Chair of Ferrous Metallurgy

Doctoral Thesis

Experimental research and mathematical modelling of the melting and dissolution behaviour of scrap in liquid hot metal

Dipl.-Ing. Florian Markus Penz, BSc

August 2019

Abstract

The production of crude steel, the basis for high quality steels, is mainly carried out with a Linz-Donawitz (LD) converter. During the process, the charged solid scrap is dissolved in the liquid hot metal. In recent years, the dynamic simulation of the entire LD process has become a challenging task. In previous works, a thermodynamic and kinetic model for the LD converter was established. For the description of the dynamic behaviour of the converter process sub routines are core elements of this model. During validation of the model with industrial data the needs for improvement of the sub routine for the scrap melting and dissolution behaviour, were detected. The focal point of this dissertation is the systematic investigation of the scrap melting and dissolution behaviour with the aim of developing a realistic scrap melting approach.

The research of the fundamental phenomenological understanding on the dissolution and melting behaviour is part of the present thesis. Based on the theoretical considerations and a comprehensive experimental investigation, a new numerical approach describing the melting and dissolution of scrap was developed.

Experiments were carried out under stagnant and turbulent flow conditions. The determination of the heat and mass transfer coefficients was realized through a standardized method of investigating the scrap melting. The findings of the electron microprobe analyses and the metallographic determinations led to a new diffusive scrap melting approach, which is based on the fundamental laws of physical chemistry and thermodynamics. This approach was successfully applied in the global process model.

Analytical descriptions of the heat and mass transfer of cylindrical specimens supported the development of a new numerical scrap melting approach. The new numerical model considers a coupled heat and mass transfer and was validated with the experimental investigations. The

new approach is valid for the whole operation temperature range of the LD process. A rigid differentiation between diffusive and forced scrap melting as used in the previous sub routine can be avoided with the new model. Also the shell freezing and its melting in the initial stages of the dissolution process is included.

Kurzfassung

Die Erzeugung von Rohstahl, welcher die Basis für hochqualitative Stähle ist, erfolgt hauptsächlich über den Linz-Donawitz (LD) Konverter Prozess. Während des Prozesses wird der dabei chargierte Stahlschrott im flüssigen Roheisen aufgelöst. In den vergangenen Jahren ist vor allem die dynamische Modellierung des gesamten LD Prozesses zur Herausforderung geworden. In vorhergehenden Arbeiten wurde ein thermodynamisches und kinetisches LD Konverter Modell entwickelt. Kernelemente des globalen Prozessmodels sind Submodelle. Während der Validierung des Prozessmodells mit Industriedaten, zeigte sich, dass Verbesserungspotential bei der Beschreibung des Auflösungs- und Aufschmelzverhaltens von Schrott enthalten ist. Der Fokus dieser Dissertation ist die systematischen Untersuchung des Auflösungs- und Aufschmelzverhaltens von Schrott mit dem Ziel einen realitätsnahen Ansatz zu definieren.

Teil dieser Arbeit ist ebenso die wissenschaftliche Beschreibung des phänomenologischen Verständnisses für den Aufschmelz- und Auflösungsprozess. Basierend auf theoretischen Überlegungen und einer umfangreichen experimentellen Studie konnte ein neues numerisches Model entwickelt werden, welches diesen Prozess beschreibt.

Die Experimente wurden unter natürlicher und erzwungener Konvektion in der Schmelze durchgeführt. Dabei konnten mit einer standardisierten Methodik Massen- und Wärmetransferkoeffizienten definiert werden. Die Ergebnisse von Mikrosondenanalysen und metallographischen Untersuchungen führten zu einem neuen Ansatz zur Beschreibung des diffusiven Schrottauflösens, welcher auf grundlegenden Gesetzen der physikalischen Chemie und Thermodynamik beruht. Der neue Ansatz konnte erfolgreich im globalen Prozessmodel integriert werden.

Die analytische Beschreibung des Wärme- und Massentransfers eines Zylinders unterstützen die Entwicklung eines neuartigen numerischen Ansatzes zur Beschreibung der Schrottauflösung. Der neue Ansatz basiert auf einer gekoppelten Massen- und Wärmeübertragung und konnte mit den experimentellen Untersuchungen validiert werden. Der Vorteil dieser Methode ist, dass sie für die gesamte Betriebstemperaturspanne des LD Prozesses gültig ist. Eine strikte Unterscheidung zwischen diffusivem und konvektivem Schmelzen beziehungsweise Auflösen, wie es im bisher verwendeten Untermodell der Schrottauflösung verwendet wurde, wird durch das neue Modell vermieden. Ebenso wird damit das Auffrieren und Abschmelzen einer Roheisenschale in den ersten Sekunden des Prozesses dargestellt.

Acknowledgement

First of all, I would like to express my sincere gratitude to my primary PhD supervisor and mentor Prof. Dipl.-Ing. Dr.techn. Johannes Schenk for all of his support and guidance over the past four years. Countless fruitful discussions with him supported me in reaching my highest level of performance at each stage of the development of this work.

I am also extremely grateful to Ao. Prof. Dipl.-Ing. Dr.techn. Christian Weiß for giving me the necessary initial broad perspectives in the field of analytical process engineering.

Big and sincere thanks go to Prof. Roberto Parreiras Tavares for his comprehensive support during my outgoing research stay in Belo Horizonte. It was an honour and a pleasure working with him and his team. It was an amazing opportunity to study and teach at the University of Minas Gerais (UFMG).

This work was carried out in the framework of a K1-MET project – a member of COMET – Competence Centres for Excellent Technologies – in collaboration with the industrial partners voestalpine Stahl GmbH, voestalpine Stahl Donawitz GmbH and Primetals Technologies Austria, including all those involved I would like to express my gratitude to each and every of them, in particular, Michael Reischl for his support during the EMPA investigations.

I would like to express special thanks to my colleagues of the Chair of Ferrous Metallurgy and K1-MET, notably Harald Mayerhofer, Carmen Grandl and Dr. mont Philip Bundschuh for all of our intensive conversations and their individual support in the course of this work.

My final thanks go to my family, specially to my parents Rudolf Wierer (with Maridl) and Sylvia Penz (with Guido) as well as my siblings Rudi, Brigitte, Romario and Sonja for their love, support, and encouragement not only throughout the course of my Ph.D. studies, but also throughout my entire life.

This work is dedicated to

my mother Sylvia, who left life far too early,

and my father Rudolf.

Affidavit

I declare on oath that I wrote this thesis independently, did not use other than the specified sources and aids, and did not otherwise use any unauthorized aids.

I declare that I have read, understood, and complied with the guidelines of the senate of the Montanuniversität Leoben for "Good Scientific Practice".

Furthermore, I declare that the electronic and printed version of the submitted thesis are identical, both, formally and with regard to content.

Date: 14.08.2019

....
Signature Author
Florian Markus, Penz
Matriculation Number: 00735183

Table of contents

Nomenclature

c_p	[J/kgK]	Specific heat capacity (isobaric)
c_i	[kg/m³]	Mass concentration
C	[kg/m³]	Mass concentration of carbon
D	[m²/s]	Diffusion coefficient
f_{liq}	[-]	Liquid fraction
f_{sol}	[-]	Solid fraction
h	[J/kg]	Specific enthalpy
H	[J]	Enthalpy
i	[-]	Control variable for the control volume
L	[J/kg]	Latent heat of fusion
n	[-]	Control variable for the simulation time
M	[g/mol]	Molar mass
m_i	[-]	Mass fraction of a specific species i
Q	[J]	Heat
S_ϕ	[-]	General source term
t	[s]	Time
T	[K]	Temperature

Tu	[-]	Tuning factor for enthalpy ($heat$) and diffusion ($diff$)
V	[m³]	Volume
v	[m/s]	melting rate
α	[m²/s]	Thermal diffusivity
Γ_ϕ	[-]	General diffusive coefficient
ξ	[-]	Dimensionless ratio of the velocity of the boundary movement and the mass transfer
λ	[W/mK]	Thermal conductivity
ϕ	[-]	General governing parameter
ρ	[kg/m³]	Density
ν	[m²/s]	Kinematic viscosity
μ	[Pa s]	Dynamic viscosity
Ψ_i	[kg]	Mass of a component i

Subscripts:

$conc$	Concentration
eut	Eutectic
HM	Hot metal
$init$	Initial
liq	Liquid
$melt$	Total liquid melt phase
mol	Molar
$mushy\ zone$	Mushy zone
scr	Scrap
$slag$	Total slag phase
sol	Solid

Superscripts:

CR	Chemical reaction

Diss	Dissolution
eut	Eutectic
HC	Consumed heat
HG	Generated heat
Melt	Melting
OC	Oxygen consumption
Tot	Total heat
0	Value on the present time step
{ }	Gas phase
[ ]	Melt
( )	Slag phase
<>	Refractory, non-metallic inclusions

Abbreviations

BOF	Basic oxygen furnace
CoFM	Chair of Ferrous Metallurgy
EMPA	Electron microprobe analysis
FDM	Finite-difference method
FEM	Finite-element method
FVM	Finite-volume method
LD	Linz Donawitz converter process
PDE	Partial differential equation
ULC	Ultra-low-carbon

List of figures

List of tables

1 Introduction and definition of the problem

The following cumulative PhD thesis is scientifically structured in peer-reviewed journal papers and the present primary work. All peer-reviewed journal articles are included in the attachment of the primary work with permission of the specific publishers. In the main text, relevant references to the peer-reviewed articles will complete the whole work and underline the scientific importance of the dissolution and scrap melting behaviour in iron-carbon melts.

1.1 Background

The LD (Linz-Donawitz) process is the dominant reactor to convert hot metal into steel and is well-described in primary literature, e.g. [1,2]. The oxidation of carbon, silicon, manganese and phosphorus delivers chemical heat to the system, which results in an increase in the hot metal temperature. To counteract the temperature increase, solid scrap is charged right at the beginning of each heat, which not only produces cooling effects, but also acts as an additional iron resource. This fact has given rise to the LD process being an important recycling process nowadays. [3–5] In the recent years, the research of the LD process and the utilization of scrap has focused on energy and resource savings, higher productivity as well as the ecological and beneficial application of scrap as a valuable raw material. [3,6,7] To achieve these objectives, the simulation of the global LD process and the specific modelling of the scrap melting and dissolution have received increasing attention in the last decades. [3]

The fundamental background of this thesis is the dynamic LD converter model developed by Lytvynyuk in [8] and improved by Bundschuh in [9]. The model connects kinetic aspects with thermodynamic knowledge according to the reaction model of Ohguchi et al. [10]. In the

previous funding period of K1-MET GmbH, several specific proposals for the improvement of the main influencing factors on the global LD process model were considered by Bundschuh in an internal report. Amongst others, the sub-routine of the dissolution and melting of scrap during the entire blowing period of the LD converter process was identified as one of the most important and process-influencing model parameters.

1.2 Objectives of the present work

The mathematical formulation of the scrap melting and dissolution in the existing global LD process model by Lytvynyuk in [8] is a connection of two approaches linked through a transition expression. The diffusive scrap melting approach is valid until the scrap melting point is reached, which is defined as the liquidus temperature in the specific scrap composition. Above the scrap melting point, the forced scrap melting approach is valid. The structure of the global dynamic LD process model will be explained in Chapter 3. The fixed point transition method shows specific disadvantages which are pointed out in this thesis.

The aim of the present thesis is the development of a scientific-methodological approach to describe the dissolution and melting of scrap in iron-carbon melts.

A comprehensive study of existing models and concepts should provide fundamental knowledge to create a new method, which implies the experimental and scientific proof.

An experimental investigation, supported by various metallographic investigations, aims to provide the main features to acquire a phenomenological understanding of the process. The behaviour of carbon at the solid-liquid interface is of particular interest.

The experiments should also be used to validate the developed modelling approach. Finally, the model illustrates the dissolution and melting of scrap realistically, which implies a coupled heat and mass transfer to avoid any numerical disadvantages through fixed point transitions.

2 Theoretical considerations

The phenomenon of the dissolution and melting of scrap is a complex simultaneous heat and mass transfer problem. In the first section of this chapter, the phenomenon of the scrap melting and dissolution is explained. It should give an overview on research carried out in previous publications. The review points out that the dissolution and melting behaviour of scrap is mainly influenced by coupled heat and mass transfer. In the second part, the fundamentals of heat and mass transfer, including the basics of numerical modelling approaches for solving the governing equations, are summarized. A short overview on the discretization methods and its rules will point out basic knowledge, which is utilized for the numerical modelling.

2.1 The dissolution and melting behaviour of scrap – a review

A review on the steel scrap melting in molten iron-carbon melts was carried out in Publication 1 in the attachment of this thesis. [3] The review contains a chapter describing the pioneering works on scrap melting by Lommel and Chalmers in [11] and on steel scrap melting in liquid iron-carbon melts by Pehlke et al. in [12] and Olsson et al. in [13]. An explicit description on the phenomenological understanding and the theoretical description can also be found in Publication 1 of the attachment. The scrap melting and dissolution behaviour can be divided into three stages [3,14–20]:

Stage 1: Solidification and melting of a liquid hot metal shell at the surface of a cold scrap particle. Heat and mass transfer have to be considered in this stage.

Stage 2: Diffusive melting of the original scrap, where only mass transfer can be considered. This is reasonable due to the heat transfer which is much faster than the mass transfer. Further the carbon content in the liquid hot metal is significantly higher than in the solid scrap.

Stage 3: Forced scrap melting stage. This stage is from particular importance especially if the carbon content of the solid is equal to that of the liquid phase or if the temperature of the hot metal exceeds the melting temperature of the scrap. [3,15,16,21–23]

Several research activities for the determination of heat and mass transfer coefficients under natural and forced convection were carried out. A summary of all published and available coefficients can be found in Publication 1 in the attachment.

2.2 Fundamentals of heat and mass transfer

In all processes in the metallurgical industry, thermo-fluid flows occur over a period of time. [24] Thereby, metals and materials tend to change their properties through transport or movement of chemical species, thermal cycling and heat fluxes. These phenomena happen because the thermodynamic equilibrium is not reached. [24,25] Scrap melting in the LD converter is one specific example for the application of transport phenomena. A quantification of the fluxes of the energy and species in the system of carbon saturated hot metal as a liquid and scrap as a solid will be described in the following chapters. These considerations have been used in this work to create the analytical and numerical model to monitor the process of the dissolution and melting behaviour of scrap. Since the experimental part of the present work used cylindrical specimens, the use of polar coordinates was more convenient. [26]

2.2.1 General forms of the conservation equations

The formulation of current transport phenomena is based on the mathematical understanding of the general conservation equations of mass, energy and chemical species and the associated formulation of the mechanics of the continuum. To describe the phenomena of scrap melting mathematically at a macro-scale level it is necessary to solve the mass and energy differential equations for the particular geometry and material. According to the first law of thermodynamics the general form of the conservation equation is shown in Equation 2.1. The parameter ϕ indicates the dependent variable and Γ_ϕ is the general diffusion coefficient of the dependent variable. [27–29]

$$\frac{\partial}{\partial t}(\rho\phi) + div(\rho\phi u) = div(\Gamma_\phi \, grad \, \phi) + S_\phi \qquad \text{Eq. 2.1}$$

The variable t defines the time in the temporal term (1st term left hand side), ρ is the density, u is the velocity and S is the source term. The second term on the left side is the convective term. In the present formulation, this term will be neglected. Its effect will be introduced by increasing the diffusion coefficient of the dependent variable. [27,30] On the right side the first term indicates the transport by diffusion for the four basic equations shown in **Table I**. [26,27,30]

Table I: Basic quantities, diffusivities and origin of the source term for general conservation transport equations [27]

Quantity	Mass	Energy	Species
ϕ	1	h	c_i
Γ_ϕ	0	$\alpha = \lambda/\rho * c_p$	D
S_ϕ	Phase motion	Phase motion and transformation	Phase motion and transformation

For the topic of the scrap melting and dissolution the transports of energy and species are utilized fundamentally. The energy is described by the enthalpy h and the general energy conservation equation is shown in Equation 2.2

$$\frac{\partial}{\partial t}(\rho h) + div(\rho h u) = div(\lambda \, grad \, T) + S_h \qquad \text{Eq. 2.2}$$

With the auxiliary equation $c_p grad \, T = grad \, h$, the conservation equation can be described as a function of enthalpy (Equation 2.3) or a function of temperature by substituting the heat flux terms with the equations of Fourier´s law.

$$\frac{\partial}{\partial t}(\rho T) + div(\rho T u) = div\left(\frac{\lambda}{c_p} grad \, T\right) + \frac{S_h}{c_p} \qquad \text{Eq. 2.3}$$

The experimental investigations in the present work were carried out by using vertical steel scrap cylinders, which were submerged into liquid hot metal. Therefore, Equation 2.3 is written in a cylindrical coordinate system. The effect of convection will further be adjusted by an increase of thermal conductivity in the liquid and mushy regions. This technique was mentioned first by Mizikar in [31] to describe the solidification of continuously casted steel slabs. Further, this approach was also used for heat transfer phenomena by Choudhary et al.

in [32], Lait et al. in [33] as well as Cho and Kim in [34]. A more specific explanation will be given in Chapter 2.2.3.4. The modified equation for three-dimensional flow is shown in Equation 2.4 and for one-dimensional heat flow in radial direction (r) in Equation 2.5. [26–28,35] The transformation of the equation to spherical and linear coordinate system is described in detail in various transport phenomena books e.g. by Seshadri et al. in [26].

$$\frac{\partial T}{\partial t} c_P \rho *= \frac{1}{r}\frac{\partial}{\partial r}\left(\lambda * r \frac{\partial T}{\partial r}\right) + \frac{1}{r^2}\frac{\partial}{\partial \theta}\left(\lambda \frac{\partial T}{\partial \theta}\right) + \frac{\partial}{\partial z}\left(\lambda \frac{\partial T}{\partial z}\right) + S_h \qquad \text{Eq. 2.4}$$

$$\frac{\partial T}{\partial t} c_P \rho = \frac{1}{r}\frac{\partial}{\partial r}\left(\lambda * r \frac{\partial T}{\partial r}\right) + S_h \qquad \text{Eq. 2.5}$$

The mass conservation of a chemical species (i) is described by Fick´s second law given Equation 2.6. The mass fraction of a chemical species is thereby defined as m_i. The mathematical expression ρm_i is further defined to be the concentration c_i in kg/m³ The modification for cylindrical coordinates and an assumed mass flow in radial direction (r) is given in Equation 2.7. For the case treated in this thesis it is defined that $c_i = C$ whereby C defines the carbon concentration in kg/m³. The further used derivation of Equation 2.7 using the carbon concentration is given in Equation 2.7a. Due to the fact, that no mass will be released through the phase change, the source term S_i can be neglected. The same assumption related to the convective term used for the heat transfer will be used in the case of mass transfer. The effect of convection will be adjusted by an increase of the mass diffusivity in the liquid and mushy regions.

$$\frac{\partial}{\partial t}(\rho m_i) + div(\rho m_i u) = div(\rho D_i \; grad \; m_i) + S_i \qquad \text{Eq. 2.6}$$

$$\frac{\partial (c_i)}{\partial t} = D_i\left(\frac{\partial^2 (c_i)}{\partial r^2} + \frac{1}{r}\frac{\partial (c_i)}{\partial r}\right) \qquad \text{Eq. 2.7}$$

$$\frac{\partial (C)}{\partial t} = D_i\left(\frac{\partial^2 (C)}{\partial r^2} + \frac{1}{r}\frac{\partial (C)}{\partial r}\right) \qquad \text{Eq. 2.7a}$$

To solve these partial differential equations (PDE) it is necessary to establish an accurate mathematical approach with appropriate boundary conditions to describe the related phenomena. [30] Usually two methods – the analytical method and the numerical method – are available to solve the PDEs. The main advantage of the analytical solution is its accuracy and concision. With specific boundary and initial conditions, the analytical solution is obtained through deduction. The most used method is the variables separation method. [30,36] A detailed description of the separation method was published by Necati Özisik in [36] and was used for the analytical solution of the heat and mass transfer, which is described in Chapter 5 and in Publication 2 in the attachment of this thesis. [37] Nevertheless, the analytical methods

suffer from many limitations, because in real life exist always more-dimensional geometries, temperature and chemical composition dependent thermal and physical properties as well as complex boundary conditions. [38] The most fundamental simulation method is the numerical approach, which is applicable for different kinds of boundary conditions and nonlinear problems. The most common methods in process simulation are the finite-element method (FEM), finite-difference method (FDM) and the finite-volume method (FVM). All of them have a characteristic procedure of transforming the PDEs into large systems of simultaneous algebraic equations. The discretized functions are finally solved. [24,30]

2.2.2 Discretization for numerical modelling

Different discretization methods like the Taylor-Series formulation and the control volume method are available. A few of them are outlined in [24] and [27]. In the present work an integral approximation for the method of finite control volumes is used, which was published by Patankar in [24]. The domain will be divided into non-overlapping control volumes, which involves a nodal point each. The differential equations are integrated throughout the control volume considering that a piecewise profile will express the variation of a function Φ between the grid points. The variable Φ is thereby only a function of one independent geometric variable. As a result, the values of Φ for a group of grid points will give the discretization equation. [24] For the conservation equation of energy, given in Equation 2.4, the control volume is shown in **Figure 1**. According to the cylindrical discretization rules proposed by Patankar, the discretization equation for an explicit scheme is given in Equation 2.8. The superscript 0 refers to the value in the present time step.

$$a_P T_P = a_E T_E^0 + a_W T_W^0 + a_N T_N^0 + a_S T_S^0 + [a_P^0 - a_E - a_W - a_N - a_S - S * \Delta V] * T_P^0 + b$$

<div align="right">Eq. 2.8</div>

where

$$a_E = \lambda_E * \Delta r / (r_E * (\delta\theta)_e)$$ <div align="right">Eq. 2.8 a</div>

$$a_W = \lambda_W * \Delta r / (r_W * (\delta\theta)_W)$$ <div align="right">Eq. 2.8 b</div>

$$a_N = \lambda_N * \Delta\theta * r_N / (\delta r)_N$$ <div align="right">Eq. 2.8 c</div>

$$a_S = \lambda_S * \Delta\theta * r_s / (\delta r)_S$$ <div align="right">Eq. 2.8 d</div>

$$a_p = a_P^0 = c_P \rho * \Delta V / \Delta t$$ <div align="right">Eq. 2.8 e</div>

$$b = S * \Delta V$$ <div align="right">Eq. 2.8 f</div>

$$\Delta V = (r_S + r_N) / 2 * \Delta\theta * \Delta r$$ <div align="right">Eq. 2.8 g</div>

A more detailed explanation of the discretization regarding this work is published in Publication 2 in the attachment of this thesis. [24,30,37]
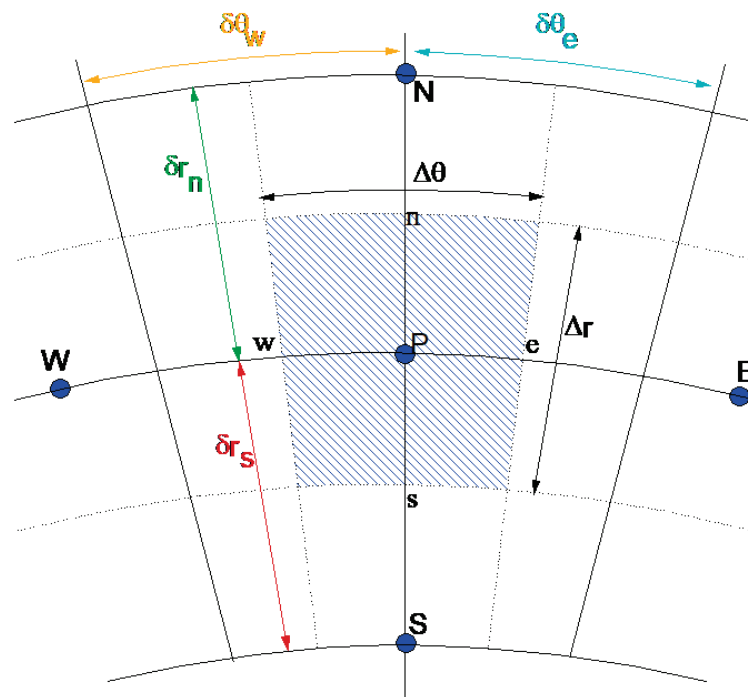
Figure 1: Control volume in polar coordinates according to Patankar´s discretization equations. [24]

To avoid any numerical errors and to ensure physical realism as well as the overall balance, four basic rules have to be adhered to the discretization equations. The four basic rules of discretization are defined as follows: [24]

1) Consistency at the control volume faces
2) All the coefficients a_P and their neighbour coefficients (a_S, a_W, a_E and a_N) must be positive
3) Negative slope linearization of the source term
4) Sum of the neighbour coefficients

The first rule defines, that the outgoing heat as well as the mass flux must be equal to the flux that enters the adjacent control volume. If this rule is not followed, the overall balance will be incorrect. This rule receives attention in the present work through the thermal conductivity, which is equalized at the boundary interface through the harmonic average between e.g. the calculated temperature dependent thermal conductivities of the points S and P in **Figure 1**. Negligence of the second and third rule will consequently lead to physically unrealistic solutions and instability. The third rule implies that the linear source term S always has to be negative. The fourth rule implies that the sum of the coefficients of all neighbours of a_P should be equal to the coefficient of the centre control volume ($a_P = \sum a_{nb}$). [24,25]

2.2.3 Non-stationary heat transfer problem through conduction with phase change and convection

A fundamental part of the numerical model for scrap melting is the solution of the energy conservation equation including the definition of the phase change accompanied with a moving boundary. These solid/liquid transformations like in solidification (e.g. casting) or melting processes involve a phase change, which is known as Stefan problem. The simulation of these phenomena can be conducted in several forms e.g. the fixed-domain method, with emphasis on the treatment of the latent heat of fusion specially in the two phase area of any alloy. [39,40] It has to be mentioned that any convection effects due to density variations in the liquid phase or density changes at the phase interface are neglected. Through simple modifications of existing numerical methods for heat transfer problems, the simulation of the phase change can be achieved. The most popular approaches are the fixed grid techniques in which the essential feature is the evolution of the released or absorbed latent heat. [38,41] Thereby, the most widely used latent heat formulations are the enthalpy method, the apparent or effective specific heat method and the source term method. [27,38,39,41]. In the published research by Voller and Swaminathan in [40–42], it is mentioned that the choice of the method will strongly depend on the problem and on the personal preferences. The most important latent heat formulations will be explained hereafter in abbreviated form. Initially, the theoretical assumptions will be explained.

According to the theoretical analyses from Szekely and Themelis in [25], the conservation Equation 2.5 can be stated at the interface as:

$$\begin{bmatrix} heat\ flux\ arriving \\ from\ the\ melt\ to \\ the\ interface \end{bmatrix} - \begin{bmatrix} heat\ flux\ leaving \\ the\ interface\ by \\ conduction\ through \\ the\ solid \end{bmatrix} = \begin{bmatrix} rate\ of\ heat \\ evolution\ due\ to \\ melting\ or \\ solidification \end{bmatrix} \qquad \text{Eq. 2.9}$$

From Equation 2.9, the rate of heat evolution can be expressed further as the product of [25]:

$$\begin{bmatrix} rate\ of\ advance \\ of\ melting\ or \\ solidification \\ boundary \end{bmatrix} * \begin{bmatrix} latent\ heat\ of \\ solidification \\ or\ melting \end{bmatrix} \qquad \text{Eq. 2.10}$$

Thus from Equation 2.10 associated with the phase change, the source term S_h can be expressed as given in Equation 2.11. [25,27]

$$S_h = \rho * L * \frac{\partial f_{liq}}{\partial t} \qquad \text{Eq. 2.11}$$

In Equation 2.11 L describes the latent heat and f_{liq} is the liquid fraction, which is rewritten as $\partial f_{liq}/\partial t = (\partial f_{liq}/\partial T)(\partial T/\partial t)$. According to the binary Fe-Fe₃C phase diagram, a dependency of the liquid fraction with the temperature is given and a two phase region exists. Possible approaches to determine the liquid fraction, which is a key feature of the fixed grid methods, are the Scheil equation and the equilibrium Lever rule approach as well as linear, linear eutectic approaches or to a power of certain constants. A compilation of possible forms for liquid fraction versus temperature is given by Voller and Swaminathan in [40] or in further literature e.g. [27,43–45]. In the present work, it is assumed that in the mushy zone – the region of coexistence of liquid and solid - f_{liq} obeys the linear variation published by Gür and Pan in [30], given in Equation 2.12. However, the temperature is expressed in terms of the enthalpy. A more detailed description will be given in the following Chapter 2.2.4.

$$f_{liq} = \frac{T_i - T_{sol}}{T_{liq} - T_{sol}}$$

Eq. 2.12

In Equation 2.12 T_i is the temperature of the specific volume element, T_{liq} and T_{sol} are the temperatures on the liquidus and solidus line, respectively, considering the carbon concentration, as schematically shown in **Figure 2**.
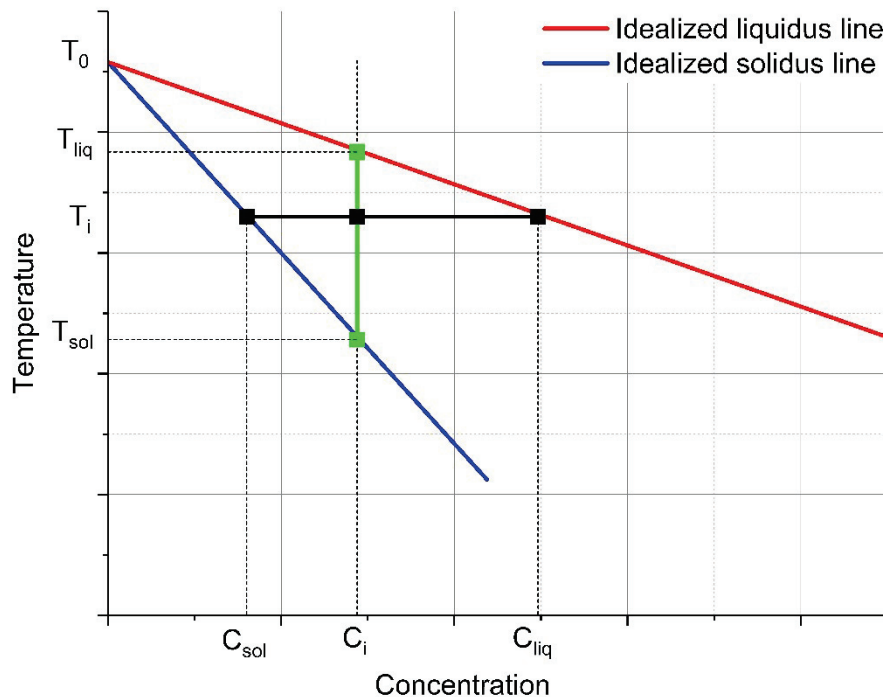
Figure 2: Scheme for the determination of the liquid fraction within the two-phase region of the binary phase diagram using a linear approach; the concentration on the x-axis denotes the carbon content according to **Figure 4**.

With the definition of the liquid fraction and the source term, the conservation equation given in Equation 2.1.5 can be rearranged through the aforementioned fixed grid techniques. [27]

2.2.3.1 Enthalpy method

The enthalpy method enjoys widespread applications as can be observed in the research of various investigators in [27,36,39,41,42,46–49] and much more. The fundamental step of this method is to transform the non-stationary part of the energy equation (Eq. 2.5) as a function of the enthalpy instead of the temperature. The enthalpy in [J/kg], including the latent heat, is defined as a piecewise linear function of the temperature. In the case of binary alloys, the enthalpy H(T) in the mushy zone will be linearized and the piecewise linear function will be as given in Equation 2.13. It has to be mentioned that the specific heat capacity is assumed to be constant. [36,38,39,47]

$$H(T) = \begin{cases} c_p * T & if: T < T_{sol} \\ c_p * T + L\dfrac{(T_i - T_{sol})}{(T_{liq} - T_{sol})} & if: T_{sol} < T < T_{liq} \\ c_p * T + L & if: T > T_{liq} \end{cases} \qquad \text{Eq. 2.13}$$

It has to be recognized that the latent heat is weighted by the liquid fraction and that on each time step a new value of the enthalpy is computed. From the new nodal enthalpy, the temperature can be determined afterwards. [38,42,47]

2.2.3.2 Apparent heat capacity method

In this approach the latent heat is included in the specific heat capacity of the material within the phase change temperature interval. The equivalent or apparent heat capacity c_p^{app} of the given temperature interval within the mushy zone is introduced in the general energy Equation 2.5. In this case, it is assumed that the latent heat is released uniformly between the liquidus and solidus temperatures. The governing form of the energy equation will be defined as given in Equation 2.14 by using the apparent heat capacity evaluated using Equation 2.15. [27,38,42,45,50,51]

$$\frac{\partial T}{\partial t} c_p^{app} \, \rho = \lambda * \frac{1}{r}\frac{\partial}{\partial r}\left(r\frac{\partial T}{\partial r}\right) \qquad \text{Eq. 2.14}$$

$$c_p^{app} = \frac{dH}{dT} = \frac{\left\{\int_{T_{sol}}^{T_{liq}} c_p(T)dT + L\right\}}{(T_{liq} - T_{sol})} \qquad \text{Eq. 2.15}$$

According to Salcudean and Abdullah in [38] as well as Swaminathan and Voller in [42], the apparent heat capacity method shows deficiencies for melting problems. If the temperature

interval for the phase change is too small, some of the heat effects may not be accounted for. [38,42,50]. This is a result of the strong variations of the specific heat capacity close to the liquidus and eutectic temperature. [27] An improvement of the apparent method is the effective capacity method were the apparent heat capacity function is integrated over the control volume. The solution is further relatively independent from the mushy range as demonstrated by Salcudean and Abdullah in [38].

2.2.3.3 Source term method

In the source term methods, the effect of the release of the latent heat is introduced in the source term of the FDM or FVM. For the numerical codes, where the discretization expression is in the form of the given Equation 2.8 from Patankar published in [24], the source term method is preferable. [38] The main objective of this method is a direct substitution of the enthalpy, including the latent heat in the form given in Equation 2.16 in the governing energy Equation 2.5. This mathematical solver will give a solution as a conduction problem, but incorporates a source term with transient formulation as given in Equation 2.17. [38,40,42,47]

$$\frac{dh}{dt} = c_p * \frac{dT}{dt} + L * \frac{df_{liq}}{dt} \qquad \text{Eq. 2.16}$$

$$c_p\,\rho\,\frac{\partial T}{\partial t} = \frac{1}{r}\frac{\partial}{\partial r}\left(\lambda * r\,\frac{\partial T}{\partial r}\right) - \rho\frac{\partial}{\partial t}\left(f_{liq} * L\right) \qquad \text{Eq. 2.17}$$

The expressions in the Equation 2.16 and 2.17 can be rearranged to a relation between the temperature and enthalpy change in form of a total derivative given in Equation 2.18.

$$dT = \frac{dh}{c_p} + L * \frac{df_{liq}}{c_p} \qquad \text{Eq. 2.18}$$

The conservation equation is turned with this substitution to the expression given in Equation 2.19, which is a solution of a heat conduction problem using the enthalpy as the dependent variable, incorporating a source term with a diffusion formulation.

$$\rho\frac{\partial h}{\partial t} = div\left(\frac{\lambda}{c_p}\,grad\,T\right) - L * div\left(\frac{\lambda}{c_p}\,grad\,f_{liq}\right) \qquad \text{Eq. 2.19}$$

2.2.3.4 Introduction of the convection

A further question beside the release of the latent heat in phase change problems with a moving boundary is, how to introduce the effect of convection – natural or forced convection – into a numerical model. Regarding this effect, several works have been published e.g. in [52–58]. The three groups of methods, which have been proposed, were summarized by Voller et al. in [52] and are the empirical, the classical and the enthalpy method.

The empirical approach is to treat the problem as a diffusion problem. In this approach the heat transfer in the liquid and mushy zones is accelerated by boosting the liquid thermal conductivity with an empirical tuning factor or a definition of an effective thermal conductivity. This approach was successfully used in the research of metallurgical processes, primarily for solidification, e.g. in [32–34,49,55,56,58–60].

The so called classical method, takes full account of the convection in the liquid region, deriving suitable governing heat and mass transfer equations and numerical techniques. [52] In the vicinity of the phase change, conditions on temperature, heat removal and velocity have to be accounted, which leads to difficulties in temperature based governing heat transfer equations. [52] According to Voller et al. [52] a huge computational effort and careful development of tailor-made codes is necessary for this approach. [52] According to the research of Sparrow et al. [61] it is also difficult to determine and validate the natural convective flows in a liquid metal bath. The classical method was amongst others successfully used in [61–64].

The third approach is the enthalpy-porosity method, which is connected with the velocity in a control volume element. The control volume element is considered to be a pseudo porous medium with a certain amount of fluid fraction inside a solid matrix. This technique is also called "Darcy-Source". [54] Therefore, a porosity-permeability relationship has to be developed, which will be substituted as an additional source term in the governing equation. A more detailed description of this method was presented by Voller et al. in [47,52–54,57]

According to the widespread acceptance and simple handling, the empirical approach will be used in this work. Therefore, the thermal conductivity has to be adjusted by the constant variable Tu_{heat} to implement the effect of convection. The following expressions in the Equations 2.20, 2.21 and 2.22 can be assumed for the artificial increase of the thermal conductivity according to the amount of f_{liq} in a certain volume element. [31,33,34,59,65]

$$f_{liq} = 1 \qquad\qquad \lambda_{liq} = Tu_{heat} * \lambda_{sol}(T) \qquad\qquad \text{Eq. 2.20}$$

$$0 < f_{liq} < 1 \qquad\qquad \lambda_{mushy\ zone} = \lambda_{sol}(T)\left[1 + (1 - Tu_{heat}) * f_{liq}^2\right] \qquad\qquad \text{Eq. 2.21}$$

$$f_{liq} = 0 \qquad\qquad \lambda_{sol} = \lambda_{sol}(T) \qquad\qquad \text{Eq. 2.22}$$

Lait et al. [33] and Mizikar [31] determined in their research about mathematical modelling of the heat flow in the continuous casting of steel that $Tu_{heat} = 7$. [31,33] Lally et al. [59], based on Brimacombes work in [65], as well as Cho and Kim in [34] stated for Tu_{heat} the range between 5 and 10.

From the aforementioned findings, the following flow sheet for an explicit numerical model to describe the non-stationary heat transfer incorporating a phase change from liquid hot metal to solid scrap is shown in **Figure 3**.

Figure 3: Flow sheet of an explicit numerical solution of a non-stationary heat transfer problem with phase change between liquid hot metal and scrap. [37]

2.2.4 Relationship among enthalpy, liquid fraction and temperature for Fe-C alloys

From the previous Chapter 2.3 and Equation 2.12, it is necessary to discuss the relationship between the temperature or enthalpy with the amount of liquid fraction in detail. The relation between enthalpy and temperature can be taken from Equation 2.13. The special case of the Fe-Fe$_3$C phase diagram is, that it has a peritectic and eutectic transformation. Due to the carbon contents in the hot metal of approximately 4.5 wt.-% the discussion of the peritectic transition will be neglected in this work. For the numerical description of the scrap melting and dissolution with a coupled heat and mass transfer, the liquidus, solidus and eutectic temperatures have to be estimated based on the Fe-Fe$_3$C phase diagram of the used scrap. For simplification, it is assumed that the specific heat capacity c_p and the latent heat of melting

L are constant. Further, the two-phase area of iron with cementite is neglected with the assumption that the carbon content in an LD converter will be rapidly below the eutectic amount of 4.38 wt.-%C if the scrap used is a common S235JR steel.

In **Figure 4** the phase diagram of a common S235JR construction steel is given, which is generated by FactSage[TM] FSstel database. To define the solidus and liquidus temperatures, two crucial approaches have to be considered. The first definition is below the maximum solubility of carbon in the austenite (≤ 2.05 wt.-% C) and the second is the eutectic area above the maximum solubility of carbon in austenite and below the eutectic point (2.05 wt.-% C < x ≤ 4.38 wt.-% C), marked as case 1 and 2 in **Figure 4**.
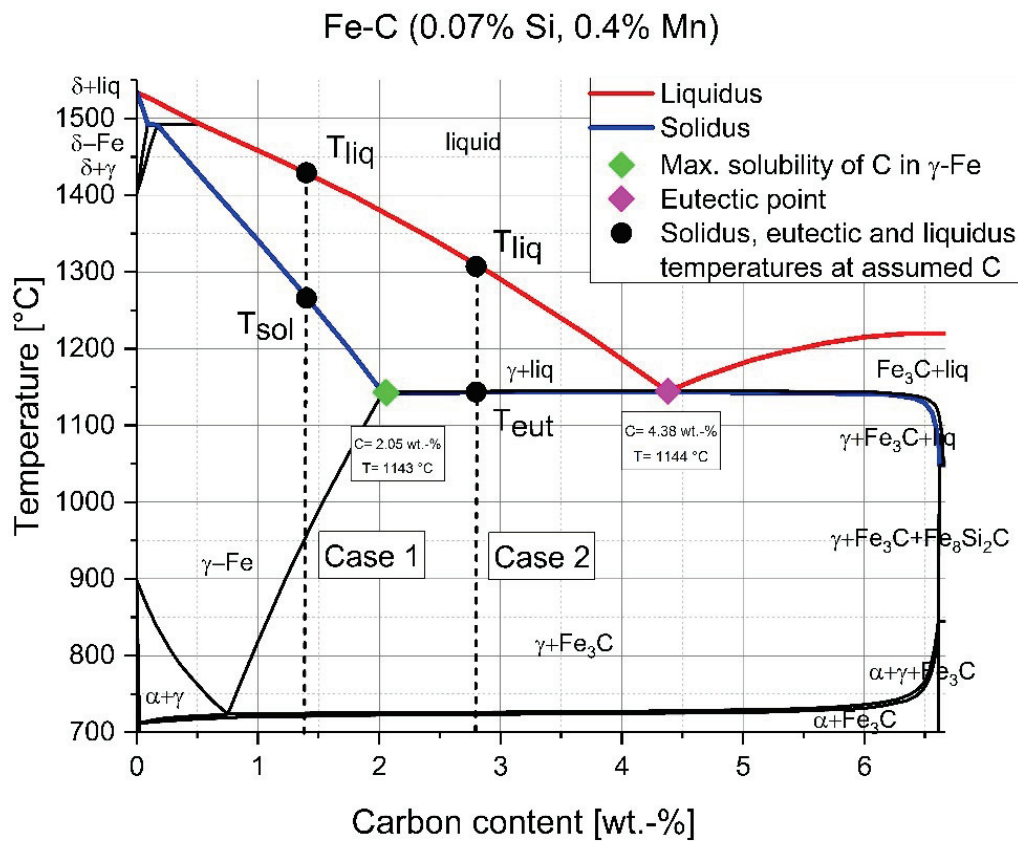
Figure 4: Fe–Fe₃C phase diagram of common S235JR construction steel scrap including schematic points of the solidus, eutectic and liquidus temperature, respectively, at assumed carbon contents.

With the temperatures and the definition from Equation 2.13, the enthalpy can be determined, which is an important step to define the amount of liquid fraction in a volume element.

According to case 1 in **Figure 4**, where the carbon composition is below the maximum solubility of carbon in austenite (≤ 2.05 wt.-% C), the linearized enthalpy in relation to the temperature is shown in the diagram in **Figure 5**. With the assumption of a constant specific heat capacity, the enthalpies at the solidus line ($H_{sol}\ in\ [J/kg]$) and the liquidus line ($H_{liq}\ in\ [J/kg]$) can be determined through Equation 2.23 and 2.24, respectively.

$$H_{sol}(i) = c_p * (T_{solidus}(i) - 298) \qquad \text{Eq. 2.23}$$

$$H_{liq}(i) = c_p * (T_{liquidus}(i) - 298) + L \qquad \text{Eq. 2.24}$$
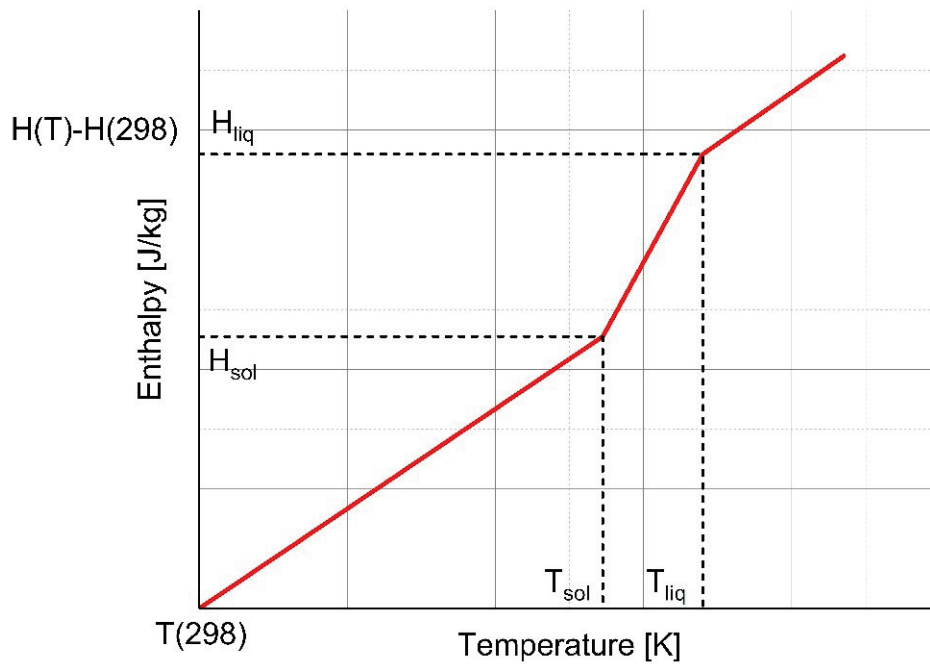
Figure 5: Linearized enthalpy function of the temperature below the maximum carbon solubility in austenite (≤ 2.05 wt.-% C) according to **Figure 4**

For case 2, where the carbon composition is between the maximum solubility of carbon in austenite and the eutectic point, the linearized temperature-dependent enthalpy diagram is shown in **Figure 6**. In this case a certain amount of scrap is already liquid and therefore the latent heat has to be incorporated. The equations for the eutectic enthalpies ($H_{eut1}\ and\ H_{eut2}$) and the eutectic liquid fraction (f_l^{eut}) are given in equation 2.25, 2.26 and 2.27. The liquidus enthalpy for temperature in the liquid region is calculated similarly to the first case. The indices of the eutectic enthalpies denote the beginning (1) and the end (2) of the step function to overcome the release of the latent heat of the eutectic transformation, which is schematically explained in **Figure 6**.

$$H_{eut1} = c_p * (T_{Eutectic}(i) - 298) \qquad \text{Eq. 2.25}$$

$$H_{eut2} = c_p * (T_{Eutectic}(i) - 298) + f_l^{eut}(i) * L \qquad \text{Eq. 2.26}$$

$$f_l^{eut}(i) = \frac{\%C(i) - 2.05}{4.3 - 2.05} \qquad \text{Eq. 2.27}$$
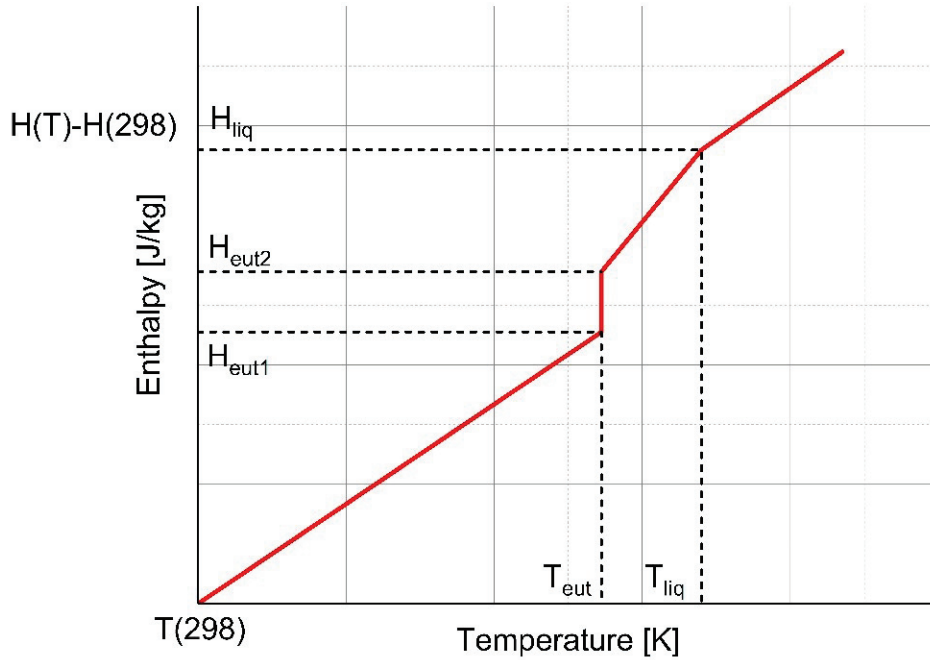
Figure 6: Linearized enthalpy function of the temperature for a binary phase change between the maximum solubility of carbon in austenite and the eutectic point according to case 2 in **Figure 4**

2.2.5 Mass transfer in non-stationary systems (temperature based)

The diffusion of a species, specifically carbon, in a solid steel cylinder is well described e.g. in [66–70]. In general, the material balance for a species "i" in a volume element can be expressed according to the theoretical analyses from Szekely and Themelis in [25], as given in Equation 2.28:

$$\begin{bmatrix} net\ flux\ of \\ i\ into \\ the\ element \end{bmatrix} - \begin{bmatrix} rate\ of\ production \\ of\ i\ by\ chemical \\ reaction \end{bmatrix} = \begin{bmatrix} rate\ of \\ accumulation\ of\ i \end{bmatrix} \qquad \text{Eq. 2.28}$$

Nevertheless, the main important point is that in the case of steel scrap melting, the diffusion is coupled with the heat transfer and the phase change. From Zhang and Oeters in [71], it is known that the heat transfer in solid steel is approximately 40 times faster than the mass

transfer. Due to this fact, the basic step for developing a numerical model is to describe the isothermal mass transfer in a non-stationary system. The development of a method to solve numerically the mass conservation Equation 2.7a is necessary. The fundamental findings and expressions from the governing heat transfer description can be converted into the mass transfer approach due to the similarity of the governing conservation equations.

From Equation 2.7 the governing equation for non-stationary mass transfer is known. The expression of the concentration of an element is defined to be $c_i = \rho m_i$ with the unit [kg/m³], with the mass fraction m_i, and D is the mass diffusivity in [m²/s]. In the special case given in Equation 2.7a $c_i = C$ whereby C is the carbon concentration in kg/m³. It is assumed that the concentration of an element is uniform inside the control volume. The discretization of the conservation equation for one-dimensional mass diffusion in a non-stationary radial system is written in Equation 2.29.

$$\int_{w}^{e} \int_{t}^{t+\Delta t} \frac{\partial C}{\partial t}\, dt\, dx = \int_{t}^{t+\Delta t} \int_{w}^{e} \frac{1}{r}\frac{\partial}{\partial r}\left(rD\frac{\partial C}{\partial r}\right) dx\, dt \qquad \text{Eq. 2.29}$$

With the use of the explicit volume element method published by Patankar in [24], the numerical model can be solved. To introduce the effect of convection in the liquid and mushy region, the same empirical approach of an artificial increase of the diffusive transport coefficient can be used. Therefore, the mass diffusivity has to be adjusted by the constant variable Tu_{diff} according to the equations 2.30, 2.31 and 2.32.

$$f_{liq} = 1 \qquad\qquad D_{liq} = Tu_{diff} * D_{sol}(T) \qquad\qquad \text{Eq. 2.30}$$

$$0 < f_{liq} < 1 \qquad\qquad D_{mushy\ zone} = D_{sol}(T)\left[1 + \left(1 - Tu_{diff}\right) * f_{liq}^2\right] \qquad\qquad \text{Eq. 2.31}$$

$$f_{liq} = 0 \qquad\qquad D_{sol} = D_{sol}(T) \qquad\qquad \text{Eq. 2.32}$$

With these theoretical findings for an explicit numerical model to describe the isothermal non-stationary mass transfer, incorporating a phase change from liquid hot metal to solid scrap, is presented in the flow sheet in **Figure 7**.
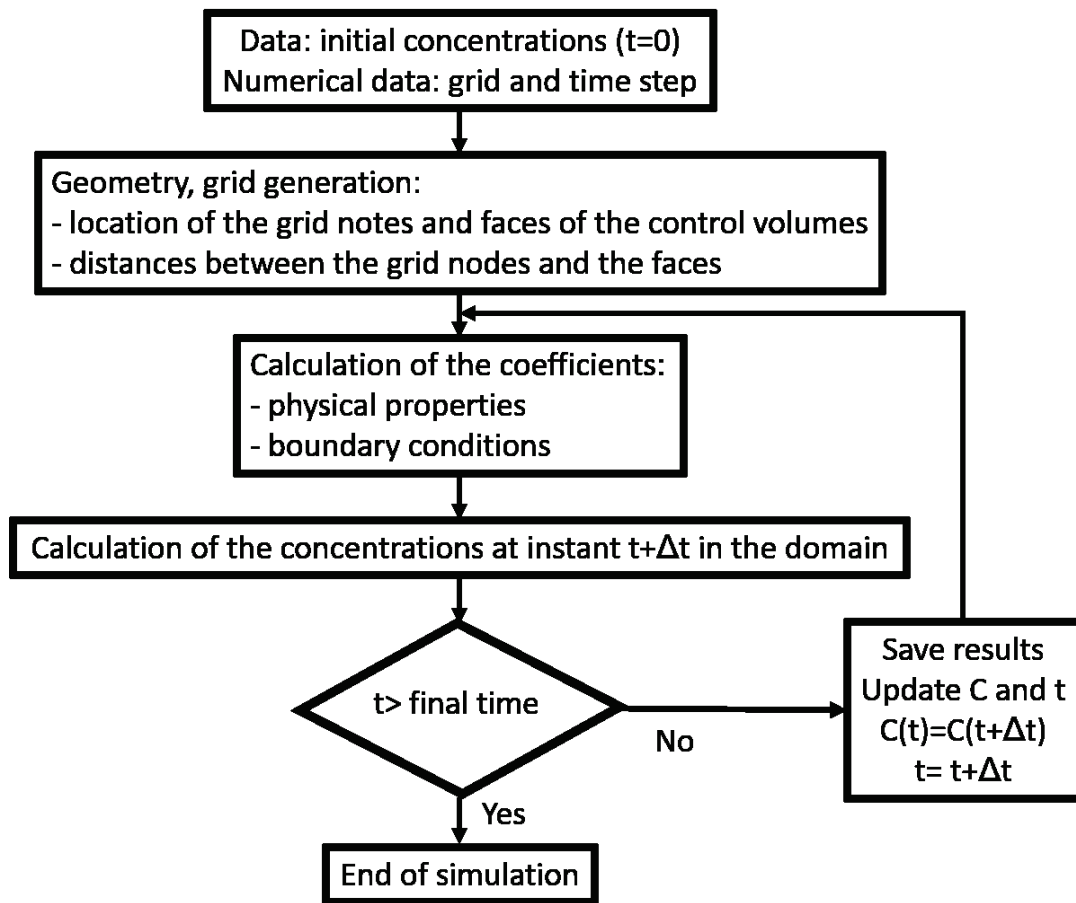
Figure 7: Flow sheet of an explicit numerical solution of a isothermal non-stationary mass transfer problem with phase change between liquid hot metal and scrap

2.2.6 Coupling heat and mass transfer during scrap melting/dissolution

In the previous chapters the single mass and heat transfer as well as further objectives to create a coupled heat and mass transfer model were described. If these findings are combined, the flow sheet for an explicit numerical model is developed as shown in **Figure 8**.
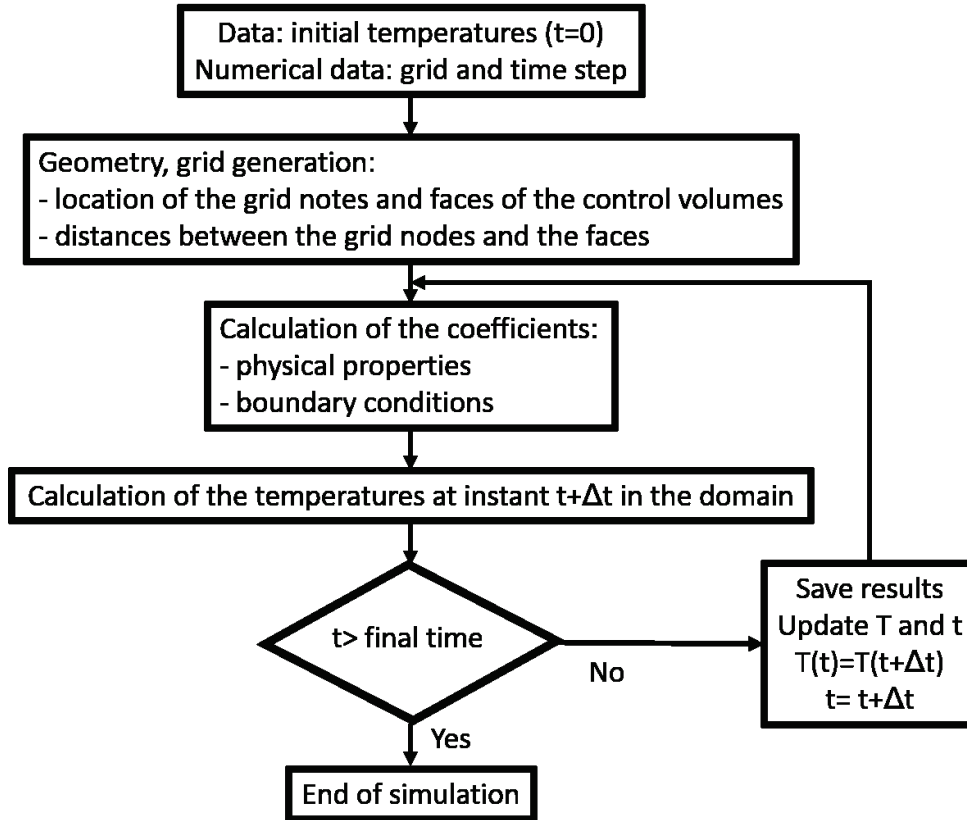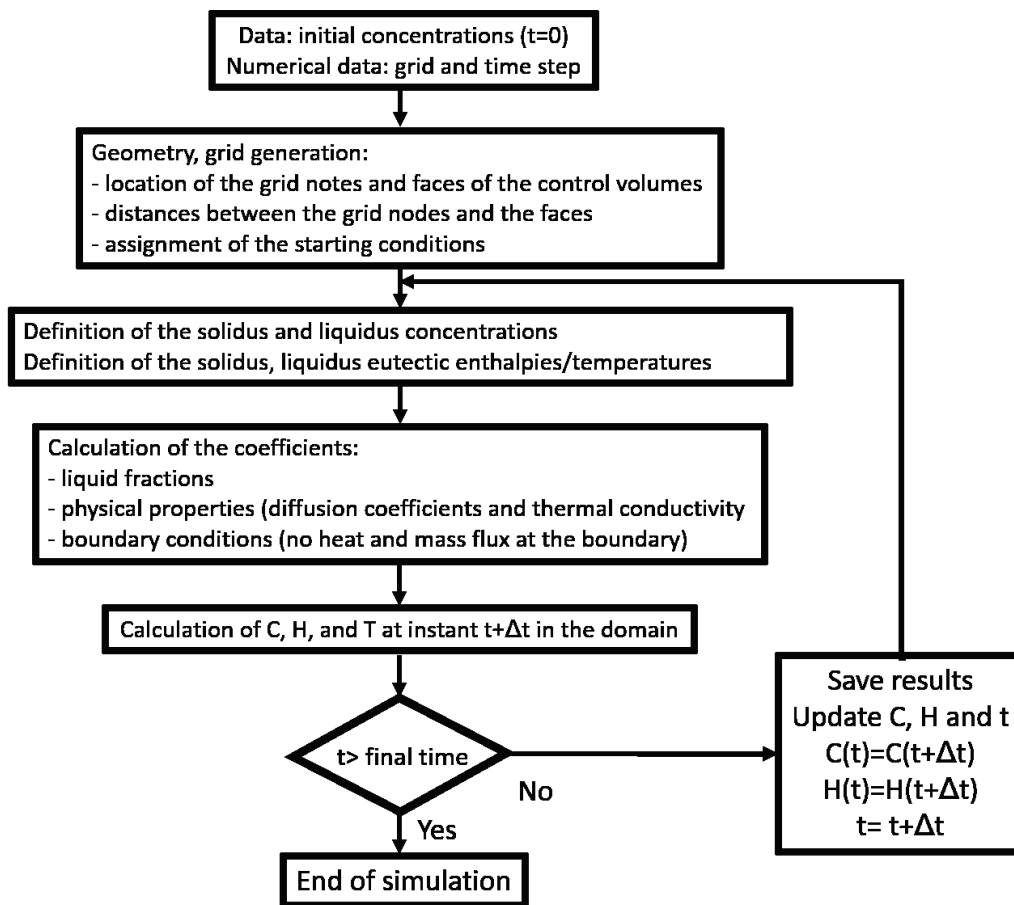
Figure 8: Flow sheet of an explicit numerical solution of a non-stationary coupled heat and mass transfer problem with phase change between liquid hot metal and solid scrap

It is necessary to highlight from **Figure 8** the determination of the physical properties, which are the proportionality factors of the governing equations for heat and mass transfer, the thermal conductivity and the diffusion coefficients, respectively. With the artificial increase of the proportionality factors to simulate the phase change, it is of particular importance to use temperature and chemical composition dependent thermal conductivities and diffusion coefficients, respectively.

Temperature dependent diffusion coefficients were published by Ågren in [72], Ueshima et al. in [73] and several other researchers in e.g. [68,74–76]. Ågren presented a comprehensive expression for the diffusivity of carbon in austenite. The diffusivity is expressed as a function of the composition variable y_C and the temperature T. The composition variable y_C is related to the ordinary mole fraction of carbon x_C with the definition of $y_C = x_C/(1 - x_C)$. This research was validated based on extensive measurements carried out by Wells et al. in [77] and is given in Equation 2.33. [72]

$$D_C = 4.53 * 10^{-7} \left(1 + y_C(1 - y_C) * \frac{8339.9}{T} \right) *$$
$$* exp \left\{ - \left(\frac{1}{T} - 2.221 * 10^{-4} \right) (17767 - 26436 y_C) \right\}$$

Eq.2.33

Ueshima et al. investigated the solute distribution in dendrites of carbon steel with δ/γ transformation during solidification. For their research, the temperature dependent diffusion coefficients for δ-iron (D_C^δ) and austenite (D_C) are given in Equation 2.34 and 2.35, respectively. The gas constant R in Equation 2.34 and 2.35 has the value of 1.987 in [cal/K mol] and the diffusion coefficients are in [m²/s]. [73,78]

$$D_C^\delta = 1.27 * 10^{-6} * exp \left(-\frac{19450}{RT} \right) = 1.27 * 10^{-6} * exp \left(-\frac{9794}{T} \right) \qquad \text{Eq. 2.34}$$

$$D_C = 7.61 * 10^{-6} * exp \left(-\frac{32160}{RT} \right) = 7.61 * 10^{-6} * exp \left(-\frac{16183}{T} \right) \qquad \text{Eq. 2.35}$$

Various authors published in their research expressions for temperature and chemical composition dependent thermal conductivities. [31,45,79–82] Through the research on a special numerical algorithm based on a phase transformation model, called IDS (interdendritic solidification model), Miettinen calculated important solidification related thermophysical properties of steel and published them in [79,80]. The research on an accurate mathematical heat transfer model for solidification of continuously casted steel slabs, published by Mizikar in [31], shows the importance to utilize a temperature dependent thermal conductivity. The definition of the thermal conductivity by Mizikar was validated by Thomas in [83] and is given in the following equations. Equation 2.38 and 2.39 include the artificial increase for the mushy zone and the liquid fraction to implement the effect of convection in a numerical model as established in the Equations 2.20, 2.21 and 2.22.

$f_{liq} = 0 \ and \ T \leq 800 \,°C$	$\lambda_{sol} = 59.4 - 0.0418 * T$	Eq. 2.36
$f_{liq} = 0 \ and \ 800 \,°C \ \leq T \leq T_{sol}$	$\lambda_{sol} = 18.4 - 0.0094 * T$	Eq. 2.37
$f_{liq} = 1$	$\lambda_{liq} = 43 * Tu_{heat}$	Eq. 2.38
$0 < f_{liq} < 1$	$\lambda_{mushy \ zone} = (18.4 - 0.0094 * T) * \left[1 + (1 - Tu_{heat}) * f_{liq}^2 \right]$	Eq. 2.39

3 The scrap melting and dissolution behaviour in LD process simulations

The modelling of the LD process started in the 1960s, where mass and energy balances of several scrap geometries were calculated. The research interest increased in modelling and empiric, kinetic or thermodynamic sub-routines to approximate process variables were introduced. Further, the process variables influence the global system and predict the required final specification to terminate the simulation. The numerical description of the scrap melting and dissolution behaviour is one of these sub-routines amongst others. In Publication 1 in the attachment a whole chapter is dedicated to the numerical descriptions of the dissolution and melting phenomenon of scrap in hot metal. [3] The chapter is thereby divided into two parts – process simulations and numerical approaches – which will be complemented with some specific approaches for steel scrap melting in LD process models in the following Chapter 3.2. The research, described in this thesis, is based on the Matlab$^{®}$ coded LD converter model developed by Lytvynyuk [8,84–86], which was improved by Bundschuh in [9,87]. The description of the scrap melting and dissolution sub-routine is outlined in Chapter 3.1.

3.1 The definition of scrap melting in the model of Lytvynyuk

Lytvynyuk developed in [8,84–86], a Matlab$^{®}$ coded LD process model, which connects thermodynamics and kinetics through the coupled reaction theory published by Ohguchi et al in [10]. Besides the reaction model, a variety of sub-routines describe both thermodynamics and kinetics of the involved phases and the melting and dissolution behaviour of the charged

materials. [8,85] The model was improved by Bundschuh in [9,87] through a new approach of the interaction area between the slag and the hot metal. Additionally, temperature and chemical composition-dependent enthalpy and heat capacity functions were implemented. A description of Lytvynyuk´s and Bundschuh´s LD process model was published in [85] and in Publication 3 in the attachment [88]. The global LD process model is based on a main iteration loop including the computation of the global heat and mass balances of the system. Each considered component in the slag, metal and gas phase is changed as a result of the simultaneous chemical oxidation-reduction reactions. Additionally, the consumption of the blown oxygen as well as the heating and melting of the charged materials are considered by the global mass balance, given in Equation 3.1. [8,85]

$$\frac{d\Psi_i}{dt} = \frac{d\Psi_i^{CR}}{dt} + \frac{d\Psi_i^{OC}}{dt} + \sum_{j=i}^{K}\frac{d\Psi_i^{Diss}}{dt} + \sum_{z=i}^{L}\frac{d\Psi_i^{Melt}}{dt} \qquad \text{Eq. 3.1}$$

In Equation 3.1 Ψ defines the mass of a component i in [kg]. The chemical reaction, oxygen consumption, dissolution and melting are indicated with the superscripts CR, OC, Diss and Melt, respectively. The number of charged materials, which are considered to be dissolved and which will melt are defined with K and L, respectively. [85] The chemical reactions of the oxidation-reduction equations resulting in the generation of heat, are included to the global heat balance and are listed in Publication 3 in the attachment. [88] The calculation of the global heat balance considers, besides the generated heat also the heat consumption. The heat consumption is the sum of sensible and latent heats required for the heating, dissolution and melting of charged materials as well as the heat fluxes of the off-gas including dusts and the losses through radiation, evaporation of H_2O, carbonate decomposition and the converter lining. The difference of the generated and consumed heats, Q^{HG} and Q^{HC}, respectively, will result in the total heat Q^{Tot} in [J] and is described through Equation 3.2. It is assumed that the temperature of the slag and the melt are identical and with the use of the total heat, the temperature change of the melt during an iteration step is described through Equation 3.3. [85]

$$\frac{dQ^{Tot}}{dt} = \frac{dQ^{HG}}{dt} - \frac{dQ^{HC}}{dt} \qquad \text{Eq. 3.2}$$

$$\frac{dT}{dt} = \frac{1}{(c_{p,Melt} * m_{Melt} + c_{p,slag} * m_{slag})} * \frac{dQ^{Tot}}{dt} \qquad \text{Eq. 3.3}$$

In Equation 3.3 the masses of the slag and the melt are defined as m_{Slag} and m_{Melt}, respectively, in [kg]. The specific heat capacities of the slag and the melt are $c_{p,Slag}$ and $c_{p,Melt}$, respectively, in [J/kgK]. [8,85] To receive the values for the global heat and mass balances, several sub-routines are implemented to the global process model, one of which is the scrap

melting and dissolution behaviour. The sub-routine is divided into two melting phenomena; the forced scrap melting and diffusive scrap melting. The transition point between these two approaches is the scrap melting point, which is considered to be the liquidus point of the scrap composition. [19,88–90]

The forced scrap melting is described through the formulation published by Medzhibozhskiy in [15], given in Equation 3.4, which is valid when the melt temperature exceeds the melt point of the scrap. [85]

$$-\frac{dr}{dt} = h_{melt} * \frac{T_{HM} - T_{liq}}{(L + (H(T_{scr}) - H(T_{liq}))) * \rho_{scr}}$$ Eq. 3.4

The ablation rate during forced scrap melting $\left(\frac{dr}{dt}\right)$ is thereby dependent on the heat transfer coefficient in the metal phase h_{melt} in [W/m²K], the temperature difference between the hot metal T_{HM} and the the liquidus temperature of the scrap T_{liq} in [K] as well as the specific enthalpy difference between the scrap at the present temperature of the scrap surface $H(T_{scr})$ and the enthalpy at the scrap melting point $H(T_{liq})$ in [J/K]. Further, ρ_{scr} is the density of the scrap in [kg/m³] and L is the latent heat in [J/kg]. [15,19,85,89,90]

The diffusive scrap melting is described through the approach published by Zhang and Oeters in [71], given in Equation 3.5 and which is used below the scrap melting point. Equation 3.5 is valid only with the assumption that the densities of the scrap and the hot metal are equal. [3,71,88]

$$-\frac{\partial r}{\partial t} = k_{melt} * ln\left(\frac{\%C_{liq} - \%C_{HM}}{\%C_{scr} - \%C_{liq}} + 1\right) = k_{melt} * ln\left(\frac{\%C_{scr} - \%C_{HM}}{\%C_{scr} - \%C_{liq}}\right)$$ Eq. 3.5

The ablation rate during the diffusive scrap melting is dependent on the mass transfer coefficient k_{melt} in [m/s] and the carbon concentration differences between the scrap ($\%C_{scr}$) and the hot metal ($\%C_{HM}$) as well as the scrap and the carbon concentrations on the liquidus line at the actual melt temperature $\left(\%C_{liq}\right)$. The carbon concentrations are in [wt.-%] in the given approach. [71,85,88]

In [19], Penz et al. showed that with the mentioned approaches as well as special chemical compositions of the bulk concentrations of the scrap and the hot metal, an increase of solid scrap mass can occur in the middle of the blowing process. This phenomenon is achieved through a negative logarithmic term of the diffusive scrap melting model published by Zhang and Oeters given in Equation 3.5. If the equilibrium is reached in diffusion controlled processes, the diffusion process itself will stop. In the case of the special configurations of the bulk concentrations for the scrap and the hot metal by Penz et al. in [19] using Zhang and Oeters´

model, the process will not stop when the thermodynamic equilibrium is reached. Due to this reasons, the sudden increase of the scrap radius is suppressed by the mathematical definition that the ablation rate will be zero. [19] The attached Publication 3 as well as the conference articles, published within the framework of this thesis, by Penz et al. in [19,89,90] evaluate the influences of the several scrap parameters, e.g. geometry, shape and chemical composition of Lytvynyuk´s model. The conference article by Penz et al. in [19] presents the effect of varying scrap compositions on the final crude steel composition after a defined blowing period, including the stagnation approach of scrap melting as described previously.

3.2 Approaches for steel scrap melting in process models

The utilization of a scrap melting sub-routine in overall LD process models is partly described in Publication 1 in the attachment. The initial approaches of the scrap melting within the framework of further comprehensive LD process models besides Lytvynyuk´s model are summarized in the following lines.

Chigwedu presented in [91] a dynamic process model with strong simplifications of the real LD process. The focus in Chigwedu´s work is situated on the scientific description of the oxidation of the tramp elements and the energy generation through their chemical reaction as well as the heat removal through the scrap dissolution. A parameter study about the advantages of an increased oxygen amount points out the critical process conditions with the aim of a more transparent fundamental understanding of the LD converter process. The proportion of a calculated driving force of an oxidation reaction on the total driving force results in the distribution of oxygen for the reactions. [91] The scrap dissolution is described by heat and mass transfer coefficients evaluated through Nusselt and Sherwood correlations of estimated incident flow conditions based on the research activities in [13,28,92–97].

A global dynamic LD process model was developed and published by Dogan et al. in [98–101] as a predictive tool for industrial application to gain a better understanding of the process. An advantage of the process model is the possibility to compare the decarburization rates in different reaction zones. [98,99] The main focus of the model from Dogan et al. lies in the emulsification using the bloated droplet theory in predicting the interaction area between the droplet and the slag in accordance with the droplet residence time. [99,100,102] amongst other process variables, also the scrap melting and composition was outlined to influence the decarburization. A disadvantage of the model is that the heat balance of the process is not considered and no FeO prediction model is employed. The kinetic model of Sethi et al. [20]

was implemented to describe the scrap melting model, which is based on an analytical solution technique using the industrial data of Asai and Muchi in [103]. The SciLab®-based source code used by Dogan, as well as the flow sheet are published in [98]. The Fourier series-based model of Sethi et al. and its derivations are summarized in Publication 1 of the attachment. [3] Dogan mentioned in [98] that the heat transfer has to be estimated through experimental studies and dimensionless analysis approaches. Dogan calculated the scrap melting as a function of the temperature, particle size and linked it to the global model to define the overall mass balance. [98] The model of Dogan et al. was improved by Rout et al. in [104–106] by employing the concept of multi-zone kinetics and focussing on the rate equation of decarburization and manganese removal. No further changes of the scrap melting sub-routine were carried out by Rout et al. in [104–106].

Schöne developed in [107] a dynamic LD converter model, which includes the pre-blowing period (charging), main blowing period and the post blowing period. The scrap melting is divided into diffusive and forced scrap melting as it is applied also in the model of Lytvynyuk and Bundschuh, described in the attached Publication 3 and [8,9,85]. Schöne modelled the heating of the scrap numerically by the finite-difference method and considers shell freezing and its melting. The same numerical approach is used to calculate the ablation rate of planar scrap particles during the diffusive scrap melting period. The diffusive and forced melting approaches are coupled. The transition between them is executed when the melting velocity of the forced scrap melting is more negative than the melting velocity of the diffusive scrap melting. [107]

Kruskopf developed in [108] new algorithms and numerical methods to simulate a gas/liquid two-phase flow, scrap melting and chemical reactions between multiple phases. These approaches are divided into three independent sub-models, which should be formed to a dynamic real-time LD process model in future work. [108,109] The chemical reaction model is based on the minimisation of the Gibbs energy to compute chemical thermodynamic equilibria to determine mass transfer between the bulk phase and reaction volume. [108,110] The developed scrap melting sub-routine is a 1-dimensional model with a moving numerical grid approach. It takes into account the mass transfer of carbon and the heat transfer from the surrounding iron melt. The numerical solution of the enthalpy and carbon mass balance equations for the solid material, using composition and temperature dependent thermal conductivities and heat capacities, are the solution strategy of Kruskopf´s scrap melting model. [4,108,111]

3.3 Resume of the available information from literature

From literature it is clear that a coupled heat and mass transfer is the challenging task to describe the scrap melting and dissolution behaviour in carbon saturated melts. The review on scrap melting (Publication 1) points out that the variety of mass and heat transfer coefficients covers a wide range of reasonable values. The classical way to define mass and heat transfer coefficients involves experiments. The most common experimental setup uses cylindrical specimens, which were immerged for a certain time into liquid hot metal. Through thermocouple measurements and the exact determination of the variation of the weight of the sample, the coefficients are determinable. From the numerical point of view numerical models describing the scrap dissolution and melting behaviour are wide-spread according to the huge variety of methods. Analytical solutions to describe the scrap melting are rare in the literature. To understand the phenomenon itself and to validate the numerical solutions, the object-oriented analytical programming is indispensable. A comparison of existing process models with their scrap melting approaches are listed in the following **Table II**. The main factors of the global model structure as well as the advantages and disadvantages of the used scrap melting sub-routines should give an overview on selected available approaches. **Table II** is supplemented with the scrap melting model of the present work and the phase field model published by Li et al., which is described in Publication 1 and in [22,23,112].

Table II: Comparison of selected LD process models and and scrap melting sub-routine approaches

Name/ Literature	Global Model structure	Advantages (+) and disadvantages (-) of the scrap sub-routine	Implementation of scrap sub-routine
Lytvynyuk [8,85]	• Dynamic model with heat and mass balance • Thermodynamic and kinetic calculations • Coupled reaction theory	+ Database of binary phase diagrams - Divided in forced and diffusive melting with single transition point - No mushy zone - Constant thermal and physical parameters - No shell formation considered	Realized
Chigwedu [91]	• Static charging materials model • Dynamic model with heat and mass balance	+ Shell formation, diffusive and forced scrap melting - Heat and mass transfer through estimated incident flow conditions with Nusselt and Sherwood approximated - No mushy zone - Single transition point	Realized
Dogan [98–101]	• Decarburization model with mass balance • Bloated droplet theory for interaction area • Multi zone model • Slag formation and heat balance are not considered	+ Fourier series based analytical model developed by Sethi in [20] - Constant thermal and physical parameters - No shell formation considered	Realized
Schöne [107]	• Dynamic model with heat and mass balance • Multi period model • Empirical approaches for thermodynamic calculations	+ Coupled heat and mass transfer of carbon concentration at solid/liquid interface + Shell formation, diffusive and forced scrap melting - Time intensive explicit FDM - Constant thermal and physical parameters	Realized with additional simplifications
Kruskopf [48,108,109]	• Dynamic model with heat and mass balance • Computation of gas/liquid two-phase flow • Chemical reaction model based on Gibbs minimization	+ Coupled heat and mass transfer of carbon concentration at solid/liquid interface + Moving boundary grid + Implicit discretization method + Temperature and composition dependent thermal and physical parameters - Constant heat and mass transfer coefficients for the estimation of the interface velocity	Realized
Li et al. [22,23,112]		+ Phase field model including description of mushy zone and shell formation + Convection in the hot metal through effective heat capacity approach by [113] - Only heat transfer considered at temperatures above 1600 °C	Not implemented in a global LD process model; No connection points available for implementation
Present work		+ Coupled heat and mass transfer of carbon concentration at solid/liquid interface + Shell formation, combined diffusive and forced scrap melting + Convection in the hot metal through artificial increase of coefficients based on experimental results ± Partly temperature and composition dependent thermal and physical parameters - Time intensive explicit FVM	Not implemented in a global LD process model; Connection points to Lytvynyuk´s [8] model available

To create a new model to describe the scrap melting and dissolution behaviour, the following practical steps are considered, experimentally investigated and will be presented in the next sections:

- Experimental investigations at various temperatures, melt conditions and scrap compositions

- Evaluation of the heat transfer coefficient through an analytical heat transfer model supported by thermocouple measurements.

- Evaluation of the carbon diffusion by optical microscopy and electron microprobe analyses as well as the development of an analytical model for mass transfer.

- Development of a numerical model considering coupled heat and mass transfer

4 Experimental investigations using small-scale experiments

According to the findings in former publications, experiments with steel cylinders submerged in liquid iron-carbon melts are the most commonly used approach to determine mass and heat transfer coefficients. In the present, work a huge variety of experimental small-scale experiments was carried out and will be described in this chapter. In all experiments (unless noted otherwise), the iron-carbon melt was common industrial hot metal from voestalpine steel GmbH, Linz. The cylindrical steel samples were made from S235JR construction steel or ultra-low-carbon (ULC) steel. The experimental results were published in the attached Publications 2, 4, 5 and 6. Publication 2 describes thermocouple measurements for the determination of heat transfer coefficients, which will be executed in Chapter 5. In Publication 4, the results of the mass transfer coefficients determined in the experimental investigations with S235JR construction steel are summarized; in Publication 5, the results of the ULC steel investigations are outlined. The phenomenological investigation at the solid-liquid interface through electron microprobe analysis is published in Publication 6.

4.1 Apparatus and procedure

The experimental setup employed is outlined in the attached Publications 2,4,5 and 6.

The procedure of the small-scale experiments carried out in the present work are outlined in the attached Publications 2,4,5 and 6.

4.2 Temperature measurements for further investigations on the heat transfer coefficient

To determine the heat transfer coefficient, the cylindrical specimens were equipped with thermocouples, as described in Publication 2 in the attachment. [37]. To guarantee the accuracy of the measurements and the experimental setup, three independent measurements of the sample core temperature were carried out at each initial temperature of the hot metal, which were 1305 °C, 1370 °C and 1450 °C (unless noted otherwise in the publications). The sample was immersed into the liquid hot metal at room temperature (25 °C). As an example the evolution of the measured core temperature of the sample submerged into hot metal with an initial temperature of 1370 °C can be derived from **Figure 9**. It is obvious that after a certain time, an equilibrium temperature between the scrap core and the hot metal will occur. The equilibria temperatures for the three initial temperatures are 1230 °C, 1300 °C and 1385 °C, respectively. The three measurements in **Figure 9** show that the temperature measurements are reproducible.
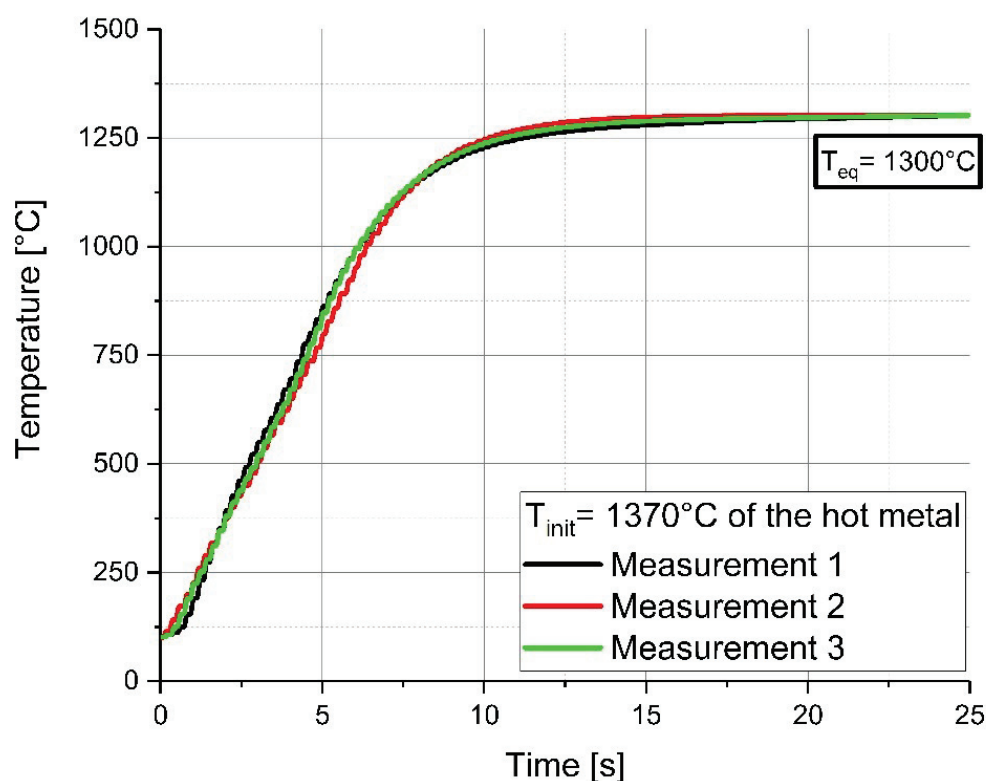
Figure 9: Time-dependent evolution of the measured temperature in the centre of the cylinder with an initial hot metal temperature of 1370 °C

The equilibrium temperature is approximately 70 °C below the initial temperature of the hot metal and this difference is the same – including the measurement tolerance of the Type S thermocouple – for all three starting temperatures. **Figure 10** shows that a specific percentage of the equilibrium temperature will be reached after less than 20 s immersion time. Furthermore, the achievement of the equilibrium temperature decreases in time with increasing temperature. **Figure 10** also includes the information on the analytic model and the numerical approach describing the heat transfer, which is published in Publication 2. [37]. Both calculation methods are consistent with the experimental measurements.
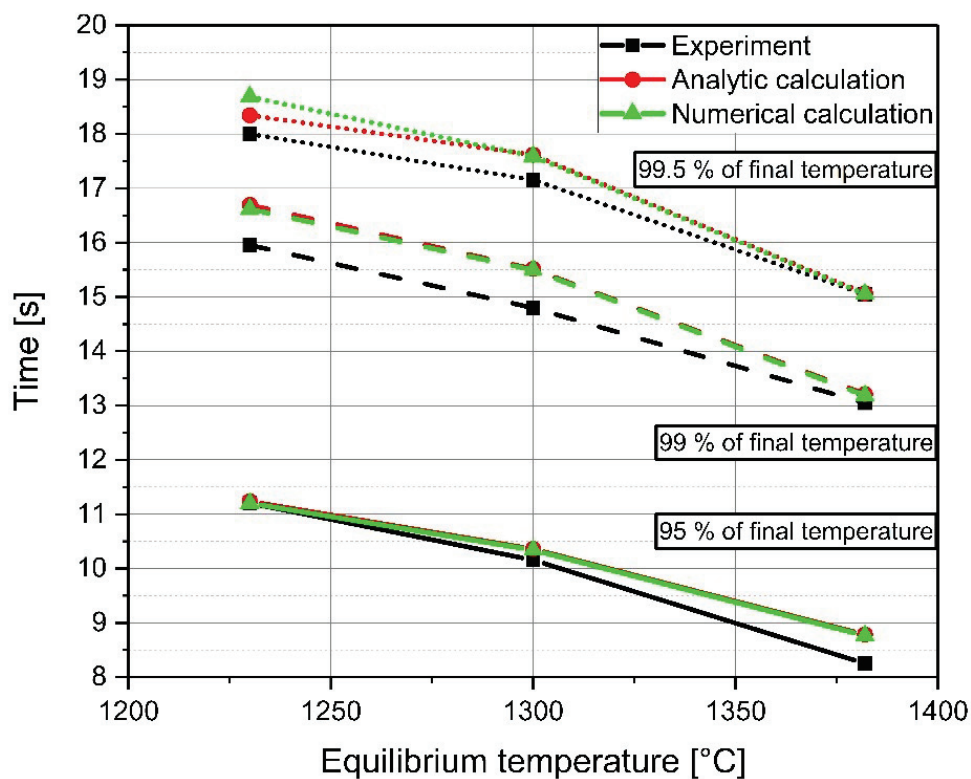
Figure 10: Elapsed time to reach the temperature equilibrium between scrap core and liquid hot metal

The findings of this approach are closely linked to the descriptions regarding a shell formation, like those published in [22,23,71,95,97,112]. Until the equilibrium temperature is reached, a coupled heat and mass transfer influences the freezing and melting of a shell on the surface of the mother scrap.

4.3 Results of the dissolution test

To determine the mass transfer coefficient of S235JR construction steel and ULC steel, cylindrical specimens were submerged for 10, 20, 30, 60, 120, 180 and 240 s into liquid hot metal, which was under stagnant or turbulent conditions. Due to the fact that completely stagnant melt conditions are not reachable it has to be mentioned that natural convection is always influencing the system. The results of the small-scale experiments were published in the attached Publications 4 and 5 and will be completed with the findings of additional tests in this chapter.

4.3.1 The dissolution behaviour of S235JR construction steel in hot metal

The experiments describing the evaluation of the mass transfer coefficient of S235JR submerged in carbon-saturated hot metal are put out in Publication 4 in the attachment. [114].

Under stagnant conditions, additional tests were carried out with an immersion time of 2.5, 5 and 7.5 s. The radius of the scrap cylinder after a certain immersion time (r(t)) is defined by the mass loss of the sample. The ablation rate (dr/dt) is approximated by the Lagrange polynomial of the second order, as described in Publication 4 [114]. Immediately after the immersion of the cylindrical specimen in the hot metal, shell freezing occurs, as shown in **Figure 11**. This finding is a result of the coupled heat and mass transfer. The shell formation and its melting is a result of the heat transfer and heating of the cold scrap until the equilibrium temperature is reached.
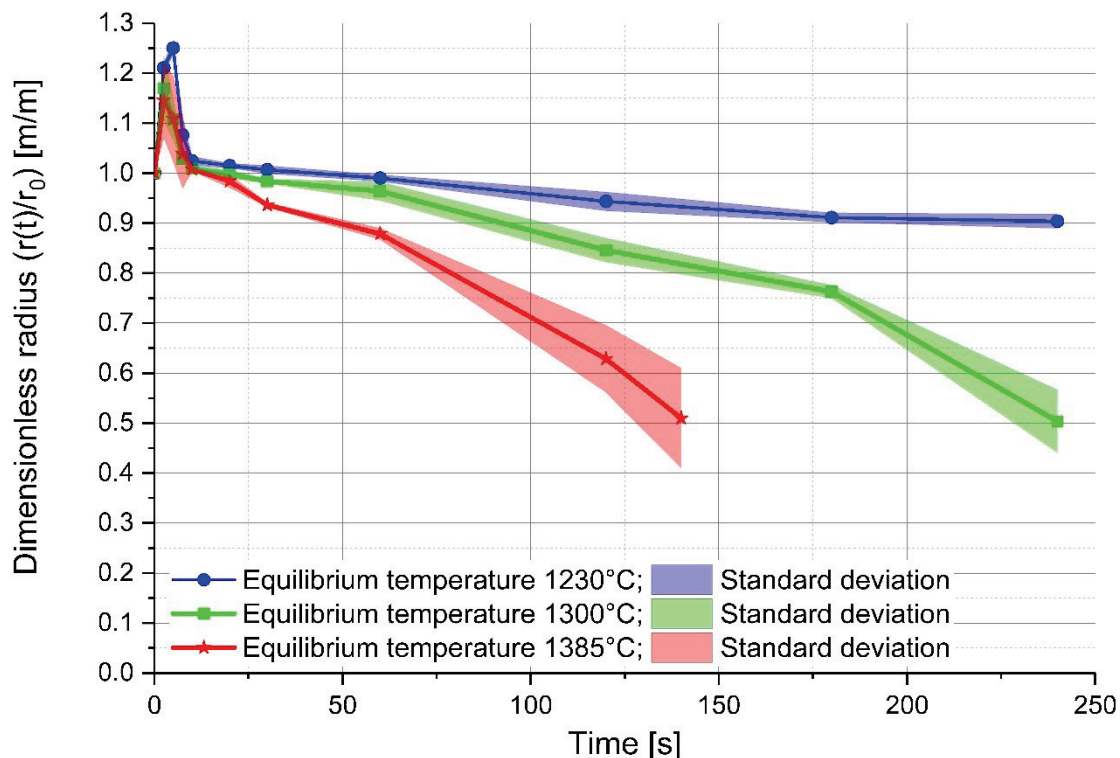
Figure 11: Dimensionless radius of the experiment in stagnant hot metal [114,115]

After reaching the equilibrium temperature, the determined mass transfer coefficients and ablation rates of the experiments show a constant evolution. The mass transfer coefficients, which are published in Publication 4 [114], were determined by the experimental ablation rate by using the diffusive scrap melting approach published by Zhang and Oeters in [71], given in Equation 3.5. For turbulent melt conditions the progress of the time dependent radius is steeper in comparison to the stagnant conditions shown in **Figure 11**. From the comparison of the investigated bath conditions in Publication 4 [114] it has to be mentioned, that the mass transfer is strongly dependent on the temperature and the conditions of the melt, which means that turbulent conditions result in higher mass transfer coefficients. The figure for turbulent bath conditions is published in Publication 4 in the attachment. The determined ablation rates and the ranges of the mass transfer coefficients under isothermal stagnant or turbulent bath conditions are given in **Table III**.

Table III: Range of the calculated ablation rate and mass transfer coefficient above 20 seconds dissolution time [114]

Equilibrium temperature [°C]	1230	1230	1300	1300	1385	1385
Experimental condition	stagnant	turbulent	stagnant	turbulent	stagnant	turbulent
Ablation rate [(m/s)x10^{-6}]	-1.98 ~ -5.30	-4.68 ~ -7.19	-7.5 ~ -12.9	-12.1 ~ -16.7	-14.6 ~ -27.7	-30.4 ~ -39.7
Mass transfer coefficient [(m/s)x10^{-6}]	7.39 ~ 20.4	18.5 ~ 27.0	16.1 ~ 26.8	25.5 ~ 36.5	18.2 ~ 31.1	33.7 ~ 44.4

4.3.2 The dissolution behaviour of ULC steel in iron carbon melts

The experiments and outcomes explaining the evaluation of the mass transfer coefficient of ULC steel submerged in carbon saturated hot metal as well as hot metal containing 1 wt.-% carbon are published in Publication 5 in the attachment. [116] The experiments described in [116] are based on the knowledge that the carbon content in the melt decreases and the temperature increases in line with the exothermic reactions during the blowing period in an LD converter.

The main finding that the mass transfer coefficient increases with increasing temperature is comparable to the dissolution experiments of the previous chapter.

In the parameter study published in the course of this project in [19], which used Lytvynyuk´s process model from [8], it was shown that the utilization of the diffusive scrap melting approach published by Zhang and Oeters in [71], given in Equation 3.5, can lead to a negative logarithmic term. This incident will result in a positive algebraic sign of the ablation rate, which is equate to an increase in the scrap radius. With the support of the experiments of Publication 5, a high melting rate of ULC scrap in hot metal, containing 1 wt.-% of carbon just above the liquidus line is demonstrated. If the temperature drops below the liquidus line, the mass transfer will not turn into an abrupt negative mass transfer coefficient. [116]

4.4 Phenomenological investigation at the solid-liquid interface

From the literature and the fundamental phenomenological understanding, found in Publication 1, it is known that scrap melting is strongly influenced by the diffusion of the dissolved carbon in the hot metal into the solid steel. [3] A systematic investigation with optical microscopy of the longitudinal area in the symmetrical axis of the cylindrical samples and selected magnified sections on the solid-liquid interface showed the diffusion of carbon qualitatively. Quantification is only possible with the help of electron microprobe analysis (EMPA), which was carried out in the certified and accredited laboratory of voestalpine Forschungsservicegesellschaft Donawitz GmbH/Section Material Analytics.

4.4.1 EMPA investigation of the construction steel samples

The sample preparation and the results of the optical microscope analysis and EMPA of the S235JR construction steel samples are published in Publication 6 [115] in the attachment.

The theoretical mass balance at the solid-liquid interface for the diffusive scrap melting approach by Zhang and Oeters, given in Equation 3.5, is defined in Equation 4.1. The balance is based on the equilibrium binary Fe-Fe₃C phase diagram given in **Figure 4**, where C_{liq}^* and C_{sol}^* define the carbon concentrations at the liquidus and solidus lines at a specific temperature, respectively. The carbon concentrations of the bulk materials are C_{HM} for the hot metal and C_{scr} for the scrap, which is needed for the surface gradient given in Equation 4.2. The densities of the hot metal and the scrap are ρ_{HM} and ρ_{scr}, respectively, and D is the diffusion coefficient. With the assumed ambient carbon concentration in the hot metal, the melting rate (v) was stated to be constant as shown in Equation 4.3. [71,115,117]

$$k_{met}' * \rho_{HM} * \left(C_{HM} - C_{liq}^*\right) = -\rho_{scr} * D * \frac{dC}{dx}_{|x=r(x,t)} - \rho_{HM} * \left(C_{liq}^* - C_{sol}^*\right)\frac{dr(x,t)}{dt} \qquad \text{Eq. 4.1}$$

$$\frac{dC}{dx}_{|x=r(x,t)} = -(C_{sol}^* - C_{scr})\frac{v}{D} \qquad \text{Eq. 4.2}$$

$$v = -\frac{dx}{dt} = -\frac{dr(x,t)}{dt} = const. \qquad \text{Eq. 4.3}$$

$$f(\xi) = \xi/\left(1 - e^{-\xi}\right) \qquad \text{Eq. 4.4}$$

The two boundary conditions are defined to be for the carbon concentration in the center of the scrap $C(r = 0) = C_{scr}$ and the carbon concentration in the hot metal far away of the boundary surface $C(r = \infty) = C_{HM}$. The mass transfer coefficient k_{met}' of Equation 4.1 is

connected to k_{met} by the approach published by Zhang and Oeters in [71], which is given by the mathematical relationship in Equation 4.4. In Equation 4.4, the dimensionless value ξ expresses the ratio of the velocity of the boundary movement to the mass transfer [71]. With the assumed constant melting rate, the mentioned boundary conditions, the definition that $\rho_{HM} = \rho_{scr}$ and Zhang and Oeters' mathematical relationship in Equation 4.4, the diffusive melting approach of Equation 3.5 is approximated. The mathematical derivation of this procedure is in detailed shown by Jeschar and Specht in [117] and Publication 6 in the attachment. [115,117] As already mentioned in Chapter 3.1 the diffusive scrap melting model of Equation 3.5 will not stop when the thermodynamic equilibrium is reached. This will result mathematically in an increase of the scrap radius during the blowing process due to the negative logarithmic term of Equation 3.5.

It is shown in Publication 6 that the carbon composition at the solid-liquid interface differs significantly, as the previous theory predicts, which is highlighted as example in **Figure 12**. The carbon content on the solid side of the interface ($C_{interface}$) is the same as on the hot metal side, where a steep concentration gradient to the hot metal carbon content exists (see **Figure 12**). The interface carbon concentration is situated between the carbon concentration on the liquidus (C_{liq}^*) and the solidus line (C_{sol}^*). Based on these results, the mass balance of the diffusive scrap melting approach of Equation 4.1 is amended to Equation 4.5 with the definition $C_{liq}^* > C_{interface} \geq C_{sol}^*$. [115]

$$k'_{met} * \rho_{HM} * \left(C_{HM} - C_{interface} \right) = -\rho_{scr} * D_s * \frac{dC}{dx}_{|x=r(x,t)} \qquad \text{Eq. 4.5}$$

$$\frac{dC}{dx}_{|x=r(x,t)} = -\left(C_{interface} - C_{scr} \right) \frac{v}{D_s} \qquad \text{Eq. 4.6}$$

$$-\frac{dr}{dt} = k_{met} * ln\left(\left(\frac{\left(\%C_{HM} - \%C_{interface} \right) * \rho_{HM}}{\left(\%C_{interface} - \%C_{scr} \right) * \rho_{scr}} \right) + 1 \right) \qquad \text{Eq. 4.7}$$

The left side of Equation 4.5 is the carbon transport in the liquid melt with the carbon difference between the hot metal composition and the interface carbon concentration according to the results of Publication 6 and exemplarily **Figure 12**. The mass balance is closed on the right side by the expression of the carbon diffusion into the scrap using the surface gradient according to Equation 4.6. With Equation 4.6 and the mathematical relationship in Equation 4.4 the amended diffusive scrap melting formulation given in Equation 4.7 is achieved, which is valid for $C_{liq}^* > C_{interface} \geq C_{sol}^*$. The obtained diffusive model is an improvement in comparison to the previous approach of Equation 3.5 because the risk of a negative logarithmic term is diminished. Nevertheless, it has to be mentioned that the

thermodynamic equilibrium concentrations at the solid-liquid interface are actually physically inaccessible and indeterminable.

As an example for all measurements, the results of the EMPA of Sample 41 are given in **Figure 12** with the carbon and the silicon distribution of the same measurement area of 240 µm x 500 µm. Additionally, in **Figure 12**, the average amount of silicon and carbon of the 80 measurement points of an area of 3 µm x 3 µm each in y-distance is given. As published in Publication 6 and mathematically described in Equation 4.7, a steep gradient from a carbon interface content of approximately 1.5 wt.-% carbon up to the hot metal composition of more than 4 wt.-% carbon is visible. Liberated grains lead to distortions in the average carbon graph in **Figure 12**. It is obvious from the EMPA investigations that the dissolution behaviour is, aside from carbon, also influenced by silicon. In each sample, an enrichment of silicon in the solid scrap close to the interface was detected and is clearly readable from the silicon distribution and the average silicon concentration in **Figure 12**. The complete range of figures of all EMPA measurements can be found on the DVD of attachment 2.
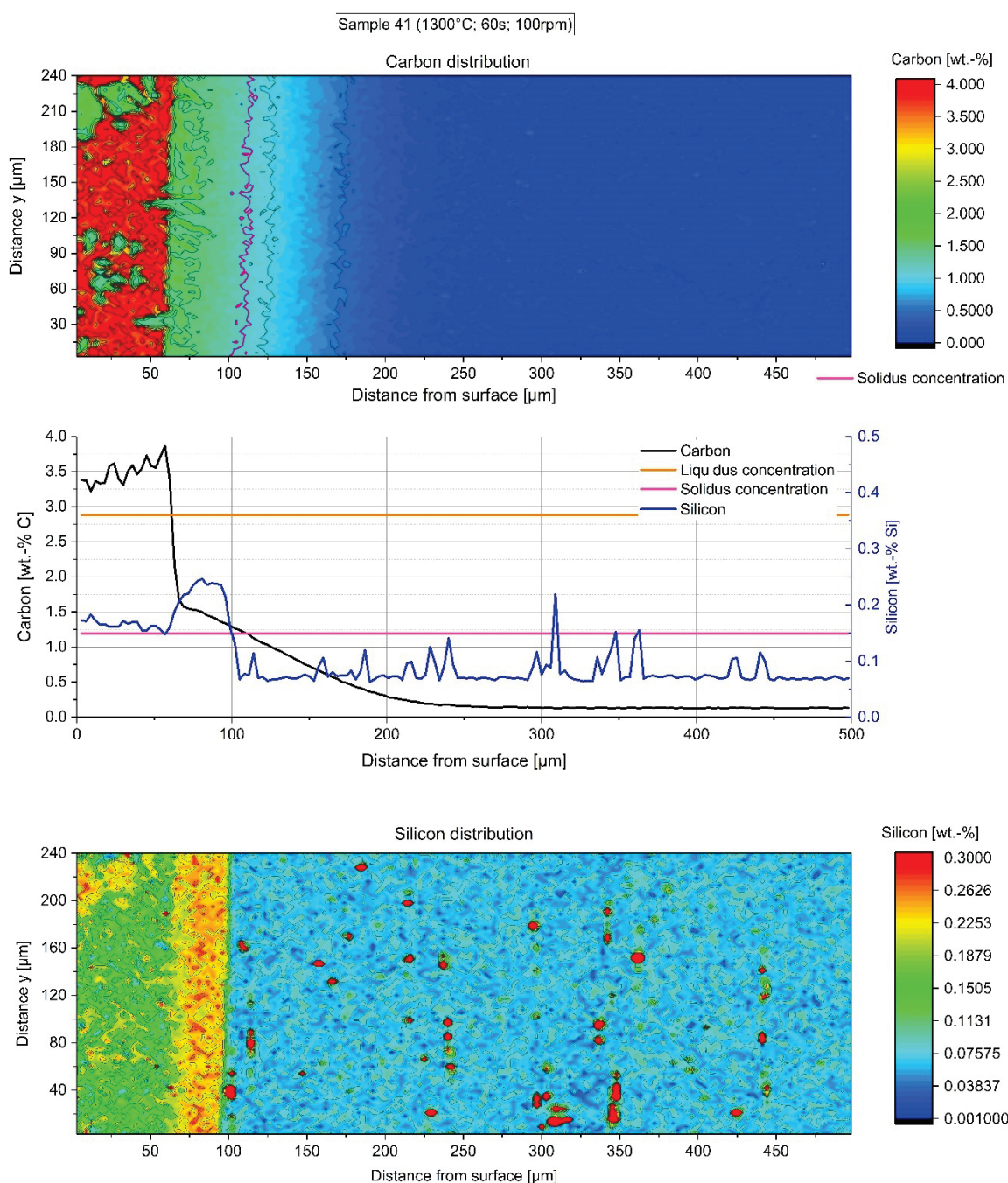
Figure 12: EMPA-measured carbon and silicon distributions of sample 41 with an immersion time of 60 s at 1300 °C equilibrium temperature; The equilibrium concentrations at the liquidus and solidus line are taken from the phase diagram in **Figure 4** at a temperature of 1300 °C;

A potentially influencing effect of the silicon amount in the layer in a shift of the phase boundaries in the equilibrium phase diagram of the scrap composition with variable carbon and silicon content can be easily neglected, as pointed out in **Figure 13**. **Figure 13** was generated by the FactSage™ FSstel database (licensed to Montanuniversität Leoben,

Department Metallurgy; Version 7.1, ©Thermfact and GTT-Technologies, Montreal, Canada and Herzogenrath, Germany).
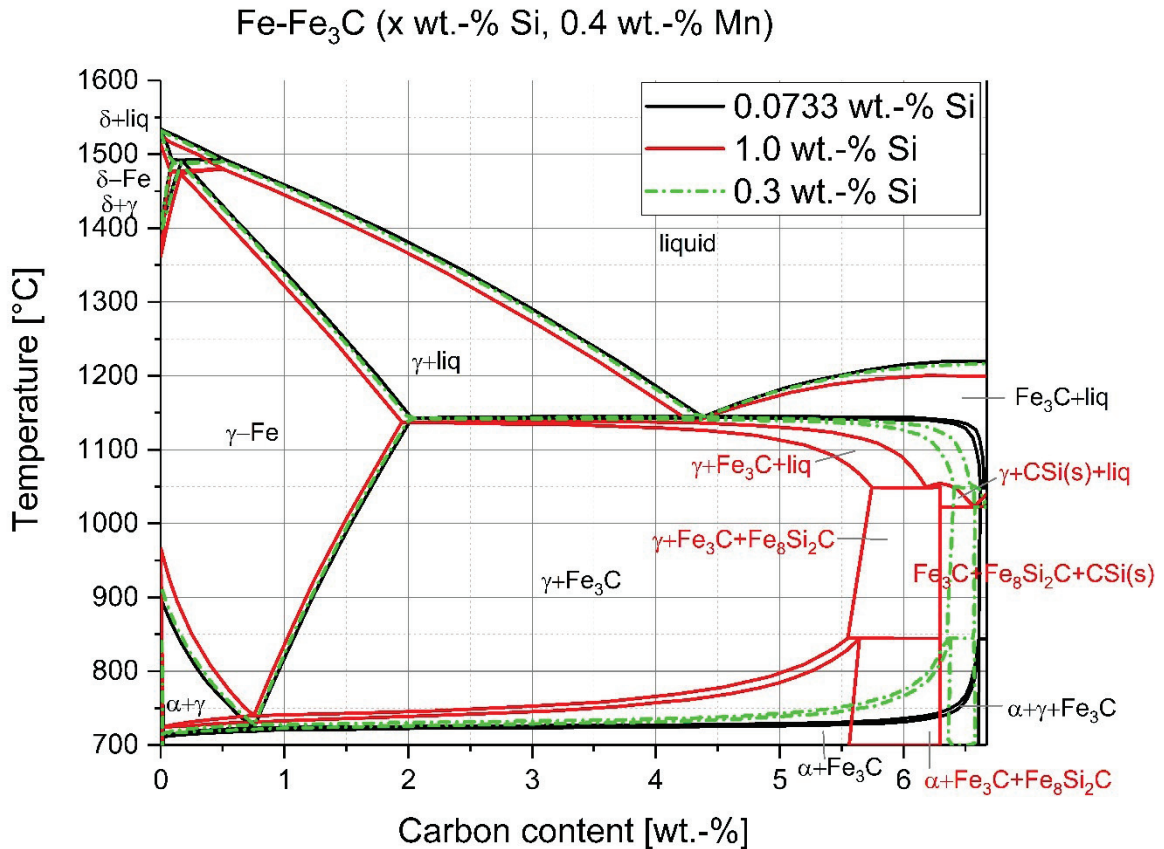
Figure 13: Fe-Fe₃C phase diagram of common S235JR construction scrap with variable carbon content and the influence of altering silicon contents

A deeper research and investigation into the appearance of the silicon layer was not executed in the framework of this thesis. The hypothesis that the solved oxygen in the hot metal diffuses into the scrap and oxidizes silicon to silicon dioxide is reasonable. A contrary effect is that the silicon dioxide is reduced through carbon, which is available in an enriched quantity. A second acceptable hypothesis is that the silicon layer is part of a primary solidified layer and a type of constitutional overheating is necessary to melt it. A third hypothesis, which has to be investigated in future, is an interaction of the activities between silicon and carbon, which results in the formation of a silicon carbide. In conclusion, it can be said that the dissolution of steel scrap in hot metal is, without a doubt, a multicomponent-diffusional process, whereby the main influencing element is carbon.

The shell freezing and melting during the first 10 s was investigated by optical microscopy and EMPA by means of the identical examination to that described in Publication 4. The

cylindrical samples were immersed in carbon-saturated hot metal for 2.5, 5 and 7.5 s at the same initial temperature as described before. **Figure 14** shows the microstructure of the Nital-etched area of sample 8, where the EMPA measurement was carried out (between the golden lines). This sample, used as an example, was submerged for 5 s in the hot metal with a starting temperature of 1450 °C. From **Figure 10** it is known that during this time, heat transfer is still the limiting factor for dissolution. Due to the temperature difference, shell freezing occurs, which is confirmed through the primary carbide on the solid scrap surface in **Figure 14** marked by the white arrow on the left side.
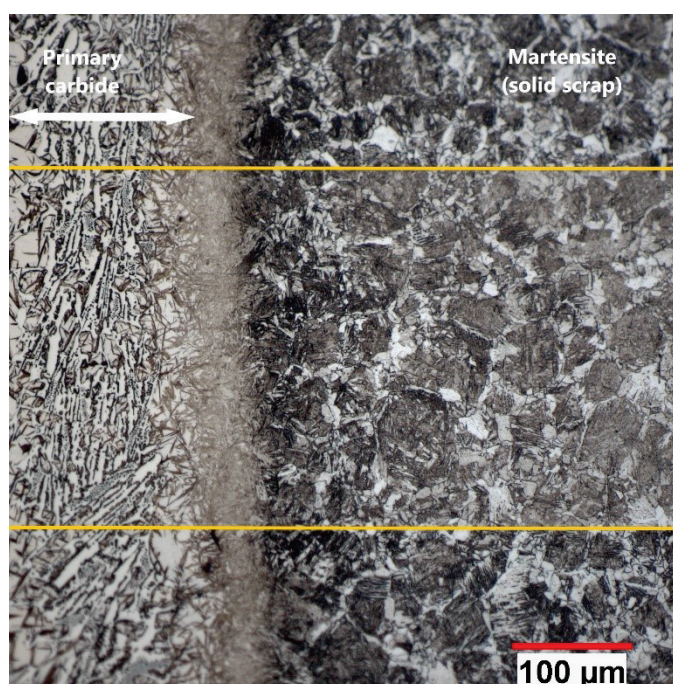
Figure 14: Section where the electron microprobe analysis (inside the golden lines) was carried out for sample 8 (5 s immersion time at 1450 °C initial temperature)

The results of EMPA measurement of the area marked in **Figure 14** is shown in **Figure 15**. It can be seen that the carbon diffusion has already resumed after 5 s, which is a result of the already present heat transfer. Due to the increasing temperature, the diffusion of carbon gets accelerated. In **Figure 16** and **Figure 17**, the increase in the diffusion depth during the initial seconds of the immersion time at initial hot metal temperatures of 1370 °C and 1450 °C, respectively, is visible. While after 2.5 s the profile of the carbon diffusion is very low it is well-developed after 7.5 s, although a frozen shell is still situated on the scrap surface. This phenomenon points out the huge importance of the utilization of a coupled heat and mass transfer for a numerical description of the scrap melting and dissolution behaviour.
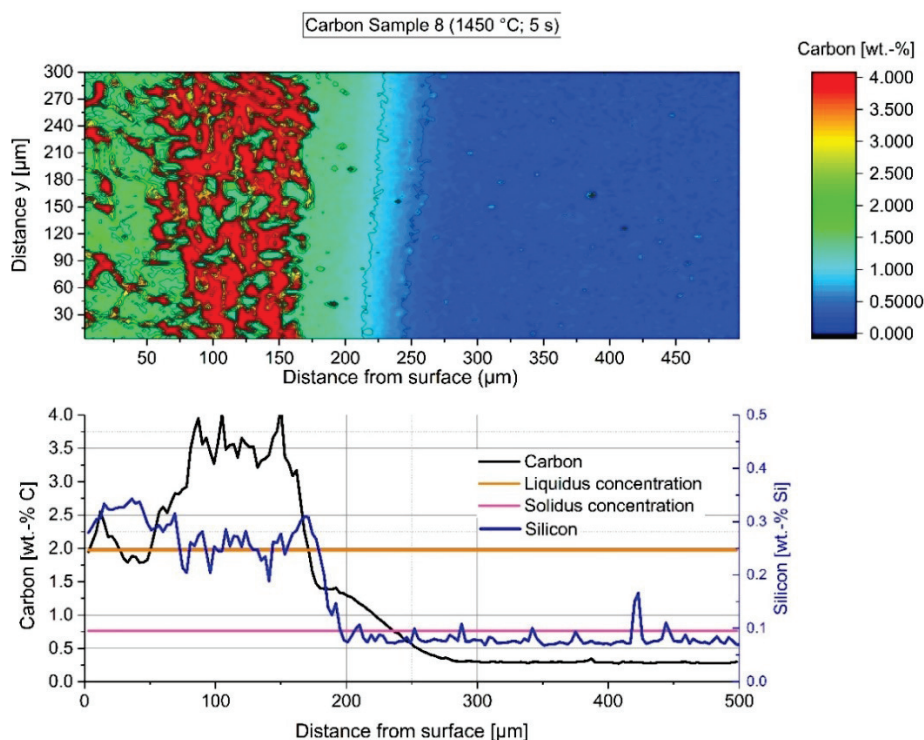
Figure 15: EMPA-measured carbon distribution of sample 8 with an immersion time of 5 s at 1450 °C initial hot metal temperature; The equilibrium concentrations at the liquidus and solidus line are taken from the phase diagram in **Figure 4** at a temperature of 1450 °C;
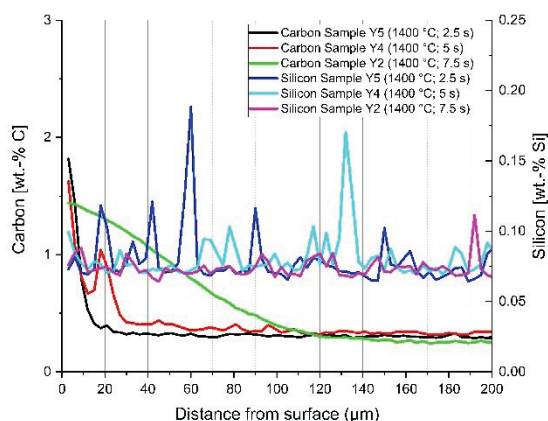
Figure 16: Average carbon and silicon composition and diffusion depth from the detected solid–liquid interface under stagnant hot metal conditions with an initial temperature of 1370 °C
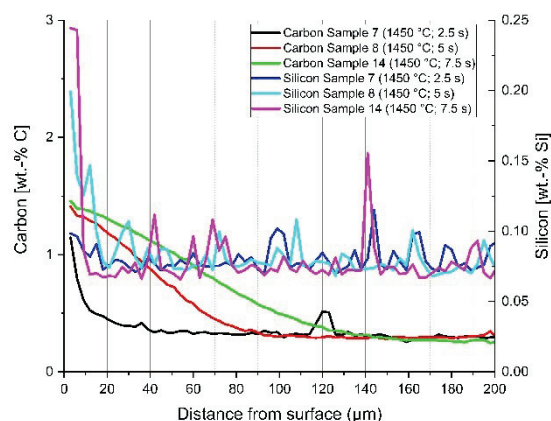
Figure 17: Average carbon and silicon composition and diffusion depth from the detected solid–liquid interface under stagnant hot metal conditions with an initial temperature of 1450 °C

The complete range of figures of all measurements associated with the present chapter can be found on the DVD of Attachment 2.

4.4.2 EMPA investigation of a scrap skull withstanding an entire converter heat

One of the main challenges in the framework of the handling and scrap charging is to avoid huge scrap pieces, which will not completely melt during the entire blowing period in a LD converter. Residues of slabs or billets in the melt are harmful and can result in damage to the oxygen or sub-lance. Sometimes pieces of scrap (scrap skulls) withstand the entire converter heat and may be found in the slag yard. In the present work, a scrap skull was prepared in the same way as the samples in the previous chapters to investigate it with the help of EMPA. The composition of the scrap skull was analyzed with the Spectromax stationary metal analyzer at the CoFM. The composition in the core of the scrap skull is given in **Table IV**.

Table IV: Chemical composition of the scrap skull

Element	Amount [wt.-%]
Carbon	0.0457
Silicon	0.295
Manganese	1.67
Phosphorus	0.011
Chromium	0.17

The colored shape image in **Figure 18** shows the carbon distribution of sample 1 of the scrap skull. The left edge (x-distance = 0) is approximately 5 µm away from the surface of the skull. The red regions are carbon-enriched perlite, embedded in a ferritic microstructure. This is documented in the same section by the Nital-etched mosaic image of the optical microscope investigations in **Figure 19**. Due to the slow cooling of the scrap skull, carbon equilibrates through diffusion in the scrap, which is comparable to the diffusion annealing process. What is of particular importance in sample 1 (**Figure 18**) is, that the heavier elements silicon, phosphorus and chromium show much lower contents at a distance of more than 750 µm from the surface than in its core. This is explainable through very low activities in the crude steel melt at the end of the blowing process. Through these activity differences, a high mobility of the above mentioned elements in the direction of the liquid melt is ensured. Additionally, the solved oxygen in the liquid crude steel diffuses into the scrap and oxidizes silicon and manganese. The resulting SiMn oxides are visible in **Figure 19** (black dots) and **Figure 20**, where the assembled shape images of Cr, Mn, Si and O of sample 7 are given.
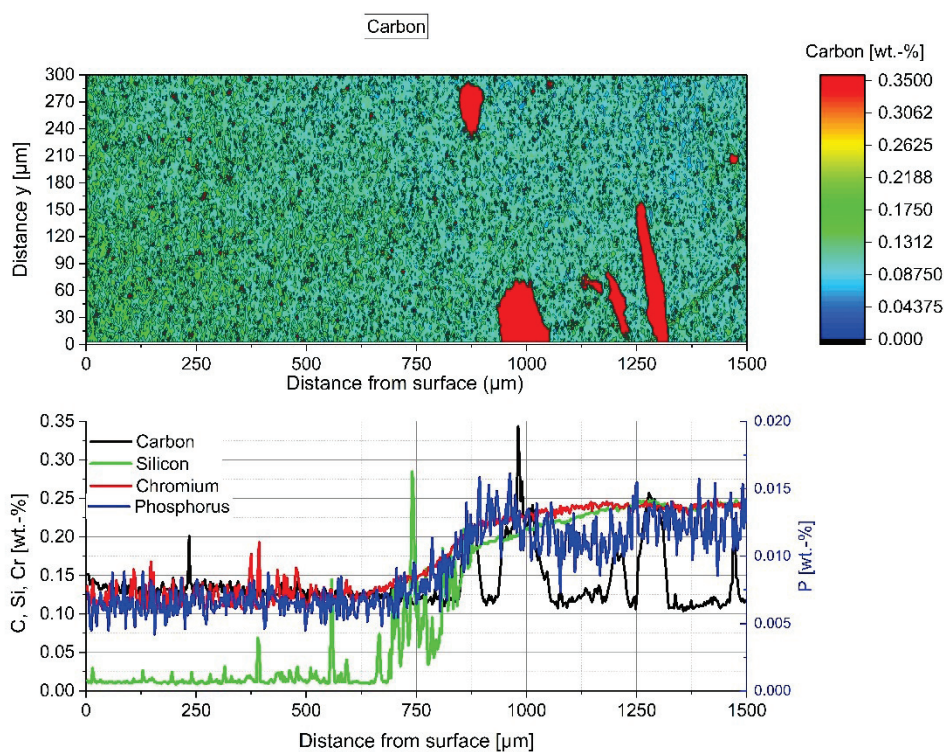
Figure 18: EMPA-measured carbon distribution of sample 1 of the scrap skull withstanding an entire converter heat
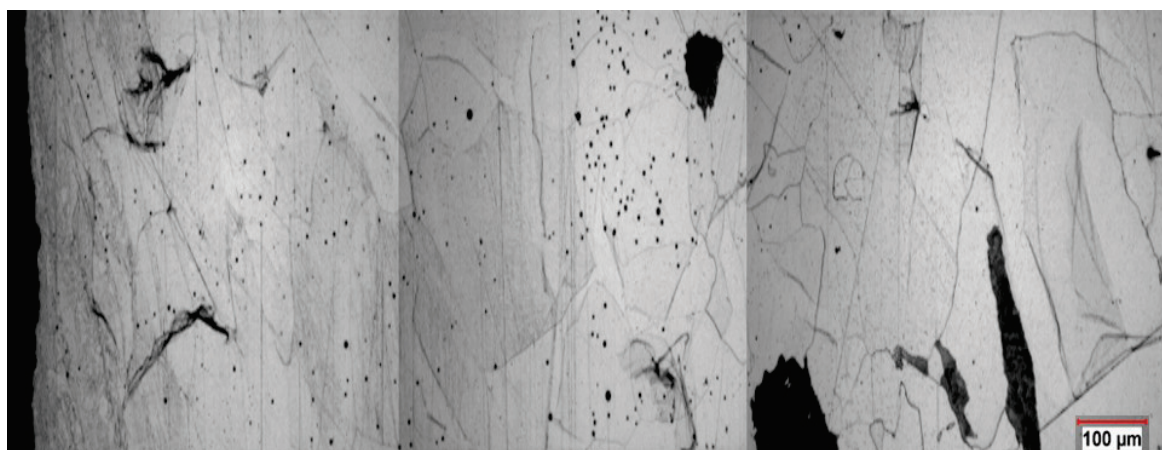
Figure 19: Nital-etched section of the EMPA investigation for sample 1 in addition to **Figure 18**

The shape images in **Figure 20** also support the hypothesis of the previous chapter that silicon is oxidized at the dissolution interface and re-reduced by increasing carbon amounts, which diffuse from the melt into the scrap. In the present system, the carbon content in the melt is very low and no diffusive process occurs. Through the diffusion of oxygen, the oxidation of silicon and manganese results in the formation of SiMn oxides, visible as small red dots in the oxygen, silicon and manganese image in **Figure 20**.
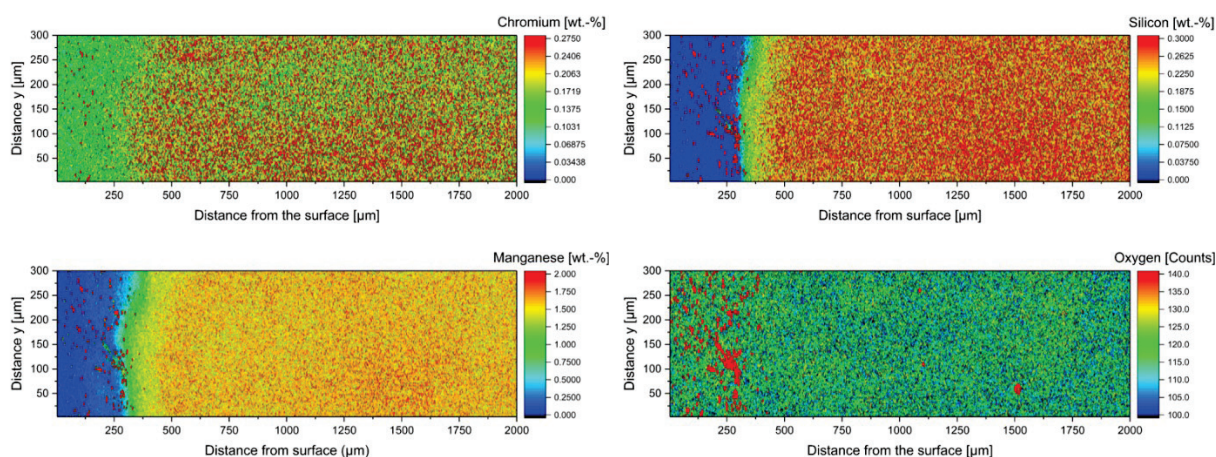
Figure 20: Comparison of the EMPA-measured Cr, Mn, Si and oxygen distribution of sample 7 of the scrap skull withstanding an entire converter heat

The irretrievable results of the mobility of big atoms like Mn, Cr and Si in the scrap underline the high complexity of the scrap-melting phenomenon. The main influencing factors describing the melting and dissolution behaviour of steel scrap in liquid iron-carbon melts are the temperature and the carbon composition. With increasing temperatures and low element activities in the melt, also the mobility of the residual elements, which are solved inside the scrap, acquire more influence. Therefore, it is of particular importance that scrap melting has to be investigated as a multicomponent diffusion problem in forthcoming studies and research. The complete range of figures of all measurements associated with the present chapter can be found on the DVD of Attachment 2.

4.5 Comparison of the modified diffusive melting equation with the existing model

In Publication 6 of the attachment, a modified approach (Equation 4.7) of the diffusive melting equation of Zhang and Oeters given in Equation 3.5, was derived. [71,115] The available Matlab®-coded LD process model by Lytvynyuk, described in Publication 3 of the attachment and Chapter 3.1, was validated by means of industrial data of the project partners voestalpine Stahl GmbH and voestalpine Stahl Donawitz GmbH by Bundschuh [9] and Lytvynyuk [8,84].

The derived new approach of the diffusive melting equation, considering only carbon diffusion, was implemented into the LD process model. Based on this adjustment, the

differences in several output parameters of the LD process model will be summarized in this chapter.

In the present chapter, the graphs with the definition "Zhang & Oeters" were calculated by means of the diffusive scrap melting approach given in Equation 3.5. The scientific findings of Publication 6 require an interface carbon composition $(C_{interface})$ in [wt.-%] according to Equation 4.7. It is assumed to be the mean value of the isothermal liquidus and solidus carbon concentration of the Fe-Fe$_3$C phase diagram in **Figure 4**. This assumption is justified due to the experimental results that $C_{interface}$ is in the range of approximately 50 % liquid fraction at the equilibrium temperatures of 1300 °C and 1385 °C. [115] Due to the prevailing melt temperatures in the LD converter of >1300 °C, the definition of $C_{interface} = C_{sol}$ can be neglected, which was found in the experiments at an equilibrium temperature of 1235 °C. [1,115] The definition of the interface carbon composition is given in Equation 4.8.

$$C_{interface}(T,t) = \frac{C_{liq}(T,t) - C_{sol}(T,t)}{2}$$

Eq. 4.8

For simplification, the required sections of the solidus and liquidus lines are fitted to polynomials of second order, which are given in **Figure 21**.
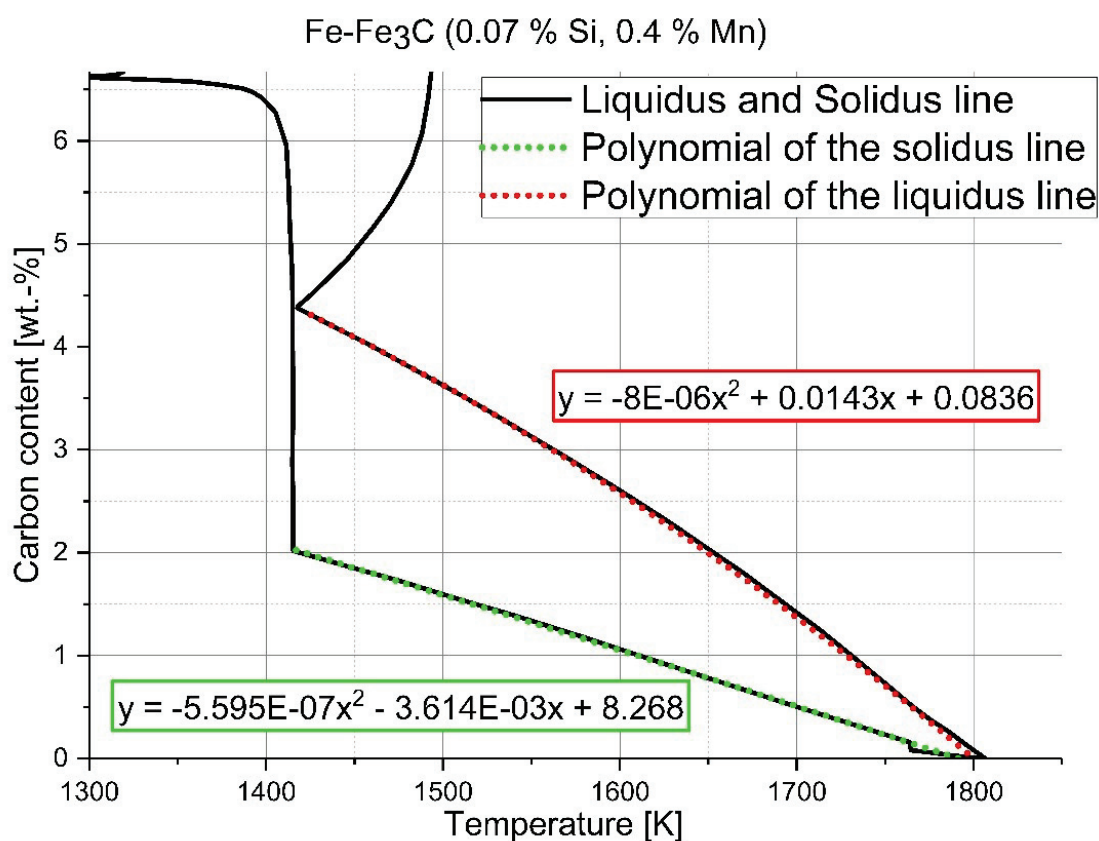
Figure 21: Polynomials for approximation of the solidus and liquidus carbon concentrations

The densities of the scrap (ρ_{scr}) and hot metal (ρ_{HM}) in Equation 4.7 are determined using the temperature and composition-dependent approach given in Equation 4.9, published by Miettinen in [79]. Zhang and Oeters´ approach assumes that $\rho_{scr} = \rho_{HM}$. [71]

$$\rho_{scr} = 7875.96 - 0.297T - 5.62 * 10^{-5}T^2 + (-206.35 + 0.00778T + 1.472 * 10^{-6}T^2) *$$
$$C_{C,scr} + 36.86 * C_{Si,scr} - 30.78 * C_{Mn,scr} \qquad \text{Eq. 4.9}$$

In the following illustrations, the influence of the aforementioned approach of the present work is compared to that of Zhang and Oeters on specific output parameters of the latest version of the LD process model developed by Lytvynyuk [8] improved by Bundschuh [9]. In total, the data sets of eight industrial heats were used. The complete range of figures of all outputs associated with the present chapter can be found on the DVD of Attachment 2.

In **Figure 22** the dissolution and melting of scrap during the entire blowing period, which is fixed at 12.6 min, is pointed out. Both approaches show between 8 and 10 a kink, which results from the change between diffusive and forced scrap melting. This is a numerical problem if a fixed point is defined as a transition between forced and diffusive scrap melting. This is amongst others a disadvantage of this concept. A smooth transition between the two melting mechanisms will occur under real process conditions because a mushy zone exists during the passage of the two-phase area. Nevertheless, the approach developed in the present work shows a more rapid and uniform melting behaviour than the previous one. The scrap will completely melt during this heat.
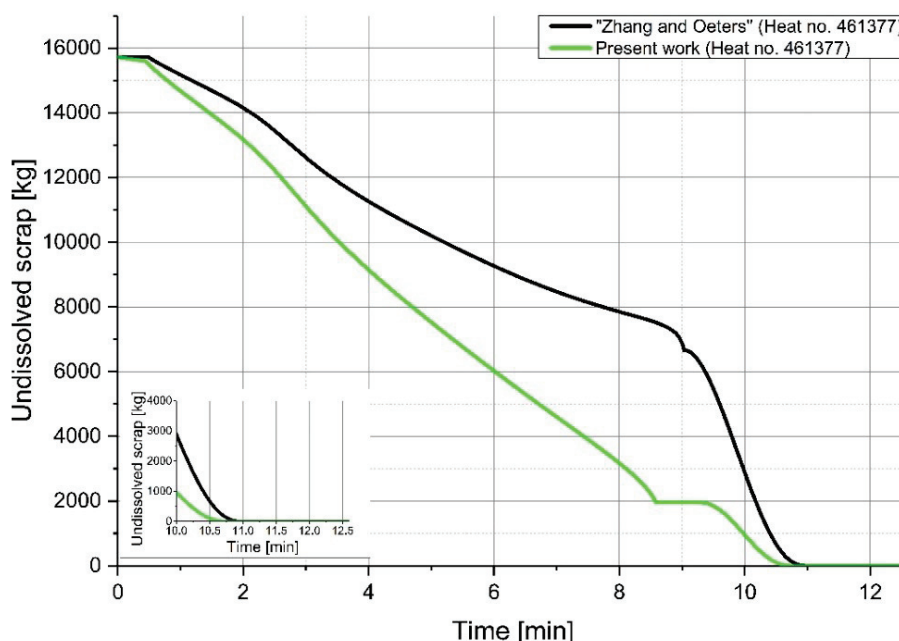
Figure 22: Influence of the diffusive melting approaches on the melting behaviour of scrap

One of the main tasks of the LD converter is the decarburization of hot metal and the simulated decarburization evolution is shown in **Figure 23**. The evolution is similar in both approaches, but slight differences in the final carbon composition are visible. The final carbon content is 9.0 % higher than with the diffusive melting approach of Zhang and Oeters (indicated as 0 %), which can be read from **Figure 24**. **Figure 24** also shows that the final carbon composition of the tapped crude steel can range from -49.6 % to 179.4 % for the investigated heats.
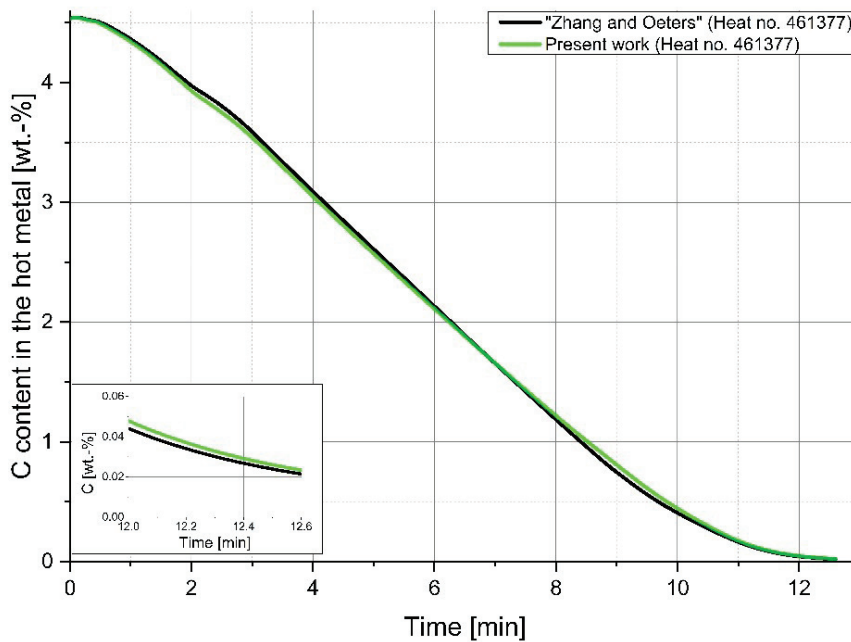
Figure 23: Influence of the diffusive melting approaches on the carbon content of the liquid steel
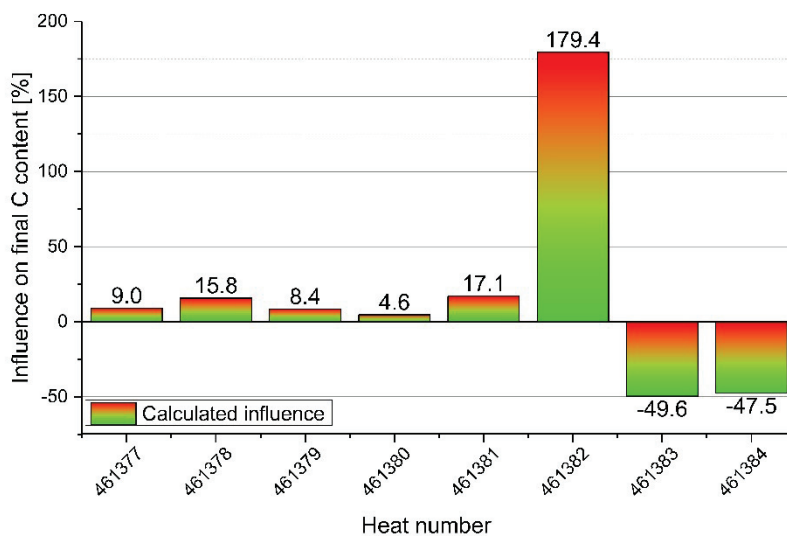
Figure 24: Percentage difference of the final carbon content between the present diffusive melting approach and Zhang and Oeters´ definition (indicated as 0 %) for all heats.

A second aim of each LD process operator is to minimize the final phosphorus content in the crude steel. The simulation shows in **Figure 25** that the trajectories of the phosphorus content in the melt are influenced during the blowing period, which is a result of the faster dissolution of the scrap and consequently the higher energy consumption needed. This means that the temperature is lowered and more time is required until the transition between the oxidation and reduction of phosphorus is reached. In the final stages of the heat, where the scrap has already melted (compare to **Figure 22**), the evolution of the dephosphorization is equalizing for the heat number shown.
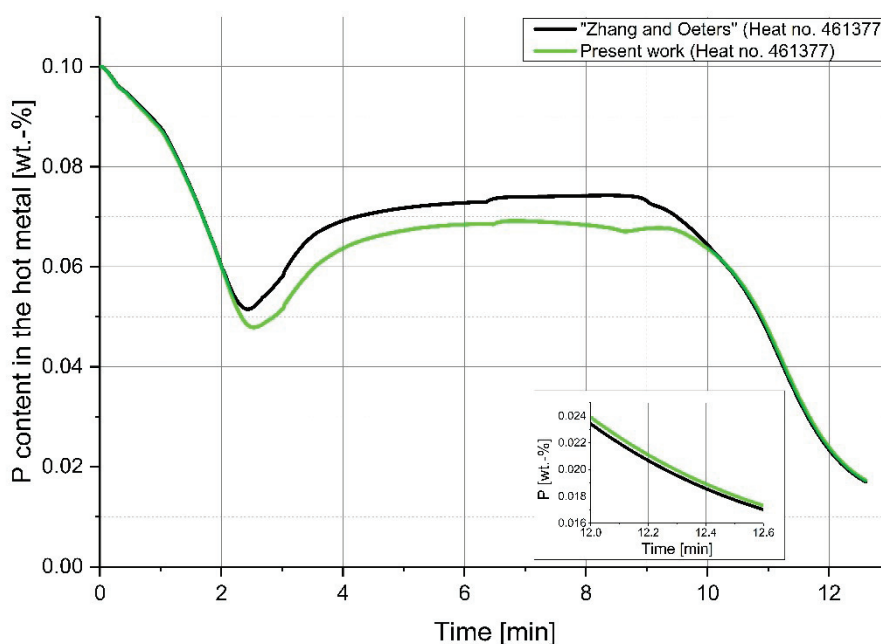
Figure 25: Influence of the diffusive melting approaches on the phosphorus content of the liquid steel

For the heat number shown in **Figure 25** the final phosphorus content is 1.7 % higher than with the approach of Zhang and Oeters (see **Figure 26**), which is indicated as 0 %. The prediction of the final phosphorus content of all heats investigated varies between -2.3 % and 104.2 %, as pointed out in **Figure 26**. Despite the close accordance of some heats, the discrepancies in the final phosphorus content are given.
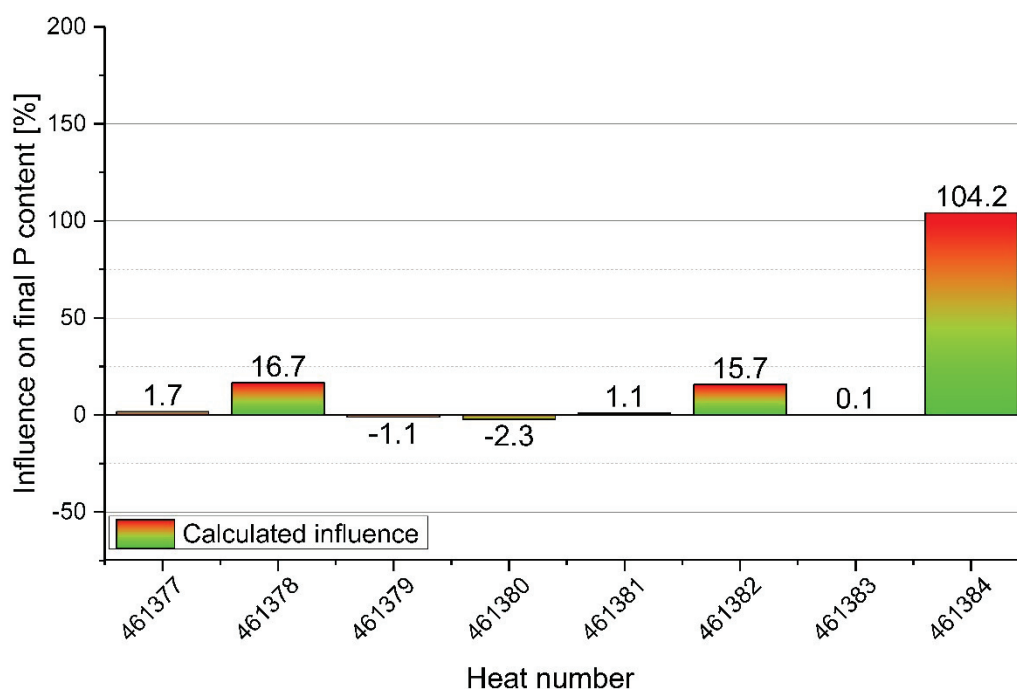
Figure 26: Percentage difference of the final phosphorus content between the present diffusive melting approach and Zhang and Oeters´ definition (indicated as 0 %) for all heats.

The utilization of the developed diffusive scrap melting approach instead of the former approach, used in the process model, shows definite discrepancies in the predicted final values. With the output of the evolution of the undissolved scrap (see **Figure 22**), the huge disadvantage of the fixed point transition definition is clearly demonstrated. The transition between the diffusive and forced scrap melting is described insufficiently. A possible solution is a coupled heat and mass transfer approach, which takes a mushy zone into account.

5 Analytic approaches for the modelling of heat and mass transfer

Analytical descriptions of the non-stationary heat and mass transfer process are common for exact solutions to one-dimensional problems. A combined analytic solution for coupled heat and mass transfer including phase change is a challenging topic. For systems where a simultaneous mass, heat and/or momentum transfer occurs in connection with a thermal or concentration gradient, it is difficult to obtain general analytical solutions. Scrap melting and dissolution is also included in this group because of all the temperature and concentration-dependent parameters, e.g. the thermal conductivity or diffusion coefficients. [25,28,30,118,119] Nevertheless, an analytical heat transfer solution with a third boundary condition, where a heat transfer coefficient between the cylindrical specimen and the environment occurs (see Equation 2.5), is a first position fixing for each numerical model. [37] The development of an analytical heat transfer model is outlined in Chapter 5.2. Mass transfer of carbon is detected, both literature and experimental based, to be the most relevant. An analytical model was developed, which neglects the moving boundary and takes into account auxiliary simplifications for a better understanding of the diffusional process during the scrap dissolution. The development of the analytical mass transfer model is described in Chapter 5.3 and is based on the literature of [39,67]. A few supporting theoretical considerations in Chapter 5.1 serve as a connecting passage.

5.1 Theoretical considerations

To develop analytical models for heat and mass transfer, the governing equations given in Equations 2.5 and 2.7a have to be solved. The calculation steps are illustrated in the following chapters.

5.1.1 Theoretical derivations for an analytical heat transfer model

The derivations and boundary conditions based on Equation 2.5 are published in Publication 2 in the attachment.

5.1.2 Theoretical derivations for an analytical mass transfer model

The results of the experimental investigations in Chapter 4.4 and Publication 6 clearly indicate that the carbon concentration in the hot metal close to the solid liquid interface is equal to the carbon concentration in the infinite environment. [115] Moreover, it is assumed that the carbon diffusion is developed under isothermal properties, so an isothermal mass transfer problem with a first boundary condition is assumed, where the surface concentration is known as shown in **Figure 27** and the Equations 5.4, 5.5 and 5.6. [30]
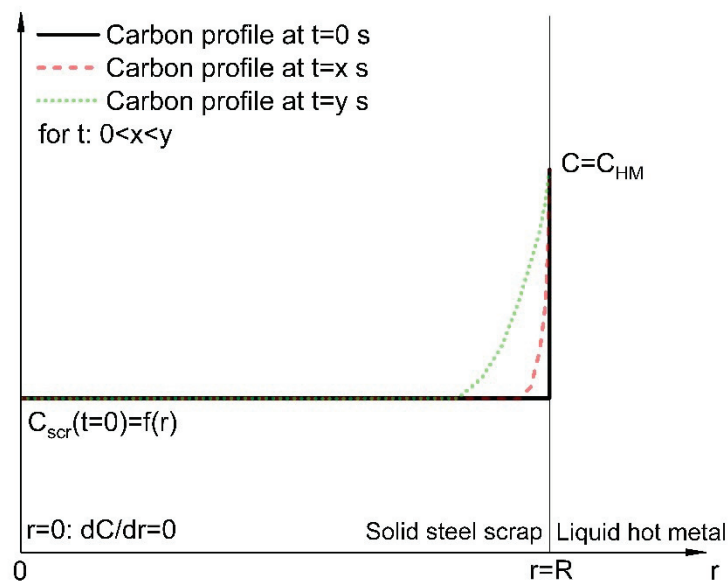
Figure 27: Schematic definition of the initial and boundary conditions for an analytical mass transfer problem with constant surface concentration

This assumption allows the utilization of a constant diffusion coefficient D estimated based on one of the three approaches given in Equations 2.33, 2.34 or 2.35. With the method of separation of the variables, a solution to Equation 2.7 is given in Equation 5.1. [67]

$$C(r,t) = u(r)\exp(-D\beta_m^2 t)$$

Eq. 5.1

In Equation 5.1, β_m is a constant and the solution provides that u satisfies

$$\frac{\partial^2 u}{\partial r^2} + \frac{1}{r}\frac{\partial u}{\partial r} + \beta^2 u = 0$$

Eq. 5.2

provided that $u(r) = 0$ and $r = 0$. The solution is a special case of the Bessel equation of order zero $\left(J_0(z)\right)$, expressed mathematically as shown in Equation 5.3. [67]

$$J_0(z) = 1 - \frac{z^2}{(1!)2^2} + \frac{z^4}{(2!)^2 2^4} - \frac{z^6}{(2!)^2 2^6} + \cdots$$

Eq. 5.3

For isothermal conditions and a cylindrical specimen of radius R, a constant surface concentration and an initial distribution $\left(f(r)\right)$ of the diffusing species is supposed, as given in Equations 5.4 and 5.5. [25,67,120]

For $0 < r < R$ $\qquad\qquad C_{scr}\ (t = 0) = f(r)$ $\qquad\qquad$ Eq. 5.4

And $r = R$ $\qquad\qquad C = C_{HM}\ (t \geq 0)$ $\qquad\qquad$ Eq. 5.5

Due to the symmetric profile of a cylinder, the following boundary condition is given [25]:

For $r = 0$ $\qquad\qquad \dfrac{dC}{dr} = 0$ $\qquad\qquad$ Eq. 5.6

the solution to the present problem is given in Equation 5.7 [67,120].

$$C(r,t) = C_{HM}\left[1 - \frac{2}{R} * \sum_{n=1}^{\infty} \frac{J_0(\beta_m r)}{\beta_m J_1(\beta_m R)} * e^{-D\beta_m^2 t}\right]$$
$$+ \left[\frac{2}{R}\sum_{n=1}^{\infty} \frac{J_0(\beta_m r)}{C_n J_1^2(\beta_m R)} * e^{-D\beta_m^2 t}\right] * \int_0^R r\, f(r) J_0(\beta_m r) * dr$$

Eq. 5.7

In Equation 5.7, the Bessel equation of first order is stated as J_1 and the constant β_m defines the positive roots of $J_0(\beta_m R) = 0$. With the assumed uniform initial concentration in the scrap (C_{scr}), defined in Equation 5.4, the following reduction of Equation 5.7 results in Equation 5.8. [67,120]

$$C(r,t) = C_{HM} - \frac{2(C_{HM} - C_{scr})}{R} * \sum_{n=1}^{\infty} \frac{J_0(\beta_m r)}{\beta_m J_1(\beta_m R)} * e^{-D\beta_m^2 t}$$

Eq. 5.8

5.2 Analytical heat transfer model

The results of the analytical heat transfer model as well as the thermal and physical properties applied are published in Publication 2 in the attachment. [37]

In Publication 2 it is shown that the numerical approach describing the one-dimensional heat transfer in a cylindrical specimen, is very close to the analytical solution of the problem in its predictions. Furthermore, Publication 2 indicates that the heat transfer coefficients determined are in the range of 4.5 kW/m² to 6.2 kW/m², which is approximately 10 times smaller than those evaluated through existing Nusselt correlations. The heat transfer coefficients worked out are in line with prior published research. The discrepancies between the analytical estimated heat transfer coefficients and the calculated ones based on Nusselt correlations are explainable through special effects of the scrap dissolution. The effects are the shell freezing and melting reported in [17,22,103,121]or air gap formations between solidified shell and the mother scrap, which are reported in [122–124]. Mentionable is also the lack of reliable information concerning the physical and thermal parameters of the liquid hot metal. [37]

A comprehensive discussion of the heat transfer coefficients was included in the framework of this work in the attached Publications 1 and 2. It demonstrated that a wide range of heat transfer coefficients is scientifically proven, making it difficult to verify their utilization and technical accuracy in the case of the LD process.

5.3 Analytical diffusion model

Based on the theoretical considerations in Chapter 5.1.2, an analytical model was developed to describe the isothermal mass transfer of carbon into a cylindrical specimen in radial direction. The temperatures used were defined to be equal to the equilibrium temperatures of the small-scale experiments detailed in Chapter 4 (1230 °C, 1300 °C and 1385 °C).

For each temperature the three diffusion coefficients were calculated from Equations 2.33, 2.34 and 2.35. The initial compositions of the scrap and hot metal are listed in **Table V**. To calculate the diffusion of carbon into the steel scrap according to the theory of Chapter 5.1.2, it is necessary to express the concentration in [mol/m³].

Table V: Chemical composition of the scrap and hot metal as well as the molar weights of the elements

Element	Scrap [wt.-%]	Hot metal [wt.-%]	Molar weight [g/mol]
Carbon	0.2	4.5	12.011
Silicon	0.073	0.1	28.086
Manganese	0.479	0.6	54.938
Iron	99.248	94.8	55.847

For simplification, the complete diffusion profile based on the Matlab® coded analytical model was cut at the solid liquid interface carbon composition, which had been detected by the EMPA measurements in Chapter 4.4. In **Figure 28** the isothermal carbon diffusion profile at 1300 °C is figured out and compared to the average carbon profiles measured by EMPA, found in Publication 6 in the attachment. The carbon profile is calculated by using the diffusion coefficient for δ-iron (D_C^δ) given in Equation 2.34 by Ueshima et al. [73]. It is instantly visible that with this method, the profile is pronounced already after 2.5 s. It has to be mentioned that the scrap composition does not cross the δ-iron region, which is why this approach is not recommendable for an improved scrap-melting model considering coupled heat and mass transfer.
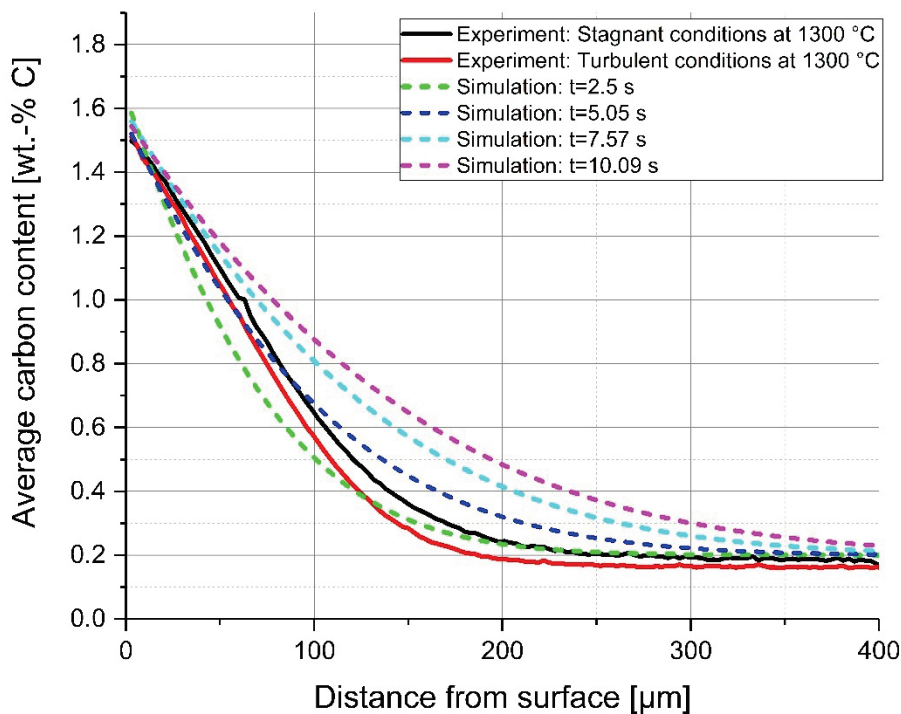
Figure 28: Isothermal carbon diffusion profile at 1300 °C using the diffusion coefficient for delta iron according to Ueshima et al. in Equation 2.34 [73,78] in comparison to the average carbon profiles of the small-scale experiments

Figure 29 and **Figure 30** show the isothermal carbon diffusion profiles at 1300 °C using the diffusion coefficient for austenite by Ueshima et al. (Eq. 2.35) and Ågren (Eq. 2.33), respectively. Both approaches look similar and differ strongly from the previous one for δ-iron. It can be seen that the carbon profile is pronounced after approximately 20 s. The same time is also needed for the specimen to heat up to the equilibrium temperature, conforming to the findings in Chapter 4.2. Due to the diffusion of the carbon into the scrap, the composition is in the range of the austenitic phase during the entire melting period, with the result that the approaches given in Equations 2.33 and 2.35 are more reasonable for a numerical model. The expression of the diffusion coefficient by Ågren [72] is dependent on both the temperature and the carbon composition, which is why it will be used in the numerical model outlined in Chapter 6.

The same behaviour was also detected at the equilibrium temperatures of 1230 °C and 1385 °C. The supplementary figures of all results associated with the present chapter can be found on the DVD of Attachment 2.
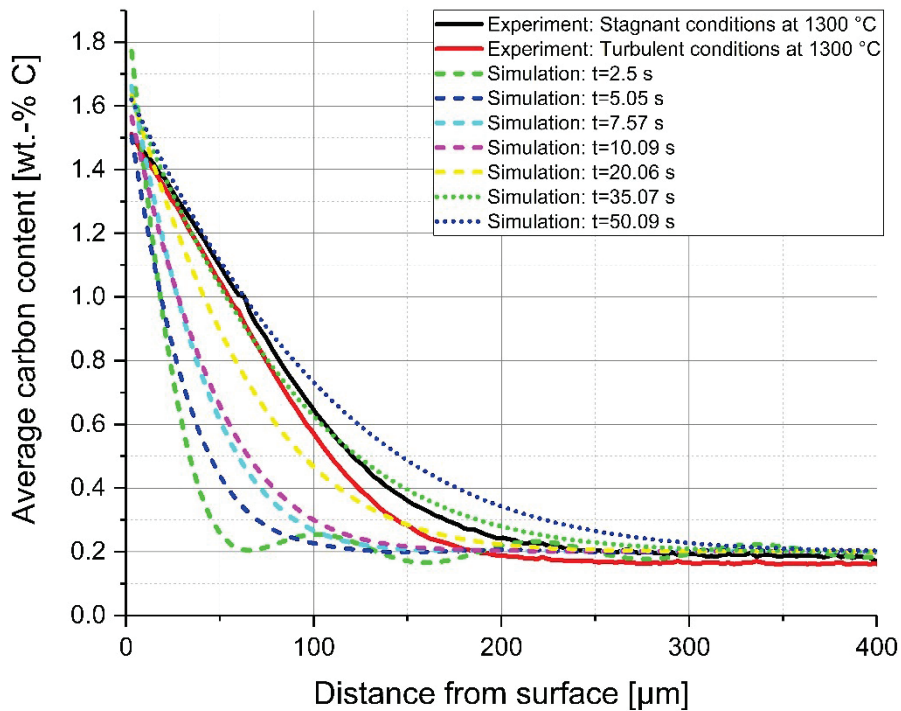
Figure 29: Isothermal carbon diffusion profile at 1300 °C using the diffusion coefficient for austenite according to Ueshima et al. in Equation 2.35 [73,78] in comparison to the average carbon profiles of the small-scale experiments
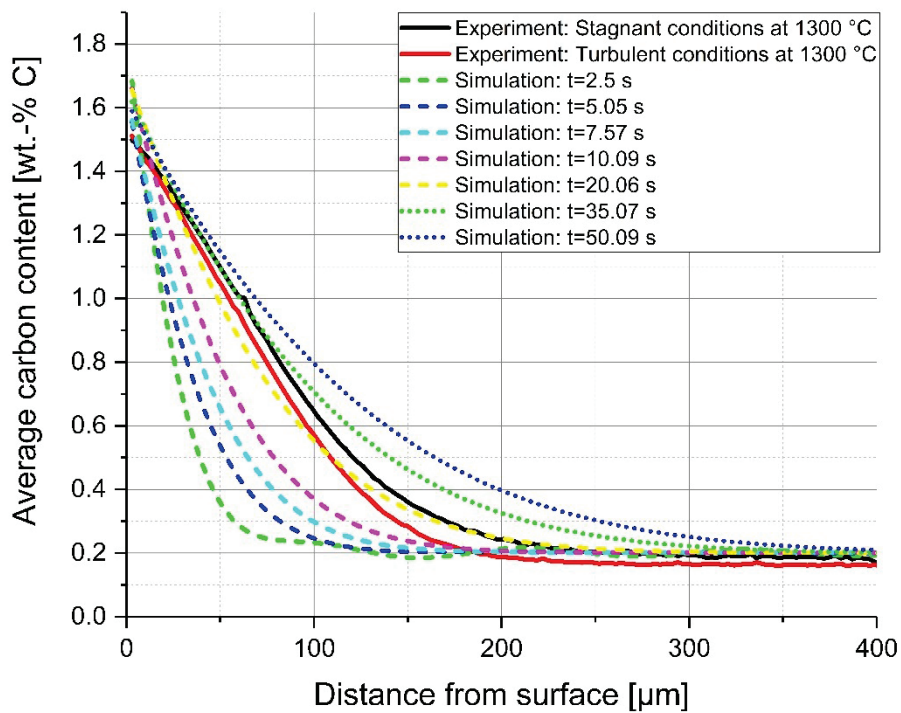
Figure 30: Isothermal carbon diffusion profile at 1300 °C using the diffusion coefficient for austenite according to Ågren in Equation 2.33 [72] in comparison to the average carbon profiles of the small-scale experiments

6 Development of a numerical model combining heat and mass transfer

Derived from the preceding chapters, a numerical model, coded on Matlab®, was developed to describe the coupled heat and mass transfer. The fundamentals of the model are the theoretical considerations presented in Chapter 2. According to the findings of the experimental investigations and to the their utilization in the developed diffusive melting approach in the LD process model developed by Lytvynyuk in [8], it is shown that the modelling of the coupled heat and mass transfer has to contain mushy-zone formulation. Furthermore, the literature discussion of the analytical model (see Publication 2, [37]) as well as the literature review on scrap melting (see Publication 1, [3]) showed that wide ranges of mass and heat transfer coefficients were scientifically outlined. The aim of the present numerical model was to describe the scrap melting by a coupled heat and mass transfer numerically, to obtain possible connection links to the global process model of Lytvynyuk and to validate it with the small-scale experiments.

6.1 Model description

A steel cylinder with a radius of 6 mm will be dissolved in a carbon rich hot metal. The steel is a common unalloyed construction steel (S235JR or 1.0038) as it was used in the small-scale experiments described in Publication 3 and Chapter 4.

6.1.1 Input parameters

The input parameters are directly written into the first part of the main code and include following points:

- Radius of the cylinder
- Number of grid points in the solid
- Factor for the number of grid points in the fluid
- Scrap and hot metal composition
- Starting temperature for the scrap and the hot metal
- Specific heat capacity
- Size of the time step
- Total calculation time
- Tuning factors for the thermal conductivity and the diffusivity, according to the definitions in Equations 2.20, 2.21, 2.30 and 2.31

The scrap is divided in 22 grid points and the amount of grid points in the liquid is four times larger, which refers to the ratio between the scrap and the inner radius of the crucible of the small-scale experiments of Chapter 4. A lower amount of grid points will lead to problems in the resolution of the model. Higher amounts will increase the calculation time dramatically since the explicit approach was adopted. It is important to mention that the time step has to fulfil the second rule of discretization, which is explained in Chapter 2.2.2. The used scrap and hot metal compositions are shown in **Table VI**, whereby the remaining part up to 100 wt.-% is iron. The initial temperature of 100 °C arises from the thermocouple measurement and is unavoidable in the experimental setup due to the radiation effect in the furnace until the sample is completely submerged in the hot metal.

Table VI: Initial temperatures as well as scrap and hot metal compositions

Material	Carbon [wt.-%]	Silicon [wt.-%]	Manganese [wt.-%]	Initial temperature [°C]
Scrap S235JR	0.10	0.07	0.5	100
Hot metal	4.5	0.10	0.2	1305/1370/1450

The values for the liquidus and solidus lines used in the model are approximated through a fitted polynomial of power two based on the solidus and liquidus lines of the Fe-Fe$_3$C-Si-Mn

diagram in **Figure 4**, generated by FactSage™ FSstel database. In **Figure 31** the polynomials are visualized.
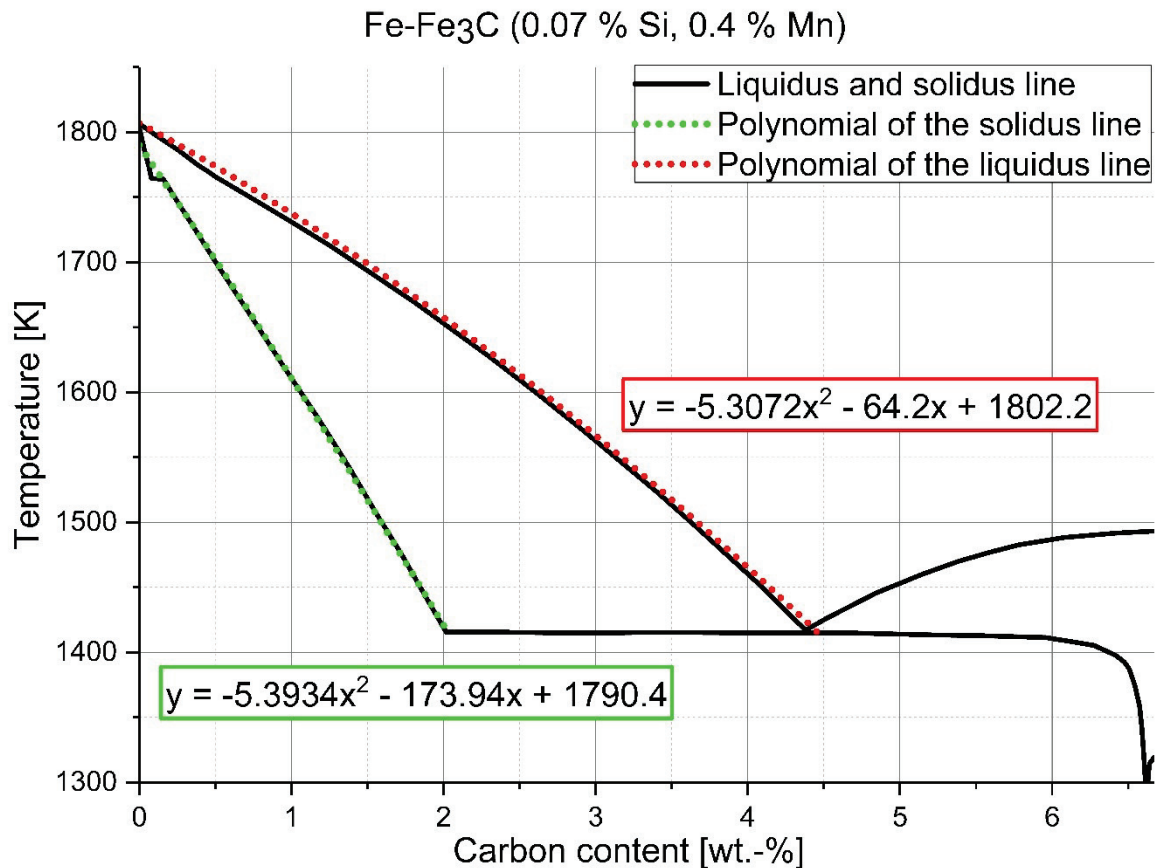
Figure 31: Polynomials for approximation of the solidus and liquidus carbon compositions

The simulated time, the size of each time step, the specific heat capacity and the two tuning factors for the heat (Tu_{heat}) and the mass transfer (Tu_{diff}) for the specific starting temperature of the hot metal and the melt conditions are listed in **Table VII**. The specific heat capacity was assumed to be constant to decrease the total simulation time, but a temperature dependent approach can be implemented in a future version in the time loop. The tuning pairs were approximated and fitted to the experimental results through several calculations. The usage of the tuning factors is necessary for the description of the mushy zone and the behaviour of the mass and heat transfer in the liquid melt, which are described in the Chapters 2.2.3 and 2.2.5. The elapsed real calculation time for each iteration step is between 0.03 s and 0.05 s with the hardware used.

Table VII: Initial parameters of the coupled heat and mass transfer model

Temperature of hot metal [°C]	Melt condition [-]	Simulated time [s]	Size of time step [s]	Specific heat capacity [W/mK]	Tu_{heat} [-]	Tu_{diff} [-]
1305	stagnant	240	0.002	780	2	10
1305	turbulent	240	0.002	780	5	400
1370	stagnant	240	0.002	780	2	10
1370	turbulent	240	0.002	780	5	400
1450	stagnant	140	0.002	780	2	10
1450	turbulent	140	0.002	780	5	400

6.1.2 Discretization of the grid and basic relations

In a first step, the whole domain is divided in equally spaced grid points. Further, the grid is divided into the parts of solid fraction, which is the scrap, and the liquid fraction, which is the hot metal. As a next step, the positions of the boundaries of the control volumes are defined. All definitions have to be saved as a vector to be properly used during the calculation. A future improvement of the model might be to insert a moving grid spacing where the spacing is smaller in the mushy zone.

Additional basic relations for the model are the conversion of the temperatures from °C to K and the definition of the constant density. The density is assumed to be the average density between the hot metal and the scrap, which are both defined through the approach of Miettinen given in Equation 4.9. A more exact solution can be realized by including the definition of a chemical composition-dependent density for each volume element into the time loop. This step was neglected in the present version in order to achieve a rational total calculation time.

The model uses enthalpy functions in [J/kg] and diffusion coefficients in [m²/s], therefore it is necessary to express the carbon concentration with the unit [kg/m³]. It is determined with the Equation 6.1.

$$C_{conc} = \%C * \frac{\rho_{scr}}{100}$$

Eq. 6.1

6.1.3 Starting conditions

The initial temperatures of the scrap and the hot metal are inserted into a vector with the same dimensions of the grid points or if necessary on the position of the boundary between two volume elements. The initial scrap temperature is placed on all grid points where $f_{sol} = 1$ otherwise it is the hot metal temperature. The same procedure is repeated with the carbon concentration on each grid point.

The liquidus and solidus temperatures as well as their direct carbon amounts in [wt.-%] are defined with the polynomials given in **Figure 21** and **Figure 31**. Based on the polynomials also the eutectic temperature of the scrap system is defined. All temperature vectors are rewritten as enthalpies in a sub-function. To decrease the overall calculation time, the enthalpy as a function of temperature, which was generated by FactSage™ FSstel database, was simplified to a linear function. The initial composition of the scrap and the hot metal can be taken from **Table VI**. Afterwards the liquidus and solidus enthalpies as well as the starting enthalpies (H_{init}) on each grid point are determined by using equations 2.23 and 2.24.

6.1.4 Time loop

The main iteration loop of the numerical model is divided into four main parts, which are explained briefly in this chapter in their chronological order of appearance in the model.

6.1.4.1 Definition of the liquid and solid fractions

After the determination of all initial vectors, the iteration with the control variable "n" starts until the total number of time steps is reached, which is defined through the simulation time. For each iteration in which n>1, the present solidus and liquidus carbon concentrations, temperatures and enthalpies are calculated in each control volume "i". The first for-loop is the definition of the liquid f_{liq} and solid fraction $f_{sol} = 1 - f_{liq}$ on the grid points. The definition is divided into two parts. A case discrimination for the calculation is based on the carbon concentration being above or below the maximum solubility of carbon in austenite (2.05 wt.-% C). For carbon concentrations in a grid point (n; i) below 2.05 wt.-% carbon, the following expressions have to be taken into account. For the exact specification, the present enthalpy is used.

for $H \geq H_{liq}$: $\qquad\qquad f_{liq} = 1$ $\qquad$ and $\qquad T = \dfrac{H - L}{c_p} + 298$ $\qquad$ Eq. 6.2

for $H_{sol} \leq H \leq H_{liq}$: $\qquad f_{liq} = \dfrac{H - H_{sol}}{H_{liq} - H_{sol}}$ $\qquad$ and $\quad T = \dfrac{(H - f_l * L)}{c_p} + 298$ $\quad$ Eq. 6.3

For $H \leq H_{sol}$: $\qquad\qquad f_{liq} = 0$ $\qquad$ and $\qquad T = \dfrac{H}{c_p} + 298$ $\qquad$ Eq. 6.4

For the grid points with carbon concentrations above 2.05 wt.-%, the following expressions are valid.

for $H \geq H_{liq}$: $\qquad\qquad f_{liq} = 1$ $\qquad$ and $\qquad T = \dfrac{H - L}{c_p} + 298$ $\qquad$ Eq. 6.5

for $H_{eut2} \leq H \leq H_{liq}$: $\qquad f_{liq} = \dfrac{T - T_{eut}}{T_{liq} - T_{eut}} * \left(1 - f_{liq}^{eut}\right) + f_{liq}^{eut}$ $\qquad$ and

$$T = \left[H + c_p * 298 - f_{liq}^{eut} * L + \left(\dfrac{T_{eut}}{T_{liq} - T_{eut}}\right) * \left(1 - f_{liq}^{eut}\right) * L\right] \bigg/ \left[c_p + \dfrac{\left(1 - f_{liq}^{eut}\right) * L}{\left(T_{liq} - T_{eut}\right)}\right] \quad \text{Eq. 6.6}$$

for $H_{eut1} \leq H \leq H_{eut2}$: $\quad f_{liq} = \dfrac{H - H_{eut1}}{H_{eut2} - H_{eut1}} * f_{liq}^{eut}$ $\quad$ and $\qquad\qquad T = T_{eut}$ $\qquad$ Eq. 6.7

for $H \leq H_{sol}$: $\qquad\qquad f_{liq} = 0$ $\qquad$ and $\qquad T = \dfrac{H}{c_p} + 298$ $\qquad$ Eq. 6.8

6.1.4.2 Definition of diffusion coefficients

The diffusion coefficients are determined by means of the theoretical description, given in Chapter 2.2.5. The artificially increase of the diffusion coefficient with the factor Tu_{diff} in the mushy zone (Eq. 2.31) and in the liquid (Eq. 2.30) is responsible for introducing the effect of the convection. Through the analytical description of the diffusion of carbon into a solid steel cylinder and the fact that with increasing temperature and carbon contents the steel gets austenitic, the diffusion coefficient was determined through the approach given in Equation 2.33 by Ågren [72]. In Equation 2.33, the mole fraction of carbon is needed. The transformation is expressed through Equation 6.9, whereby $M_{mol,C} = 12.01 \; g/mol$ is the molar mass of carbon.

$$C_{mol} = \dfrac{\dfrac{C_{Conc}}{\rho} * 100}{M_{mol,C}} \qquad\qquad \text{Eq. 6.9}$$

Afterwards, the whole simulation has to be checked on its compatibility through the basic rules of discretization. Rule number 2 in Chapter 2.2.2 implies that all coefficients must be positive and requires Equation 6.10 to be satisfied.

$$\Delta t < \frac{(\Delta x)^2}{2 * D_C}$$

<div align="right">Eq. 6.10</div>

Equation 6.10 is only valid for equidistant grid nodes with the distance Δx between two adjacent grid points. The time step is Δt and therefore dependent on the size of the diffusion coefficient D_C and the grid point distance. For the solution of the differential equation, the diffusion coefficients on the boundary interface have to be determined using the harmonic average between two adjacent volume elements.

6.1.4.3 Definition of thermal conductivities

The thermal conductivities are determined by means of the theoretical descriptions, given in the Chapters 2.2.3.4 and 2.2.6. The approach published by Thomas [83], which is given in the Equations 2.36 until 2.39, is used. The effect of convection is incorporated through the artificial increase of the heat conductivity with the factor Tu_{heat}. For the solution the conductivity on the boundary interface between volume elements is also defined by the harmonic average. After the determination of the thermal conductivity, it is also necessary to check if the basic rule number 2 of the discretization is true. The required equation therefore is given in Equation 6.11 and is only valid for equidistant grid nodes with the distance Δx between two adjacent grid points.

$$\Delta t < \frac{\rho * c_p (\Delta x)^2}{2\lambda}$$

<div align="right">Eq. 6.11</div>

6.1.4.4 Determination of the discretization coefficients and solution of the iteration

The final step of the time loop is the determination of the discretization coefficients for the diffusion and the enthalpy according to the equations given 2.8 a – h. With the discretization coefficients and Equation 2.8, the explicit solution of the carbon concentrations and enthalpies for time step $t + \Delta t$ is obtained. The solution calculates the carbon concentration in the liquid and mushy regions by solving the mass diffusion equation with the incremented value of diffusivity. The new values of the temperatures are determined through the temperature approaches given between the Equation 6.2 until 6.8. Until the final iteration step is reached, the enthalpies, temperatures and carbon concentrations are updated at the end of each loop. In an additional step every volume element where $f_{liq} = 1$ the carbon concentration is reset to the initial carbon concentration of the hot metal. This assumption and simplification was

included regarding the phenomenological investigation at the solid-liquid interface described in Chapter 4.4. From the EMPA investigations it is assumed that the hot metal has always a constant carbon amount which is explainable with the rapid homogenisation in the liquid phase. From the EMPA investigations in Chapter 4.4 it is obvious that this assumption is justified. It has to be mentioned that no global mass balance on the whole domain exists, which means that the system in the present form is open. However, this alleged disadvantage of the numerical model is one main connection point to the global LD process model of Lytvynyuk for future improvements.

6.1.5 Structural summary of the numerical scrap melting model

The model allows a coupled heat and mass transfer description of the melting and dissolution of steel scrap in hot metal. To summarize briefly the model, all the steps of the program are listed below and the flow sheet is presented in **Figure 8**.

Based on the initial conditions (t=0). the generation and discretization of the grid is conducted, the initial conditions and basic relations are evaluated.

In each iteration loop following steps are calculated:
- Calculation of f_{liq}
- Determination of D_C and λ and their harmonic average for the boundary interface
- Calculate the discretization coefficients for mass diffusion and heat transfer
- Solve the iteration equations to determine the new carbon concentrations and enthalpies
- Update the values
- Repeat the calculation loop until the final simulation time is reached

6.2 Results of the numerically determined solid/liquid fractions with the small-scale experiments

Based on the initial parameters of **Table VII**, the results of the numerical scrap melting model are compared and validated in the present chapter with the small-scale experiments from Chapter 4. It has to be mentioned that a validation of the heat transfer was technically only possible for non-rotating specimens, which means under stagnant bath conditions. For the rotating specimen, an experimental set-up with a slip ring transmitter might be a solution to

validate the temperature evolution in the core of the sample. This equipment was not available for the present work.

6.2.1 Stagnant bath conditions

As described in Publication 1 in the attachment, totally stagnant conditions are not possible to reach. The effect of natural convection is always present. Due to this fact the tuning factors for the thermal conductivity $(Tu_{heat} = 2)$ and the diffusion $(Tu_{diff} = 10)$ are estimated to be relatively small in comparison to the reported from Lait et al. in [33] and Mizikar in [31] in their associated research on continuous casting of steel, where $Tu_{heat} = 7$. [31,33] Tuning factors to increase artificially the diffusion coefficient to introduce a convection term are not reported so far. The experimental and modelled temperature evolution in the core of the specimen $\left(T_{scr}^{init} = 100\,°C\right)$ is shown in **Figure 32**. The dotted lines display the experimental investigations and the solid lines the results of the present model with the initial parameters of **Table VII**.
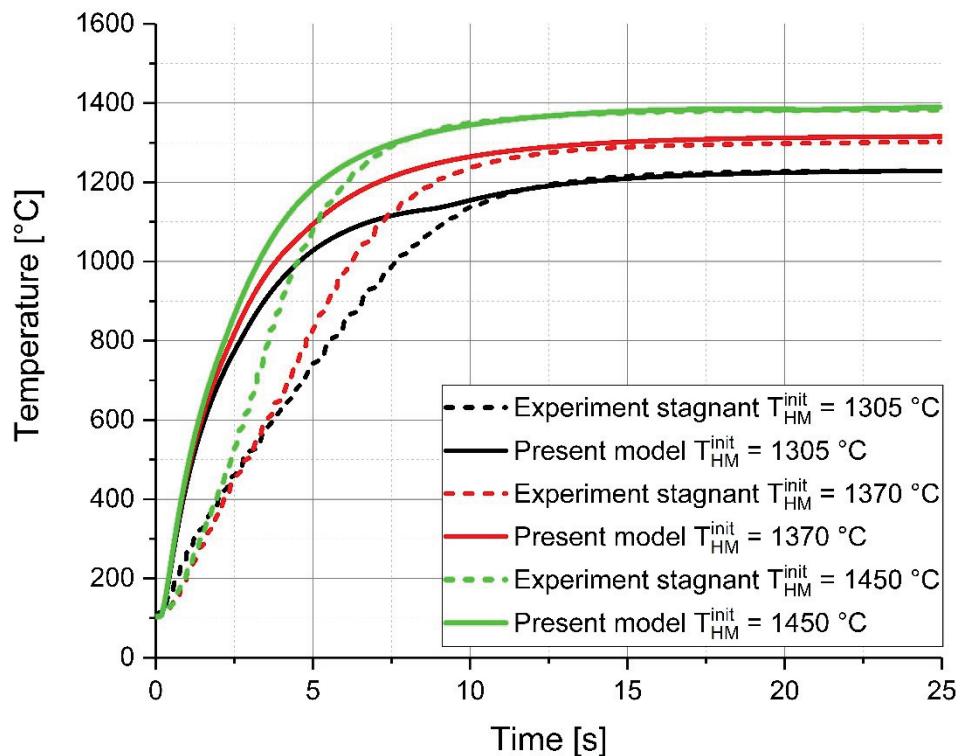
Figure 32: Experimental and modelled temperature evolution in the core of the cylindrical specimen with an initial temperature of 100 °C

In **Figure 32** it is visible that in the initial seconds the temperature of the scrap is increasing faster as the measured one. This is a result of the constant specific heat capacity in the

numerical model and has to be improved in future versions. As already mentioned in Publication 2 and Chapter 4.2, the temperature of the scrap sample and the hot metal become equal after a certain heating time. This achievement is obviously in very good agreement with the present coupled heat and mass transfer model.

In the following three graphs – **Figure 33**, **Figure 34** and **Figure 35** – the evolution of the modelled radii are compared with the small-scale experiments (see Chapter 4). In all figures the red lines define the last volume element where $f_{sol} = 1$ and the blue line describes the first volume element where $f_{liq} = 1$. Between both lines, the mushy zone is located. The step function is a result of the selected mesh.
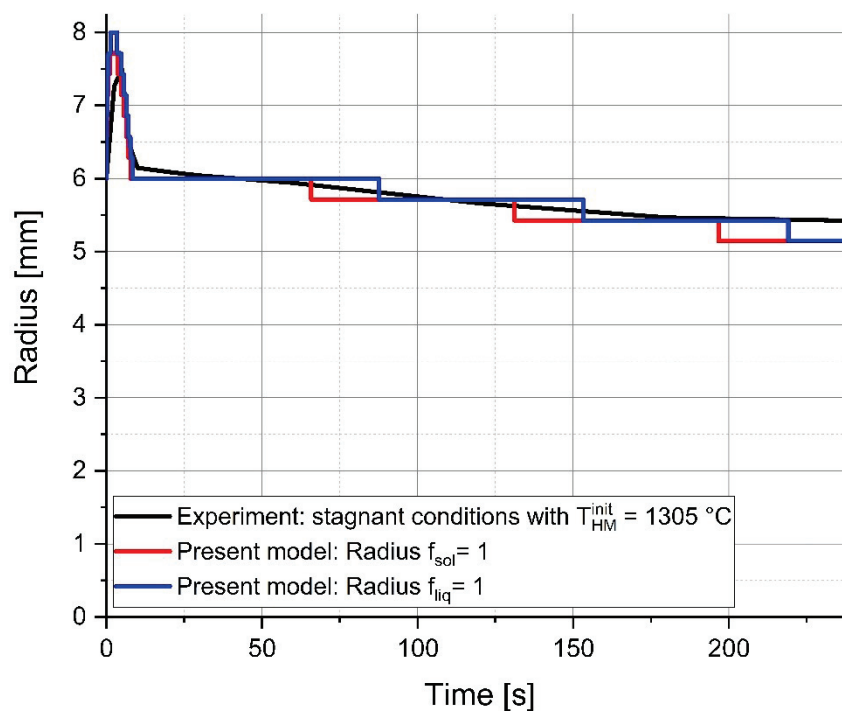
Figure 33: Modelled radii of the last completely solid and first completely liquid volume element in comparison to the experimentally determined radius evolution of the small-scale experiments at an initial temperature of 1305 °C
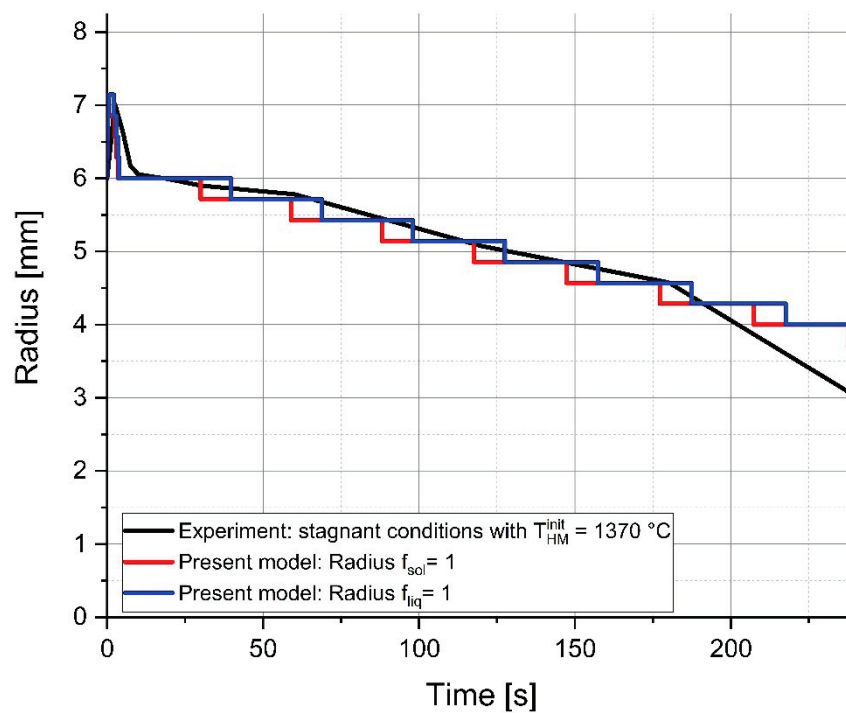
Figure 34: Modelled radii of the last completely solid and first completely liquid volume element in comparison to the experimentally determined radius evolution of the small-scale experiments at an initial temperature of 1370 °C
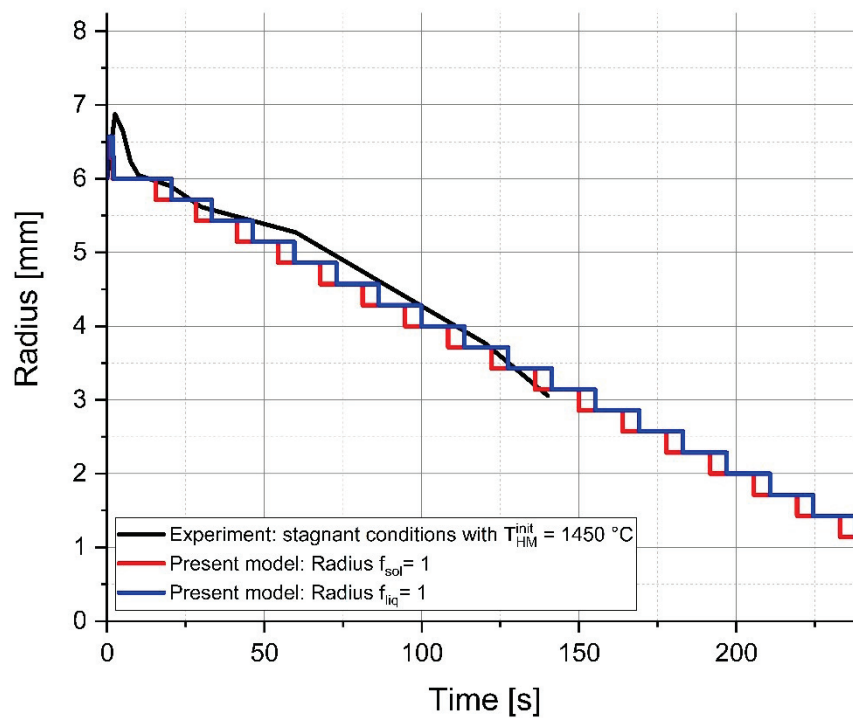
Figure 35: Modelled radii of the last completely solid and first completely liquid volume element in comparison to the experimentally determined radius evolution of the small-scale experiments at an initial temperature of 1450 °C

It is clearly visible that the modelled radius evolution is in a very good agreement with the small scale experiments. The initial shell freezing as well as the thin mushy-zone can be displayed as it was evaluated in the small-scale experiments and the EMPA investigations. The overlapping of the lines describing the last solid volume element and the first completely liquid volume element occurs due to the selected coarse grid. During the overlapping period the carbon diffusion is continuing.

It can be concluded that for the used stagnant system, the chosen tuning parameters and the model developed predicts the melting and dissolution behaviour of scrap very well. The results of small-scale experiments under stagnant conditions validate the present modelling achievements.

6.2.2 Turbulent bath conditions

The turbulent conditions in the small-scale experiments were realized through a rotating sample as described in Publication 4. According to the reported Tu_{heat} values by Lally et al. [59], Brimacombe [65] as well as Cho and Kim in [34] Tu_{heat} was set equal 5 for turbulent conditions. The literature reported a range between 5 and 10 for the turbulent conditions for the continuous casting of steel between the submerged entry nozzle and the solidifying shell. Tu_{diff} was set equal 400 for turbulent conditions. In the following three graphs – **Figure 36**, **Figure 37** and **Figure 38** – the evolution of the modelled radii are compared with the small-scale experiments under turbulent conditions described in Chapter 4. The structure of the following figures is identical to the previous chapter. The initial parameters are listed in **Table VII**.
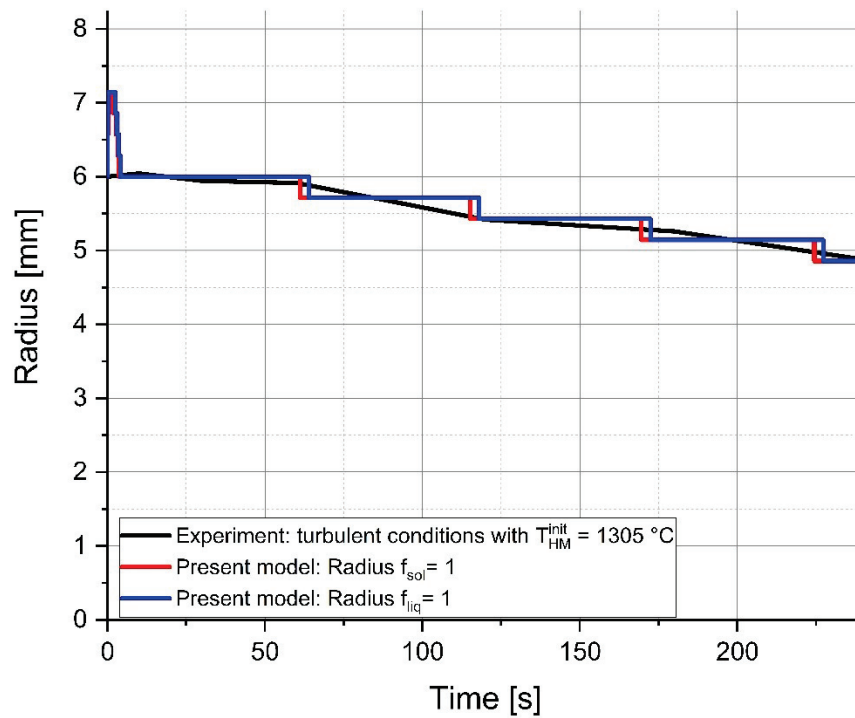
Figure 36: Modelled radii of the last completely solid and first completely liquid volume element in comparison to the experimentally determined radius evolution of the small-scale experiments under turbulent conditions at an initial temperature of 1305 °C
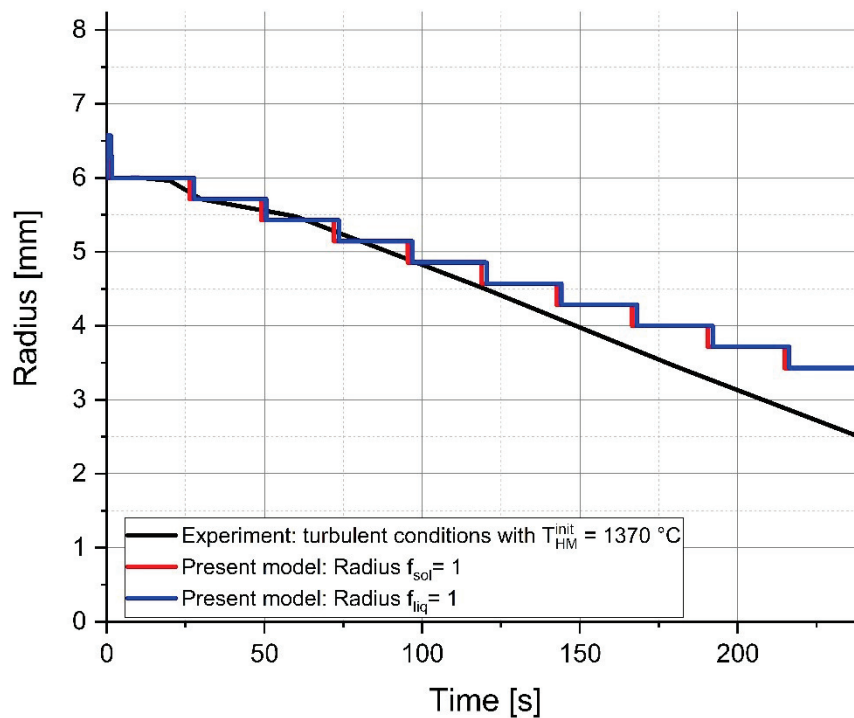
Figure 37: Modelled radii of the last completely solid and first completely liquid volume element in comparison to the experimentally determined radius evolution of the small-scale experiments under turbulent conditions at an initial temperature of 1370 °C
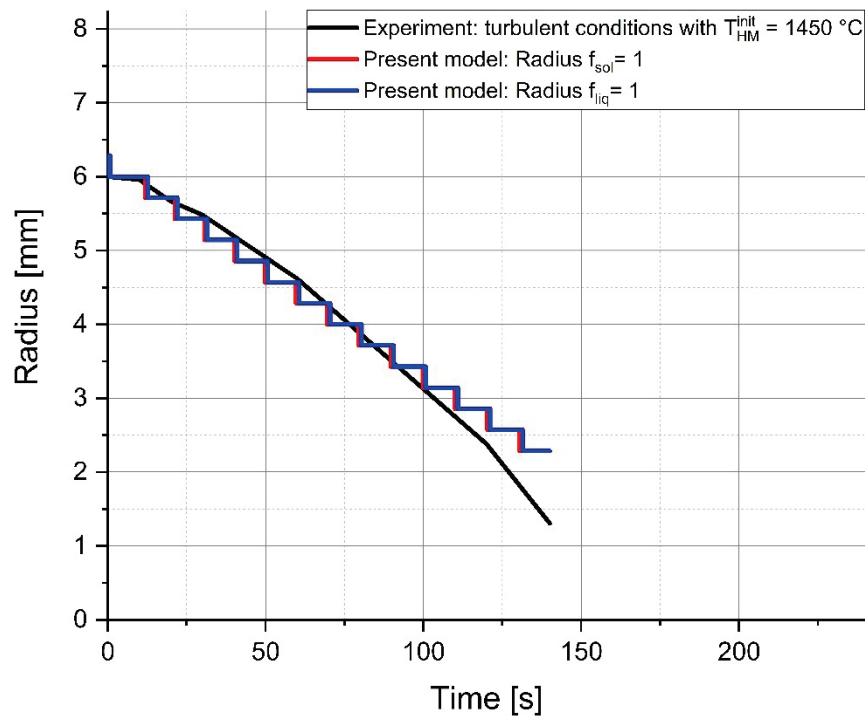
Figure 38: Modelled radii of the last completely solid and first completely liquid volume element in comparison to the experimentally determined radius evolution of the small-scale experiments under turbulent conditions at an initial temperature of 1450 °C

Identically to the previous chapter, the chosen tuning parameters and the model predicts the melting and dissolution behaviour of the scrap under turbulent conditions very well. Due to the 40 times higher Tu_{diff} in comparison to the stagnant conditions, a more narrow mushy-zone exists, which is also in accordance to the results of the EMPA measurements, where the hot metal composition reaches up to the solid-liquid interface. Therefore, the assumption mentioned in Chapter 6.1.4.4 that the hot metal is a rapid and homogeneous liquid mixture, can be assumed to be accurate.

According to the coupled heat and mass transfer, the last open question is the behaviour of the model, if the initial temperature of the hot metal is above the liquidus temperature of liquid hot metal or pure iron. There, according to the definition published by Medzhibozhskiy in [15] (see Equation 3.4), forced scrap melting occurs. In **Figure 39** the evolution of the modelled radii for an initial hot metal temperature of 1600 °C and 1700 °C, respectively, are given. The red and black line define the last volume element where $f_{sol} = 1$ and the blue and green line describe the first volume element where $f_{liq} = 1$ for the given initial temperatures, respectively.
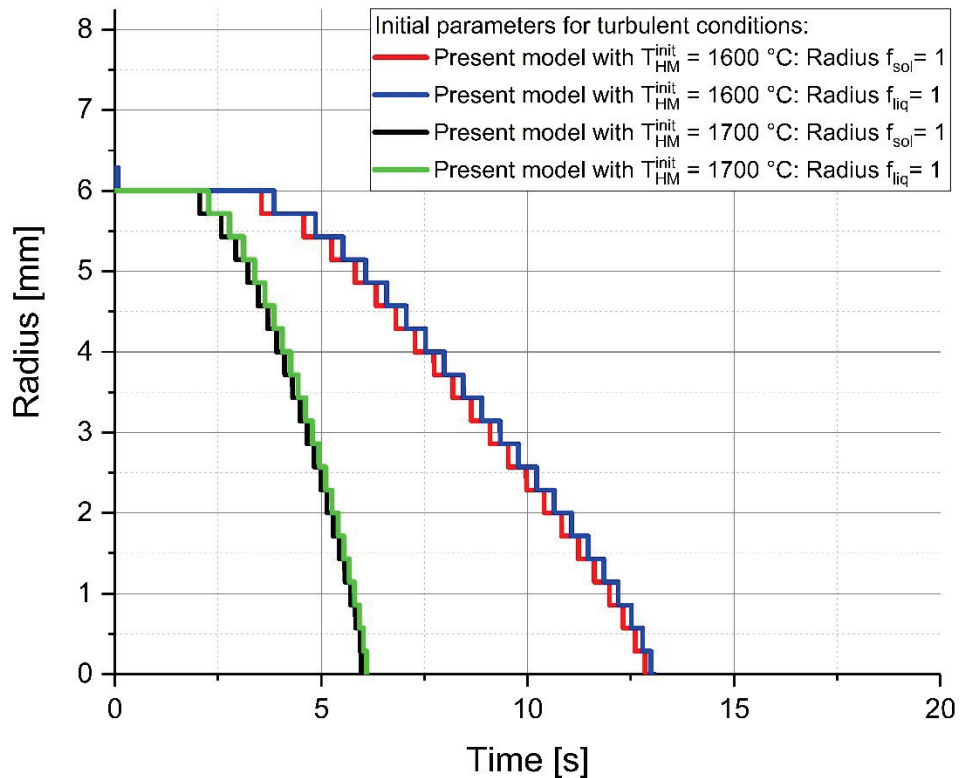
Figure 39: Modelled radii of the last completely solid and first completely liquid volume element under turbulent conditions at an initial temperature of 1600 °C and 1700 °C

In both cases it is visible that the scrap melts very fast as it is predicted by means of the global process model described in Chapter 4.5. However, diffusion of carbon is modelled, which results in a small mushy zone. Due to the investigations of the scrap skull in Chapter 4.4.2, this finding in the simulation might be reasonable because the mass transfer in the solid increases dramatically with increasing temperatures. The specific examples in **Figure 39** show that the model is working in every range of scrap melting and dissolution, which means that forced and diffusive scrap melting are coupled too. The numerical artefacts at the transition of forced and diffusive scrap melting, as they occur in fixed point approaches (see Chapter 4.5), can be avoided with the present numerical approach of a coupled heat and mass transfer.

6.3 Outlook on improvements and description of possible conjunctions to the dynamic BOF model

The developed model in the present research is already in a good agreement with the experiments carried out in the frame of this work. Nevertheless, science is always an iterative process and improvements of the model are necessary to be included for further versions and to improve the accuracy of the model.

My first recommendation for an improvement is the transition of the model into an implicit approach. Actually the model uses the explicit method which requires very small time steps. Probably total calculation time will not decrease but the model will become compatible with the global LD process model of Lytvynyuk and Bundschuh. A gradual alignment of the time steps will be reached. The necessary connection points are the definition of the temperature and the carbon composition in the volume elements where $f_{liq} = 1$.

The model was validated with the experiments carried out in the frame of this work. Further validations, also with available data from literature, should be considered.

Temperature and chemical composition dependent parameters are important to attain more accurate predictions. The implementation of a variable specific heat capacity and density as a function of the temperature and if possible of the carbon content in each grid point during every iteration step should be considered in future versions.

The last point, which should be considered in future models, is the implementation of the diffusion behaviour of other alloying elements of steel (e.g. Mn, Si, P and Cr). The scrap skull investigations in Chapter 4.4.2 point out that these elements behave quite mobile at higher temperatures.

7 Discussion of the results

The detailed description of the melting and dissolution behaviour of scrap in iron-carbon melts requires the consideration of parallel processes of heat and mass transfer. A comprehensive literature study based on all associated and available references showed the huge variety and complexity of experimental and modelling approaches. In this context, it showed that a coupled heat and mass transfer is the most important requirement to receive accurate predictions in the modelling of the melting and dissolution behaviour of scrap. In a study of several scrap parameters, the used technique of a fixed point transition in the model, developed by Lytvynyuk and improved by Bundschuh, cast serious doubts. With a fixed point as a transition between diffusive and forced scrap melting, a non-logical increase in the scrap radius can occur. This is actually suppressed by the definition that if the ablation rate gets positive it is replaced by the value 0, which is equal to a dissolution stop.

It turned out that one of the main challenging points was the proper definition of the heat and mass transfer coefficients. With specified small-scale laboratory investigations, a targeted approach was developed to investigate and evaluate the heat as well as the mass transfer coefficients. The results showed, compared to previously published research, close conformity and interesting side effects. The evaluated heat transfer coefficients, supported by the analytic model developed within this thesis, showed huge discrepancies in comparison to existing Nusselt correlations, but are in absolute agreement with published research from other scientists. These findings pointed out that the development of a numerical model without the use of Nusselt correlations is expedient.

A pragmatic procedure with the aim understanding the phenomenological effects specifically at the solid-liquid interface was developed by means of connecting optical microscopy with electron microprobe investigations. Through the EMPA investigations, a new approach was

derived to describe the diffusive scrap melting, where the interface carbon concentration is located in the two-phase area between the liquidus and solidus lines. The derived approach was implemented into the existing global LD process model. A strong influence on the melting and dissolution evolution of the scrap, resulting in deviations of the final chemical composition, was visualized. Nevertheless, the resulting approach connected with the equation for forced scrap melting points out yet again the reasonable doubts about the fixed point approach used.

During the EMPA investigations, a silicon enrichment, located in the solid section, was identified. A closer examination of its formation is not included in this work but a few hypotheses should provide the basis for future investigations. Within the framework of the EMPA investigation, a high mobility of heavy elements inside the scrap was also identified, which will require more time for an intense and sustainable description in future.

In addition, an analytical solution for the heat transfer, an analytical model to investigate the isothermal diffusion of carbon into the solid steel was developed, as well. This model supports the choice of the diffusion coefficient´s sub model to be used in a numerical model. The development of the diffusion profile over the time was estimated.

Due to the mathematical difficulties of combining the two analytical models developed with a coupled heat and mass transfer model, the theoretical fundamentals for the numerical description of phase change problems were reviewed. With the combination of several methods, a numerical description of the melting and dissolution of scrap was created. The numerical model couples the heat and mass transfer. A huge advantage is that in this model, no fixed transition point between forced and diffusive scrap melting exists and a small mushy zone is considered. The model is consistent with the small-scale experiments and the findings of the EMPA, which validates the accuracy. The model developed, is based on an explicit calculation technique and gives preferential and recommended connection points for its implementation into Lytvynyuk´s global LD process model. A further advantage in comparison to other scrap melting models is that this model considers temperature and composition-dependent physical parameters to a certain degree.

The total amount of the research conducted, serves as a basis for future developments and improvements in the description of scrap melting with coupled heat and mass transfer. The target of this work to develop a model for an improved description of this topic was successfully achieved.

8 Outlook

Science does not stop in the last chapter of any thesis or book. A fundamental work to understand the melting and dissolution behaviour of scrap in iron-carbon melts is included in this thesis. Several outstanding results have been pointed out and should now give the opportunity to focus on further topics for scientific research.

As mentioned in the previous chapter, the EMPA investigation points out several particular incidents. The formation of a silicon enrichment on the solid side of the solid liquid interface can be a result of oxidation and reduction processes due to oxygen diffusion into the solid scrap. Additionally, the formation of silicon carbide can be a reasonable explanation for the silicon layer. The formations of the interstitial phases might need some kind of constitutional overheating to convert them into a liquid phase. These findings definitely require intensive investigation to be solved in future.

A second new discovery of the present research was the increased mobility of heavy elements in the steel scrap. Through favourable circumstances, a scrap skull, which withstands the entire blowing period of an LD converter and reaches temperatures above 1600 °C, was investigated regarding the phenomena on its surface. The diffusive removal of heavy elements like Cr, Mn, P and Si from a distance of up to 1 mm below the surface into the melt still leaves open questions requiring additional efforts to be solved. It is imperative to note that the description of the carbon diffusion is the most important factor in the scrap melting and dissolution behaviour, but due to the discoveries in this work, it has to be concluded that a multicomponent mass transfer has to be incorporated into the efforts of future work.

The developed coupled heat and mass transfer model presents an essential development of this thesis to improve the predictions about the scrap melting behaviour in an LD converter.

Links have been pointed out in the present work to establish a conjunction with the global LD process model of Lytvynyuk. Nevertheless, a few improvements, listed in Chapter 6.3, and the transformation into the implicit simulation technique, are important to be considered.

9 Publications published within this PhD thesis

In the course of the preparation of this thesis several publications were established. In all publications the author of this thesis wrote 100 % of the original draft. The complete contribution of the author is given in **Table VIII**. All peer-reviewed journal articles are attached with permission of the publishing companies. Additionally, all conference papers, published in the frame of this thesis are listed in Chapter 9.8. In all conference papers 100 % of the original draft were written by the author of this thesis.

9.1 Contribution of the author to the papers

Table VIII: Contribution of the author to the appended publications in percent

Publication	Conception and planning	Experiments	Analysis and interpretation	Manuscript preparation
1	100 %	100 %	100 %	100 %
2	100 %	100 %	100 %	100 %
3	100 %	100 %	100 %	100 %
4	100 %	100 %	100 %	100 %
5	100 %	100 %	100 %	100 %
6	100 %	100 %	100 %	100 %

9.2 Publication 1: A Review of Steel Scrap Melting in Molten Iron-Carbon Melts

A Review of Steel Scrap Melting in Molten Iron-Carbon Melts

Florian Markus Penz, Johannes Schenk

Steel research International, 2019, Early view online Version, article no.: 1900124 (1-20); DOI: 10.1002/srin.201900124

Work load:

Florian Markus Penz: Conceptualization; Data curation; Investigation, Methodology; Project administration; Resources; Software; Supervision; Visualization; ***Writing—original draft (100 %)***; Writing—review and editing;

Johannes Schenk: Project administration; Validation; Writing—review and editing;

9.3 Publication 2: Analytical and numerical determination of the heat transfer coefficient between scrap and hot metal based on small-scale experiments

Analytical and numerical determination of the heat transfer coefficient between scrap and hot metal based on small-scale experiments

Florian Markus Penz, Roberto Parreiras Tavares, Christian Weiss, Johannes Schenk, Rainer Ammer, Krzysztof Pastucha and Gerald Klösch

International Journal of heat and mass transfer, Volume 138, 2019, pp. 640 -646;
DOI: 10.1016/j.ijheatmasstransfer.2019.04.085

Work load:

Florian Markus Penz: Conceptualization; Data curation; Investigation, Methodology; Project administration; Resources; Software; Supervision; Visualization; ***Writing—original draft (100 %)***; Writing—review and editing;

Roberto Parreiras Tavares: Supervision; Validation; Writing—review and editing;

Christian Weiss: Supervision; Validation; Writing—review and editing;

Johannes Schenk: Project administration; Supervision; Validation; Writing—review and editing;

Krzysztof Pastucha: Project administration; Validation; Writing—review and editing;

Rainer Ammer: Validation; Writing—review and editing;

Gerald Klösch: Validation; Writing—review and editing;

9.4 Publication 3: Evaluation of the Influences of Scrap Melting and Dissolution during Dynamic Linz–Donawitz (LD) Converter Modelling

Evaluation of the Influences of Scrap Melting and Dissolution during Dynamic Linz–Donawitz (LD) Converter Modelling

Florian Markus Penz, Johannes Schenk, Rainer Ammer, Gerald Klösch and Krzysztof Pastucha

Processes Volume 7, 2019, article no.:186 (1-15); DOI: 10.3390/pr7040186

Work load:

Florian Markus Penz: Conceptualization; Data curation; Investigation, Methodology; Project administration; Resources; Software; Supervision; Visualization; ***Writing—original draft (100 %)***; Writing—review and editing;

Johannes Schenk: Project administration; Supervision; Validation; Writing—review and editing;

Krzysztof Pastucha: Project administration; Validation; Writing—review and editing;

Rainer Ammer: Validation; Writing—review and editing;

Gerald Klösch: Validation; Writing—review and editing;

9.5 Publication 4: Dissolution of Scrap in Hot Metal under Linz–Donawitz (LD) Steelmaking Conditions

Dissolution of Scrap in Hot Metal under Linz–Donawitz (LD) Steelmaking Conditions

Florian Markus Penz, Johannes Schenk, Rainer Ammer, Gerald Klösch and Krzysztof Pastucha

Metals Volume 8, 2018, article no.:1078 (1-10); DOI: 10.3390/met8121078

Work load:

Florian Markus Penz: Conceptualization; Data curation; Investigation, Methodology; Project administration; Resources; Software; Supervision; Visualization; ***Writing—original draft (100 %)***; Writing—review and editing;

Johannes Schenk: Project administration; Software; Supervision; Validation; Writing—review and editing;

Krzysztof Pastucha: Project administration; Validation; Writing—review and editing;

Rainer Ammer: Validation; Writing—review and editing;

Gerald Klösch: Validation; Writing—review and editing;

9.6 Publication 5: Dissolution behaviour of ULC steel in carbon saturated hot metal

Dissolution behaviour of ULC steel in carbon saturated hot metal

Florian Markus Penz, Johannes Schenk, Rainer Ammer, Krzysztof Pastucha and Bernhard Maunz

La Metallurgia Italiana Volume 11/12, 2018, 36-45;

Work load:

Florian Markus Penz: Conceptualization; Data curation; Investigation, Methodology; Project administration; Resources; Software; Supervision; Visualization; ***Writing—original draft (100 %)***; Writing—review and editing;

Johannes Schenk: Project administration; Supervision; Validation; Writing—review and editing;

Krzysztof Pastucha: Project administration; Validation; Writing—review and editing;

Rainer Ammer: Validation; Writing—review and editing;

Bernhard Maunz: Validation; Writing—review and editing;

9.7 Publication 6: Diffusive steel scrap melting in carbon-saturated hot metal – phenomenological investigation at the solid-liquid interface

Diffusive steel scrap melting in carbon-saturated hot metal – phenomenological investigation at the solid-liquid interface

Florian Markus Penz, Johannes Schenk, Rainer Ammer, Gerald Klösch, Krzysztof Pastucha and Michael Reischl

Materials Volume 12(8), 2019, 1358 (1-22); DOI: 10.3390/ma12081358

Work load:

Florian Markus Penz: Conceptualization; Data curation; Investigation; Methodology; Project administration; Resources; Software; Supervision; Visualization; ***Writing—original draft (100 %)***; Writing—review and editing;

Johannes Schenk: Project administration; Software; Supervision; Validation; Writing—review and editing;

Krzysztof Pastucha: Project administration; Validation; Writing—review and editing;

Rainer Ammer: Validation; Writing—review and editing;

Gerald Klösch: Validation; Writing—review and editing;

Michael Reischl: Investigation; Validation; Writing—review and editing;

9.8 Conference articles (not attached to this thesis):

1. **Penz, F. M.** *(Writing—original draft: 100 %)***;** Bundschuh, P.; Schenk, J.; Panhofer, H.; Pastucha, K. and A. Paul: Effect of Scrap Composition on the Thermodynamics of Kinetic Modelling of BOF Converter. In Proceedings of the 2nd VDEh-ISIJ-JK Symposium, Stockholm, Sweden, 12–13 June 2017; pp. 124–135.

2. **Penz, F. M.** *(Writing—original draft: 100 %)***;** Bundschuh, P.; Schenk, J.; Panhofer, H.; Pastucha, K. and A. Paul: Impact of carbon, silicon and manganese contents on the dissolution and melting behaviour of scrap in a dynamic BOF model. In Proceedings of the European steel technology and application days 2017 (ESTAD), Vienna, Austria, 26–29 June 2017;

3. **Penz, F. M.** *(Writing—original draft: 100 %)***;** Bundschuh, P.; Schenk, J.; Panhofer, H.; Pastucha, K. and B. Maunz: Scrap melting in BOF: Influence of particle surface and size during dynamic converter modelling. In Proceedings of the 3rd ABM week, São Paulo, Brazil, 2–6 October 2017.

4. **Penz, F. M.** *(Writing—original draft: 100 %)***;** Schenk, J.; Ammer, R.; Pastucha, K. and B. Maunz: Dissolution behaviour of ULC steel in carbon saturated hot metal. In Proceedings of the 7th International Congress on science and technology of steelmaking (ICS 2018), Venice/Mestre, Italy, 12–13 June 2018;

10 References

[1]   A. Ghosh, A. Chatterjee (Eds.), Ironmaking and Steelmaking: Theory and Practice, PHI Learning Private Limited, Dehli, 2008.

[2]   Turkdogan, E.T., Fundamentals of steelmaking, Institute of Materials, London, 2010, ©1996.

[3]   Penz, F.M. and J. Schenk, A Review of Steel Scrap Melting in Molten Iron-Carbon Melts, steel research international (2019), Early view online Version, 1900124 (1-20).

[4]   Kruskopf, A. and L. Holappa, Scrap melting model for steel converter founded on interfacial solid/liquid phenomena, Metall. Res. Technol. 115 (2018), 2, 201 (1-7).

[5]   Deng, S., A. Xu, G. Yang and H. Wang, Analyses and Calculation of Steel Scrap Melting in a Multifunctional Hot Metal Ladle, steel research int. 90 (2019), 1 early view, 1–10.

[6]   Bureau of International Recycling Ferrous Division, World steel recycling in figures 2013 – 2017: Steel scrap - a raw material for steelmaking, https://www.bdsv.org/fileadmin/user_upload/180222-Ferrous-report-2017-V07.pdf, Abgerufen am: 03.01.2019.

[7]   Ohnuki, K., T. Hiraoka, T. Inoue, K. Umezawa and N. Matsumoto, Development of steel scrap melting process, Nippon Steel Technical Report 61 (1994), April, 52–57.

[8]   Y. Lytvynyuk, Thermodynamic and kinetic modeling of metallurgical reactions, PhD thesis, Montanuniversitaet Leoben, Austria, 2013.

[9]   Bundschuh, P., Thermodynamische und kinetische Modellierung von LD-Konvertern, Dissertation, Montanuniversitaet Leoben, Austria, 2017.

[10]   S. Ohguchi, D. G. C. Robertson, B. Deo, P. Grieveson, and J. H. E. Jeffes, Simultaneous dephosphorization and desulphurization of molten pig iron, Ironmaking and Steelmaking Vol. 11 (1984), No. 4, 202–213.

[11]   Lommel, J.M. and B. Chalmers, The Isothermal Transfer from Solid to Liquid in Metal Systems, Transactions of the Metallurgical Society of AIME 215 (1959), 6, 499 - 508.

[12]   Pehlke, R.D., P.D. Goodell and R.W. Dunlap, Kinetics of Steel Dissolution in Molten Pig Iron, Transactions of the Metallurgical Society of AIME 233 (1965), 7, 1420–1427.

[13]   Olsson, R.G., V. Koump and T.F. Perzak, Rate of dissolution of Carbon-Steel in Molten Iron Carbon Alloys, Transactions of the Metallurgical Society of AIME 233 (1965), 9, 1654–1657.

[14]   Brabie, L.C. and M. Kawakami, Kinetics of Steel Scrap Melting in Molten Fe-C Bath, High Temperature Materials and Processes 19 (2000), 3-4, 241–255.

[15]   Medzhibozhskiy, M.Y., Basis of thermodynamic and kinetic of steelmaking, Publishing house "Vischa shkola". Kyiv, (1979).

[16]   Gaye, H., P. Destannes, J.L. Roth and M. Guyon, Kinetics of scrap melting in the converter and electric arc furnace, Proceedings of the 6th International Iron and Steel Congress, Nagoya, Japan, Vol. 4, Steelmaking II (1990), 11–17.

[17]   Gaye, H., M. Wanin, P. Gugliermina and P. Schittly, Kinetics of scrap dissolution in the converter. Theoretical Model and Plant Experimentation, In Proceedings of the 68th Steelmaking Conference, AIME, Detroit, MI, USA (1985), 68, 91–104.

[18]   Gol'dfarb, M. and B.I. Sherstov, Heat and mass transfer when melting scrap in an oxygen converter, Journal of Engineering Physics and Thermophysics 18 (1970), 3, 342–347.

[19]   Penz, F., P. Bundschuh, J. Schenk, H. Panhofer, K. Pastucha und A. Paul, Effect of Scrap Composition on the Thermodynamics of Kinetic Modelling of BOF Converter, Stockholm, 2017.

[20]   Sethi, G., A.K. Shukla, P.C. Das, P. Chandra and B. Deo, Theoretical Aspects of Scrap Dissolution in Oxygen Steelmaking Converters, AISTech 2004 Proceedings, Nashville, Tenn., USA (2004), Volume II, 915–926.

[21]   Glinkov, M.A., V.Y. Bakst, M.Y. Medzhibozhskiy and V.I. Sel'skii, Melting of cold steel scrap in a superheated iron carbon melt, Steel in the USSR (1972), March, 195–196.

[22]   Li, J., G. Brooks and N. Provatas, Kinetics of scrap melting in liquid steel, Metallurgical and Materials Transactions B 36 B (2005), 2, 293–302.

[23]   Li, J., G.A. Brooks and N. Provatas, Phase-Field Modeling of Steel Scrap Melting in a Liquid Steel Bath, AISTech 2004 Proceedings, Nashville, Tenn., USA (2004), Volume I, 833–843.

[24]   Patankar, S.V., Numerical Heat Transfer and Fluid Flow, Hemisphere Publishing Corporation, Washington, 1980.

[25]   Szekely, J. und N.J. Themelis, Rate Phenomena in Process Metallurgy, 1. ed., John Wiley & Sons, Inc, New York, 1971.

[26]   Seshadri, V., R. Parreiras Tavares, C. Antonio da Silva und I. Alves da Silva, Transport phenomena: fundamentals and applications in Metallurgical and Materials Engineering, ABM, Sao Paulo, 2011.

[27]   Stefanescu, D.M., Science and Engineering of Casting Solidification, 3rd ed., Springer International Publishing Switzerland, Cham, 2015.

[28]   Jeschar, R., R. Alt und E. Specht, Grundlagen der Wärmeübertragung, 3. Auflage, Viola Jescher Verlag, Goslar, 1990.

[29]   Hertwig, K. und L. Martens, Chemische Verfahrenstechnik: Berechnung Auslegung und Betrieb chemischer Reaktoren, 2nd ed., revised, Oldenbourg Verlag, München, 2012.

[30]   Gür, C.H. und J. Pan, Handbook of Thermal Process Modeling of Steels, CRC Press, Boca Raton, 2009.

[31]   Mizikar, E.A., Mathematical Heat Transfer Model for Solidification of Continuously Cast Steel Slabs, Transactions of the Metallurgical Society of AIME 239 (1967), 11, 1747–1753.

[32]   Choudhary, S.K., D. Mazumdar and A. Ghosh, Mathematical Modelling of Heat Transfer Phenomena in Continuous Casting of Steel, ISIJ International 33 (1993), 7, 764–774.

[33]   Lait, J.E., J.K. Brimacombe and F. Weinberg, Mathematical modelling of heat flow in the continous casting of steel, Ironmaking and Steelmaking (Quarterly) 1 (1974), 2, 90–97.

[34]   Cho, K.H. and B.M. Kim, Numerical Analysis of Secondary Cooling in Continuous Slab Casting, Journal of Materials Science & Technology 24 (2008), 3, 389–390.

[35]   S. Kabelac (Ed.), VDI-Wärmeatlas: [Berechnungsunterlagen für Druckverlust, Wärme- und Stoffübergang], 11. Auflage, Springer-Verlag Berlin Heidelberg, Berlin, Heidelberg, 2013.

[36]   Necati Özisik, M., Heat Conduction, second edition, John Wiley & Sons, Inc, New York, 1993.

[37]   Penz, F.M., R. Parreiras Tavares, C. Weiß, J. Schenk, R. Ammer, K. Pastucha and G. Klösch, Analytical and numerical determination of the heat transfer coefficient between scrap and hot metal based on small-scale experiments, International Journal of Heat and Mass Transfer 138 (2019), 8, 640–646.

[38]   Salcudean, M. and Z. Abdullah, On the numerical modelling of heat transfer during solidification processes, International Journal for Numerical Methods in Engineering 25 (1988), 2, 445–473.

[39]   Crank, J., Free and moving boundary problems, Clarendon Press, Oxford, 1984.

[40]   Voller, V.R. and C.R. Swaminathan, General source-based method for solidification phase change, Numerical Heat Transfer, Part B: Fundamentals 19 (1991), 2, 175–189.

[41]   Voller, V.R., C.R. Swaminathan and B.G. Thomas, Fixed grid techniques for phase change problems: A review, International Journal for Numerical Methods in Engineering 30 (1990), 4, 875–898.

[42]   Swaminathan, C.R. and V.R. Voller, On the enthalphy method, International Journal of Numerical Methods for Heat & Fluid Flow 3 (1993), 3, 233–244.

[43]   Kurz, W. und D.J. Fisher, Fundamentals of solidification, 2. ed., Trans Tech Publications, Aedermannsdorf, Switzerland, 1989.

[44]   Gabathuler, J.P. and F. Weinberg, Fluid flow into a dendritic array under forced convection, Metallurgical Transactions B 14 (1983), 4, 733–741.

[45]   Kim, Y., B. Farouk and Keverian J., A Mathematical Model for Thermal Analysis of Thin Strip Casting of Low Carbon Steel, ASME Journal of Engineering for Industry 113 (1991), 1, 53–58.

[46]   Voller, V.R., Implicit Finite - difference Solutions of the Enthalpy Formulation of Stefan Problems, IMA Journal of Numerical Analysis 5 (1985), 2, 201–214.

[47]   Voller, V.R. and C. Prakash, A fixed grid numerical modelling methodology for convection-diffusion mushy region phase-change problems, International Journal of Heat and Mass Transfer 30 (1987), 8, 1709–1719.

[48]   Kruskopf, A., A Model for Scrap Melting in Steel Converter, Metallurgical and Materials Transactions B 46 (2015), 3, 1195–1206.

[49]   Brent, A. d., V.R. Voller and K.J. Reid, Enthalpy-porosity technique for modeling convection-diffusion phase change: Application to the melting of a pure metal, Numerical Heat Transfer 13 (1988), 3, 297–318.

[50]   Comini, G., S. Del Guidice, R.W. Lewis and O.C. Zienkiewicz, Finite element solution of non-linear heat conduction problems with special reference to phase change, International Journal for Numerical Methods in Engineering 8 (1974), 3, 613–624.

[51]   Konishi, J., M. Militzer, I.V. Samarasekera and J.K. Brimacombe, Modeling the formation of longitudinal facial cracks during continuous casting of hypoperitectic steel, Metallurgical and Materials Transactions B 33 (2002), 3, 413–423.

[52]   Voller, V.R., M. Cross and N.C. Markatos, An enthalpy method for convection/diffusion phase change, International Journal for Numerical Methods in Engineering 24 (1987), 1, 271–284.

[53]   Voller, V.R., N.C. Markatos and M. Cross, Techniques for accounting for the moving interface in a convection/diffusion phase change, In Numerical Methods in Thermal Problems (Edited by R.W. Lewis and K. Morgan); Pineridge Press, Swansea 4 (1985), 595–609.

[54]   Voller, V.R., N.C. Markatos and M. Cross, Solidification in Convection-Diffusion, In Numerical Simulation of Fluid Flow and Heat/Mass Transfer Processes (Edited by N.C. Markatos, D.G.Tatchell, M. Cross and N. Rhodes); Springer Berlin (1986), 425–432.

[55]   Chiesa, F.M. and R.I.L. Guthrie, Natural Convective Heat Transfer Rates During the Solidification and Melting of Metals and Alloy Systems, Journal of Heat Transfer 96 (1974), 3, 377.

[56]   Szekely, J. and P.S. Chhabra, The effect of natural convection on the shape and movement of the melt-solid interface in the controlled solidification of lead, Metallurgical and Materials Transactions B 1 (1970), 5, 1195–1203.

[57]   Morgan, K., A numerical analysis of freezing and melting with convection, Computer Methods in Applied Mechanics and Engineering 28 (1981), 3, 275–284.

[58]   Gau, C. and R. Viskanta, Melting and solidification of a metal system in a rectangular cavity, International Journal of Heat and Mass Transfer 27 (1984), 1, 113–123.

[59]   Lally, B., L. Biegler and H. Henein, Finite difference heat-transfer modeling for continuous casting, Metallurgical Transactions B 21 (1990), 4, 761–770.

[60]   Lait, J.E., Solidification and heat transfer in the continuous casting of steel, Master Thesis, University of British Columbia, Vancouver, Canada, 1973.

[61]   Sparrow, E.M., S. v. Patankar and S. Ramadhyani, Analysis of Melting in the Presence of Natural Convection in the Melt Region, Journal of Heat Transfer 99 (1977), 4, 520–526.

[62]   Kroeger, P.G. and S. Ostrach, The solution of a two-dimensional freezing problem including convection effects in the liquid region, International Journal of Heat and Mass Transfer 17 (1974), 10, 1191–1207.

[63]   Ramachandran, N., J.P. Gupta and Y. Jaluria, Thermal and fluid flow effects during solidification in a rectangular enclosure, International Journal of Heat and Mass Transfer 25 (1982), 2, 187–194.

[64]   Gadgil, A. and d. Gobin, Analysis of Two-Dimensional Melting in Rectangular Enclosures in Presence of Convection, Journal of Heat Transfer 106 (1984), 1, 20–26.

[65]   Brimacombe, J.K., Design of continuous casting machines based on a heat-flow analysis: state-of-the-art review, Canadian Metallurgical Quarterly 15 (1976), 2, 163–175.

[66]   Tsai, C.L. and C.C. Lin, diffusion in a solid cylinder PartI: advancing model, Journal of Marine Science and Technology 22 (2015), 2, 133–144.

[67]   H. Mehrer (Ed.), Diffusion in Solids: Fundamentals, Methods, Materials, Diffusion-Controlled Processes, Springer-Verlag GmbH, Berlin Heidelberg, 2007.

[68]   Goldberg, D. and G.R. Belton, The diffusion of carbon in iron-carbon alloys at 1560°C, Metallurgical Transaction 5 (1974), 7, 1643–1648.

[69]   Ohnaka, I., Mathematical analysis of solute redistribution during solidification with diffusion in solid phase, ISIJ International 26 (1986), 12, 1045–1051.

[70]   Höglund, L. and J. Ågren, Simulation of Carbon Diffusion in Steel Driven by a Temperature Gradient, Journal of Phase Equilibria and Diffusion 31 (2010), 3, 212–215.

[71]   Zhang, L. und F. Oeters, Schmelzen und Mischen von Legierungsstoffen in Stahlschmelzen: Methoden der mathematischen Modellierung, Verlag Stahleisen GmbH, Düsseldorf, Germany, 2012.

[72]   Ågren, J., A Revised expression for the diffusivity of carbon in binary Fe-C austenite, Scripta Metallurgica 20 (1986), 1057–1510.

[73]   Ueshima, Y., S. Mizoguchi, T. Matsumiya and H. Kajioka, Analysis of solute distribution in dendrites of carbon steel with δ/γ transformation during solidification, Metallurgical Transactions B 17 (1986), 4, 845–859.

[74]   Bester, H. and K.W. Lange, Abschätzung mittlerer Werte für die Diffusion von Kohlenstoff, Sauerstoff, Wasserstoff, Stickstoff und Schwefel in festem und flüssigen Eisen, Arch. Eisenhüttenwesen 43 (1972), 3, 207–213.

[75]   Wanibe, Y., S. Takai, T. Fujisawa and H. Sakao, Temperature-dependency of Interdiffusion in Molten Fe-C Alloy, Transactions ISIJ 22 (1982), 560–565.

[76]   Parris, D.C. and R.B. McLellan, The diffusivity of carbon in austenite, Acta Metallurgica 24 (1976), 6, 523–528.

[77]   Wells, C., W. Batz and R.F. Mehl, Diffusion coefficient of carbon in austenite, JOM 2 (1950), 3, 553–560.

[78]   Won, Y.-M. and B.G. Thomas, Simple model of microsegregation during solidification of steels, Metallurgical and Materials Transactions A 32 (2001), 7, 1755–1767.

[79]   Miettinen, J., Calculation of solidification-related thermophysical properties for steels, Metallurgical and Materials Transactions B April (1997), Volume 28 B, 281–297.

[80]   Miettinen, J. and S. Louhenkilpi, Calculation of Thermal Properties of Carbon and Low Alloyed Steels for Modeling of Solidification Processes, Metallurgical and Materials Transactions B December (1994), Volume 25B, 909–916.

[81]   Mills, K.C., S. Karagadde, P.D. Lee, L. Yuan and F. Shahbazian, Calculation of Physical Properties for Use in Models of Continuous Casting Process-Part 2: Steels, ISIJ International 56 (2016), 2, 274–281.

[82]   O'Connor, T.G. and J.A. Dantzig, Modeling the thin-slab continuous-casting mold, Metallurgical and Materials Transactions B 25 (1994), 3, 443–457.

[83]   Thomas, B.G., Investiagation of panel crack formation in steel ingots using mathematical and physical models, PhD thesis, University of British Columbia, Vancouver, Canada, 1985.

[84]   Lytvynyuk, Y., J. Schenk, M. Hiebler and A. Sormann, Thermodynamic and Kinetic Model of the Converter Steelmaking Process. Part 2: The Model Validation, steel research international 85 (2014), 4, 544–563.

[85]   Lytvynyuk, Y., J. Schenk, M. Hiebler and A. Sormann, Thermodynamic and Kinetic Model of the Converter Steelmaking Process. Part 1: The Description of the BOF Model, steel research international 85 (2014), 4, 537–543.

[86]   Lytvynyuk, Y. Schenk, J. Hiebler, M. Mizelli, H., Thermodynamic and kinetic modelling of the De-vanadization process in the steelmaking converter, Proceedings of EOSC (2011), Program No. 06-06.

[87]   Bundschuh, P., J. Schenk, S. Schütt, H. Panhofer and A. Sormann, Impact of Different Heat Capacity Functions on Thermodynamic and Kinetic Modeling of the Basic Oxygen Furnace, Proceedings of AISTech (2015), 2090–2098.

[88]   Penz, F.M., J. Schenk, R. Ammer, G. Klösch and K. Pastucha, Evaluation of the Influences of Scrap Melting and Dissolution during Dynamic Linz–Donawitz (LD) Converter Modelling, Processes 7 (2019), 4, 186.

[89]   Penz, F.M., P. Bundschuh, J. Schenk, H. Panhofer, K. Pastucha and A. Paul, Impact of Carbon, Silicon and Manganese contents on the dissolution and melting behaviour of scrap in a dynamic BOF model, In Proceedings of the European steel technology and application days 2017 (ESTAD), Vienna, Austria, 26–29 June 2017; CD-ROM.

[90]   Penz, F.M., J. Schenk, P. Bundschuh, H. Panhofer, K. Pastucha and B. Maunz, Scrap melting in BOF: Influence of particle surface and size during dynamic

converter modelling, In Proceedings of the 3rd ABM Week 02.-06.10.2017, Sao Paolo, Brazil (2017), 1–12.

[91]   Chigwedu, C., Beitrag zur Modelierung des LD-Sauerstoffblasverfahrens zur Stahlerzeugung, PhD thesis, TU Clausthal, Clausthal-Zellerfeld, Germany, 1997.

[92]   Szekely, J., Y.K. Chuang and J.W. Hlinka, The melting and dissolution of low-carbon steels in iron-carbon melts, Metallurgical Transactions 3 (1972), 11, 2825–2833.

[93]   Chuang, Y.K. and J. Szekely, On the use of Green's functions for solving melting or solidification problems, International Journal of Heat and Mass Transfer 14 (1971), 9, 1285–1294.

[94]   Olsson, R.G., V. Koump and T.F. Perzak, Rate of Dissolution of Carbon in Molten Fe-C alloys, Transactions of the Metallurgical Society of AIME 236 (1966), 4, 426–429.

[95]   Oeters, F., Metallurgie der Stahlherstellung, Springer Berlin Heidelberg, Berlin, Heidelberg, 1989.

[96]   Ehrich, O., Y.K. Chuang and K. Schwerdtfeger, The melting of metal spheres involving the initially frozen shells with different material properties, International Journal of Heat and Mass Transfer 21 (1978), 3, 341–349.

[97]   Ehrich, O., Y.K. Chuang and K. Schwerdtfeger, The melting of sponge iron spheres in their own melt, Arch. Eisenhüttenwesen 50 (1979), 8, 329–334.

[98]   Dogan, N., Mathematical modelling of oxygen steelmaking, PhD thesis, Swineburne University of Technology, Melbourne, Australia, 2011.

[99]   Dogan, N., G.A. Brooks and M.A. Rhamdhani, Comprehensive Model of Oxygen Steelmaking Part 1: Model Development and Validation, ISIJ Int. 51 (2011), 7, 1086–1092.

[100]   Dogan, N., G.A. Brooks and M.A. Rhamdhani, Comprehensive Model of Oxygen Steelmaking Part 2: Application of Bloated Droplet Theory for Decarburization in Emulsion Zone, ISIJ Int. 51 (2011), 7, 1093–1101.

[101]   Dogan, N., G.A. Brooks and M.A. Rhamdhani, Comprehensive Model of Oxygen Steelmaking Part 3: Decarburization in Impact Zone, ISIJ Int. 51 (2011), 7, 1102–1109.

[102]   Brooks, G., Y. Pan, B. Subagyo and K. Coley, Modeling of trajectory and residence time of metal droplets in slag-metal-gas emulsions in oxygen steelmaking, Metallurgical and Materials Transactions B 36B (2005), 525–535.

[103]   Asai, S. and I. Muchi, Effect of Scrap Melting on the Process Variables in LD Converter Caused by the Change of Operating Conditions, Transactions ISIJ Vol. 11 (1971), 107–115.

[104]   Rout, B.K., G. Brooks, M.A. Rhamdhani, Z. Li, F.N.H. Schrama and J. Sun, Dynamic Model of Basic Oxygen Steelmaking Process Based on Multi-zone Reaction Kinetics: Model Derivation and Validation, Metallurgical and Materials Transactions B 49 (2018), 2, 537–557.

[105]   Rout, B.K., G. Brooks, M. Akbar Rhamdhani, Z. Li, F.N.H. Schrama and A. Overbosch, Dynamic Model of Basic Oxygen Steelmaking Process Based on Multizone Reaction Kinetics: Modeling of Decarburization, Metallurgical and Materials Transactions B 49 (2018), 3, 1022–1033.

[106]   Rout, B.K., G. Brooks, M. Akbar Rhamdhani, Z. Li, F.N.H. Schrama and W. van der Knoop, Dynamic Model of Basic Oxygen Steelmaking Process Based on Multizone Reaction Kinetics: Modeling of Manganese Removal, Metallurgical and Materials Transactions B 49 (2018), 5, 2191–2208.

[107]   Schöne, D., Praxisnahe Entwicklung eines dynamischen LD-Konvertermodells unter besonderer Berücksichtigung betrieblich bedingter Einflussfaktoren und statistischer Modellauswertungen, Dissertation, RWTH Aachen, Germany, 2013.

[108]   Kruskopf, A., Multiphysical Modeling Approach for Basic Oxygen Steelmaking Process, PhD thesis, Aalto University, School of Chemical Technology, Finland, 2018.

[109]   Kruskopf, A., A 2D Axisymmetric Mixture Multiphase Model for Bottom Stirring in a BOF Converter, Metallurgical and Materials Transactions B 48 (2017), 1, 619–631.

[110]   Kruskopf, A. and V.-V. Visuri, A Gibbs Energy Minimization Approach for Modeling of Chemical Reactions in a Basic Oxygen Furnace, Metallurgical and Materials Transactions B 48 (2017), 6, 3281–3300.

[111]   Kruskopf, A. and S. Louhenkilpi, 1-Dimensional scrap melting model for steel converter (BOF), Proceedings of METEC & 2nd ESTAD, june 15-19, Düsseldorf, Germany (2015), 1–4.

[112]   Li, J. and N. Provatas, Kinetics of Scrap Melting in Liquid Steel: Multipiece Scrap Melting, Metallurgical and Materials Transactions B 39 (2008), 2, 268–279.

[113]   Li, G. and B.G. Thomas, Transient thermal model of the continuous single-wheel thin-strip casting process, Metallurgical and Materials Transactions B 27 (1996), 3, 509–525.

[114]   Penz, F.M., J. Schenk, R. Ammer, G. Klösch and K. Pastucha, Dissolution of Scrap in Hot Metal under Linz–Donawitz (LD) Steelmaking Conditions, Metals 8 (2018), 12, 1078 (1-9).

[115]   Penz, F.M., J. Schenk, R. Ammer, G. Klösch, K. Pastucha and M. Reischl, Diffusive Steel Scrap Melting in Carbon-Saturated Hot Metal-Phenomenological Investigation at the Solid-Liquid Interface, Materials 12 (2019), 8, 1358.

[116]   Penz, F.M., J. Schenk, R. Ammer, K. Pastucha and B. Maunz, Dissolution behaviour of ULC steel in carbon saturated hot metal, La Metallurgia Italiana (2018), 11/12, 36–45.

[117]   Specht, E. and R. Jeschar, Kinetics of steel melting in carbon-steel alloys, Steel Research Vol. 64 (1993), 1, 28–34.

[118]   Shih, T.-M., Heat transfer: Lessons with examples solved by matlab, Cognella Academic Pub, San Diego, CA, USA, 2012.

[119]   Magrab, E.B., S. Azarm, B. Balachandran, Duncan, J.H. und K.E. Herold et al., An engineer's guide to MATLAB, 3rd edition, Prentice-Hall, Upper Saddle River, NJ, USA, 2011.

[120]   Crank, J., The mathematics of diffusion, 2. ed., 9. reprinted., Clarendon Press, Oxford, 1995.

[121]   Shukla, A.K., B. Deo and D.G.C. Robertson, Scrap Dissolution in Molten Iron Containing Carbon for the Case of Coupled Heat and Mass Transfer Control, Metallurgical and Materials Transactions B 44 (2013), 6, 1407–1427.

[122]   Lagerstedt, A., J. Kron, F. Yosef and H. Fredriksson, Measurements and modeling of air gap formation in iron-base alloys, Materials Science and Engineering: A 413-414 (2005), 44–51.

[123]   Kron, J., A. Lagerstedt and H. Fredriksson, Measurements and modelling of air gap formation in aluminium based alloys, International Journal of Cast Metals Research 18 (2005), 1, 29–40.

[124]   Shukla, A.K., B. Deo and Robertson, D. G. C., Role of Air Gap in Scrap Dissolution Process, Metallurgical and Materials Transactions B 44 (2013), 6, 1398–1406.

1 Attachment A: Publications

Publication 1:

A Review of Steel Scrap Melting in Molten Iron-Carbon Melts

A Review of Steel Scrap Melting in Molten Iron-Carbon Melts

Florian M. Penz* and Johannes Schenk

In the current economic climate, the recycling of steel scrap is become one of the most interesting tasks for the optimization of integrated steel plants. Steelmaking aspects such as jet/bath interaction, slag formation or foaming, lime dissolution as well as slag/metal reactions have received more attention in recent years than the melting and dissolution phenomena of steel scrap in molten steel baths. Since the dynamic modeling of steelmaking processes - especially the Linz Donawitz oxygen steelmaking process (LD) - is becoming more important, interest in the melting and dissolution behaviour is increasing. Several researchers have investigated the complex transactions of coupled heat and mass transfer in the past. Small-scale experiments are carried out under conditions where only mass transfer or heat transfer were considered. A few authors have reported on pilot-scale investigations or commercial converters. The coupled heat and mass transfer has also been analyzed by several authors in mathematical models and numerical simulations. The present paper reviews the research on steel scrap melting and dissolution done in the last 50 years. A summary of all reported heat and mass transfer coefficients will be given and the differences between natural and forced convection will be explained. In addition, an overview of recently published numerical simulation describing the problem will give an outlook for future work.

1. Introduction

In modern steelmaking, the LD converter, invented in the early 1950s in Linz and Donawitz (LD), is the dominant reactor to convert hot metal into crude steel.[1] Through the oxidation of carbon, silicon, manganese, and phosphorus with technically pure oxygen, heat is generated. The oxygen is supplied through a water-cooled lance and blown onto the liquid hot metal at supersonic speed during the process. Therefore, right at the beginning of each heat, scrap is charged, which acts, beside hot metal, as both an iron source and a coolant. The oxygen steelmaking process nowadays is also an important recycling process.[1-3] Due to economic reasons, for example, increasing emissions of carbon dioxide, scrap has become a valuable iron source because it needs no reduction energy as compared with iron ore.[4]

An increase in crude steel production up to 1670 million tons has been registered in the recent years. The share of crude steel produced by the Basic Oxygen Furnace (BOF) was 72.7% in 2017. The total scrap used for crude steel production in 2017 increased steadily to 600 million tons.[5] The biggest steel scrap user is China while the EU-28 is the world's leading steel scrap exporter. These values show that the recycling of used materials has become a worldwide trend, as symbolized by the issues of the global environment. Steel scrap has become an ecological and beneficial raw material as well as an internationally traded commodity.[5] It is more than desirable to utilize scrap from the viewpoint of energy and resource saving and to improve its application as a raw material to receive higher yields in production. The melting and dissolution behaviour of scrap is the main parameter to use scrap as a raw material, which is why scrap melting and dissolution should be investigated in detail. The last few decades brought up research activities regarding the acquirements of the optimum conditions such as the size and shape of scrap, its chemical composition or the degree of preheating and so on.[4,6] The modeling of the scrap melting has been emphasized over the past 20 years.

In the following chapters, the authors will critically summarize the work and findings from almost all previous publications about steel scrap melting in molten hot metal. An overview to the phenomenological understanding as well as theoretical considerations will lead into the research topic in the first two chapters. Further, this review classifies the past research work into the following categories:

- Single mass transfer experiments[7-17]
- Heat transfer experiments[18-26]
- Simultaneous heat and mass transfer in small-scale experiments[9,24,27-31]
- Simultaneous heat and mass transfer in converter experiments[32-38]
- Modeling of scrap melting[2,21,26,39-49]

F. M. Penz
K1-MET GmbH
Stahlstraße 14, 4020 Linz, Austria
E-mail: florian-markus.penz@k1-met.com

Prof. J. Schenk
Chair of Ferrous Metallurgy Montanuniversitaet
Franz Josef Straße 18, 8700 Leoben, Austria

CSO of K1-MET GmbH
Stahlstraße 14, 4020 Linz, Austria

The ORCID identification number(s) for the author(s) of this article can be found under https://doi.org/10.1002/srin.201900124.

ADVANCED
SCIENCE NEWS

www.advancedsciencenews.com

steel
research
international

www.steel-research.de

Additional references will support the reader to get an additional overview of possible overlaps with other research areas. These overlaps are necessary to understand the complex topic of the melting and dissolution behavior of scrap and will provide a fundamental collection for further research work in this specific field.

2. Pioneer Work and Phenomenological Understanding

The first published research on the isothermal transfer from solid to liquid was done by Lommel and Chalmers in ref. [11]. They investigated the transport behavior from solid lead into liquid lead-tin alloy, whereby the diffusion of tin atoms into the solid lead was not a necessary condition for mass transfer in the absence of stirring the liquid. Furthermore, Lommel and Chalmers assumed that in a stirred liquid phase, the mass transport in the liquid adjacent to the interface occurs by volume diffusion through a boundary layer of thickness δ. As they refer their work to a lead/lead-tin-alloy system, the initial concentration of the liquid (C_{HM}) is lower than the initial concentration of the solid (C_{scrap}). In their research they also mentioned that the absolute rate of reaction at the solid liquid interface must have a certain activation energy for melting or freezing.[11]

Based on the work of Lommel and Chalmers, the research groups around Pehlke et al. [9] and Olsson et al. [12] pioneered on carbon-steel scrap dissolution in molten iron-carbon alloys during small-scale experiments. In their experiments, rotating or static cylindrical rods of various sizes were submerged into hot metal baths under different conditions and temperatures. While Pehlke et al. submerged scrap samples at room temperature into the liquid bath,[9] Olsson et al. only reported on mass transfer measurements at equilibrium temperature between scrap and hot metal.[12]

Pehlke et al. carried out their experiments in a 90 kg induction furnace in the range of 1260 °C up to 1454 °C and carbon contents of approximately 4 wt% down to 2 wt%. In order to evaluate the ablation rate of the samples, the radius was measured manually after a specific submerging time (30 s–6 min). The different bath conditions were listed as induction stirring by the furnace power, mechanical stirring and induction stirring, mechanical stirring with switched off furnace or stagnant fluid without any stirring. They concluded, for large specimens and low temperatures, a shell formation on the surface of the steel bar, which retards the dissolution. Additionally, the radius decreases linearly with time and the dissolution rate is higher at higher temperature, increasing stirring velocity and increasing carbon contents in the melt.[9]

Olsson et al. used graphite crucibles containing graphite-saturated hot metal, in a vertical purified argon flushed silica tube, heated by an induction coil. The mass of the hot metal was 1200 g and the temperature kept constant at a desired value between 1274 °C and 1500 °C. The carbon concentration of the sample was between 0.008 wt% and 1 wt.% and the mechanical stirring speed of the cylindrical rod was between 32 and 1210 rpm. They based their findings on the more fundamental investigations of rotating disk investigations of Shurygin and Shantarin,[50] who proposed that the rate of dissolution of the iron disk was limited by the diffusion of the elements in the

Florian Markus Penz did his Master degree in Metallurgy in 2015 at Montanuniversitaet Leoben and is currently working as PhD-researcher at the Austrian Metallurgical Competence Center K1-MET in Leoben. His main research interests are the numerical simulation of the scrap melting and dissolution behaviour for dynamic LD converter modeling.

Dr. Johannes Schenk is Professor for Ferrous Metallurgy at the Montanuniversitaet Leoben since 2008 and Chief Scientific Officer (CSO) of the Austrian Metallurgical Competence Center K1-MET since 2015. He did his PhD in Chemical Engineering at Graz University of Technology in 1989 and was than working in Siemens VAI in the research and development of new direct and smelting reduction technologies. One of his current research focus is thermodynamic and kinetic modeling of iron and steelmaking processes.

boundary layer. The expression for the boundary layer thickness they used, commonly defined as δ, is given by Levič[51] at page 69. The proposed rate of dissolution, N, including Levič's expression is given in Equation (1).[12,50,51]

$$N = \frac{D}{\delta} A (C_{scrap} - C_{HM})$$
$$= 1.95 * r^2 D^{2/3} v^{-1/6} \omega^{1/2} (C_{scrap} - C_{HM}) \qquad (1)$$

In Equation (1), D is the diffusion coefficient, A is the surface area and r defines the radius of the sample. The parameters v and ω describe the kinematic viscosity and the angular velocity.

In the research article of Olsson et al.,[12] they did not mention any shell formation in the initial seconds of scrap melting. They concluded that if the dissolution of the carbon steel samples is controlled by counter diffusion of iron and carbon in the boundary layer, the liquid and solid at the interface will be in equilibrium. They assumed that therefore, the liquid at the interface would have the liquidus composition in (wt%) corresponding to the bath temperature (C_{liq}), which would result in the modified dissolution equation by Lommel and Chalmers in Equation (2), with equal densities in the solid and liquid.[11,12]

$$-\frac{dr}{dt} = k_{met} * \ln\left(1 + \left(\frac{\%C_{liq} - \%C_{HM}}{\%C_{Scrap} - \%C_{liq}}\right)\right) \qquad (2)$$

In Equation (2), $k_{met} = D/\delta$ is the mass transfer coefficient in (m/s), which is expressed by Lommel and Chalmers as the ratio between the diffusion coefficient D and the boundary layer

**ADVANCED
SCIENCE NEWS**

www.advancedsciencenews.com

**steel
research**
international

www.steel-research.de

thickness δ. The concentrations in the logarithmic term are in (wt%). Mentionable is, that Lommel and Chalmers used a concentration independent diffusion coefficient.[11]

To sum up the phenomenological understanding, it is necessary to mention that two main occurrences are important for scrap melting. The first is the mass transfer, especially from carbon, and the second is the heat transfer, especially in non-isothermal systems, that could lead to the formation of a frozen shell of hot metal on the scrap surface. The pioneer work also showed that bath agitation and temperature influences the dissolution and melting behavior of scrap. It is essential to know that commonly constant material properties have been used. The upcoming chapters will deal with theoretical consideration of the scrap melting, the dissolution of scrap focusing on the mass transfer as well as the heat transfer and the modeling.

3. Theoretical Description

If a solid particle is charged into a liquid with the same chemical composition, the melting consists of two parts: the heating of the particle to the liquidus temperature and the phase transition to liquid state. In this case, the melting process is only dependent on the heat transfer. The fundamentals of this process are well summarized by Oeters.[52] To solve this problem analytically, the Fourier differential equation for heat conduction (second Fourier law) has to be solved including a moving boundary problem. The phenomenon of a shell formation during the initial moments of submerging a cold solid particle into a liquid melt is also reported, which will melt rapidly after reaching its maximum.[19,21,22,26,53,54]

Assuming that the solid steel scrap has a different composition from the liquid hot metal, as usual in an LD converter, the melting is extended with dissolution phenomena including multiphase systems with temperature as well as chemical composition-dependent liquidus and solidus lines. This leads to a coupled heat and mass transfer at the solid-liquid interface, especially if the temperature of the liquid phase is below the liquidus temperature of the solid scrap.[53] It has been reported in several publications that the melting rate is dependent on the difference in carbon content between the scrap and the liquid hot metal as given already in Equation (2).[9,12] **Figure 1** shows the Fe-Fe$_3$C phase diagram of a common S235JR construction steel scrap with variable carbon content. The square blue points in Figure 1 show the specific isothermal carbon concentrations of the scrap (C_{scrap}) and the assumed composition of the liquid hot metal (C_{HM}) as well as the solidus (C_s^*) and liquidus (C_l^*) concentrations at 1300 °C. Further, **Figure 2** shows the concentration and temperature profiles at the solid-liquid interface. The subscript init stands for the initial concentration or temperature. The liquid metal has an initial temperature of T_{HM} and a carbon concentration of C_{HM} before the cold specimen is submerged into the liquid. The scrap initial carbon concentration C_{scrap}^{init} and temperature T_{HM}^{init} is uniform over the whole transverse section. Immediately after immersion of the sample, temperature, and concentration gradients will occur in the liquid and solid. At the interface, a slightly lower temperature T_s than the hot metal will be reached. The equilibrium concentration achieved in the liquid for the
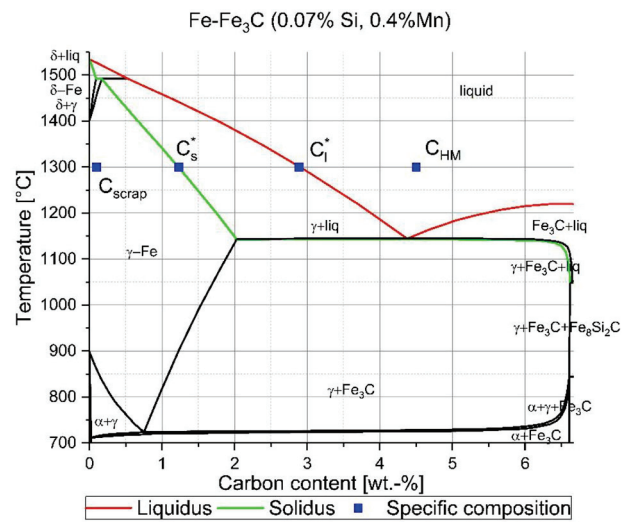
Figure 1. Fe-Fe$_3$C phase diagram of common S235JR construction steel scrap with variable carbon content including schematic points of carbon concentrations.

temperature T_s is C_l^* and C_s^* in the solid. The boundary layers in the liquid for heat and mass transfer are δ_T and δ_C, respectively. Both are related to each other due to convective flow in the liquid. According to temperature-dependent physical and chemical parameters like the density the liquid melt will be under natural convection or the bath is under forced convection.[4,6,21,26,29,35,55] Krupennikov and Filimonov describe in ref. [56] the direct solution of steel in iron carbon melts in two successive stages: the transition of iron atoms through the phase boundary (kinetic stage) and their subsequent diffusion through the boundary layer into the melt (diffusion stage). Their theoretical consideration produces the result, that the carbon concentration on the surface of the solid has to be equal to C_s^* at

Figure 2. Schematic diagram of mass and heat transfer between cold scrap and liquid hot metal.

ADVANCED
SCIENCE NEWS

www.advancedsciencenews.com

steel
research
international

www.steel-research.de

the solidus temperature. This leads to a chemical potential difference $\Delta\mu(C_s^*, C_l^*)$ between the iron atoms on the surface of the solid and in the melt at the phase boundary. Additionally, they mention that the formation of liquid phase in the decomposition of supersaturated solid solution is due to a breakdown of the solid's crystalline structure, which results in a reduction of activation energy characterizing the kinetic stage. However, no significant kinetic factors retarding the melting process have been observed as yet.[56]

In Figure 2 it is shown that the heat is transported from the liquid into the solid scrap. The heat transport in the interior is executed solely by heat conduction. Carbon is transported steadily to the interface through convection and will diffuse into the solid scrap. As the scrap is dissolved or melted, there also has to be a transfer from the dissolved material into the bulk. Through the dissolution of the scrap, latent heat for phase transformation will be released. The general equations for the diffusion (Fick,s second law) and the heat conduction (Fourier's second law) are given in Equations (3) and (4) with the three dimensional differential operator ∇.[20,57–60]

$$\frac{\partial C}{\partial t} = \nabla \cdot (D\nabla C) \tag{3}$$

$$c_p\rho\frac{\partial T}{\partial t} = \nabla \cdot (\lambda\nabla T) \tag{4}$$

Regarding the pioneering work of Olsson et al.[12] and Pehlke et al.,[9] who conducted their research on cylindrical specimens, the general equations can be transferred to the more common forms for cylindrical coordinates, given in Equations (5) and (6). The axial flow in radial direction (r) is given if $\partial/\partial z = \partial/\partial\theta = 0$ and $0 < r < r(t)$:

$$\frac{\partial C}{\partial t} = D\left(\frac{\partial^2 C}{\partial r^2} + \frac{1}{r}\frac{\partial C}{\partial r}\right) \tag{5}$$

$$\frac{\partial T}{\partial t} = \frac{\lambda}{C_P\rho}\left(\frac{\partial^2 T}{\partial r^2} + \frac{1}{r}\frac{\partial T}{\partial r}\right) \tag{6}$$

where T and C are the temperature and concentration, respectively. The diffusion coefficient is D, c_p is the specific heat capacity, ρ is the density and λ is the thermal conductivity of the scrap. As it is well known that D, c_p, ρ, and λ are functions of temperature and/or chemical composition, they are assumed to be constant in most previous publications.[12,19–21,29,55] Information about temperature and chemical composition-dependent parameters can be found in ref. [61–65] for D, in ref. [66–72] for λ or in ref. [69,70,73,74] for ρ. Temperature-dependent functions for the specific heat capacity can be determined with thermodynamic software, for example FactSage™.

The boundary conditions for the heat transfer are defined as follows:

$$\frac{\partial T}{\partial r} = 0 \text{ at } r = 0, \ t \geq 0 \tag{7}$$

$$-\lambda * \frac{\partial T}{\partial r} = h * (T_S - T_{HM}) + S \text{ at } r = r(t), t \geq 0 \tag{8}$$

where the heat transferred into the solid is dependent on the heat transfer coefficient h in the liquid and S is the source term for the released latent heat of phase transformation. In Equation (8), $r(t)$ states that the solid liquid interface is moving and therefore the actual radius is a function of time.[6] Assuming that the boundary layer thickness is moving toward 0, it can be supposed that the surface concentration is a constant and equal to the carbon concentration of the melt. For this case, an analytical solution was found by Mehrer in ref. [57] on page 50.

According to the theory by Lommel Chalmers in ref. [11] modified by Olsson et al. in ref. [12] given in Equation (2), the rate of movement at the interface in a isothermal liquid-solid system is described by using the weight fraction. Glinkov et al. explained in ref. [7] that the distribution of carbon concentration in (kg m^{-3}) in both the liquid phase and in the boundary layer was assumed to be constant with time. A specific carbon concentration at the phase boundary ($C_{interface}$ in [kg m^{-3}]) was not given. The published expression from Glinkov et al. for the mass transfer is given in Equation (9) and was appropriate for their experiments on mass transfer. Equation (9) is only valid if the densities of the solid and liquid are assumed to be equal.[7]

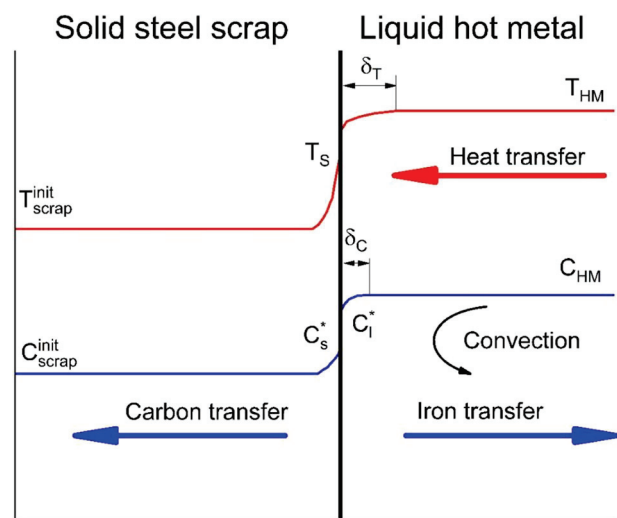$$-\frac{dr}{dt} = k'_{met} * \left(\frac{C_{HM} - C_{interface}}{C_{HM} - C_{scrap}}\right) \tag{9}$$

In Equation (9), the concentrations are given in kg m^{-3}. The mass transfer coefficient k'_{met} used is connected to k_{met} by the function $f(\xi) = \xi/(1-e^{-\xi})$ using the dimensionless value ξ. It is the ratio of the velocity of the boundary movement with the mass transfer. With high values of ξ the mass transfer will increase, resulting in the mass transfer only being dependent on the boundary movement velocity. A detailed description of this explanation is given by Zhang and Oeters.[53]

It can be seen that the dissolution rates are controlled by the interdiffusion of iron and carbon in the liquid boundary layer. For the reason, the kinetics of scrap dissolution essentially belongs to the class of moving boundary problems with phase change, also known as a Stefan problem. A comprehensive theoretical explanation of Stefan problems can be found in various research articles, for example[75–77] It should be kept in mind that the values of mass transfer also depend on the scrap geometry and the condition of the liquid bath as well as various physical parameters that include the diffusion coefficients. It could be concluded that scrap melting and dissolution is divided into three stages, all of which are illustrated in literature by several authors[6,23,35,36,43,44,78]:

- Initial solidification stage of liquid hot metal at the surface of cold scrap, which remelts fast after enough superheat is available from the heat transfer.
- Dissolution stage of the original scrap, depending on liquid and solidus compositions. The superheat is consumed to promote the necessary mass transfer. This stage is also defined as diffusive melting. Especially if the heat transfer is much faster than the mass transfer and the carbon content in the solid steel is much lower than in the liquid melt, only mass transfer has to be considered.

**ADVANCED
SCIENCE NEWS**

www.advancedsciencenews.com

**steel
research**
international

www.steel-research.de

- If the temperature of the hot metal exceeds the melting point of the scrap or the carbon content in the solid is equal to that of the melt, only heat transfer should be considered. This stage is defined as forced scrap melting, as well.[18,21,23,26,35]

Generally, a simultaneous heat and mass transfer should be considered.

4. Mass Transfer

To determine the mass transfer, two types of experimental procedures are available. The first procedure to perform experiments is, where a static specimen is submerged into a stagnant fluid or a fluid is tapped onto a surface of a specimen with no further forced convection. In this case, the mass transfer under natural convection can be described. Those experiments require less equipment and are more simple to perform. Natural convection occurs during all processes, where a portion of the melt is at a higher temperature than the melting point of the solid phase. These conditions usually have a temperature gradient and hence, a density gradient. These gradients appear in the liquid close to the reaction surface with a normal component in the direction of gravity. A complete stagnant bath could therefore not be realized.[13,20,79] The second procedure is that forced convection leads to agitation of the bath. This might be realized mechanically through a rotating specimen or through gas-stirred systems. Especially in an LD converter, the blown oxygen results in a high bath agitation favorable for bath homogenization and accelerated mass transfer as well as increasing transfer rates.

4.1. Mass Transfer Under Natural Convection

In most cases the experimental apparatus to determine the mass transfer under natural convection was designed that under isothermal conditions the liquid melt is in a crucible and the specimen is submerged into it. A second procedure reported in literature is, that the sample is premelt and solidified in a crucible and the low-melting liquid is tilted onto the surface under isothermal conditions. With this setup the reaction area is assumed to stay constant. The reported results of both setups will be explained in this chapter.

Pehlke et al. carried out only one reported experiment without forced bath agitation in ref. [9]. However, they showed with this experiment that there is an influence of the bath agitation on the dissolution rate ($-dr/dt$) of a 0.0254 m diameter steel bar at 1371 °C. Without stirring, a linear dissolution rate of $36 * 10^{-5}$ m s^{-1} was attained.[9] In **Table 1** a selection of various reported mass transfer coefficients are listed.

Kosaka and Minowa investigated in a series of experiments the dissolution of steel cylinders in liquid Fe-C alloy. They correlated their static experiments on dimensionless relations by using the following dimensionless numbers, which allows a comparison of experimental results: Sherwood $\left(\text{Sh} = \frac{k_{\text{met}} * L}{D}\right)$, Reynolds $\left(\text{Re} = \frac{\rho_{\text{fluid}} VL}{\eta_{\text{fluid}}} = \frac{VL}{\nu_{\text{fluid}}}\right)$, Schmidt $\left(\text{Sc} = \frac{\nu_{\text{fluid}}}{D}\right)$ and Grashof $\left(\text{Gr} = \frac{g * L^3}{\nu_{\text{fluid}}^2} * \beta * (T_{\text{interface}} - T_{\text{HM}})\right)$. The characteristic length (L) is the diameter for cylinders or spheres; η_{fluid} and ν_{fluid} are the dynamic and kinematic viscosities of the liquid. The rotational speed on the cylinder surface is V. The acceleration of gravity is g and $\beta = -\frac{1}{\rho}\left(\frac{\partial \rho}{\partial T}\right)_p$ is the isobar thermal expansion coefficient with the pressure p.[8,80] The correlation Kosaka and Minowa established is given in Equation (10) and valid for $10^9 < \text{GrSc} < 10^{11}$.[8]

$$\text{Sh} = 0.11(\text{GrSc})^{1/3} \tag{10}$$

A further finding of Kosaka and Minowa was that the cylindrical rod takes on the shape of a truncated cone in a

Table 1. Selection of various mass transfer coefficients under natural convection reported in literature.

Initial diameter [m]	Hot metal temperature [°C]	Carbon content of the sample [wt%] or grade	Carbon content of the hot metal [wt%]	Mass transfer coefficient [m/s] * 10^{-6}	Maximum immersion time [s]	Literature
0.0254	1371	AISI 1020	3.84	9.9[13]	150	[9]
0.01	1350	0.15	3.64	23.1	120	[8]
0.0254	1482	0.10	4.74	12.3	150	[13]
0.0381	1482	0.10	4.74	11.5	240	[13]
0.0762	1471	0.10	4.71	14.6	480	[13]
0.012	1200	0.005	C-saturated iron	11.5	200	[14]
0.0121	1400	0.26	4.00	~30	150	[16]
0.012	1230	0.1	4.58	7.39–20.4	240	[27]
0.012	1300	0.1	4.58	16.1–26.8	240	[27]
0.012	1385	0.1	4.58	18.2–31.1	140	[27]
Constant area	1230	>0.001	2.17	63	60	[17]
Constant area	1325	>0.001	3.29	96	60	[17]
Constant area	1415	>0.001	4.23	124	60	[17]
0.04	1420	0.17	3.74	250	No time estimation possible	[30]

ADVANCED
SCIENCE NEWS
www.advancedsciencenews.com

steel
research
international
www.steel-research.de

non-external agitated melt. This effect arises due to density differences according to the dissolution of carbon, which results in a descending flow along the surface of the rod.[8] Guthrie and Stubbs carried out experiments to analyze the mass transfer from immersed steel rods with different radii in carbon saturated melt in ref. [13]. The dissolution rate was estimated as a function of radius diameter, bath temperature and bath carbon content. The mass transfer coefficient, k_{met} was predicted by the dimensionless correlation given in Equation (11).[13]

$$Sh = 0.13(GrSc)^{1/3} \tag{11}$$

Experimentally, Guthrie and Stubbs obtained the following equation for the mass transfer coefficient k_{GS} [m s^{-1}], given in Equation (12), whereby their conclusion indicated that the experimental mass transfer k_{GS} is 0.3 to 0.6 times the predicted k_{met}.[13]

$$k_{GS} = \frac{dr}{dt} * \frac{\frac{\rho_{solid}}{\rho_{liq}} * \%C_{liq} - \%C_{scrap}}{\%C_{HM} - \%C_{liq}} \tag{12}$$

Dissolution of pure iron and solid iron-carbon alloy into hot metal was studied under isothermal conditions by Kim and Pehlke.[10] Cylinders 0.127 and 0.0254 m in diameter were preheated to bath temperature and submerged into the melt with undefined carbon content for a specific time. They observed the same melting shape formation of a truncated cone as Kosaka and Minowa.[8] The mass transfers were derived from the equation of Lommel and Chalmers[11] given in Equation (2). Their results of the isothermal experiments are represented in the dimensionless correlation given in Equation (13), valid for $6.9 * 10^8 < GrSc < 7.7 * 10^9$.[10]

$$Sh = 0.149(GrSc)^{0.294} \tag{13}$$

An observation of Kim and Pehlke was a decreasing total dissolution time with increasing temperature. This could be derived from the increasing dissolution rate with increasing temperature from their research results. The thickness of the boundary layer was estimated to be 58 μm for 1242 °C and stationary conditions.[10]

In their research in ref. [14], Mori and Sakuraya investigated the influence of the evolution of CO, which forms, if there is a high oxygen concentration in the specimen. Through the evolution of CO, a forced convection indirectly arises. Nevertheless, they observed the same cone shape in Al-killed steels, where no CO formation occurs, as already stated in ref. [8,10]. The lowest mass transfer coefficient observed for aluminum-killed iron at 1200 °C was $11.5 * 10^{-6}$ ms^{-1}. The mass transfer also increases with rising temperature, comparable to the other authors mentioned before.

In quiescent iron-carbon melts, Wright investigated the dissolution rates of commercial black iron rods in ref. [16], finding the dimensionless correlation for a turbulent natural convective flow, given in Equation (14). The correlation is valid for $GrSc > 10^9$ and is closely related to that of Guthrie and Stubbs.[13] The steel rods, 0.0121 m in diameter, with varying immersion depths and a carbon content of 0.26 wt%, were submerged either in a 1 kg or 25 kg iron bath, the temperature of the bath ranging from 1260 °C to 1460 °C and the carbon concentrations of the melt from 2 to 4.5 wt% carbon.[16]

$$Sh = 0.13(GrSc)^{0.34} \tag{14}$$

Wright was able to show that the dissolution rates increase with increasing carbon content and temperature of the bath. Moreover, he demonstrated that the dissolution rates are virtually independent of the rod immersion depth.[16]

Penz et al. carried out dissolution tests using S235JR construction steel samples in hot metal in ref. [27] They reported that after 20 s of immersion time, the core of the specimen has the same temperature as the liquid hot metal; thus, only mass transfer is in action. Similar results were also reported by Penz et al..[81] In ref. [27] the mass transfer was estimated through the relation based on Equation (2) of Lommel and Chalmers,[11] deduced by Oeters and Zhang.[53] Their published ranges of mass transfer for experimental temperatures of 1230, 1300, and 1385 °C under natural convection are comparable to the range put forth by previously mentioned researchers in ref. [8,9,13,14,16].

The experimental setup of a constant reaction area was used by Shin et al. in their investigations in ref. [17]. The same experimental design was also used by Nomura and Mori.[15] The initial carbon concentration of the bulk liquid Fe-C alloy was set as 4.23, 3.29, and 2.17 wt% for experiments at 1230, 1325, and 1415 °C, respectively. For the rate constant k_{met} in ms^{-1}, the temperature-dependent relation given in Equation (15) was obtained and the activation energy estimated to be 74 kJ mol^{-1}.[17]

$$\ln(k_{met}) = -3.47 - \frac{8905}{T} \tag{15}$$

Their measured values showed reasonable agreement with the calculated values using a dimensionless analysis based on the correlation by Jang et al.[82] presented in Equation (16).

$$Sh = 0.209\,Re^{0.739}Sc^{1/3} \tag{16}$$

From their results, they concluded that the mass transfer in the liquid boundary layer is the rate determining step for the dissolution of solid iron in liquid iron carbon melts. By using the temperature and carbon-dependent extrapolated diffusion coefficient published by Wanibe et al.,[65] they amounted the thickness of the boundary layer for carbon diffusion to be 114, 108, and 57 μm at 1230 °C, 1325 °C, and 1415 °C, respectively. Nomura and Mori reported an estimated diffusion boundary layer thickness of 50 μm to 100 μm at decreasing temperatures in the range of 1420 to 1200 °C, respectively. Compared to Kim and Pehlke,[10] the estimated boundary layer thickness of Shin et al. and Nomura and Mori is two times higher, which might be a result of two different test realizations.[15,17]

Nugumanov et al. used a mass transfer coefficient of $250 * 10^{-6}$ m s^{-1} for unmixed baths and temperatures below 1500 °C. In comparison to other published mass transfer coefficients, Nugumanov et al. value is approximately 10 times larger. Unfortunately, the literature where they took the mass

**ADVANCED
SCIENCE NEWS**
www.advancedsciencenews.com

**steel
research**
international

www.steel-research.de

transfer coefficient from was unavailable for the authors. An interesting theoretical assumption of theirs was that the carbon concentration at the external surface of the transition zone in the sample corresponds to the solidus line, rather than the liquidus line, as usually assumed in previous publications.[30]

Table 1 shows that the mass transfer coefficients explored under natural convection reported in literature are more or less in the same range if only mass transfer is considered. One exception is the investigations of Shin et al. [17] who carried out their experiments by using the constant reaction area approach. The published correlations given in Equations (10–16) provide a convenient method for calculating mass transfer coefficients under bath conditions of natural convection. The more recommended approach to determine mass transfer coefficients under natural convection is, according the presented results, to submerge a specimen of known geometry into the liquid melt.

4.2. Mass Transfer Under Forced Convection

In ref. [9], Pehlke et al. used the furnace power of a 90 kg induction melting unit for inductive stirring of the melt or a hand rotation with a chain and sprocket to achieve an angular velocity of approximately 200 rpm. They used the same material, cold finished 1020 steel cylinders with several diameters, as they did under non-forced convective conditions, as explained in the previous chapter. In general, the immersed specimen showed a linearly decreasing diameter with increasing bath agitation. **Figure 3** shows the change in the radius of a 0.0254 m diameter steel bar at 1371 °C as a function of the immersion time under various stirring conditions, investigated by Pehlke et al. They also indicated a boundary-layer thickness through carbon diffusion in the solid scrap of 254 μm, which, in comparison to the results reported by Shin et al.,[17] without stirring, is more than double the thickness. The measurement was performed by means of a metallographic examination, which allows only the
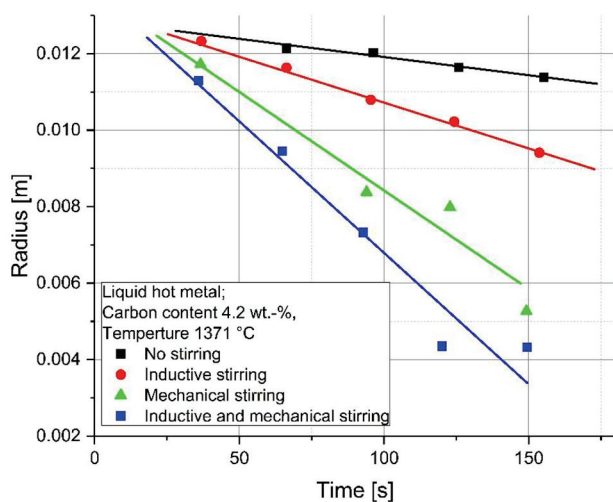
Figure 3. Influence of the stirring on the dissolution behaviour of a 0.0254 m diameter steel bar at 1371 °C.

usage as an order-magnitude measurement of the boundary layer.[9]

Rotating cylindrical samples with a speed of revolution from 32 rpm to 1210 rpm, obtained by a variable-speed motor, were investigated in a 1200 g carbon-saturated iron bath under isothermal conditions at 1274 °C to 1500 °C by Olsson et al.[12] The sample diameter varied from 0.0147 m to 0.0172 m with a carbon content of 0.008 wt% or 1 wt%. The samples were preheated under argon atmosphere to 100 °C below the bath temperature and then submerged into the melt. They compared their findings on a generalized relationship from Eisenberg et al. for mass transfer from a cylinder rotating in a stationary concentric crucible, which is given in Equation (17).[12,83]

$$J_D = \frac{k_{met}}{V}\left(\frac{v}{D}\right)^{0.644} = 0.0791\left(\frac{d*V}{v}\right)^{-0.3} \quad (17)$$

J_d defines the dimensionless modified mass transfer (J-factor), V is the rotational speed of the rotating cylinder [ms^{-1}], d is the diameter in [m] and v is the kinematic viscosity [m^2 s^{-1}]. It is obvious that the J-factor is a function of the Schmidt and Reynolds number, respectively, which was basically predicted in the analogy of heat transfer published by Chilton and Colburn.[84] The generalized relationship of Eisenberg et al.[83] provided in Equation (17) was analyzed by Olsson et al.[85] They could demonstrate that Eisenberg et al.'s correlation is applicable for molten Fe-C systems. Furthermore, Olsson et al. obtained a correlation between mass transfer coefficient and the rotational speed given in Equation (18).[12]

$$k_{met} = (const) * V^{0.7} \quad (18)$$

Kosaka and Minowa established in ref. [8], for rotated cylinders and temperatures between 1300 °C and 1500 °C, the following correlation for the J-factor seen in Equation (19) and valid for $10^2 < Re < 10^4$. Just as Olsson et al.[12] Kosaka and Minowa based their measurements on the relation of Shurygin and Shantarin.[8,50]

$$J_D = 0.064(Re)^{-0.25} \quad (19)$$

A rotating specimen was also used by Kim and Pehlke[10] deriving a J-factor given in Equation (20), which is slightly different from that derived by Kosaka and Minowa.[8] It has to be mentioned that both correlations found, do not consider the fact that the rotational speed increases with the decrease in the diameter of the rotating cylinder.[10]

$$J_D = 0.112(Re)^{-0.330} \quad (20)$$

The correlation found between the mass transfer coefficient and the rotational speed is shown in Equation (21).[10]

$$k_{met} = (const) * V^{0.670} \quad (21)$$

Penz et al. in addition to their investigations under natural convection, also reported forced convection measurements in ref. [27]. In order to realize turbulent conditions in the hot metal,

ADVANCED
SCIENCE NEWS
www.advancedsciencenews.com

steel
research
international
www.steel-research.de

Table 2. Selection of various mass transfer coefficients under forced convection through mechanical stirring reported in literature.

Initial diameter [m]	Hot metal temperature [°C]	Carbon content of the sample [wt%]	Carbon content of the hot metal [wt%]	Stirring	Mass transfer coefficient [m/s] * 10^{-6}	Rotational speed [rpm]	Literature
0.051	1371	0.2	4.1	Mechanical and inductive	23.8[13]	200	[9]
0.015	1274	0.008	1.5	Mechanical	87.4	450	[12]
0.017	1398	0.008	C-saturated iron	Mechanical	39.1	96	[12]
0.018	1302	0.008	C-saturated iron	Mechanical	24.8	85	[12]
0.015	1500	0.008	4.6	Mechanical	45.1	200	[12]
0.01	1400	0.15	3.87	Mechanical	15.3	200	[8]
0.01	1300	0.15	3.99	Mechanical	10.6	200	[8]
0.0254	1247	0.007	C-saturated iron	Mechanical	21.4	20	[10]
0.0254	1406	0.007	C-saturated iron	Mechanical	381	1800	[10]
0.012	1230	0.1	4.58	Mechanical	18.5–27.0	100	[27]
0.012	1300	0.1	4.58	Mechanical	25.5–36.5	100	[27]
0.012	1385	0.1	4.58	Mechanical	33.7–44.4	100	[27]

they rotated the sample at 100 rpm. They based their assumption concerning turbulent conditions on geometric and physical parameters of the experiment using the theory of Taylor-Couette flows. Based on the published system, a turbulent mixing regime was established.[27,86,87] The mass transfer coefficients are listed in **Table 2** and are comparable in the range of previous investigations using a similar experimental setup.[27]

A few published mass transfer coefficients are listed in Table 2, where mechanical stirring was carried out. It has to be noted that the mass transfer coefficient is increasing at an increasing rotation speed of the sample as well as the temperature. The rotational speed of the cylindrical sample is further influenced by the decreasing sample radius. The chemical composition of the bath and the sample itself also influences the mass transfer coefficient.

A different approach to obtain forced convection in the melt is through gas stirring, which was experimentally investigated by the following authors. The published mass transfer coefficients obtained in gas-stirred melts are listed in **Table 3**.

Glinkov et al. carried out in ref. [7] experimental investigations on the melting rate by blowing nitrogen through a quartz tube of 5 mm bore diameter into an induction furnace with a crucible of

about 50 kg pig iron bath (4.1 wt% C) at temperatures between 1300 and 1500 °C. The specimen of steel cylinders, containing 0.2 wt% carbon, were immersed into the melt after its temperature became steady. They observed an increase in the mass transfer coefficient from approximately $9 * 10^{-5}\,\mathrm{ms}^{-1}$ to $20 * 10^{-5}\,\mathrm{ms}^{-1}$ at 1350 °C with increasing nitrogen consumption from $5 * 10^{-5}\,\mathrm{m}^3\,\mathrm{s}^{-1}$ to $18.9 * 10^{-5}\,\mathrm{m}^3\,\mathrm{s}^{-1}$.[7]

The technique of gas-stirred Fe/C melts was also investigated by Wright in ref. [16]. The nitrogen stirring flow rates were given between $8.3 * 10^{-5}\,\mathrm{m}^3\,\mathrm{s}^{-1}$ and $66.6 * 10^{-5}\,\mathrm{m}^3\,\mathrm{s}^{-1}$. The derived mass transport coefficients under gas stirring conditions were reported to have dependence on the gas injection rate (Q) given in Equation (22). The gas was injected through a bottom tuyere with 2 mm diameter into a 25 kg hot metal bath.[16]

$$k_{\mathrm{met}} \propto Q^{0.21} \tag{22}$$

Mori and Sakuraya[14] studied the influence of gas stirring in an indirect way by dissolving iron rods containing up to 1.14 wt% oxygen in carbon–saturated iron alloys. During the dissolution, carbon monoxide (CO) was formed. They reported that the mass transfer coefficient tends to increase with increasing oxygen

Table 3. Selection of various mass transfer coefficients under forced convection through gas stirring reported in literature.

Initial diameter [m]	Hot metal temperature [°C]	Carbon content of the sample [wt%]	Carbon content of the hot metal [wt%]	Stirring	Mass transfer coefficient [m/s] * 10^{-6}	Gas flow rate [m³/s]	Literature
0.03	1350	0.2	4.1	Gas stirring (N_2)	90	$5 * 10^{-5}$	[7]
0.03	1350	0.2	4.1	Gas stirring (N_2)	200	$18.9 * 10^{-5}$	[7]
0.0121	1400	0.26	3.95	Gas stirring (N_2)	145	$10 * 10^{-5}$	[16]
0.012	1400	0.004 (0.96 wt% O)	C-saturated iron	Gas stirring (CO formation)	840	Not quantifiable	[14]
0.03	1600	Not specified steel	0.25	Gas stirring (N_2) in small-scale converter	83–208	8.33	[29]
Experiments on a 5 t converter				5 t converter	83.3–194	3500–12 000 W/t mixing power	[37,38]

content of the specimen as well as increasing temperature. They concluded that between 1350 °C and 1450 °C, the mass transfer is proportional to the volumetric evolution rate of CO, $\dot{V}_{CO}$, to a power of 0.45. Further rotational dissolution tests were done and a finding was that for a rotational speed >250 rpm, the effect of rotation becomes predominant. Below 250 rpm, the mass transfer coefficient is mainly controlled by the extent of CO evolution.[14]

The gas injection has a considerable importance in high-temperature metallurgy, particularly in an LD converter. Through the injection of gas into liquid melts, the mass transfer accelerates significantly with increasing injection rate, as could be seen from the reported data in Table 3. It has to be noted that the mass transfer coefficient is increasing at an increasing gas flow rate as well as the temperature. The chemical composition of the bath and the sample itself also influences the mass transfer coefficient.

Additionally, two estimated mass transfer coefficients reported from a laboratory-scale converter and a 5 t converter are added in the end of Table 3 to compare the experimental results. The experimental procedure of those two values reported from converters will be explained in detail in the chapters 6.1 and 6.2. It is clearly visible that the experimentally determined mass transfer coefficients in gas stirred melts are in the same range than the estimated values reported from converter experiments. Therefore, the more recommended approach to determine mass transfer coefficients under forced convection is, according the presented results, to use gas as a stirring device to reach turbulent bath conditions. Nevertheless, the experimental apparatus is more complex and difficult to realize to carry out investigations with a gas stirred melt.

5. Heat Transfer

According to the theoretical description in Chapter 3, the dissolution and melting behaviour is also dependent on the heat transfer. Especially during the initial stages of immersion of a cold steel into a hot liquid iron-carbon alloy, heat, and mass transfer are concurrent and the heat transfer has to be taken into account. This combination will be explained in Chapter 6. If the temperature of the melt exceeds the liquidus temperature of the scrap, the scrap melting and dissolution behavior, are controlled solely by the heat transfer. The present chapter summarizes a few papers, where the heat transfer of steel scrap submerged in iron carbon melts is evaluated and determined. A selection of reported values for the heat transfer coefficients is presented in **Table 4**, where only heat transfer was investigated. Beside steel scrap it is also possible to charge hot briquetted iron (HBI), direct reduced iron (DRI) or pellets as coolants into an LD converter. Several researchers published their investigations on those alternatives where mostly only the heat transfer was determined. To get a complete overview on this field, the authors also summarize in this chapter these findings and outline in **Table 5** the reported heat transfer coefficients.

One of the first observations regarding the topic of the melting of cold steel scrap in a superheated iron-carbon melt was published by Glinkov et al.[18] A cylindrical sample 0.02 m in diameter and 0.03 m in length was submerged in superheated iron carbon melt at 1540 °C to 1690 °C, containing 0.9 wt% to 4.0 wt% carbon. The cold specimens were immersed with a molybdenum support, which acts as a holding device, into the superheated melt and water-quenched after their removal. Through the weight change, the melting rate was determined. Immediately after the submersion, a solid shell formed in all melt compositions. They assumed the starting time at the end of the melting of the solidified shell, which results in their measured points are on the same curve. According to Glinkov et al. this is an indication that during the melting process, at the determined temperatures, the process of carbon diffusion has no substantial effect. The published melting rate at 1600 °C was $6.15 * 10^{-3}\ \text{kg s}^{-1}$ and their evaluated heat transfer coefficient was specified at 6163.9 $\text{W m}^{-2}\ \text{K}^{-1}$.[18]

Research was carried out by Guthrie and Gourtsoyannis[20] who created a heat transfer model to obtain the melting times of various sized annealed and ground steel hemispheres (0.05 to 0.076 m in diameter and 0.85 wt% carbon) immersed in stagnant liquid hot metal (∼5 wt% carbon). The model was validated with experiments. They also concluded that specifically the laminar natural convection flows play an important role in determining

Table 4. Selection of various heat transfer coefficients reported in literature where only heat transfer was investigated.

Initial diameter [m]	Hot metal temperature [°C]	Carbon content of the sample [wt%] or grade	Carbon content of the hot metal [wt%]	Type of experiment	Heat transfer coefficient [W/m²K] * 10³	Information	Literature
0.02	1600	Pure iron	Pure iron	Small scale	32	Spherical scrap	[19]
0.02	1600	Not specified steel	0.9–4.0	Small scale	6.164		[18]
0.025	1650	0.02	0.02	Small scale	13.4		[21,22]
0.025	1650	0.02	0.02	Small scale	5	Multi-piece scrap	[22]
0.012	1229	S235JR	4.5	Small scale	4.2	Immersion time 25 s	[25]
0.012	1302	S235JR	4.5	Small scale	5.0	Immersion time 25 s	[25]
0.012	1382	S235JR	4.5	Small scale	6.2	Immersion time 25 s	[25]

ADVANCED
SCIENCE NEWS

www.advancedsciencenews.com

steel
research
international

www.steel-research.de

Table 5. Selection of heat transfer coefficients of pellets reported in literature.

Initial diameter [m]	Hot metal temperature [°C]	Material	Carbon content of the hot metal [wt%]	Type of experiment	Heat transfer coefficient [W/m²K] * 10³	Literature
0.02	1600	Iron ore Pellets	Pure iron	Small scale	25	[19]
0.0093	1580	Iron ore Pellets	0.15	Small scale	8.3–25	[92]

melting times. In their developed model, they used the Nusselt correlation for the heat transfer coefficient in a stagnant melt, published by Eckert[88] for vertical planes. The correlation is also valid for vertical cylinders with the multiplication of 2.5 times the diameter, resulting in the correlation in Equation (23).[20,88]

$$\mathrm{Nu} = 0.508 * \left[\frac{\mathrm{Pr}}{0.952 + \mathrm{Pr}} * (\mathrm{Gr} * \mathrm{Pr}) * 2.5d \right]^{0.25} \tag{23}$$

Eckert's correlation was also used by Szekely and Chhabra[79] in the solidification of lead, where they made a study of natural convection effects under steady state and transient conditions. Their apparatus was designed to allow the establishment of a thermal convective field between the liquid and solid phases under conditions of controlled, unidirectional, horizontal heat flow. Guthrie and Gourtsoyannis analyzed the effects of the size of hemispherical scrap and preheating temperature as well as the bath temperature. Beside their observation of shell formation, they concluded that the preheating temperature could play an important role in decreasing the overall melting time by more than 25%. Their mathematical model shows a fair agreement with their experiments for the conditions where heat transfer alone controls the melting, which is the case for experimental temperatures above the liquidus temperature of the scrap hemisphere.[20]

The melting behavior of metal spheres and sponge iron pellets in their own melts were the topics of the research of Ehrich et al.[19,54], respectively. In both publications, they solved the heat transfer Equation (4) for spherical coordinates and with the application of the Greeńs function method. The theory using Greeńs functions for solving melting or solidification problems was described in detail by Chuang and Szekely[89] and Chuang et al.[90,91] For the validation of their numerical simulation, they carried out experiments with spherical samples 0.015 m in diameter in a 20 kg induction furnace under argon atmosphere. Through a fitting process with the numerical model, using constant material data, a heat transfer coefficient of $32\,000\,\mathrm{W\,m^{-2}\,K^{-1}}$ was determined for metal spheres. Additionally, they reported that a shell freezing and melting occurs in the initial seconds after the cold sample has been immersed into the melt. The thickness of the shell reached a maximum of 10% of the initial radius. The melting time of the sponge iron pellets (radius 0.01 m) was noted to be in the range of 10 to 25 s very quickly, due to their high porosity and despite its unfavorable heat conductivity. The published heat transfer coefficient for iron ore pellets was fitted with their numerical model to be $25\,000\,\mathrm{W\,m^{-2}\,K^{-1}}$.[19]

Medzhibozhskiy defined the ablation rate for scrap $-dr/dt$ in ref. [23] with Equation (24). The reported Equation (24) is assumed to be valid if the bath temperature T_{HM} exceeds the

scrap melting temperature T_{liq}, which is defined as a single temperature on the liquidus line of a phase diagram. The latent heat, released through the melting of the scrap, is included in Equation (24) with the variable L_f.

$$-\partial r/\partial t = h_{\mathrm{met}} * \frac{(T_{\mathrm{HM}} - T_{\mathrm{liq}})}{(L_f + (T_{\mathrm{HM}} - T_{\mathrm{liq}}) * c_p) * \rho_{\mathrm{scrap}}} \tag{24}$$

The melting rate of steel bars in a 70 kg liquid steel bath at temperatures of 1650 °C was analyzed by Li et al. [21,26] to investigate the kinetics in melting and to validate their phase field model. The sample and melt carbon contents were equal, in the range of 0.15 to 0.2 wt% carbon. Since the carbon contents are similar, they assumed that the mass transfer has no significant effect on the melting process in their investigation. The cold sample (25 °C) was immersed for a specific time into the melt, where shell freezing and melting were achieved, lasting much longer in comparison to the other reported periods. In **Figure 4**, the comparison of samples with several initial radii from Li et al. experiments are shown. The ratios of the measured radii after a specific immersion time with the initial radius of the sample are applied.

During the immersion, the electric power of the induction furnace was turned off to minimize forced convection. For their model, the heat transfer coefficient used was determined by the Nusselt correlation given in Equation (25) whereby h_{still} is the heat transfer coefficient for the stagnant interface. The modified
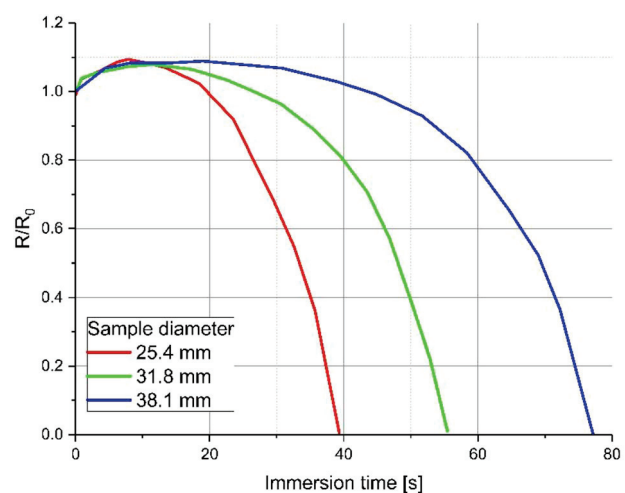

Figure 4. Comparison of samples with several initial radius as ratio of measured radius after a specific immersion time to the initial at 1650 °C obtained by Li et al.[21,26] Copyright © 2005 by The Minerals, Metals & Materials Society and ASM International. Used with permission.

**ADVANCED
SCIENCE NEWS**

www.advancedsciencenews.com

**steel
research**
international

www.steel-research.de

heat transfer coefficient h for a traditional sharp interface depends on the local normal interface velocity u and can be taken from Equation (26). The heat transfer coefficient $\tilde{h}$ used for the phase-field model, given in Equation (27), was calculated based on their assumptions on the derivation of the sharp-interface limit of their phase-field model to the lowest order.

$$\text{Nu} = \frac{h_{\text{still}} * L}{\lambda} = 0.686 * (\text{Gr} * \text{Pr})^{0.25} \tag{25}$$

$$h = \frac{\rho * c_p * u}{\exp(\rho * c_p u / h_{\text{still}}) - 1} \tag{26}$$

$$\tilde{h} = \frac{3 * \sqrt{2}}{4} \frac{h}{w * \rho * c_p} \tag{27}$$

In Equation (25), L was defined by Li et al.[21] as the immersed length of the cylinder. In Equation (26), u indicates the local normal interface velocity, which is calculated from the evolution of the phase field at $\Phi = 0$. The phase-field function Φ is the degree of crystallinity, where $\Phi = 1$ is a fully crystal solid and $\Phi = -1$ is a disordered liquid. In Equation (27), w defines the order, which controls the numerical thickness of the interface. This application noted by Li et al. is used in modeling microstructure to control surface tension. The Nusselt correlation in Equation (25) is applicable for $10^4 < \text{GrSc} < 10^9$. By the use of constant parameters, Li et al. obtained for $h_{\text{still}} = 13\,400\,\text{Wm}^{-2}\,\text{K}^{-1}$. They concluded that $\tilde{h}$, is in reality not constant, because it depends on the fluid flow conditions. Due to the phenomenon of the two-phase region at the interface, they used a modified heat conduction to elucidate the role of the interfacial gap and its heat conduction properties based on the considerations of Li and Thomas.[72] When they used a constant heat conductivity over the whole solid phase, they could not reproduce the experiments quantitatively.[21] Li and Provatas continued their investigations with multi-piece scrap melting in ref. [22], where they concluded that the porosity between scrap pieces plays a critical role in the melting process and rate. The best fitting heat transfer coefficient was thereby found to be $5000\,\text{Wm}^{-2}\,\text{K}^{-1}$ for the case of the melting of a structural component containing 19 steel cylinders at an equal distance to each other, which are fixed to a ground plate.[22]

Analytical investigations on the sectional surface by optical microscopy were carried out by Xi et al.[24] for round bearing steel bars (GCr15) with a carbon content of approximately 1 wt%. The samples were submerged in a non-specified liquid steel bath in a 10 kg induction furnace at bath temperatures between 1450 °C and 1600 °C. This range is above the liquidus temperature of the scrap, so only heat transfer control for melting was expected. In the analyses with an optical microscope, primary carbide was also detected on the surface after longer immersion times. Due to the solidification of liquid steel, carbon, and the other alloying elements were enriched and as a consequence, metastable eutectic ledeburite was formed. The inner regions of the scrap showed martensite, which was expected after water quenching. In their microstructure images, a light layer could also be seen

between the martensite and the primary carbide on the surface. This layer was unfortunately not described in detail.[24]

Penz et al. describe an analytical and numerical heat transfer model in ref. [25]. With the help of experimental measurements, the heat transfer coefficient was fitted to the models. For the investigation, cylindrical specimens of S235JR construction steel were immersed into liquid hot metal with a carbon content of 4.5 wt.% at temperatures of 1300 °C, 1370 °C, and 1450 °C. Within approximately 15 s, they reached a thermal equilibrium between the scrap core and the melt which was approximately 70 °C lower than the initial temperature. Their experiments were analyzed using their analytical and numerical model to determine the best fitting heat transfer coefficients in the initial stage of scrap melting. Mass transfer was not considered. An additional finding of theirs was that existing Nusselt correlations, for example, published by Windisch in ref. [80], will result in an approximately 10 times higher heat transfer coefficients. will result in an approximately 10 times higher heat transfer coefficients.[25]

Beside scrap also HBI, pellets, DRI, or sponge iron are charged into an LD converter as coolants. Their melting and dissolution behavior is only described by a few researches in literature. The research focus was in case mostly on the heat transfer. As an important substitute of scrap in the LD process the authors included parts of the reported experimental investigations of those coolants and the determined heat transfer coefficients in this chapter.

As described in the chapter 4.2 Mori and Sakuraya[14] studied the indirect influence of gas stirring through CO formation on the mass transfer coefficient. Similar investigations, but on the heat transfer coefficient, were reported by Seaton et al.[92] and Caffery et al. ref. [93]. While Seaton et al. determined the rate of dissolution of pre-reduced iron (Midrex and HyL pellets) in molten steel,[92] Caffery et al. published their research on the melting characteristics of HBI in iron and steel melts.[93] Both research groups figured out CO formation due to the relatively high oxygen content in those alternatives of scrap. Seaton et al. obtained the heat transfer by curve fitting and reported it to be in the range of $8300\,\text{W}\,\text{m}^{-2}\text{K}$ to $25\,000\,\text{Wm}^{-2}\,\text{K}^{-1}$.[92] With respect to changes in the physical properties of the pellets and the radius decrease during dissolution, discrepancies between the experimental and modeling results were observed. By the use of the expression given in Equation (28) (published first by Ehrich et al.[19]), for the variation of the heat transfer coefficient with the pellet radius (r), better fittings of the results were obtained.[92]

$$h_{\text{Seaton}} = h/\sqrt{r} \tag{28}$$

Both research groups reported that the rate of heat transfer increases with increasing CO evolution. Further, Caffrey et al. mentioned that at high bath carbon levels, carbon diffusion does not control the CO formation reaction.[93] More information about the melting behaviour of pellets or iron oxide coolants was published by Sato et al.[94,95] and Oya et al.[32,96] A fundamental description of the effects of gas release and changing diameter on heat and mass transfer to spheres was summarized by Brian and Hales.[97] Jiao and Themelis published a piece of research on the melting of DRI pellets in a liquid slag or metal bath in ref. [98]. They created a mathematical model for the heat transfer

ADVANCED
SCIENCE NEWS

www.advancedsciencenews.com

steel
research
international

www.steel-research.de

during the melting of solid particles and reported that DRI pellets might agglomerate and form "floating islands" or "icebergs" on the top of the slag. The computed results of the melting times for DRI/slag and DRI/liquid iron systems show critical differences. A pellet with a diameter of 0.03 m immersed in molten slag melts in 155 s, whereas in hot metal in only 10 s.[98]

The publications dealing exclusively with heat transfer showed a huge variety of heat transfer coefficients. A few of them are listed in **Table 6**. To get a better overview of the whole variation of heat transfer coefficients regarding the topic of scrap melting as an iron source and coolant in the LD converter the authors gave also a short summery of the published experiments and heat transfer coefficients is shown Table 5. It is visible that the heat transfer of pellets is much higher than of solid steel scrap. Derived from the published experiments the most recommended setup for heat transfer investigations is with a specimen of simple geometry equipped with thermocouples. From the practical point of view, it is difficult to define which heat transfer coefficient is favorable. Beside the chemical compositions of the scrap and the melt also the temperatures and the temperature-dependent physical parameters for example specific heat capacity, density, or viscosity will influence the heat transfer-relevant melting behaviour of scrap. Due to the temperature-dependence of the physical parameters the approach of Li et al.[21] in Equations (25–27) might be difficult to realize. Therefore, the authors will recommend, especially for the description of the heat transfer-driven forced scrap melting the approach of Medzhibozhskiy[23] given in Equation (24).

As stated in the theoretical part of this review and as a conclusion of the chapters 4 and 5 the dissolution and melting behaviour of scrap is a coupled heat and mass transfer problem. Beside the publications dealing with only one of those elements a few research groups investigated in their experiments both effects simultaneous in small-scale experiments or investigations in a commercial converter, which will be summarized in the following chapter.

6. Heat and Mass Transfer

As mentioned in preceding sections, the melting and dissolution behaviour of scrap is a complex phenomenon coupling heat and mass transfer. Several investigations have been published in the past considering heat and mass transfer in their small-scale experiments or investigations in converters. In the following two paragraphs the authors will provide an overview on these reports.

6.1. Small-Scale Experiments in Converters

In their pioneering work, Pehlke et al. observed in ref. [9] that the initial rate of dissolution was smaller for larger bars and lower bath temperatures. The hot metal shell, which freezes on the surface of steel bars that are immersed for extremely short times into the hot metal, delays the dissolution process. Through the growth and melting of this shell, the heat flow into the rod is also delayed. In their investigation, they carried out thermocouple measurements which were positioned in the center of a rod. A result was that the rate of heating was decreased with increasing diameter. It was reported in ref. [9] that a 0.0127 m diameter steel bar is heated through to the melt temperature in more than 10 s. However, they did not estimate a heat transfer coefficient but declared the rate of heating of the steel as a limiting factor for delays in the dissolution process.[9]

The practical motivation in the early 70s for studies on the scrap melting behavior in the LD converter was pointed out by Szekely et al.[28] on the recent interest in increasing the fraction of scrap charged in the LD converter. They published a mathematical interpretation that includes the mass transfer of carbon and heat transfer within a moving boundary system, which takes into account the initial temperature of steel and the heat of fusion as well as the carbon content of the bath. In their experimental investigations, steel rods with various diameters were submerged into an induction furnace containing 295 kg molten hot metal. The carbon contents were in the range of 2. to 4.4 wt%. They assumed turbulent flow and used the correlation of the heat and mass transfer coefficient given in Equation (29), which was solved by a manipulation of Green's function.

$$\frac{k_{met}}{h} = Sc^{1/3} Pr^{-4/5} \frac{D}{\lambda} \tag{29}$$

However, both mass and heat transfer coefficients were obtained by data fit to their experimental results. The best fitting heat transfer was fixed at $3400 \, Wm^{-2} K^{-1}$.[28]

Another experimental investigation was carried out by Kawakami et al.,[29] who investigated the dissolution of

Table 6. Selection of various heat transfer coefficients reported in literature based on coupled heat and mass transfer investigations.

Initial diameter [m]	Hot metal temperature [°C]	Carbon content of the sample [wt%]	Carbon content of the hot metal [wt%]	Type of experiment	Heat transfer coefficient [W/m²K] * 10³	Information	Literature
0.0192	1380	0.22	4.21	Small scale	3.4	Immersion time 120s	[28]
0.03	1600	0.25	0.25	Small scale	66.4	Gas purging	[29]
0.03	1600	0.25	4	Small scale	69.2	Gas purging	[29]
0.03	1400–1600	0.25	0.25–4	Small scale	27.7–77.2	Various experimental conditions	[29]
0.04	1550	0.17	3.74	Small scale	11.63		[30]
	Experiments in a commercial converter				17–25		[35,36]
	Experiments in a 5 t converter				23–47		[37,38]

**ADVANCED
SCIENCE NEWS**

www.advancedsciencenews.com

**steel
research**
international

www.steel-research.de

cylindrical rods (diameters of 30, 40, and 50 mm) in hot metal with various carbon contents at 1600 °C. The iron carbon alloy was homogenized through nitrogen gas purging with a gas flow rate of $8.33 * 10^{-5} \, \text{m}^3 \, \text{s}^{-1}$. Some of the reported experiments were carried out with no gas injection. The estimated heat and mass transfer coefficients reported are in the ranges of $27\,700 \, \text{Wm}^{-2} \text{K}^{-1}$ to $77\,200 \, \text{Wm}^{-2} \text{K}^{-1}$ and $83 * 10^{-6}$ to $208 * 10^{-6} \, \text{ms}^{-1}$. Furthermore, Kawakami et al. stated that both coefficients are independent of the carbon content in the steel bath and both coefficients increase with an increase in temperature. Their estimated dimensionless correlations for heat and mass transfer are given in Equations (30) and (31), respectively.[29]

$$Sh = 0.017 \, Re^{0.8} \, Sc^{1/3} \tag{30}$$

$$Nu = 0.017 \, Re^{0.8} \, Pr^{1/3} \tag{31}$$

Nugumanov et al. investigated the scrap dissolution and melting behavior in ref. [30] with experiments in a 60 kg electric arc furnace, using cylindrical low-carbon steel samples with a diameter of 40 mm containing 0.17 wt% carbon. The samples were submerged into liquid hot metal in the temperature range of 1400 °C to 1690 °C. They showed that above 1550 °C, the ablation rate of the radius does not depend on the carbon content in the melt anymore and only correlates with the heat flux supplied to the phase interface. The heat transfer coefficient fitting the best with the experiments was described to be $11\,630 \, \text{Wm}^{-2} \text{K}^{-1}$ above 1550 °C melt temperature.[30]

Experimental observations of spherical scrap containing 0.1–3.7 wt% carbon in hot metal containing 2–4.5 wt% carbon in a temperature range of 1300 and 1600 °C were reported by Sun et al. [31]. The solid spherical scrap of 0.24 kg on average was fixed to a molybdenum rod and immersed into a hot metal bath of 70 kg heated in an induction furnace. In their work, they did not present any mass and heat transfers, but reach the conclusions that scrap with a higher carbon content will dissolve faster in a liquid carbon alloy bath than low-carbon scrap. The sectional surfaces of the spheres were investigated by electron microprobe analysis (EMPA) for their carbon content. They demonstrated that the shell, which freezes in the initial stages (19.8 s) of scrap melting, is solidified hot metal. In a sample immersed for 359 s, the surface shows a slightly higher number of carbon counts than those deep inside of the sample.[31]

6.2. Experiments and Investigations in Converters

The main focus in LD converter steelmaking is to produce as much crude steel as possible in a safe and economical way with minimal costs. For that reason, experiments in converters are not easy to perform during the production process. A strong disadvantage is undissolved heavy scrap at turndowns in the process, because it disturbs the end-point control, lowers the steel output, affords sub-lance breakage, and brings a hazard for operators in front of the converter.[35,36,40] Nevertheless, a few experiments on scrap melting and dissolution have been carried out and published. Oya et al. observed ref. [32] that cold charged

pig iron and scrap are sometimes not melted after the blowing process in an LD converter, which is why they charged pig iron containing a certain amount of the radioisotope 60 Co. With regard to the measurement of the cobalt-60 emissions, they concluded that after 15 min, 50% of the charged scrap had melted. After this period, the dissolution rate rapidly increased. The scrap size was given as 1400 mm × 500 mm, weighing less than 1 t. The melting of cold-charged pig iron was faster than scrap. After 1 to 2 min of blowing, approximately 20–30% of the cold charged pig iron had already melted.[32]

In a 100 t converter, Burdakov and Varshavskii investigated the tendency to increase the consumption of scrap in LD converters in ref. [33]. From their published data it could be estimated that the scrap ratio is 1 t scrap on 4 t of hot metal. They stated that the scrap surface, carbon composition and superheat are important parameters for scrap melting. In their converter, the average melt down of the scrap was quantified with 10 to 12 min. After a blowing time between 10 to 15 min the melt temperature exceeds 1500 °C. The initial hot metal temperature is given with approximately 1300 °C.[33]

With frequent turndowns (every 2–4 min), Bondarenko and Afanaśev investigated the scrap dissolution in a 130 t converter in ref. [34]. The scrap charge was specified to be 23–27% of the metallic charge. Light scrap like discard from thin sheets was observed to have melted already during the charging of hot metal, which leads to a noticeable super cooling of the melt. Heavy scrap in the form of slab croppings was observed to be completely dissolved after 12–16 min blowing time. The charging of heavy scrap also diminished the hot metal temperature by approximately 100 °C. The scrap dissolution was estimated in accordance with the copper balance. The total blowing time was 23–26 min, with an average specific oxygen consumption of $50 \, \text{m}^3 \, \text{t}^{-1}$.[34]

Experimental investigations on scrap melting in various converter types were published by Gaye et al.[35,36] The experiments were used to support the dynamic model which had been developed by their research group. Activated 133 xenon was placed in carbon steel capsules of 20 mm inside the scrap and used to determine the scrap melting time. Due to the emission of xenon in the exhausted gas, the time of melting of the scrap was able to be determined. In their theoretical considerations, the heat transfer depends essentially on the mixing conditions. The heat transfer coefficient of the liquid phase was found to be a function of blowing conditions with the following correlation given in Equation (32),

$$h = 5000 * \dot{\varepsilon}^{0.2} \tag{32}$$

where h is the mass transfer coefficient in $[\text{Wm}^{-2} \text{K}^{-1}]$ and $\dot{\varepsilon}$ is the average mixing power $[\text{Wm}^{-3}]$ which is a function of blowing conditions. Specially for LD converters a heat transfer coefficient of $17\,000 \, \text{Wm}^{-2} \text{K}^{-1}$ and for LD vessels with bottom oxygen flow, $25\,000 \, \text{W/m}^{-2} \text{K}^{-1}$ was mentioned. In ref. [35,36] they recommended that the scrap thickness should not exceed 0.1 m to 0.12 m in a 300 t converter. They stated in their experimental findings that the type of scrap is relatively more important than its thickness or shape.

To acquire the required data for a single-scrap melting model, Isobe et al. carried out experiments on a rotating rod in a 300 kg

**ADVANCED
SCIENCE NEWS**

www.advancedsciencenews.com

**steel
research**
international

www.steel-research.de

heating furnace and on scrap melting in a 5 t converter in ref. [37,38]. For the mass transfer of the rotating rod, the non-dimensional correlation given in Equation (33) was obtained.

$$Sh = 0.163 \, Re^{0.78} \, Sc^{0.356} \tag{33}$$

This relation correlates well with those described in Chapter 4.1 on small-scale experiments, for example.[10,16,82] In the 5 t converter the values obtained for the heat transfer are in the range of $23\,000\,Wm^{-2}K^{-1}$ and $47\,000\,Wm^{-2}K^{-1}$. For the mass transfer, they were published to be in the range of $83.3 * 10^{-6}\,ms^{-1}$ and $194 * 10^{-6}\,ms^{-1}$. The melting rates in the experiments were measured by the dissolution of added copper tracers similar to the investigations of Bondarenko and Afanaśev in ref. [34]. In comparison to the small-scale experiments it is obvious − due to the risks of production delay and occupational safety − that long-term experiments on commercial converters are not welcome nowadays. Based on the results for heat and mass transfer coefficients and correlations, the previously mentioned publications show no huge differences compared with small-scale experiments. In Table 3 and 6, the mass and heat transfer coefficients received from commercial converter experiments are also listed to complete the values reported up to now. It is again mentionable that investigations with gas purging result in higher heat transfer coefficients. If the mixing power of a converter is known, which is usually a function of for example the blowing and purging conditions as well as the lance tip geometry or lance height, the approach published by Gaye et al.[35] given in Equation (32) will be recommendable. Although some outliers have been reported, most of the publications mentioned the simulation and modeling of the process, which will be reviewed in the following chapter.

7. Modeling of the Scrap Melting and Dissolution Process

In the last decades the numerical modeling of LD converters became more and more important. Most of the published converter models describing the whole process based on mass and energy balances and supported by a variety of sub routines, where among others the scrap melting and dissolution process is placed. Often the scrap melting sub routine is not described in detail, which makes it difficult to analyze it and make it comprehensible. The authors will summarize in the present chapter all reported numerical scrap melting approaches, which were published and available for them. Additionally, a few dynamic process simulations, where a more detailed description of the scrap melting routine was mentioned should give an overview on the whole process simulation.

7.1. Process Simulations of Converters

The first metallurgical models for solidification of continuously cast steel were published as early as the end of the 1960s, treating heat transfer between a solid and liquid iron carbon alloy, for example in ref. [99–101]. One of the first theoretical analyses of an LD converter by the use of a mathematical model was described by Asai and Muchi.[102] The model consists of 13 differential equations and an algebraic equation, which are solved simultaneously by means of the Runge-Kutta-Gill method. For simplification, it was considered that the scrap and pig iron charged had immediately reached the same temperature as the liquid hot metal. The function for melting and dissolution of scrap is not mentioned in detail. In a second publication closely related to ref. [102] Muchi et al.[103] describe the scrap melting only by a basic balance equation. The same research team of Asai and Muchi published the first description of modeling scrap melting in ref. [39], based on their LD converter model by use of experimental data obtained by other authors, for example Oya et al.[32] They analyzed the behavior of the carbon content and the temperature of the melt, caused by changes in the operating conditions. For the research, the liquidus line of the Fe-Fe₃C diagram was linearized. In the mass and heat balance, it was assumed that the temperature and the carbon concentration on the surface of the scrap are identical with the values given by the linearized liquidus line. In a parameter study, the effects of the fluctuations of the carbon concentration and temperature of the melt as well as the effects of the flow rate of oxygen and the assumed product of the effective scrap surface area and the mass transfer coefficient in the metal side were examined. The heat transfer coefficient ($70\,000\,Wm^{-2}\,K^{-1}$) and mass transfer coefficient ($200 * 10^{-6}\,ms^{-1}$) used are comparable to the experimental investigations described in the previous chapters in the upper ranges. All in all, it was considered from the assumption of a lumped parameter system that the thermal resistance in scrap may be concentrated only on the surface of the scrap and in the analysis of the melting process only the decarburization reaction is taken into account.[39]

A dynamic model of the dissolution of scrap in the LD process was published by den Hartog et al. ref. [40], with the special feature of calculating the simultaneous dissolution of scrap with different sizes and carbon compositions. The basis of their model was a static heat and mass balance model with an overall oxygen balance. In a second step, the differential equations of heat and mass transfer were involved for subsequent time steps. To derive the heat transfer coefficient used, charged ingots in the LD converter of the BOF plant No. 2 in Ijmuiden were measured before charging. The remaining scrap pieces after tapping were measured again and a heat transfer coefficient of the stagnant surface was derived through a trial and error calculation and was quantified to $47\,500\,Wm^{-2}K^{-1}$. By the use of the Chilton-Colburn analogy (see also[84]), a mass transfer was estimated. Various quantities were implemented as variables in the model. For scrap melting, the most important ones were the shape, weight, temperature, and composition of the scrap. In their results, they argued that the scrap dissolution is heavily dependent on the distribution of the scrap weight over heavy pieces and small-sized scrap. Through their experiments, they also concluded that the temperature of the bath is influenced by the scrap size distribution. A conclusion reached was, that the dissolution of scrap is dependent on the heat transfer between scrap and hot metal and almost independent from the blowing rate.[40] The latter is in contrast with the findings of Gaye et al.,[35] who considered in Equation (32) that the heat transfer coefficient is a function of the mixing power.

**ADVANCED
SCIENCE NEWS**

www.advancedsciencenews.com

**steel
research**
international

www.steel-research.de

As a sub routine for a dynamic model of the LD process, Yorucu and Rolls created a numerical solution for the scrap melting in the LD process, published in ref. [42]. Their input data to the sub routine was characterized by a constant bath temperature and carbon content in each time step. The carbon concentration on the scrap surface was defined to be equal to that of the bath. Further the temperature of the same point was assumed to be the melting point of the bath. What was different to previous models was their consideration that the melting temperatures of the bath and the scrap are estimated using a linearized form of the solidus line of the Fe-Fe₃C diagram published by Hansen et al.[104] Due to coupled mass and heat transfer, the melting rate of a volume element was calculated for both heat and mass transfer. The slower rate was further taken to be the "true" melting rate. The last step in the model was the heat balance. No information was given by Yorucu and Rolls about a validation of the model.[42]

In ref. [49], Kruskopf mentioned a process model for LD converters which is under development. The model should include beside a 2-dimensional axisymmetric flow model for iron melt and a chemical reaction model also a steel scrap model. The numerical approach of Kruskopfs steel scrap melting model will be explained in the following chapter.

In ref. [105], Penz et al. described the sub model for scrap melting and dissolution of the dynamic process model developed by Lytvynyuk et al.[106,107] in detail. The scrap melting is divided two mechanisms, the diffusive scrap melting and the forced scrap melting. The diffusive scrap melting uses the equation of Olsson et al. given in Equation (2), modified with the assumptions of Zhang and Oeters[53] and unequal densities of hot metal and scrap according to Chigwedu.[108] According to the explanations of Penz et al., the forced scrap melting starts in Lytvynyuḱs process model when the melt temperature exceeds the scrap melting point and follows the equation of Medzhi-bozhskiy[23] given in Equation (24).[105,106]

7.2. Numerical Approaches for Scrap Melting

An approximated and strongly simplified analytical solution to the scrap melting process of a spherical particle was presented by Goĺdfarb and Sherstov ref. [43]. In their theoretical description, the freezing and melting of a hot metal shell was also considered as a result of the intensive absorption of heat by the cold solid scrap. The analytical model is established in Biot and Fourier correlations. To solve the general equation of diffusion analytically, the carbon ratio $(C_{solidus} - C_{scrap})/(C_{liquidus} - C_{solidus})$ was taken to be equal to 0.8, whereby $C_{solidus}$ and $C_{liquidus}$ are the carbon concentrations on the solidus and the liquidus line, respectively. In the results, the diffusive dissolution period is about ¾ of the overall dissolution time and only a little dissolution activity was reported during this period.[43]

The use of Greeńs functions for solving moving boundary problems like melting or solidification processes was mathematically described by Chuang and Szekely ref. [89]. In some simple examples, using constant physical and transport parameters, the melting of a steel slab in carbon-saturated hot metal was realized. They concluded that the involvement of Greeńs functions is a flexible and economical procedure for

accommodating complex boundary conditions. In ref. [28], Szekely et al. compared the theory with the use of Greeńs function with experimental investigations. In this way, heat and mass transfer coefficients were obtained by means of data fit and the mentioned correlation of the heat and mass transfer coefficient given in Equation (29) was reported.

The initial stages of scrap melting were investigated by Kim and Pehlke[41] on the transient heat transfer. They derived an analytical model for the process and compared the numerical solution with experimental results. Comparable to other authors, for example Penz et al.[25], they found that in preheated cylindrical specimens with a diameter of 0.013 m, the shell freezing and melting ends after a short period of less than 10 s. After this time range, a thermal equilibrium is derived and the dissolution of the solid continues under isothermal conditions.[41] Kim and Pehlke developed their model based on the explicit method of computing the temperature distribution and location of the solid interface. Constant physical and transport properties were assumed. The heat transfer coefficient used in the model was 11 300 Wm⁻² K⁻¹ and the third degree Lagrange polynomial was used to evaluate the new temperature at the grid points. They also mentioned that a precise quantitative confirmation of their results was difficult because they could not measure the temperature change in the liquid bath.[41]

In Chapter 5, the heat transfer experiments of Li et al.[21,26] were already described. In their investigation, the mass transfer was neglected due to the fact that the carbon content of steel scrap and the steel bath in an electric arc furnace is similar. Their experimental results served to introduce a new phase-field model of melting in the presence of convection. While previous studies consider a sharp interface between scrap and liquid metal, the phase-field model replaces the need to track the explicit dynamics of the boundary by an equation of motion of a continuum phase field Φ.[26] The order parameter Φ takes a constant value in each bulk phase, for example $\Phi = 1$ in the solid and $\Phi = -1$ in the liquid, and interpolates continuously from 1 to −1 at the interface. The method is widely used for simulating dendritic growth and other solidification microstructures in two or three dimensions, for example in ref. [109–112]. The problem of convection in the liquid bath was solved by introducing a convective heat transfer term into the heat equation. The heat transfer $\tilde{h}$ of the phase-field model is proportional to sharp interface models and was already given in Equation (27). In their simulations, the heat resistance of an air gap between the initial steel bar and the solidified layer was included by the use of an effective heat capacity for the air gap.[21,26] The use of the effective heat capacity was motivated by Li and Thomas from strip casting[72] and described in detail for other phase transition models, for example in ref. [22,99,100,113–116]. Li et al. phase-field model in ref. [21,26] showed reasonable accuracy to simulate the melting process. However, they noted the following possible reasons for the differences between experiments and simulation: One reason was given through the assumed heat transfer coefficient, that was not a function of the sampleś shapes and sizes, which could lead to a systematic error. They also mentioned that it is difficult to find a scientific basis to determine the accurate contact heat conduction of a possible air gap between the solidified shell and the original bar. Finally, the lost heat from bath and steel samples in the experiments was,

**ADVANCED
SCIENCE NEWS**

www.advancedsciencenews.com

**steel
research**
international

www.steel-research.de

according to them, hard to calculate and the natural convection patterns were not considered.[26]

A Fourier series-based solution of the temperature distribution in the solid scrap was used in the model developed and published by a research group around Sethi, Shukla and Deo in ref. [44,45]. In their research, the effect of different heat transfer coefficients on the kinetics of scrap dissolution and the solid-liquid ratio are examined and discussed. Basic assumptions they used in their analytical model were: No mass transfer control during the solidification and fast melting stage, convective heat transfer in the melt and a constant ablation rate during a single time step. They included the amount of carbon consumed by CO reaction in the weight balance and the specific heat of the scrap varies by a temperature-dependent function using an average temperature between scrap surface and its core temperature. Constant thermal conductivity and densities are used and they are equal for scrap and liquid hot metal. They mentioned that in the initial stages of shell freezing, the formed shell is not in perfect contact with the parent iron rod. This formation of an air gap was assumed to be a possible reason why the solution using the finite difference method has a significant deviation from the analytic solution. Differences in the temperature profile predicted between the analytical and numerical solution occur because of an inaccurate assumption of the mushy zone in the latter.[44]

The research group around Shukla et al. improved their model by comparing different approaches to model the scrap dissolution phenomenon in ref. [46]. The use of Green's function, a quasi-static approach as well as an integral profile method and a finite difference approach were compared for different Biot numbers and fed into an artificial neural network to select the best approach to describing the problem. The heat transfer coefficient was estimated through a function of the mixing energy $\dot{\varepsilon}_{total}$ (see Equation (34)) comparable to the work of Gaye et al.[35]

$$h = 5000*(7.0*\dot{\varepsilon}_{total})^{0.2} \tag{34}$$

In the case of Shukla et al.[46] research, the total mixing energy [Wm^{-3}] is a combined function of the influence of top lance geometry and type, the bottom stirring flow rate and decarburization reactions based on previous publications in ref. [117–119]. The mass transfer coefficient is further determined by the Chilton-Colburn analogy for forced convection. Their recommendations were to use a quasi-static modeling approach, which can be employed to study the effect of parameters such as scrap ratios or heating rates of the melt.[46]

The previously reported role of an air gap between the solidified shell and the mother scrap during the scrap dissolution process was investigated by Shukla et al.[120] As soon as liquid hot metal comes in contact with cold steel scrap, a shell formation will start. This process is associated with density changes from liquid to solid state, which causes stress in the material. A result of the induced stress is the formation of an air gap between the parent scrap and the solidified shell.[120] Gas and air have a low thermal conductivity, which will act as a resistor for the heat transfer between scrap and liquid melt. A mathematical model assuming radiation and conduction-dependent heat transfer coefficient in the air gap was developed and compared

with the research results of Li et al.[21,120] By fitting the model with Li et al. experiments, a good agreement was found if the heat transfer coefficient in the air gap was considered as $5000\,Wm^{-2}\,K^{-1}$. Shukla et al. concluded that the calculated value of heat transfer coefficient for air gaps of 10 to 100 μm thickness lies in the range of 1000 to $10\,000\,Wm^{-2}\,K^{-1}$. Finally, a significant finding was that the air gap affects the path of melting, particularly if the Biot number is less than 50 and the ratio of air gap to liquid melt heat transfer coefficient is low (< 0.25). The total dissolution time remains unaffected.[120] The formation of air gaps during the dissolution process has also been observed in non-ferrous metallurgy, for example by Lagerstedt et al.[121,122]

A 2-D tool was developed by Guo et al.[47] to describe the melting of heavy scrap in LD steelmaking. The simulations showed that, for slab type scrap, the thickness is an essential parameter for the melting time, and the location of the scrap piece relative to an oxygen jet has a significant influence.[47]

The latest publications about modeling of the scrap melting and dissolution phenomena were published by Kruskopf et al.[2,48,49] The steel scrap melting model is part of a process model for an LD converter. One of the most important factors Kruskopf included in his work was temperature and carbon concentration-dependent material data for the heat capacity, thermal conductivity and the diffusion coefficient. In order to increase the accuracy of the model, the enthalpy method is taken into account to bring the heat capacity into a conservative form. This will allow a solution in a fixed space grid to be obtained and takes into account the sudden changes in the heat capacity related to phase changes.[49,123]

Using the control volume method in a moving grid with the implicit Crank-Nicolson method the 1-D general equations of the enthalpy and carbon concentrations are discretized. For the density, a constant value was used. The use of the implicit discretization method was seen as an improvement in comparison to using the more unstable explicit method.[49] Kruskopf validated his results by providing literature data from Isobe et al. study presented.[37] The experimental results agreed well with the model to predict the melting curves of the scrap. It was necessary to modify the Nusselt and Sherwood correlations, published by Kawakami et al.[29] which are given in Equations (30) and (31), with a coefficient of 0.04 and 0.0082, respectively. The modified correlations, shown in Equations (35) and (36), gave the best fit with the literature data used in Kruskopf's model[48,49]

$$Sh = 0.04\,Re^{0.8}\,Sc^{1/3} \tag{35}$$

$$Nu = 0.0082\,Re^{0.8}\,Pr^{1/3} \tag{36}$$

In **Figure 5** the melting curves of scrap, predicted by Kruskopf's model, are compared with Isobé's experiments.

In ref. [2], Kruskopf and Holappa improved their previous model with the inclusion of an interfacial solid/liquid phenomena tool connecting the scrap melting model with the melt model of their LD converter process simulation. The improvement took into account that after the melting of the solidified shell, the interface velocity vector could be positive. A
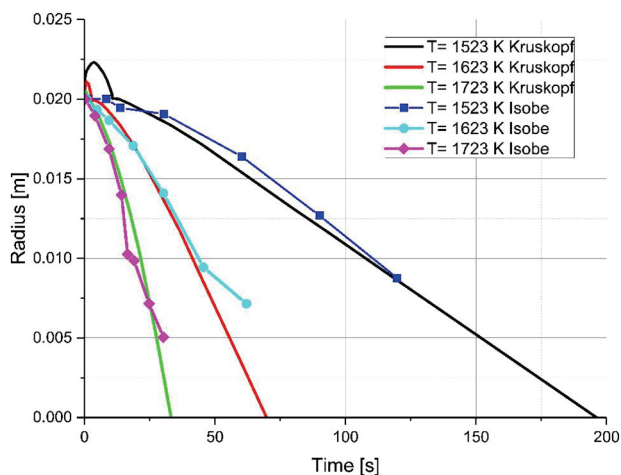
**ADVANCED
SCIENCE NEWS**

www.advancedsciencenews.com

**steel
research**
international

www.steel-research.de

Figure 5. Comparison of Kruskopf's model[49] with Isobés experiment results.[37] Copyright © 2015 by The Minerals, Metals & Materials Society and ASM International. Used with permission.

positive interface velocity was defined as renewed solidification of hot metal on the surface and that the scrap does not melt. This is based on the assumption that the solidus and liquidus temperatures are equal, since they are the eutectic isotherm of a binary Fe-Fe$_3$C phase diagram. To explain the non-existing phase change, the interface velocity was set to zero for this situation. It is mentionable that in their research work, only carbon and iron were considered to build the melt and the scrap.[2]

According to the recent publications about the numerical modeling, the main factors for a proper description of the scrap melting and dissolution behavior are the definition of the heat and mass transfer coefficients, which close the loop to the experimental investigations done by all researchers and published works in the chapters 4 to 6. Due to the safety and economic reasons experiments on a commercial converter are nowadays impossible to execute or related with an enormous time-consuming and financial effort. Small-scale experiments are therefore necessary to find the ideal values for a proper description of the problem. One important factor beside the heat and mass transfer coefficient is also the application of temperature and composition-dependent physical and ther-modynamic properties in the models. In the more complex dynamic process simulations, these parameters should be included too. The last important consideration for the numerical description of the dissolution behavior of scrap is an accurate execution of the mushy zone, which will appear due to the Fe-Fe$_3$C phase diagram. The approaches of the phase field model published by Li et al.[21,26] and the interfacial solid/liquid description of the control volume method-based model of Kruskopf[2,49] are recommendable for further research activities. Further, the methods of Green"s functions and the enthalpy method for the numerical description of the moving boundary problem have been applied. A recommendation to use a quasi-static modeling approach for the description of the moving boundary problem was given by Shukla et al.[46]

8. Concluding Remarks

Scrap melting is indeed a complex and complicated process including simultaneous heat and mass transfer. The present study was carried out to present the knowledge and give an overview as to which research work has been carried out on this process in the past 60 years. The main factors controlling the melting and dissolution process reported are heat and mass transfer. While mass transfer, namely the diffusion of carbon into the scrap, is widely investigated under natural and forced convection, heat transfer has received less attention. The main influencing factors of the melting and dissolution behaviour of scrap can be summarized to be the chemical compositions of the scrap and the liquid as well as the temperatures. From the fundamental theory of scrap melting the carbon concentration on the solid/liquid interface was estimated to be the liquidus concentration at the hot metal side and the solidus concentration on the scrap side. However, this theory exists since decades but it was never investigated and validated in detail through measurements. Furthermore, the theory is understood to be in a thermodynamic equilibrium but from experiments it is already well known that always natural or forced convection in the fluid will influence the scrap melting and dissolution. An additional theory says that the crystalline structure will break down in a kinetic stage but in this case also no significant and validated kinetic factors exists. Therefore, the authors would suggest that the most common mathematical equation to describe the diffusive scrap melting behavior is the approach given in Equation (9), considering the modification of the densities and the ratio of the velocity of the boundary movement as described in chapter 3. This estimation will be useful either for small scale and industrial applications. For the definition of the heat transfer the Equation (32) and (34) might be the most convincing mathematical formulations. Combined with Equation (24) the scrap ablation rate also conditions where forced scrap melting might occur.

The temperatures of the melt in an LD converter rise during one heat from approximately 1250 up to 1700 °C, depending on the process control. In the main part, the temperatures are below the melting point of pure iron or the solidus temperature of scrap. In this period, the carbon content is also higher in the melt than in the scrap. These circumstances led to the fact that the melting and dissolution are exclusively controlled by the mass transfer of carbon. Due to reasonable facts experimental investigations on commercial converters are nowadays extremely complex to perform. Small-scale experiments are therefore the most convenient method to estimate heat and mass transfer coefficients, which are a suitable basis for the validation of numerical descriptions or dynamic process simulations. All available and published small-scale experiments and investigations on commercial converters were described by the authors in this review, to guarantee the best possible documentation of the obtainable scientific information and technology. The obtained mass transfer coefficients and dimensionless correlations were collected and summarized. All of them only consider carbon as the main element for mass transfer.

The heat transfer becomes more important at the beginning of the process, when the scrap does not have the same temperature as the melt. The freezing and melting of a shell of

bulk composition on the scrap surface are reported and investigated during this process. Heat transfer is also the main reason for melting the scrap if the melt temperature exceeds the melting point of the scrap. In most publications, the melting point is defined as the liquidus temperature of the initial chemical composition of the scrap. The reported values for the heat transfer coefficients and established correlations were also collected and summarized in this review.

Scientific investigations on simultaneous heat and mass transfer have been published and also described in this review. In those works, similar results of the heat and mass transfers were published to those in articles only dealing with either heat or mass transfer investigations.

The simultaneous heat and mass transfers have received more attention in the past 20 years in the mathematical modeling of the scrap dissolution and melting. Most of the recent numerical models are sub tools of dynamic process models of the LD converter. In detail, it could be seen from the reported articles that temperature and chemical composition-dependent physical and thermal parameters are necessary to yield more accurate results. This will certainly make the models more complex and difficult to program. The estimations of the heat and mass transfers were partly fitted to empirical results from previous research. One of the most difficult questions is therefore the simulation of the mushy zone during the diffusive melting process. Additionally, topics like the formation of an air gap between the scrap and hot metal shell in the initial stages still lead to open questions as well as in the simulation and experimental analyses.

As a whole, the reported values for the heat and mass transfer coefficients vary significantly and individual cases are still open to question. Furthermore, it is still questionable how other elements like silicon, manganese, or phosphorus may influence the scrap melting and dissolution behavior in carbon melts.

In summary, the outcomes of this review clearly indicate that based on all previous investigations and simulations, open questions have to be solved in future research work. The present review should have shown the present status of know-how and technique and should serve as a basis for new investigations.

Conflict of Interest

The authors declare no conflict of interests.

[1] A. Ghosh, A. Chatterjee, *Ironmaking and Steelmaking: Theory and Practice*, PHI Learning Private Limited, Delhi **2008**.
[2] A. Kruskopf, L. Holappa, *Metall. Res. Technol.* **2018**, *115*, 201.
[3] S. Deng, A. Xu, G. Yang, H. Wang, *Steel Res. Int.* **2019**, *90*, 1.
[4] K. Ohnuki, T. Hiraoka, T. Inoue, K. Umezawa, N. Matsumoto, *Nippon Steel Techn. Rep.* **1994**, *61*, 52.
[5] Bureau of International Recycling Ferrous Division, *World steel recycling in figures 2013–2017: Steel scrap - a raw material for steelmaking*, https://www.bdsv.org/fileadmin/user_upload/180222-Ferrous-report-2017-V07.pdf, accessed: **2019**.
[6] L. C. Brabie, M. Kawakami, *High Temp. Mater. Process* **2000**, *19*, 241.
[7] M. A. Glinkov, Y. P. Filimonov, V. V. Yurevich, *Steel USSR* **1971**, 202.
[8] M. Kosaka, S. Minowa, *Tetsu-to-Hagane* **1967**, *53*, 983.
[9] R. D. Pehlke, P. D. Goodell, R. W. Dunlap, *Trans. Metall. Soc. AIME* **1965**, *233*, 1420.
[10] Y.-U. Kim, R. Pehlke, *Metall. Trans.* **1974**, *5*, 2527.
[11] J. M. Lommel, B. Chalmers, *Trans. Metall. Soc. AIME* **1959**, *215*, 499.
[12] R. G. Olsson, V. Koump, T. F. Perzak, *Trans. Metall. Soc. AIME* **1965**, *233*, 1654.
[13] R. Guthrie, P. Stubbs, *Can. Metall. Quart.* **1973**, *12*, 465.
[14] K. Mori, T. Sakuraya, *Transactions ISIJ* **1982**, *22*, 984.
[15] H. Nomura, K. Mori, *Tetsu-to-Hagané* **1969**, *55*, 1134.
[16] J. K. Wright, *Metall. Mater. Trans. B* **1989**, *20B*, 363.
[17] M. Shin, J. S. Oh, J. Lee, S. Jung, J. Lee, *Met. Mater. Int.* **2014**, *20*, 1139.
[18] M. A. Glinkov, V. Y. Bakst, M. Medzhibozhskiy, V. I. Sel'skii, *Steel in the USSR* **1972**, 195.
[19] O. Ehrich, Y. K. Chuang, K. Schwerdtfeger, *Arch. Eisenhüttenwesen* **1979**, *50*, 329.
[20] R. Guthrie, L. Gourtsoyannis, *Can. Metall. Quart* **1971**, *10*, 37.
[21] J. Li, G. Brooks, N. Provatas, *Metall. Mater. Trans. B.* **2005**, *36B*, 293.
[22] J. Li, N. Provatas, *Metall. Mater. Trans. B* **2008**, *39*, 268.
[23] M. Medzhibozhskiy, *Publishing house "Vischa shkola". Kyiv*, **1979**.
[24] X. Xi, S. Yang, J. Li, X. Chen, M. Ye, *Ironmak Steelmak.* **2018**, *52*, 1.
[25] F. M. Penz, R. Parreiras Tavares, C. Weiß, J. Schenk, R. Ammer, K. Pastucha, G. Klösch, *Int. J. Heat Mass Transf.* **2019**, *138*, 640.
[26] J. Li, G. A. Brooks, N. Provatas, *AISTech 2004 Proceedings*, Nashville, Tenn., USA **2004**, 833.
[27] F. M. Penz, J. Schenk, R. Ammer, G. Klösch, K. Pastucha, *Metals* **2018**, *8*, 1078.
[28] J. Szekely, Y. K. Chuang, J. W. Hlinka, *Metall. Trans.* **1972**, *3*, 2825.
[29] M. Kawakami, K. Takatani, L. C. Brabie, *Tetsu-to-Hagané* **1999**, *85*, 658.
[30] R. F. Nugumanov, E. V. Protopopov, P. S. Kharlashin, V. Y. Bakst, *Steel Transl.* **2009**, *39*, 624.
[31] H. Sun, Y. Liu, C. Lin, M. Lu, *Proceedings of the 6th ICS 12.-14. May, 2015*, Beijing, China **2015**, 136.
[32] T. Oya, I. Furugaki, H. Matsunaga, T. Tominaga, K. Miyagawa, E. Nomura, *Tetsu-to-Hagané* **1965**, *51*, 1925.
[33] D. D. Burdakov, A. P. Varshavskii, *Stal English* **1967**, *8*, 647.
[34] V. P. Bondarenko, S. G. Afanaśev, *Steel USSR* **1971**, *1*, 185.
[35] H. Gaye, M. Wanin, P. Gugliermina, P. Schittly, *In Proceedings of the 68th Steelmaking Conference*, AIME, Detroit, MI, USA **1985**, 91.
[36] H. Gaye, P. Destannes, J. L. Roth, M. Guyon, *Proceedings of the 6th International Iron and Steel Congress*, Nagoya, Japan, Vol. 4, Steelmaking II **1990**, 11.
[37] K. Isobe, H. Maede, K. Ozawa, K. Umezawa, C. Saito, *Tetsu-to-Hagané* **1990**, *76*, 2033.

**ADVANCED
SCIENCE NEWS**

www.advancedsciencenews.com

**steel
research**
international

www.steel-research.de

[38] K. Ozawa, K. Umezawa, K. Isobe, C. Saito, *Proceedings of the 6th International Iron and Steel Congress*, Nagoya, Japan, Vol. 4, Steelmaking II **1990**, 33.

[39] S. Asai, I. Muchi, *Transactions ISIJ* **1971**, *11*, 107.

[40] H. W. den Hartog, P. J. Kreyger, A. B. Snoeijer, *C.R.M.* **1973**, *37*, 13.

[41] Y. U. Kim, R. D. Pehlke, *Metall. Trans. B* **1975**, *6*, 585.

[42] H. Yorucu, R. Rolls, *Iron Steel Int.* **1976**, *49*, 35.

[43] M. Gol'dfarb, B. I. Sherstov, *J. Eng. Phys. Therm.* **1970**, *18*, 342.

[44] G. Sethi, A. K. Shukla, P. C. Das, P. Chandra, B. Deo, *AISTech 2004 Proceedings*, Nashville, Tenn., USA **2004**, p. 915.

[45] A. K. Shukla, B. Deo, *Proceedings of the International Symposium for Research Scholars on Metallurgy, Materials Science & Engineering*, Chennai, India, December 18–20, **2006**, 1.

[46] A. K. Shukla, B. Deo, D. Robertson, *Metall. Mat. Trans. B* **2013**, *44*, 1407.

[47] D. Guo, Swickard, D. Alavanja, M., J. Bradley, *Iron Steel Technol.* **2013**, *10*, 125.

[48] A. Kruskopf, S. Louhenkilpi, *Proceedings of METEC & 2nd ESTAD*, june 15–19, Düsseldorf, Germany **2015**, 1–4.

[49] A. Kruskopf, *Metall. Mat. Trans. B* **2015**, *46*, 1195.

[50] P. M. Shurygin, V. D. Shantarin, *Izvestiya vysshikh uchebnykh zavedenii, Chernaya metallurgiya* **1963**, *6*, 5–11.

[51] V. G. Levič, *Physicochemical Hydrodynamics*, Prentice-Hall, New York **1962**.

[52] F. Oeters, *Metallurgie der Stahlherstellung*, Springer Berlin Heidelberg, Berlin, Heidelberg **1989**.

[53] L. Zhang, F. Oeters, *Schmelzen und Mischen von Legierungsstoffen in Stahlschmelzen: Methoden der mathematischen Modellierung*, Verlag Stahleisen GmbH, Düsseldorf, Germany **2012**.

[54] O. Ehrich, Y. K. Chuang, K. Schwerdtfeger, *Int. J. Heat Mass Transf.* **1978**, *21*, 341.

[55] E. Specht, R. Jeschar, *Steel Research* **1993**, *64*, 28.

[56] S. A. Krupennikov, Y. P. Filimonov, *Steel Transl.* **2007**, *37*, 217.

[57] H. Mehrer, *Diffusion in Solids: Fundamentals, Methods, Materials, Diffusion-Controlled Processes*, Springer - Verlag GmbH, Berlin Heidelberg **2007**.

[58] J. Szekely, N. J. Themelis, *Rate Phenomena in Process Metallurgy*, John Wiley & Sons, Inc, New York **1971**.

[59] V. Seshadri, R. Parreiras Tavares, C. Antonio da Silva, I. Alves da Silva, *Transport Phenomena: Fundamentals and Applications in Metallurgical and Materials Engineering*, ABM, Sao Paulo **2011**.

[60] M. Necati Özisik, *Heat Conduction*, John Wiley & Sons, Inc, New York **1993**.

[61] J. Ågren, *Scripta Metallurgica* **1986**, *20*, 1057.

[62] Y. Ueshima, S. Mizoguchi, T. Matsumiya, H. Kajioka, *Metall. Trans. B* **1986**, *17*, 845.

[63] D. Goldberg, G. R. Belton, *Metall. Trans.* **1974** *5*, 1643.

[64] H. Bester, K. W. Lange, *Arch. Eisenhüttenwesen* **1972**, *43*, 207.

[65] Y. Wanibe, S. Takai, T. Fujisawa, H. Sakao, *Transactions ISIJ* **1982**, *22*, 560.

[66] B. G. Thomas, I. V. Samarasekera, J. K. Brimacombe, *Metall. Trans. B* **1987**, *18*, 119.

[67] J. Miettinen, S. Louhenkilpi, *Metall. Mat. Trans. B* **1994**, 909.

[68] J. Miettinen, *Metall. Mat. Trans. B* **1997**, 281.

[69] K. C. Mills, S. Karagadde, P. D. Lee, L. Yuan, F. Shahbazian, *ISIJ Int.* **2016**, *56*, 274.

[70] Y. Kim, B. Farouk, J. Keverian, *ASME J. Eng. Ind.* **1991**, *113*, 53.

[71] T. G. O'Connor, J. A. Dantzig, *Metall. Mat. Trans. B* **1994**, *25*, 443.

[72] G. Li, B. G. Thomas, *Metall. Mat. Trans. B* **1996**, *27*, 509.

[73] J. Miettinen, *Report TKK-V-B126* **1996**.

[74] S. Joo, J. W. Han, R. I. L. Guthrie, *Metall. Trans. B* **1993**, *24*, 767.

[75] A. Kumar, S. Abhishek Kumar, Rajeev, *J. King Saud Univ.-Sci.* **2018**, 1, in press. https://doi.org/10.1016/j.jksus.2018.09.009

[76] M. Turkyilmazoglu, *Int. J. Thermal Sci.* **2018**, *126*, 67.

[77] V. R. Voller, F. Falcini, *Int. J. Heat Mass Transf.* **2013**, *58*, 80.

[78] F. Penz, P. Bundschuh, J. Schenk, H. Panhofer, K. Pastucha, A. Paul, presented at 2nd VDEh-ISIJ-JK Symposium, Stockholm, 2017, Stockholm **2017**.

[79] J. Szekely, P. S. Chhabra, *Metall. Materi. Trans. B* **1970**, *1*, 1195.

[80] H. Windisch, *Thermodynamik: Ein Lehrbuch für Ingenieure*, Oldenbourg Verlag, München **2011**.

[81] F. M. Penz, J. Schenk, R. Ammer, K. Pastucha, B. Maunz, *La Metallurgia Italiana* **2018**, *11/12*, 36.

[82] D. Jang, Y. Kim, M. Shin, J. Lee, *Metallurgical and Materials Transactions B* **2012**, *43*, 1308.

[83] M. Eisenberg, C. W. Tobias, C. R. Wilke, *Chem. Eng. Prog., Symp. Ser.* **1955**, *51*, 1.

[84] T. H. Chilton, A. P. Colburn, *Ind. Eng. Chem.* **1934**, *26*, 1183.

[85] R. G. Olsson, V. Koump, T. F. Perzak, *Trans. Metall. Soc. AIME* **1966**, *236*, 426.

[86] A. Esser, S. Grossmann, *Phys. Fluids* **1996**, *8*, 1814.

[87] A. Racina, *Vermischung in Taylor-Couette Strömung*, Universitätsverlag Karlsruhe, Karlsruhe **2009**.

[88] E. R. G. Eckert, *Einführung in den Wärme- und Stoffaustausch*, Springer Berlin Heidelberg, Berlin Heidelberg New York **1966**.

[89] Y. K. Chuang, J. Szekely, *Int. J. Heat Mass Transfer* **1971**, *14*, 1285.

[90] Y. K. Chuang, W. Wepner, K. Schwerdtfeger, *Archiv für das Eisenhüttenwesen* **1973**, *44*, 243.

[91] Y. K. Chuang, O. Ehrich, *Int. J. Heat Mass Transf.* **1974**, *17*, 945.

[92] C. E. Seaton, A. A. Rodriguez, M. González, M. Manrique, *ISIJ Int.* **1983**, *23*, 14.

[93] G. Caffery, P. Rafiei, T. Honeyands, D. Trotter, *Proceedings of AISTech Volume I*, September 2014, Nashville, USA **2004**, p. 503.

[94] A. Sato, R. Nakagawa, S. Yoshimatsu, A. Fukuzawa, T. Ozaki, *Trans. ISIJ* **1981**, *21*, 879.

[95] A. Sato, R. Nakagawa, S. Yoshimatsu, A. Fukuzawa, T. Ozaki, *Trans. ISIJ* **1981**, *21*, 66.

[96] E. Honma, S. Okubo, T. Oya, H. Matsunaga, *Tetsu-to-Hagane* **1964**, *50*, 2166.

[97] P. Brian, H. B. Hales, *AIChE J.* **1969**, *15*, 419.

[98] Q. Jiao, N. J. Themelis, *Can. Metall. Quart.* **1993**, *32*, 75.

[99] E. A. Mizikar, *Trans. Metall. Soc. AIME* **1967**, *239*, 1747.

[100] E. A. Mizikar, *Iron Steel Eng.* **1970**, *47*, 53.

[101] J. J. Gautier, Y. Morillon, J. Dumont-Fillon, *J. Iron Steel Inst.* **1970**, *208*, 1053.

[102] S. Asai, I. Muchi, *Trans. ISIJ* **1970**, 250.

[103] I. Muchi, S. Asai, M. Miwa, *Proceedings ICSTIC, Suppl. Trans. ISIJ* **1971**, *11*, 347.

[104] M. Hansen, *Constitution of Binary Alloys*, McGraw-Hill, New York **1958**.

[105] F. M. Penz, J. Schenk, R. Ammer, G. Klösch, K. Pastucha, *Processes* **2019**, *7*, 186.

[106] Y. Lytvynyuk, *Thermodynamic and Kinetic Modeling of Metallurgical Reactions*, Montanuniversitaet Leoben, Leoben **2013**.

[107] Y. Lytvynyuk, J. Schenk, M. Hiebler, A. Sormann, *Steel Res. Int.* **2014**, *85*, 537.

[108] C. Chigwedu, *Beitrag zur Modelierung des LD-Sauerstoffblasverfahrens zur Stahlerzeugung*, TU Clausthal, Clausthal **1997**.

[109] A. Karma, W.-J. Rappel, *Phys. Rev. E* **1998**, *57*, 4323.

[110] N. Provatas, N. Goldenfeld, J. Dantzig, *Phys. Rev. Lett.* **1998**, *80*, 3308.

[111] K. R. Elder, M. Grant, N. Provatas, J. M. Kosterlitz, *Phys. Rev. E Stat. Nonlin. Soft Matter. Phys.* **2001**, *64*, 21604.

[112] J. H. Jeong, N. Goldenfeld, J. A. Dantzig, *Phys. Rev. E Stat. Nonlin. Soft Matter Phys.* **2001**, *64*, 41602.

[113] B. Lally, L. Biegler, H. Henein, *Metall. Trans. B* **1990**, *21*, 761.

[114] J. E. Lait, *Solidification and heat transfer in the continuous casting of steel*, University of British Columbia, Vancouver, Canada **1973**.

[115] K. H. Cho, B. M. Kim, *J. Mat. Sci. Technol.* **2008**, *24*, 389.

[116] J. E. Lait, J. K. Brimacombe, F. Weinberg, *Ironmaking. Steelmaking (Quarterly)* **1974**, *1*, 90.

[117] K. Mori, M. Sano, *Tetsu-to-Hagane* **1981**, *67*, 672.

[118] P. Mink, G. van Unen, B. Deo, R. Boom, *Proceedings 1st European Oxygen Steelmaking Congress EOSC*, June 21 −23 Düsseldorf/ Neuss, Germany **1993**, p. 65.

[119] K. Nakanishi, T. Fujii, J. Szekely, *Ironmaking Steelmaking (Quarterly)* **1975**, *3*, 193.

[120] A. K. Shukla, B. Deo, D. G. C. Robertson, *Metall. Mat. Trans. B* **2013**, *44*, 1398.

[121] J. Kron, A. Lagerstedt, H. Fredriksson, *Int. J. Cast Met. Res.* **2005**, *18*, 29.

[122] A. Lagerstedt, J. Kron, F. Yosef, H. Fredriksson, *Mat. Sci. Eng.: A* **2005**, *413*–*414*, 44.

[123] C. R. Swaminathan, V. R. Voller, *Int. J. Numer. Method H* **1993**, *3*, 233.

Publication 2:

Analytical and numerical determination of the heat transfer coefficient between scrap and hot metal based on small-scale experiments

Analytical and numerical determination of the heat transfer coefficient between scrap and hot metal based on small-scale experiments

Florian Markus Penz [a,*], Roberto Parreiras Tavares [b], Christian Weiss [c], Johannes Schenk [d], Rainer Ammer [e], Krzysztof Pastucha [f], Gerald Klösch [g]

[a] K1-MET GmbH, Linz, Austria
[b] Department of Metallurgical and Materials Engineering, Federal University of Minas Gerais, Belo Horizonte, Brazil
[c] Chair for Process Technology and Industrial Environmental Protection, Montanuniversitaet Leoben, Austria
[d] Chair of Ferrous Metallurgy, Montanuniversitaet Leoben, Austria
[e] voestalpine Stahl GmbH, Linz, Austria
[f] Primetals Technologies Austria GmbH, Linz, Austria
[g] voestalpine Stahl Donawitz GmbH, Donawitz, Austria

ARTICLE INFO

ABSTRACT

Dynamic modelling of the Linz-Donawitz oxygen steelmaking process (LD) is one of the most challenging tasks in the current economic situation for the optimization of integrated steel plants. One of the main influencing parameters is the melting and dissolution behaviour of scrap. Scrap is used as an iron source and coolant for the exothermic reactions inside the LD converter. Literature-based dissolution equations are commonly used in modelling. As a basis for developing a new numerical model for scrap melting with coupled heat and mass transfer, laboratory-scale experiments were conducted. The aim of the experiments was the determination of the heat transfer coefficient between scrap and liquid hot metal through a combination of thermocouple measurements with analytical and numerical solutions. The heat transfer coefficients achieved were in the range between 4.5 and 6.2 kW/m^2 K. The heat transfer coefficients estimated in the present work are approximately 10 times smaller than those evaluated through existing Nusselt correlations. These discrepancies may be explainable through specific effects of scrap dissolution, e.g. shell freezing and successive melting or air-gap formation between solidified shell and mother scrap increasing the heat transfer resistance at the solid scrap to melt interface. The numerical solution to the heat transfer problem shows identical results to the analytical solution of the problem and provides a feasible basis for further research and development.

© 2019 Elsevier Ltd. All rights reserved.

1. Introduction

In modern steelmaking, the LD converter, invented in the early 1950s in Linz and Donawitz (LD), is the dominant reactor to convert hot metal into crude steel [1]. During the process, technically pure oxygen is blown onto the liquid hot metal at supersonic speed. Through the oxidation reactions of carbon, silicon, manganese and phosphorus, heat is generated. Therefore, right at the beginning of each heat, scrap is charged. It acts, beside hot metal, as an iron source, but also as an important coolant. In other words, the oxygen steelmaking process is an important recycling process too. [1,2] As shown in previous publications by the authors in [3,4], the dissolution and melting behavior of scrap influences the whole process cycle in the converter. Melting and dissolution behaviour of scrap in liquid hot metal is a complex phenomenon coupling heat and mass transfer, as reported in several publications e.g. [2,5–8]. The work to be reported in this paper forms part of a project aimed to create an improved scrap melting sub-model for further usage in a dynamic LD converter model, which was published by Lytvynyuk et al. in [9,10].

Many experimental studies have been performed evaluating the heat transfer coefficient between hot metal and scrap. Gaye et al. published the results of their experimental investigation of the scrap melting time in [6,11]. The heat transfer coefficient of the liquid phase was obtained as a function of blowing conditions with expressed by the correlation presented in Eq. (1)

$$h = 5000 * \dot{\varepsilon}^{0.2} \tag{1}$$

where h is the mass transfer coefficient in [W/m^2 K] and $\dot{\varepsilon}$ is the average mixing power. Especially for LD heats, a heat transfer coefficient of 17 kW/m^2 K was mentioned [6]. Den Hartog et al. in [7]

estimated a heat transfer coefficient between bath and scrap of approximately 47.5 kW/m^2 K from special experiments carried out in a converter and using the Chilton Colburn analogy. Szekely et al. presented in [8] direct experimental proof of the melting and dissolution behaviour of low carbon steels in hot metal where a fixed heat transfer coefficient of approximately 3.4 W/m^2 K was required to match with the measured results. They expected barely lower heat transfer coefficients in the case of stagnant melts and considerably larger heat transfer coefficients exceeding 56 kW/m^2 K for highly agitated melts, such as those in LD converters [8]. In a further publication solving melting and solidification problems with the use of Greeńs function Chuang and Szekely assumed a heat transfer coefficient of 5680 W/m^2 K [12]. Another experimental investigation was carried out by Kawakami et al. [13] investigating the dissolution of cylindrical rods in high carbon melts. The estimated heat transfer coefficient varied from 27.7 kW/m^2 K to 77.2 kW/m^2 K [13]. Isobe et al. performed scrap melting experiments in a 300 kg induction furnace and in a 5 ton converter and reported a range of heat transfer coefficients between 23.26 kW/m^2 K and 46.5 kW/m^2 K in [14]. Li and Provatas [15] investigated the kinetics of scrap melting in liquid steel where their experimental investigation followed the trends with the use of an assumed heat transfer coefficient of 5 kW/m^2 K.

As could be seen, the variation of determined heat transfer coefficients in previous publications ranges from 5 up to 75 kW/m^2 K for the same problem.

To develop a numerical scrap melting model using new approaches, considering mass and heat transfer, a first step was to understand the heat transfer from the liquid melt into the scrap. Therefore, an experimental investigation of the heating of steel scrap in hot metal was executed. Based on an analytical model for transient heat transfer, the heat transfer coefficient was evaluated. With these findings, a numerical heat transfer model was created for further purposes.

2. Analytical model and theoretical assumptions

For the determination of the heat transfer coefficient, a one-dimensional heat flow in radial direction (r) of a steel cylinder is assumed. A schematic overview of the analytical problem and the position of the considered one-dimensional profile is shown in Fig. 1.
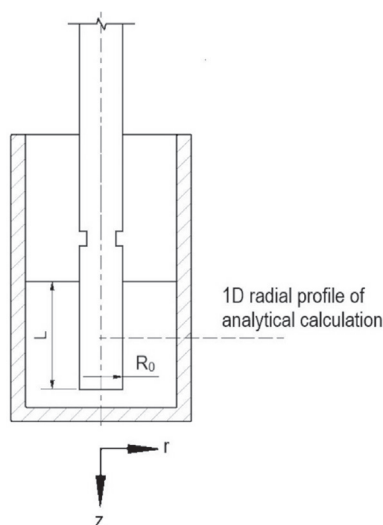

Fig. 1. Schematic overview of the analytical problem.

The considered geometrical parameters used in the analytical model are L for the height and R_0 for the radius of the cylinder are shown in Fig. 1. Assuming no inner heat source and one-dimensional heat flow, the Fourier differential equation for heat conduction becomes for cylindrical coordinates

$$\frac{\partial T}{\partial t} c_P \rho = \lambda * \frac{1}{r} \frac{\partial}{\partial r}\left(r \frac{\partial T}{\partial r}\right) \tag{2}$$

where T is the temperature in K, c_P is the specific heat capacity in J/kgK, ρ is the density in kg/m^3 and λ is the thermal conductivity of the scrap in W/mK. It is well known that c_P, ρ and λ are functions of temperature, nevertheless they were assumed to be constant. Eq. (2) was solved adopting the following boundary conditions: at the surface of the cylinder (radius $r = R_0$):

$$-\lambda * \frac{\partial T}{\partial r} = h * (T_{if} - T_{HM}) \tag{3}$$

and at $r = 0$:

$$\frac{\partial T}{\partial r} = 0. \tag{4}$$

The analytical solution according to [16] for the temperature profile with the separation of variables $T(r,t) = \Psi(r) * \Phi(t)$ of the Fourier differential equation is:

$$T(r,t) = \frac{2}{R_0^2} \sum_{m=1}^{\infty} \frac{C_m^2 * J_0(C_m r)}{\left(C_m^2 + \left(\frac{h}{\lambda_{HM}}\right)^2 * J_0^2(C_m R_0)\right)} * e^{-\alpha C_m t}$$
$$* \int_0^R r' J_0(C_m r') * f(r') dr' \tag{5}$$

With the assumptions also used in [16] of an initial scrap temperature $T_{scr} = f(r) = constant$ and a hot metal temperature $T_{HM} = constant$ the required solution becomes:

$$T(r,t) = T_{HM} + \frac{2(T_{scr} - T_{HM})}{R_0} \sum_{m=1}^{\infty} \frac{1}{C_m} * \frac{J_1(C_m R_0) * J_0(C_m r)}{J_1^2(C_m R_0) + J_0^2(C_m R_0)} * e^{-\alpha C_m^2 t} \tag{6}$$

The eigenvalues C_m are obtained from the roots of the following transcendental equation with the Biot number $Bi = h * R_0 / \lambda_{scr}$:

$$C_m * R_0 * J_1(C_m R_0) - Bi * J_0(C_m R_0) = 0 \tag{7}$$

The common way of deriving the heat transfer coefficient h is with the use of Nusselt correlations, where a few correlations can be found in several publications e.g. [13,17–20] According to the experimental measurements, explained in the next chapter, a system with natural convection is investigated in the current work, where the Nusselt number is a function of the Grashof number (Gr) and the Prandtl number [17,20].

$$Nu = \frac{hL}{\lambda} = f(Gr, Pr) = f(Ra) \tag{8}$$

The Grashof number approximates the ratio of buoyancy to viscous force acting on fluid and is described in following equation.

$$Gr = \frac{g * L^3}{v_{fluid}^2} * \beta * (T_{if} - T_{HM}) \tag{9}$$

In this equation, g is the acceleration of gravity and $\beta = -\frac{1}{\rho}\left(\frac{\partial \rho}{\partial T}\right)_p$ is the isobar thermal expansion coefficient with the temperature T. The Grashof and the Prandtl numbers joined together result in the Rayleigh number (Ra), defined as follows:

$$Ra = Pr * Gr = \frac{g * L^3}{v_{fluid}^2} * \frac{\lambda_{fluid}}{c_{P,fluid} * \rho_{fluid}} * \beta * (T_{if} - T_{HM}) \tag{10}$$

Unfortunately, the heat transfer from vertical cylinders has received less attention in literature than that for horizontal cylinders in cross-flow. At least for the consideration of natural convection, the cylinder surface could be treated like the system of a planar vertical plate. One specific correlation for free convection along a vertical cylinder was derived by Windisch in [20] and is valid for $10^{-1} < Ra < 10^{12}$ and $Pr \geq 10^{-3}$ where L is the height and $d = 2 * R_0$ is the diameter of the cylinder in m.

$$Nu_m = \left[0.825 + 0.387 \left(\frac{Ra}{[1 + (0.492/Pr)^{9/16}]^{8/27}} \right)^{1/6} \right]^2 + 0.87 * \frac{L}{d}$$
(11)

The thermal and physical properties as well as geometric parameters of scrap and hot metal used in the present work are listed in Table 1. Additional parameters are listed as well, to present the variation of thermal and physical properties published in previous publications.

The density of the scrap ρ is defined by Eq. (12), published by Miettinen in [23] and is dependent on the temperature in °C and the scrap composition. The scrap is assumed to be ferritic and the density for a multicomponent system (composition $C_{i,scr}$ in wt.-%) is, according to the considered elements i of the scrap, defined with Eq. (11) according to [23].

$$\rho_{scr} = 7875.96 - 0.297T - 5.62 * 10^{-5}T^2$$
$$+ \left(-206.35 + 0.00778T + 1.472 * 10^{-6}T^2 \right) * C_{C,scr}$$
$$+ 36.86 * C_{Si,scr} - 30.78 * C_{Mn,scr}$$
(12)

3. Numerical considerations

To create an improved scrap melting sub-model to describe the melting and dissolution behaviour of scrap in a dynamic LD converter model based on the model published by Lytvynyuk et al. in [9,10], a first step is to prove the theoretical assumptions for the heat transfer. In a future final version of the model, the physical and thermal parameters are planned to be a function of the temperature or the carbon concentration, which is why a numerical solution is strived to be developed. To validate the finite volume code, the analytical model from Section 2 and the experimental measurements described in Section 4. This section will give an overview of the numerical model itself. In Section 5, the validation and results will be presented and discussed.

For the present transient explicit numerical model, the method of finite volume is used. To be able to validate the basic numerical model with the analytical model a numerical solution for the heat transfer coefficient is searched for a radial temperature profile within the cylinder in radial direction. The profile should be on the same position of the analytical model given in Fig. 1. The size of the volume elements is equally distributed along the whole cylinder radius. For the basic model of heat transfer, the mass transfer, which is the second main parameter in the melting and dissolution behaviour scrap, will not be discussed in the present work.

As also assumed for the analytical model, the thermal conductivity will be constant, but for further improvements it is considered that the thermal conductivity on the interface between two control volumes will be estimated by the usage of the harmonic average. For transient numerical modelling of the axisymmetric problem the one-dimensional conservation equation of heat conduction for cylindrical coordinates is given in Eq. (13). The grid and control volumes are indicated according to Patankar's discretization scheme published in [26].

$$c_P \rho \frac{\partial T}{\partial t} = \frac{1}{r} \frac{\partial}{\partial r} \left(r\lambda \frac{\partial T}{\partial r} \right) + S$$
(13)

Discretized by means of the control volume formulation of Patankar [26], the discretization equation for an explicit scheme is written as Eq. (14), whereby 0 in superscript defines the value on the present time step.

$$a_P T_P = a_E T_E^0 + a_W T_W^0 + a_N T_N^0 + a_S T_S^0$$
$$+ \left[a_P^0 - a_E - a_W - a_N - a_S - S * \Delta V \right] * T_P^0 + b$$
(14)

where

$$a_E = \lambda_E * \Delta r / (r_E * (\delta\theta)_e)$$
(15a)

$$a_W = \lambda_W * \Delta r / (r_W * (\delta\theta)_W)$$
(15b)

$$a_N = \lambda_N * \Delta\theta * r_N / (\delta r)_N$$
(15c)

$$a_S = \lambda_S * \Delta\theta * r_s / (\delta r)_S$$
(15d)

$$a_p = a_P^0 = c_P \rho * \Delta V / \Delta t$$
(15e)

$$b = S * \Delta V$$
(15f)

$$\Delta V = (r_S + r_N)/2 * \Delta\theta * \Delta r$$
(15g)

Table 1
Thermal and physical properties as well as geometric parameters for scrap and hot metal used in analyses.

Parameter	Nomenclature	Data	Literature
Initial radius	$r = R_0$	0.006 m	
Cylinder height	L	0.03 m	
Specific heat capacity of the fluid	$c_{P,fluid}$	780 J/kgK	[18]
		910 J/kgK	[21]
Specific heat capacity of the scrap	$c_{P,scrap}$	480 J/kgK at 100 °C	[22]
Density	ρ	7819 kg/m³	[23]
Thermal conductivity of the scrap	λ_{scr}	42.5 W/mK at 25 °C	[22]
Thermal conductivity of the liquid hot metal	λ_{HM}	34 W/mK	[24]
		16.5 W/mK at 1550 °C	[21]
Thermal expansion coefficient	β	6.2 * 10⁻⁵ 1/K	[24]
		1.4 * 10⁻⁴ 1/K	[21]
Viscosity	μ	0.01 Pa s at 1200 °C	[25]
		0.00795 Pa s at 1300 °C	[25]
		0.0062 Pas at 1400 °C	[25]
		1400 °C ≤ T≤1600 °C:	
		$(-0.0105*T + 22.9) * 10^{-3}$ Pa s	[21]

Assuming a one-dimensional system in radial direction, all elements with index E and W will become 0 and $\Delta\theta$ is defined to be 1. The source term S is expressed by the surrounding fluid temperature such that Eq. (3) is valid as a boundary condition. A detailed description of its determination can be found in [26] and results in an interface boundary definition for the coefficient b_{if} given in equation (16).

$$b_{if} = T_{HM} * h * R_0 \qquad (16)$$

In Eq. (16) b_{if} forms the discretized coefficient of heat flux into the scrap at the solid/liquid interface. When the explicit scheme is used, there is a limitation for the time step. To ensure that the coefficient a_P^0 will not become negative (see Patankar [26]), the time step has to be lower than the value given by Eq. (17).

$$\Delta t < c_P \rho * (\Delta r)^2 / (2 * \lambda) \qquad (17)$$

The end simulations were developed to reproduce the duration of the experiments. A flowsheet for the description of the explicit approach to solve the heat transfer problem shown in Fig. 2.

4. Experimental evaluation of the temperature profile

The experimental measurements were performed in a high temperature vertical tube furnace. An alumina crucible was charged with 320 g to 345 g of hot metal. The heating rate was 300 K/min to reach the starting temperatures of 1305 °C, 1370 °C and 1450 °C. At each temperature, three measurements were performed. Before the first and between each further dissolution experiment, a holding time of 30 min was set for the homogenization of the initial temperature. To prevent oxidation of the hot metal, the vertical tube furnace was purged with nitrogen during the heating and melting process. The scrap geometry was cylindrical with a diameter of 12 mm and a length of 40 mm. 30 mm of the cylinder were submerged into the liquid hot metal. A 5 mm screw thread was machined to fix the sample on a holding device. In the centre of the cylinder, a bore of 1.7 mm in diameter was drilled until the middle of the submerged depth (15 mm from the cylinder
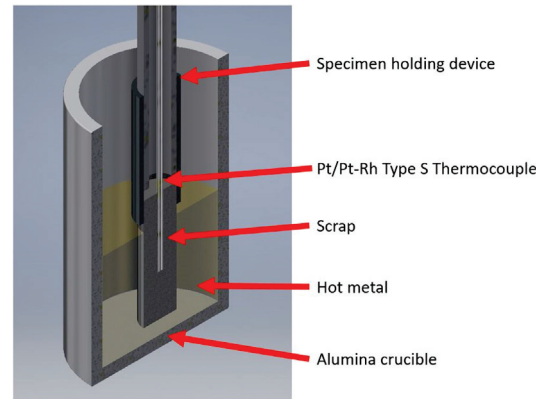

Fig. 3. Schematic technical set-up of the experiments.

tip). A Type S Pt/Pt-10%Rh Thermocouple, with an uncertainty of +/−1.5 °C, was placed in the bore. Through the axial movement of the cylinder, carried out by a fast pneumatic cylinder, the sample was transported into the melt where a starting temperature of the specimen centre of 100 °C was determined. The temperature measurement were carried out for 25 s. A sketch of the technical structure of the experiment is shown in Fig. 3.

In a previous test series of this research work, the authors published the melting and dissolution behaviour of Ultra Low Carbon (ULC) scrap in hot metal in [27]. In the course of these investigations, scrap specimens were used for verification of the equilibrium temperature between the liquid metal and the submerged sample, which results from the heat exchange between hot melt and cold scrap [27]. The same determination was used for this work and it was verified that the measurements are reproducible.

5. Results and discussion

For the determination of the heat transfer coefficient, the temperature in the centre of the cylinder was measured by a Type S
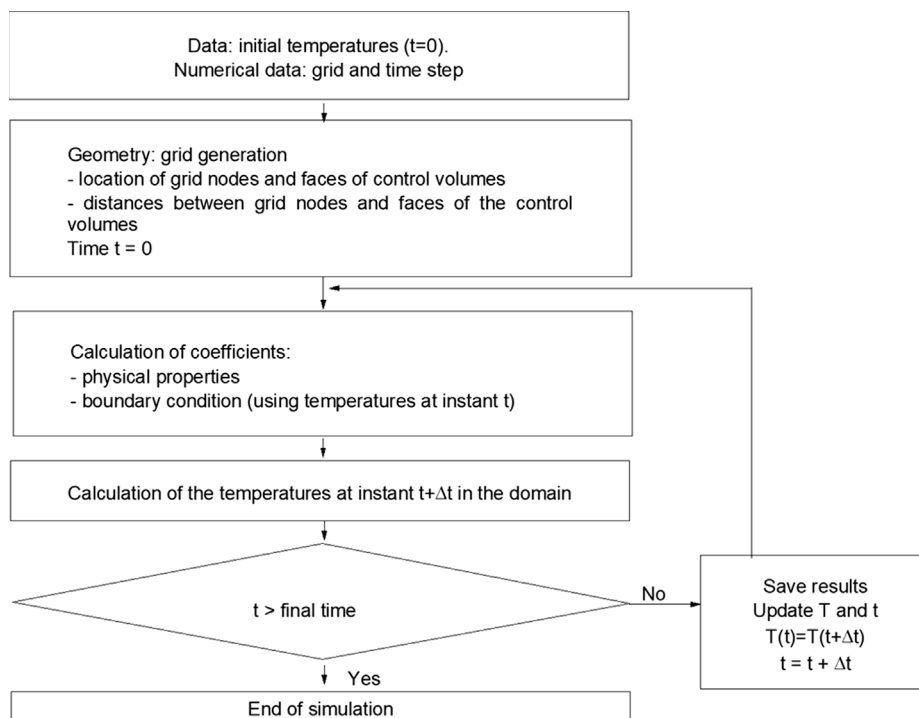

Fig. 2. Flowsheet on the explicit numerical model for transient heat transfer between liquid hot metal and scrap.
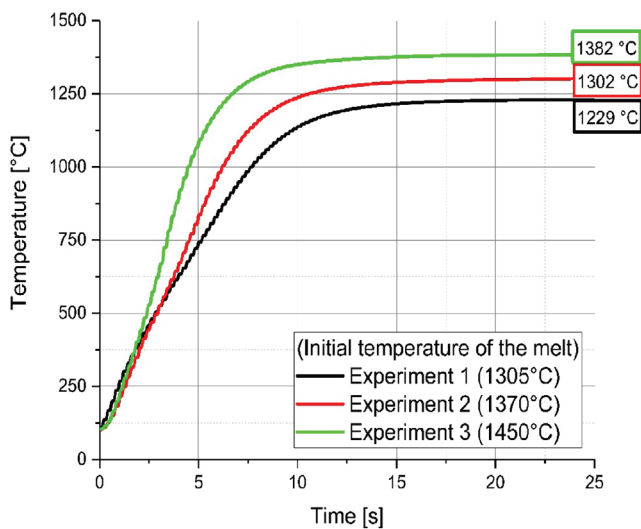
Fig. 4. Transient evolution of the measured temperature in the centre of the cylinder; initial melt temperature as curve parameter.

Fig. 5. Experimental and modelled temperature development in the centre of the scrap for an initial melt temperature of 1300 °C.

thermocouple as described in Section 4. The transient evolution of the measured temperature in the core of the cylinder, based on the three investigated starting temperatures of the melt, are shown in Fig. 4. Three measurements were carried out at each initial hot metal temperature.

Fig. 4 illustrates that in the present system, an equilibrium temperature between the core of the scrap and the hot metal melt is reached within approximately 15 s. Higher initial temperatures lead to a steeper variation of the temperature with time. The measurements also show that the equilibrium temperature is approximately 70 °C below the starting temperature of the melt. In Table 2 the measured starting and equilibrium temperatures of the hot metal and the scrap are listed.

Using the Nusselt correlation from Eq. (11), the relation between the Nusselt number and the heat transfer coefficient in Eq. (8) as well as the thermal properties and geometries from Table 1, the heat transfer coefficient can be estimated. As an approximation, the specific heat was assumed as an harmonic average between 780 J/kgK from [18] and 480 J/kgK from [22]. For simplification, the thermal conductivity was assumed to be constant and equal for the scrap and the hot metal at 42.5 W/mK [22]. The calculated heat transfer coefficients, using Eq. (11) are in the range between 41 kW/m^2 K and 46 kW/m^2 K.

Based on the analytical considerations of Section 2, a computational model was created using the software Matlab™. The only changeable value in this model is the heat transfer coefficient. A planned output of the analytical and numerical program is the temperature increase in the centre of the cylinder. With the use of the temperature measurements and the calculated temperature profile of the analytical model, the heat transfer coefficient was fitted and presented in Fig. 5 at an initial hot metal temperature of 1300 °C. The best solution is a heat coefficient of 4500 W/m^2 K for this temperature, which is around 10 times smaller than the
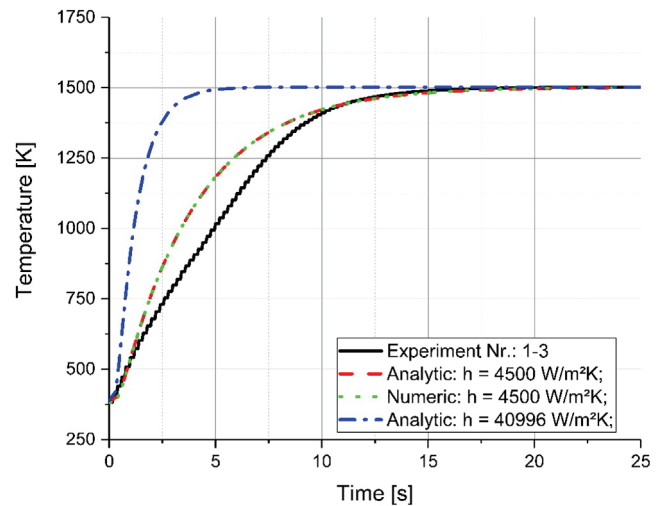
approximated heat transfer coefficient using the Nusselt correlation from Eq. (11). This uncertainty may have several reasons. Scrap melting is indeed a complex combination of heat and mass transfer. One can be a shell formation of hot metal in the initial stages which is reported to occur in most published articles e.g. [5,6,19,24,28]. The release of the latent heat of melting should be another factor. A possible influence might also be an air-gap formation, reported in [29–31], between the frozen shell and the mother scrap, which decreases the heat transfer coefficient. Finally, there is a lack of information related to the thermal and physical parameters for carbon-saturated liquid iron melts like hot metal. This is one point explaining the slight differences in the analytical result and the experimentally measured temperature increase. What is notable is definitely the usage of constant specific heat capacity, thermal conductivity and density resulting in minor deviations during analytical and numerical modelling. Those parameters are naturally a function of the temperature. Fig. 5 shows that the results of the numerical method fit perfectly with the analytical solution. This result shows that the basic assumptions of the numerical model are definitely correct, which allows an ongoing improvement for the creation of an improved scrap melting and dissolution sub-model for further application in a dynamic LD converter model.

Similar results for an initial melt temperatures of 1375 °C and 1450 °C can be found in Figs. 6 and 7. In both cases, an equilibrium temperature between the scrap core and the melt will be reached within approximately 15 s (1302 °C and 1382 °C respectively). The best fitting heat transfer coefficients (5 kW/m^2 K and 6.2 kW/m^2 K, respectively) are about 7 to 8 times smaller than the calculated ones (45 kW/m^2 K and 41.8 kW/m^2 K, respectively) based on the Nusselt correlation given in Eq. (11).

The heat transfer coefficients estimated in the present work are partly lower than the coefficients found in the literature. This was

Table 2
Starting and final temperatures of the hot metal and scrap as well as the determined heat transfer coefficients between scrap and hot metal.

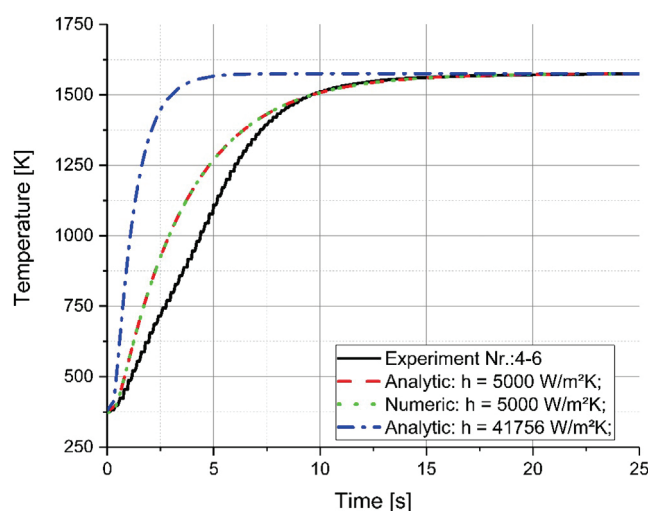|	Initial melt temperature [°C]	Final melt and scrap core temperature [°C]	Experimental Heat transfer coefficient [kW/m^2 K]	Heat transfer coefficient based on Eq. (11) [kW/m^2 K]
Experiment 1 – 3	1305	1229	4.5	41.0
Experiment 4 – 6	1370	1302	5.0	41.8
Experiment 7 – 9	1450	1382	6.2	45.0

Fig. 6. Experimental and modelled temperature development in the centre of the scrap for an initial melt temperature of 1370 °C.
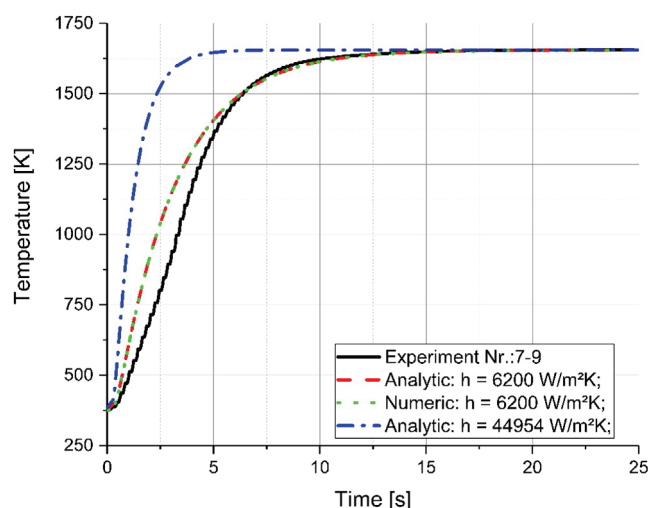

Fig. 7. Experimental and modelled temperature development in the centre of the scrap for an initial melt temperature of 1450 °C.

expected because the present system was only under natural convection. The present heat transfer coefficients are comparable to those reported by Szekely et al. in [8], who matched their measurements to a fixed heat transfer coefficient of 3.4 kW/m^2 K, from Chuang and Szekely in [12] with 5.7 kW/m^2 K and Li and Provatas in [15] with a constant heat transfer coefficient of 5 kW/m^2 K. The present equilibrated temperature ranges of 1229–1382 °C result in a heat transfer range of 4.5–6.2 kW/m^2 K. However, higher heat transfer coefficients around 50 kW/m^2 K, which are reported in several publications [7,13,14], could only be reached theoretically by means on the Nusselt correlation from Eq. (11), but it isńt consistent with the experimental heat transfer coefficient. Through an increase in temperature, the natural convection will lead to a higher heat transfer coefficient. Consequently, it might be reasonably assumed that only in the limit case of highly turbulent and agitated melts, the heat transfer might be even higher than 50 kW/m^2 K, but this case is not reachable with the present experimental equipment.

In summary, the outcomes of this work clearly indicate that the numerical considerations for a new scrap melting model are accurate, but several improvements have to be taken into account.

Additional measurements in highly agitated melts would definitely increase the heat transfer coefficient. A further experimental method to register hot and cold regions in the interface between solid and liquid will be the thermography. The method might be well adapted to visualize the results of the findings in the present paper. However, a modified experimental setup has to be installed to realize similar investigations. The employment of temperature-dependent thermal and physical parameters would also provide less uncertainty in the reported models. The scrap melting and dissolution in the LD process is indeed a very complex combination of heat transfer and mass transfer combined with the kinetics of chemical reactions and the bath conditions. Every small and experimentally validated step will lead to the final aim of creating an improved model for dynamic LD converter steelmaking.

6. Conclusions

In the present research study, the heat transfer between solid scrap and liquid hot metal is investigated. Laboratory-scale experiments on the dissolution and melting behaviour of scrap are carried out. Thermocouple measurements were used to determine the temperature increase in the centre of the cylindrical scrap specimen. These measurements are processed analytically as well as numerically and the heat transfer coefficients are determined. These coefficients obtained are instrumental for further studies in regard to the creation of a numerical scrap melting sub-model for a dynamic LD converter model.

The results of the present work show that the analytical solution gives predictions that are very close to those of the numerical solution. The heat transfer coefficients determined are in the range from 4.5 kW/m^2 K to 6.2 kW/m^2 K, showing an increase with increasing initial temperature of hot metal. The heat transfer coefficients estimated in the present work are approximately 10 times smaller than those evaluated through existing Nusselt correlations. These discrepancies are explainable through typical effects of scrap dissolution, e.g. shell freezing and melting or air-gap formation between solidified shell and mother scrap as well as the release of the latent heat of melting. It should be mentioned, that there exists also a lack of reliable information concerning the thermal and physical parameters for carbon saturated liquid iron melts like hot metal.

Conflicts of interest

The authors declare no conflict of interest.

Appendix A. Supplementary material

Supplementary data to this article can be found online at https://doi.org/10.1016/j.ijheatmasstransfer.2019.04.085.

References

[1] A. Ghosh, A. Chatterjee (Eds.), Ironmaking and Steelmaking: Theory and Practice, PHI Learning Private Limited, Dehli, 2008, pp. 285–292.

[2] A. Kruskopf, L. Holappa, Scrap melting model for steel converter founded on interfacial solid/liquid phenomena, Metall. Res. Technol. 115 (201) (2018) 1–7.

[3] F.M. Penz, J. Schenk, P. Bundschuh, H. Panhofer, K. Pastucha, B. Maunz, Scrap melting in BOF: Influence of particle surface and size during dynamic converter modelling, Proceedings of the 3rd ABM Week, Sao Paulo, Brazil, 2017.

[4] F.M. Penz, P. Bundschuh, J. Schenk, H. Panhofer, K. Pastucha, A. Paul, Effect of scrap composition on the thermodynamics of kinetic modelling of BOF converter, in: Proceedings of the 2nd VDEh-ISIJ-JK Symposium, Stockholm, Sweden, 2017, pp. 124–135.

[5] S. Asai, I. Muchi, Effect of scrap melting on the process variables in LD converter caused by the change of operating conditions, Trans. ISIJ 11 (1971) 107–115.

[6] H. Gaye, M. Wanin, P. Gugliermina, P. Schittly, Kinetics of scrap dissolution in the converter. theoretical model and plant experimentation, in: Proceedings of the 68th Steelmaking Conference, AIME, Detroit, MI, USA, 1985, pp. 91–103.

[7] H.W. den Hartog, P.J. Kreyger, A.B. Snoeijer, Dynamic model of the dissolution of scrap in the BOF process, C.R.M. 37 (1973) 13–22.

[8] J. Szekely, Y.K. Chuang, J.W. Hlinka, The melting and dissolution of low-carbon steels in iron-carbon melts, Metall. Trans. 3 (11) (1972) 2825–2833.

[9] Y. Lytvynyuk, J. Schenk, M. Hiebler, H. Mizelli, Thermodynamic and kinetic modelling of the De-vanadization process in the steelmaking converter, in: Proceedings of 6th EOSC, Stockholm, Sweden, Program No. 06-06, 2011, pp. 1–8.

[10] Y. Lytvynyuk, J. Schenk, M. Hiebler, A. Sormann, Thermodynamic and kinetic model of the converter steelmaking process. Part 1: the description of the BOF model, Steel Res. Int. 85 (4) (2014) 537–543.

[11] H. Gaye, P. Destannes, J.L. Roth, M. Guyon, Kinetics of scrap melting in the converter and electric arc furnace, in: Proceedings of the 6th International Iron and Steel Congress, Nagoya, Japan, Vol. 4, Steelmaking II, 1990, pp. 11–17.

[12] Y.K. Chuang, J. Szekely, On the use of Greeńs functions for solving melting or solidification problems, Int. J. Heat Mass Transf. 14 (1971) 1285–1294.

[13] M. Kawakami, K. Takatani, L.C. Brabie, Heat and mass transfer analysis of scrap melting in steel bath, Tetsu-to-Hagané 85 (9) (1999) 658–665.

[14] K. Isobe, H. Maede, K. Ozawa, K. Umezawa, C. Saito, Analysis of the scrap melting rate in high carbon molten iron, Tetsu-to-Hagané 76 (11) (1990) 2033–2040.

[15] J. Li, N. Provatas, Kinetics of scrap melting in liquid steel: multipiece scrap melting, Metall. Mater. Trans. B 39 (2) (2008) 268–279.

[16] M. Necati Özisik, Heat Conduction, second ed., John Wiley & Sons, Inc, New York, 1993, pp. 99–153.

[17] S. Kabelac (Ed.), VDI-Wärmeatlas: Berechnungsunterlagen für Druckverlust, Wärme- und Stoffübergang, 11th ed., Springer-Verlag Berlin Heidelberg, Berlin, Heidelberg, 2013.

[18] E. Specht, R. Jeschar, Kinetics of steel melting in carbon-steel alloys, Steel Res. 64 (1) (1993) 28–34.

[19] A.K. Shukla, B. Deo, D.G.C. Robertson, Scrap dissolution in molten iron containing carbon for the case of coupled heat and mass transfer control, Metall. Mater. Trans. B 44 (6) (2013) 1407–1427.

[20] H. Windisch, Thermodynamik: Ein Lehrbuch für Ingenieure, 4th ed., Oldenbourg Verlag, München, 2011, pp. 269–278.

[21] K. Shibata, Y. Kimura, M. Shimizu, S. Inaba, Dynamics of dead-man coke and hot metal flow in a blast furnace hearth, ISIJ Int. 30 (3) (1990) 208–215.

[22] Ovako, Material Data Sheet S235JR, https://steelnavigator.ovako.com/steel-grades/s235/, last control: 13.01.2019.

[23] J. Miettinen, Calculation of solidification-related thermophysical properties for steels, Metall. Mater. Trans. B 28 (4) (1997) 281–297.

[24] J. Li, G. Brooks, N. Provatas, Kinetics of scrap melting in liquid steel, Metall. Mater. Trans. B 36 (2) (2005) 293–302.

[25] H.T. Angus, Cast Iron: Physical and Engineering Properties, second ed., Butterworth & Co, London - Boston, 1976, pp. 124–126.

[26] S.V. Patankar, Numerical Heat Transfer and Fluid Flow, Hemisphere Publishing Corporation, Washington, 1980, pp. 40–77.

[27] F.M. Penz, J. Schenk, R. Ammer, K. Pastucha, B. Maunz, Dissolution behaviour of ULC steel in carbon saturated hot metal, La Metall. Italiana (11/12) (2018) 36–45.

[28] G. Sethi, A.K. Shukla, P.C. Das, P. Chandra, B. Deo, Theoretical aspects of scrap dissolution in oxygen steelmaking converters, in: Proceedings of AISTech 2004, Nashville, Tenn., USA, Volume II, 2004, pp. 915–926.

[29] A.K. Shukla, B. Deo, D.G.C. Robertson, Role of air gap in scrap dissolution process, Metall. Mater. Trans. B 44 (6) (2013) 1398–1406.

[30] J. Kron, A. Lagerstedt, H. Fredriksson, Measurements and modelling of air gap formation in aluminium based alloys, Int. J. Cast Met. Res. 18 (1) (2005) 29–40.

[31] A. Lagerstedt, J. Kron, F. Yosef, H. Fredriksson, Measurements and modelling of air gap formation in iron-base alloys, Mater. Sci. Eng., A 413–414 (2005) 44–51.

Publication 3:

Evaluation of the Influences of Scrap Melting and Dissolution during Dynamic Linz–Donawitz (LD) Converter Modelling

Reproduced with permission of open access Creative Commons CC BY 4.0 license

Evaluation of the Influences of Scrap Melting and Dissolution during Dynamic Linz–Donawitz (LD) Converter Modelling

Florian Markus Penz [1,*], **Johannes Schenk [1,2]**, **Rainer Ammer [3]**, **Gerald Klösch [4]** **and Krzysztof Pastucha [5]**

[1] K1-MET GmbH, Stahlstraße 14, A-4020 Linz, Austria; Johannes.Schenk@unileoben.ac.at
[2] Chair of Ferrous Metallurgy, Montanuniversität Leoben, Franz Josef Straße 18, A-8700 Leoben, Austria
[3] voestalpine Stahl GmbH, voestalpine Straße 3, A-4020 Linz, Austria; Rainer.Ammer@voestalpine.com
[4] voestalpine Stahl Donawitz GmbH, Kerpelystraße 199, A-8700 Leoben, Austria; Gerald.Kloesch@voestalpine.com
[5] Primetals Technologies Austria GmbH, Turmstraße 44, A-4020 Linz, Austria; Krzysztof.Pastucha@primetals.com
* Correspondence: Florian-Markus.Penz@K1-MET.com; Tel.: +43-3842-402-2244

check for
updates

Abstract: The Linz–Donawitz (LD) converter is still the dominant process for converting hot metal into crude steel with the help of technically pure oxygen. Beside hot metal, scrap is the most important charging material which acts as an additional iron source and coolant. Because of the irrevocable importance of the process, there is continued interest in a dynamic simulation of the LD process, especially regarding the savings of material and process costs with optimized process times. Based on a thermodynamic and kinetic Matlab®coded model, the influences of several scrap parameters on its melting and dissolution behavior were determined, with a special focus on establishing the importance of specific factors on the crude steel composition and bath temperature after a defined blowing period to increase the accuracy of the process model. The calculations reported clearly indicate that the dynamic converter model reacts very sensitively to the chemical composition of the scrap as well as the charged scrap mass and size. Those results reflect the importance of experiments for validation on the diffusive scrap melting model in further research work. Based on that, reliable conclusions could be drawn to improve the theoretical and practical description of the dissolution and melting behavior of scrap in dynamic converter modelling.

Keywords: scrap dissolution; scrap melting; thermodynamics; kinetics; dynamic converter modelling

1. Introduction

The Linz–Donawitz (LD) converter steelmaking process was patented in Austria in the early 1950s. The invention of the LD converter enabled the refinement of hot metal to crude steel in short blowing periods of around 20 min, enabling the high productivity of the steelmaking industry today. Technically pure oxygen is blown onto the surface of the liquid melt inside the vessel, which leads to an increase of the reaction surface through the ejection of iron droplets and further to a stronger oxidation of the dissolved elements like carbon, silicon, manganese and phosphorus. These chemical reactions are exothermic, which results in a sharp temperature rise. As a coolant, steel scrap is added at the beginning of each blowing period [1–5].

As process and material costs are getting more important, the modelling of the process is crucial. Several authors gave different approaches for modelling the scrap melting during the LD converter process e.g., by Kruskopf in [6–8], Guo in [9] and Sethi and Shukla et al. in [10–12]. In previous

publications by Y. Lytvynyuk et al. [13,14], a single reaction zone model was developed. This paper should point out the sensitivity of various scrap parameters on the simulation results. Therefore, the only parameters which will be changed are scrap parameters.

2. Description of the Dynamic LD Converter Model

Lytvynyuk's model is based on thermodynamic and kinetic calculations [13,14]. It is assumed that in the heterogeneous thermodynamic reaction zone, all components can be conveyed between the slag and metal phases except carbon, which is oxidized to become gaseous carbon monoxide. The chemical oxidation reactions are assumed to be simultaneous at the interfacial surface between the slag and metal phases, whereby the oxidized carbon is removed instantly, and the equilibrium thermodynamics of the post combustion is neglected according to a non-reversible oxidation process. The flowsheet of the LD converter model is presented in Figure 1. Two simulation targets can be attained. During the main calculation loop, the mass and heat balances are calculated. Every single element is considered due to the results of chemical reactions, the consumption of the blown oxygen and the heating and melting of the charged materials. In the heat balance the consumed and generated heats are considered. Additionally, a structure of sub models will be solved during the main calculation loop. In this paper only the sub model of the scrap melting will be explained in detail. A more detailed description of the whole model is given in [4,13,15,16].
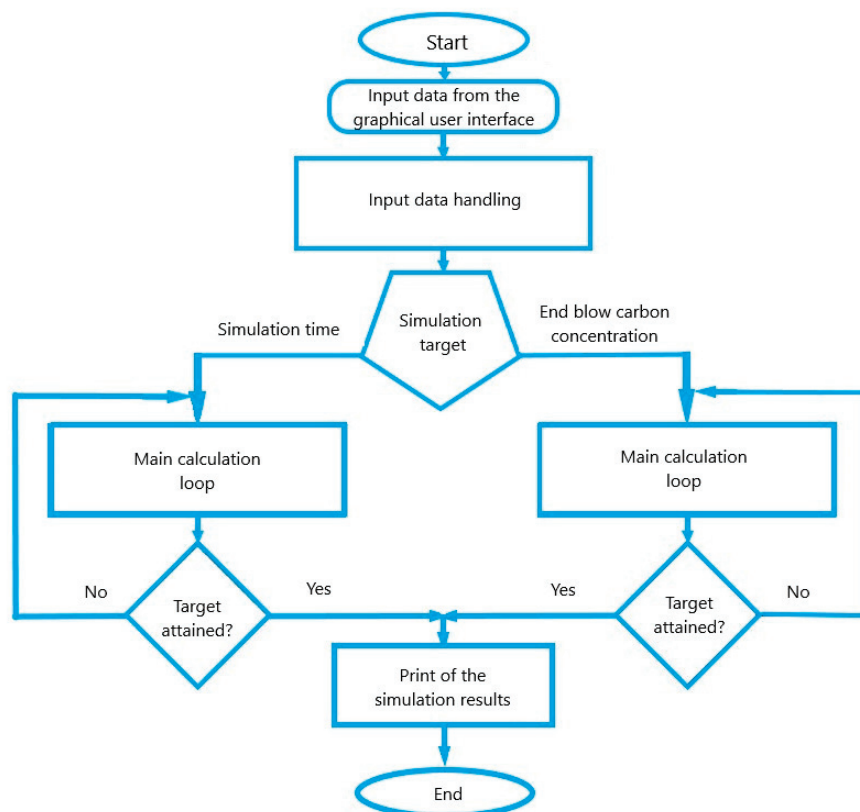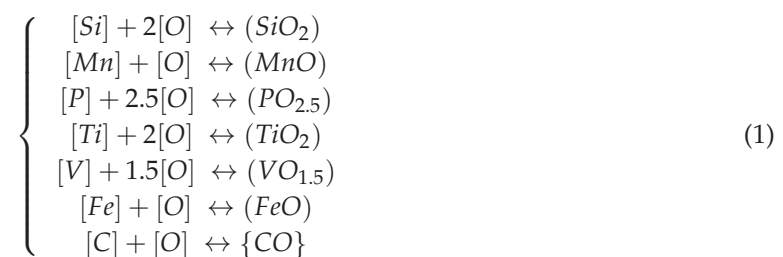

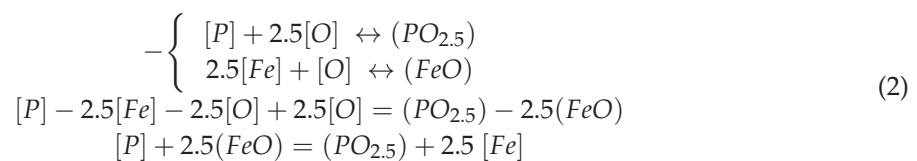**Figure 1.** Flow sheet of the Linz–Donawitz (LD) converter model.

During the entire process, the chemical composition of the metal and slag phases changes due to the blowing oxygen consumption theory by V.E. Grum-Grzhimaylo for Bessemer converters [17]. In this theory, it is assumed that only iron is oxidized by blown oxygen and the remaining elements in the metal phase react with the iron oxide. The slag phase is formed by chemical reactions, melting and dissolution of charge materials and iron oxide, which is generated in the hot spot as a result of iron burning. Beside the oxidation, the dissolution and melting behavior of all charged materials influences

the melt and slag composition during the entire blowing period. It is considered that the metal phase consists of the charged hot metal. Further, the solid scrap will be dissolved only in the hot metal due to its higher density. The other materials, which able to be charged, like lime, pellets, magnesia or dolomite, are assumed to dissolve only in the slag phase. They can be charged in portions during the heat [13,14].

The coupled reaction model published by Ohguchi et al. in [18] is used to describe the concurrent oxidation–reduction reactions between slag and metal, which is commonly utilized for the determination of the influence of kinetic parameters on chemical reaction rates and dephosphorization processes. [18–25]. In the present model, the simultaneous chemical reactions between the two different phases of the heterogeneous thermodynamic system can be determined by the system of chemical reactions listed in Equation (1). The reactions take place on the interfacial area between the slag and metal phase. Hess´s law is utilized for all calculated reactions. [13] In Equations (1) and (2) following metallurgical convention was used: [], () and {} indicate the metal, slag and gas phases, respectively.

$$\begin{cases} [Si] + 2[O] & \leftrightarrow (SiO_2) \\ [Mn] + [O] & \leftrightarrow (MnO) \\ [P] + 2.5[O] & \leftrightarrow (PO_{2.5}) \\ [Ti] + 2[O] & \leftrightarrow (TiO_2) \\ [V] + 1.5[O] & \leftrightarrow (VO_{1.5}) \\ [Fe] + [O] & \leftrightarrow (FeO) \\ [C] + [O] & \leftrightarrow \{CO\} \end{cases} \tag{1}$$

For example, the oxidation of phosphorus by iron oxide is expressed by combining two reactions of Equation (1), which will result in Equation (2).

$$-\begin{cases} [P] + 2.5[O] & \leftrightarrow (PO_{2.5}) \\ 2.5[Fe] + [O] & \leftrightarrow (FeO) \end{cases}$$
$$[P] - 2.5[Fe] - 2.5[O] + 2.5[O] = (PO_{2.5}) - 2.5(FeO)$$
$$[P] + 2.5(FeO) = (PO_{2.5}) + 2.5[Fe] \tag{2}$$

By the use of the system of the chemical reactions, any change of one component parameter, e.g., the concentration or the activity coefficient, will lead to a change in the whole system of the considered chemical reactions. [13,14,26].

The dynamic LD converter model used is mainly focused on cost reduction due to shorter process times and specified amounts of charged materials. This parameter study on scrap melting and dissolution behavior was performed since alterations in component parameters influence the whole system because of the thermodynamic and kinetic principles of the model and its equation of oxygen balance. For all mathematical and chemical expressions, the following assumptions were taken into account:

- At the interfacial surface all reactions are expeditious and equilibrated at each time step.
- The mass transfer kinetics in the metal and slag phases are the limitation for reaction rates.
- Fluctuations in iron concentration as well as lime concentrations are neglected [13,27].

The fundamental equation to solve the calculation is one algebraic equation, which includes the bulk chemical compositions of the metal and the slag phases as well as thermodynamic and kinetic parameters. The flowchart of the reaction model is given in Figure 2. Further descriptions of the kinetic and thermodynamic calculations and for the melting behavior of slag formers, pellets and FeSi were published by Lytvynyuk et al. [13,26].
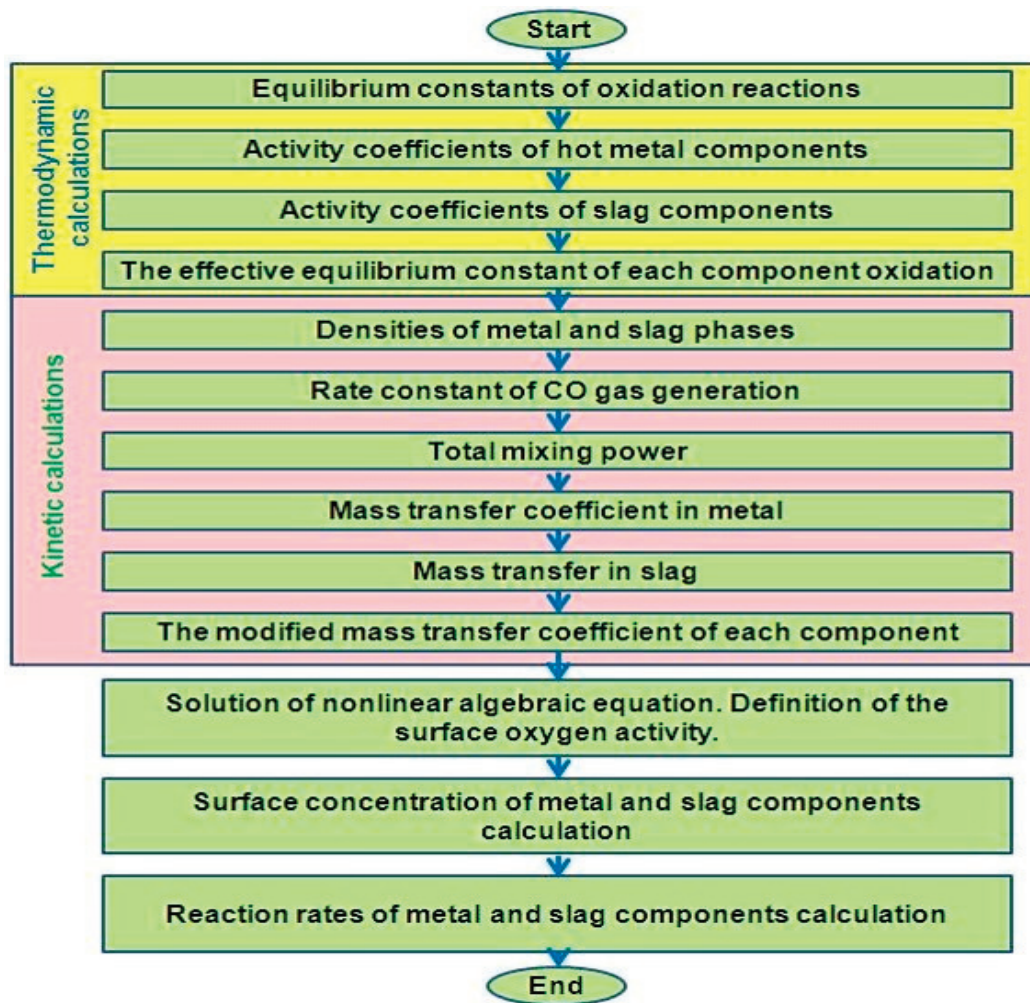
Figure 2. Flowsheet of the reaction model used [14].

To receive the effective equilibrium constant E of the oxidation reaction as a result of the thermodynamic calculation, the equilibrium constants, as well as the activity coefficients of the hot metal components, γ_{HM} and the slag components γ_S have to be determined. [26] Thus will result in Equation (3). The activity coefficients of the slag components are calculated by the collective electron theory described by Grigoryan et al. in [28] or Kolesnikova et al. in [29]. For the determination of the activity coefficients the Wagner–Lupis–Elliot method was chosen, published by Sigworth and Elliott in [30].

$$E = \frac{K \times \gamma_{HM}}{\gamma_S} \tag{3}$$

The equilibrium constant K for example for the oxidation reaction of phosphorus was derived from Equation (4). [28]

$$\log K = \frac{27050}{T} - 14.25 \tag{4}$$

The model of Lytvynyuk et al. was validated based on the output parameters of a commercial 170 t converter, which was published by Lytvynyuk et al. in [31]. The model was in a good agreement with the measured industrial data. The behavior of the temperature, the composition of the metal and slag phases, as well as the melting and dissolution of charge materials requires shutdowns during a converter heat. This kind of research is difficult to realize, due to the high costs incurred by the loss of

production. The trends of the temperature or the off gas composition as well as the composition of the metal and slag phases is comparable by information from literature. Lytvynyuk also carried out a validation in this direction and could present in [14] and [31] a good agreement between the model and literature-based information.

3. Mechanisms of Scrap Melting in the LD Model

Two mechanisms describe the scrap melting and dissolution behavior in the LD model used. The scrap is charged into the vessel at the beginning of the process. The scrap geometry is assumed to be spherical. It is also possible to define the scrap to be cylindrical in shape, but in this case a melting only in radial direction can be simulated. Further, a manipulation of the overall surface of the scrap particle can be executed by introducing the form factor sphericity. The sphericity of a particle is defined as the ratio of the surface area of a sphere to the surface area of the particle, whereby the sphere has the same volume as the given particle. [32,33] In this work only a spherical shaped scrap is determined. A study on the differences between cylindrical, spherical and particles manipulated by the use of sphericity was published by the authors in [27] to give a first estimation on scrap melting behavior on the influence of heat balance. For simplification, it is assumed that the surface temperature of the scrap is equal to the hot metal temperature and that the scrap is heated up through thermal conduction. Due to the fact that the solid scrap is denser than hot metal, it assumed that the scrap is covered by liquid hot metal. Therefore, the influence of radiation can be neglected [1,4,34,35].

Forced or convective scrap melting appears if the melt temperature exceeds the melting point of the scrap and diffusive scrap melting occurs at temperatures below the scrap melt point. Forced scrap melting controls the scrap dissolution in the final stage of the LD converter process and the temperature difference between hot metal and scrap acts as the driving force. In this case, heat transfer determines the scrap melting [34,35]. Equation (5) characterizes the model for forced scrap melting of a spherical scrap particle:

$$- \partial r / \partial t = h_{met} \times \left(T_{HM} - T_{liq} \right) / \left(L + \left(H(T_{scrap}) - H\left(T_{liq} \right) \right) \right) \times \rho_{scrap} \tag{5}$$

The scrap particle´s radius is r in unit (m). The heat transfer coefficient in the metal phase is h_{met} in (W m^{-2} K^{-1}) and the density of the scrap is ρ_{scrap} in (kg m^{-3}). The latent heat of scrap melting is L in (J kg^{-1}). T_{HM} and T_{liq} are the temperatures of the metal phase and the liquidus temperature of the scrap in (K) [13,31]. $H(T_{scrap})$ is the specific enthalpy of scrap at the actual temperature of the scrap surface and $H(T_{liq})$ is the specific enthalpy of the scrap melting point, both in (J kg^{-1}) [4,27].

Equation (6) describes the diffusive melting of a spherical scrap particle, where the driving force is the difference of carbon concentration in the liquid phase and the scrap. It is strongly dependent on the mass transfer coefficient of the system. According to the binary Fe-Fe$_3$C diagram, low carbon scrap has a higher melting point than hot metal, with around 4.5 wt.% of carbon. [3]

$$- \partial r / \partial t = k_{met} \times \ln\left(\left(\%C_{HM} - \%C_{liq} \right) \times \rho_{liquid} / \left(\%C_{liq} - \%C_{scrap} \right) \times \rho_{scrap} + 1 \right) \tag{6}$$

The mass transfer coefficient in the metal phase is k_{met} in (m s^{-1}). C_{scrap} and C_{HM} are the carbon concentrations in the scrap and hot metal in (wt.%). C_{liq} describes the carbon concentration on the liquidus line. The density of the liquid hot metal is ρ_{liquid} and of the scrap is ρ_{scrap}, both in (kg m^{-3}) [3,27]. The values for the liquidus lines are approximated by a database of Fe-Fe$_3$C-Si-Mn diagrams, generated by the FactSage^{TM} FSstel database (licensed to Montanuniversität Leoben, Department Metallurgie; Version 7.1, ©Thermfact and GTT-Technologies, Montreal, Canada and Herzogenrath, Germany) [13,36].

The specific mixing power, which is created by bottom stirring and oxygen blowing, provides the basis for the mass transfer coefficient in the metal phase. The mass transfer coefficient is calculated

through a function of the total mixing power including the bath depth, the converter geometry, position and geometry of the oxygen lance and the number of bottom-stirring nozzles as well as the flow rate of oxygen and bottom-stirring gas [14,26]. The heat transfer coefficient of the metal phase is defined by the function given in Equation (7), which is dependent on the specific mixing power $\dot{\varepsilon}$ [35]. According to Lytvynyuk et al. the total mixing power is a sum of the mixing power by top-blown oxygen and the mixing power by bottom-blown gas [13].

$$h_{met} = 5000 \times \dot{\varepsilon}^{0.3} \tag{7}$$

4. Simulation Parameters

Based on industrial materials and their chemical composition, the influence of small adjustments in carbon, phosphorus and silicon contents as well as the size and charged mass of scrap were investigated. The variations of the carbon and silicon contents were taken according to their quantity in scrap. The phosphorus content is rather small in common steels; still, through the scrap melting, small quantities of phosphorus are always delivered through to the liquid melt and may influence the final phosphorus content. The aim is to clarify the relevance of the obtained deviation in comparison to the adjustments to maintain the future focus on the detailed description of the melting and dissolution behavior of scrap in an LD converter. In particular, it is necessary to evaluate the sensitivity of the dynamic LD converter model on the adjusted charged scrap for further purposes.

The input parameters are listed in Table 1; Table 2. For modelling, a common rail steel grade was used. It has to be mentioned that the blowing time was fixed at 12.6 min and the amount of blown oxygen was also constant. Hot metal, scrap, solid LD slag and sand are charged at the beginning of the blowing period, whereby for simplification, only lime is charged stepwise during the entire process time. In Table 1, the initial composition, the charged mass and charging temperature of the hot metal and scrap are listed. The charged mass of scrap and the hot metal are constant for all investigations except when the scrap mass was modified.

Table 1. Charging parameters of the hot metal and the standard scrap used.

Definition	Unit	Hot Metal	Standard Scrap
Carbon content	wt.%	4.536	0.737
Silicon content	wt.%	0.410	0.349
Manganese content	wt.%	1.171	1.060
Phosphorus content	wt.%	0.100	0.013
Iron content	wt.%	93.783	97.841
Mass	t	53.60	15.72
Temperature	°C	1318	20

Table 2. Selected chemistry of added slag, sand and lime.

Name	Unit	Initial Slag	Dust Pellets	Sand	Lime
SiO_2 content	wt.%	11.32	-	92.79	0.980
MnO content	wt.%	11.93	2.960	-	-
P_2O_5 content	wt.%	1.330	-	-	-
FeO content	wt.%	29.66	-	-	-
CaO content	wt.%	40.08	7.320	-	92.37
MgO content	wt.%	4.380	4.580	-	3.080
CO_2 content	wt.%	-	-	-	2.400
H_2O content	wt.%	-	-	-	0.170
Fe_2O_3 content	wt.%	-	67.88	-	-
Fe content	wt.%	-	11.09	-	-
Amount of charged material	t	0.001	1.000	0.172	2.800

The chemistry of the initial slag as well as their compositions and the amounts of the charged dust pellets, sand and the added lime are shown in Table 2.

The standard scrap parameters from Table 1 were adjusted to analyze the melting and dissolution behavior of scrap in the BOF process. The phosphorus content in the scrap is very low, at 0.013 wt.%. The adjustment of the phosphorus was therefore set only to a higher content than usual, for example, which can be found in weathering steel. The changed values are listed in Table 3 and their percentage relative adjustment in comparison to the standard scrap is noted. It is assumed that the shape of the scrap is a sphere, whereby the size is defined to be its radius.

Table 3. Variation of the initial parameters of the scrap and their percentage.

Name and Unit	Standard Scrap	Lower Value		Higher Value	
Carbon content (wt.%)	0.7370	0.40	−45.7%	1.00	35.68%
Silicon content (wt.%)	0.3488	0.10	−71.3%	0.70	100.7%
Phosphorus content (wt.%)	0.0130	-	-	0.05	273.1%
Size (m)	0.1	0.08	−20.0%	0.12	20.00%
Mass (t)	15.72	13.0	−17.3%	17.0	%

5. Results and Discussion

This publication displays in the following illustrations of the scrap melting and dissolution behavior during the LD process with the aforementioned parameters. The calculated influence of the adjusted parameters is also shown by the trajectories of carbon, phosphorus and the melt temperature.

5.1. Influence on the Melting and Dissolution Behavior of Scrap

In Figures 3 and 4, the dissolution and melting behavior of scrap is pointed out. Between minutes 8 and 10, a kink occurs in all figures, resulting from the change between diffusive and forced scrap melting. At this point, the melt temperature exceeds the melting temperature of the scrap. Under real process conditions, a smooth transition between the two melting mechanisms will take place. While the melting takes place under real conditions in the two-phase area between the solidus and liquidus lines, in this model, the assumption is used that the melting point of scrap is specific to the liquidus line [27].

It is illustrated in Figure 3 that the rate of diffusive melting is faster for higher carbon content in the scrap. In the model, the denominator of the logarithmic term in Equation (4) decreases, since the difference of $\%C_{liq}$ and $\%C_{scrap}$ becomes smaller in comparison to the standard case. A lower carbon content results in the opposite. Also, a higher silicon content in the scrap leads to faster diffusive melting. The effect of the higher silicon content is a decrease of $\%C_{liq}$, which also reduces the value of the denominator of the logarithmic term in Equation (4). Changes in the phosphorus contents do not show a big difference, because they are already too small to influence the melting behavior of scrap.

In Figure 4, it is shown that low-dimension scrap melts a little bit slower in the initial phase of melting because of the higher cooling effect due to a higher specific surface. Once the low-dimension scrap is heated up—between minutes three and four—the melting of low dimension scrap accelerates. The complete melting time of the big dimension scrap with a radius of 0.12 m is higher; however, the time difference is about 1 min in comparison to the low dimension scrap with a radius of 0.08 m. It is obvious that the amount of scrap has an influence on the trajectories of melting behavior. There is a strong increase in the scrap melting of high scrap amounts shortly before the transition point between diffusive and forced scrap melting. This is explainable through Equation (6), where the logarithmic term increases in value. According to the increasing temperatures and decreasing carbon concentrations in the hot metal at this stage of the process, the denominator of the logarithm decreases faster than the numerator.
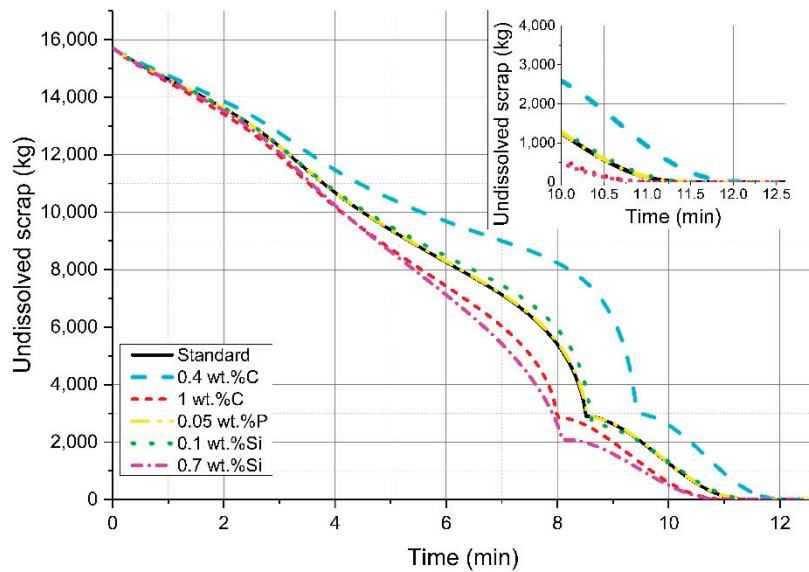
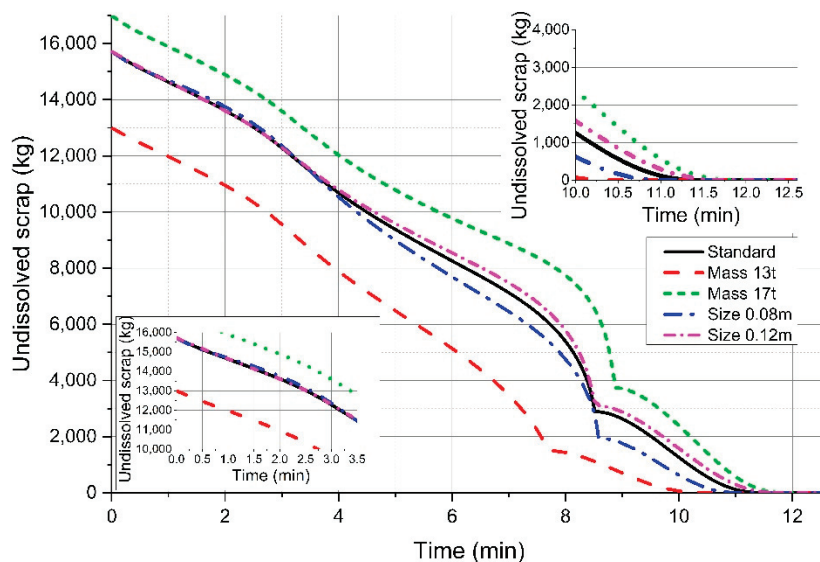**Figure 3.** Influence of adjustment on chemical composition on the melting behavior of scrap.

Figure 4. Influence of variable charging scrap amounts and scrap size on the melting behavior.

5.2. Influence on the Final Crude Steel Temperature

Influenced by the varying melting behavior, the calculated final temperature of the liquid crude steel changes slightly. As shown in Figure 5, the highest influence on the final temperature will be reached if the mass of charged scrap is modified. Due to the energy balance, less energy for heating the scrap will be needed with decreasing scrap amounts, which will result in higher tapping temperatures. But in comparison to the relative adjustments used, the influence on the final temperature is still small, whereby 1% means 16 °C.
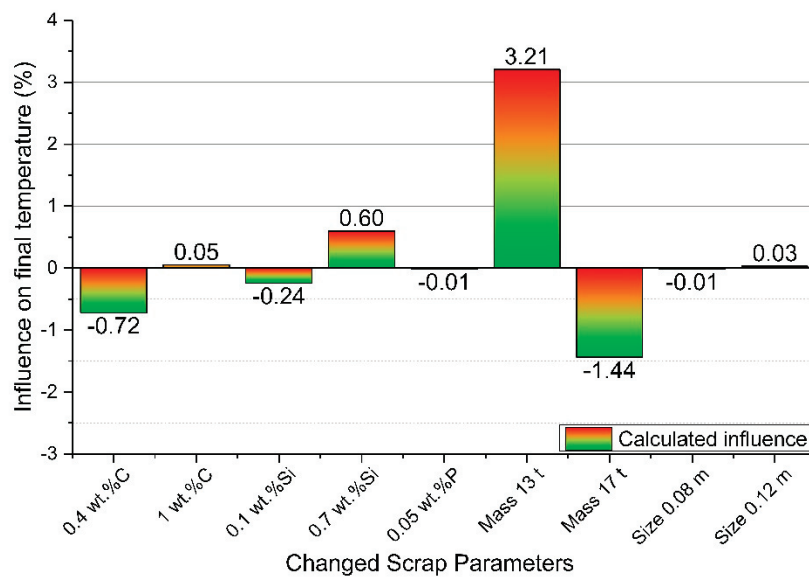
Figure 5. Influence on the final melt temperature; 1% defines a difference of 16 °C.

The influence of the mass and the scrap size can be seen in Figure 6. It is obvious that a lower charged mass of scrap will consume less heat from the system, resulting in a higher final temperature. The variation of the scrap size will only influence the melt temperature in the initial stages of the blowing period. Due to the higher overall surface of small scale scrap (0.08 m in diameter) the exchange area of heat is increasing. This fact results in a higher cooling effect at the beginning of the blowing period.
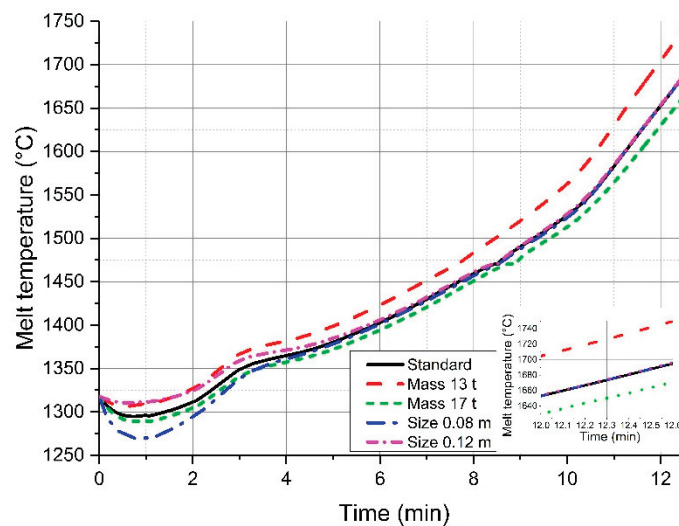
Figure 6. Influence of variable charging scrap amounts and scrap size on the melt temperature.

5.3. Influence on the Final Carbon Content

Decarburization is one of the two main tasks of an LD converter. How strongly the calculated final carbon content is influenced by the assumed modifications is shown in Figures 7 and 8. What is interesting to mention is that lower silicon contents in the scrap have a positive effect on decarburization and result in, besides low carbon contents in the scrap, lower final carbon contents in the liquid melt (Figure 7). In Figure 8, it is shown that a lower mass and therefore a lower input of carbon through scrap will also result in lower final values. The same behavior was determined for silicon. There is no large effect of the scrap size and the scrap phosphorus content on the final carbon content visible.
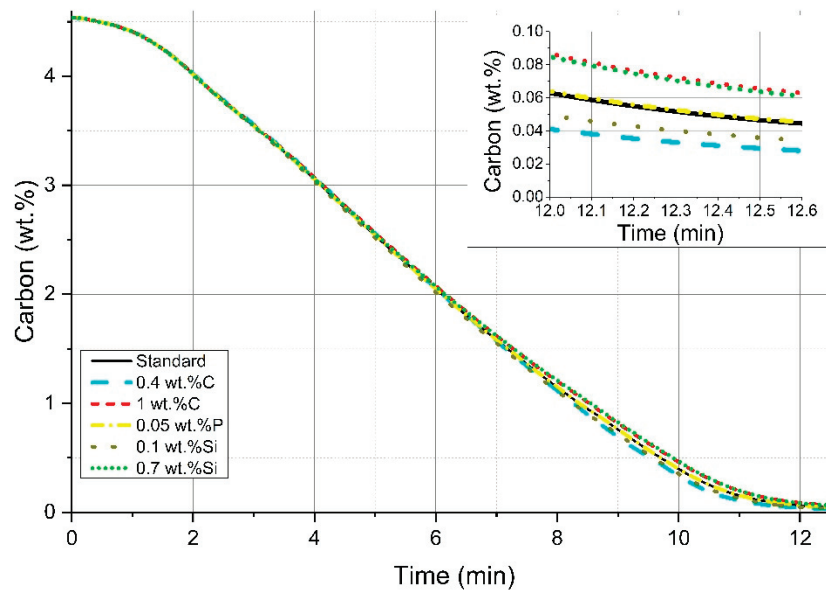
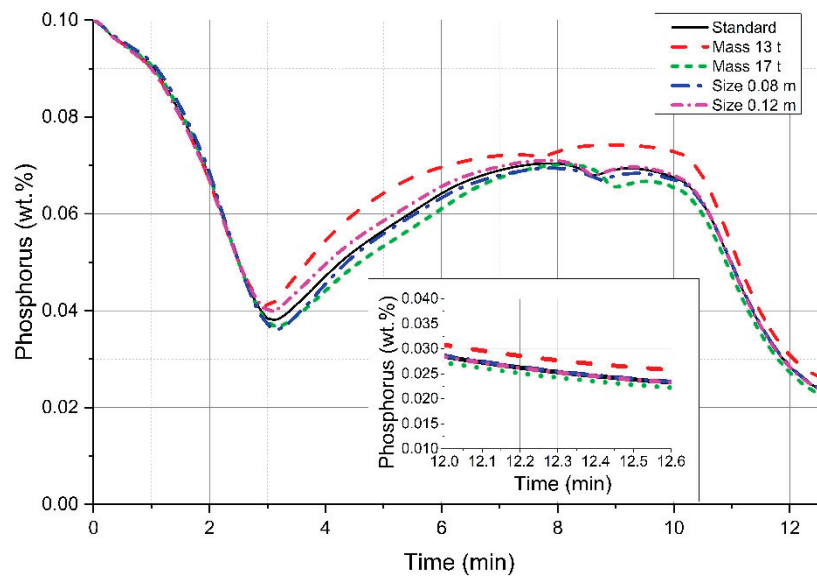**Figure 7.** Influence of variable carbon and silicon contents on the carbon content of the liquid crude steel.
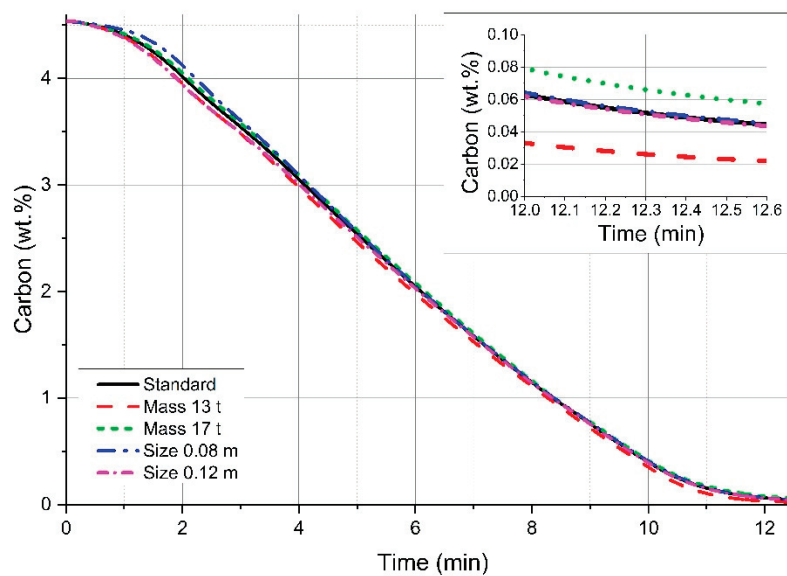
Figure 8. Influence of variable charging scrap amounts and scrap size on the carbon content of the liquid crude steel.

Even though the difference seems to be small in the final carbon content, it has to be carefully analyzed because a discrepancy of around 50% in the scrap carbon composition results in a final deviation of 40% in the final melt carbon composition. Similar values are detected in variations of the silicon content of the scrap and the scrap mass, as shown in Figure 9. A discrepancy in the final carbon composition of 50.67% was detected, if less scrap is charged. This high value results in the chosen rail scrap with a carbon content of 0.737 wt.%. Due to the faster melting of the reduced scrap mass, less carbon is transported into the melt and therefore lower amounts can be reached in the final content. The phosphorus content in the scrap and the particle size show no significant influence.
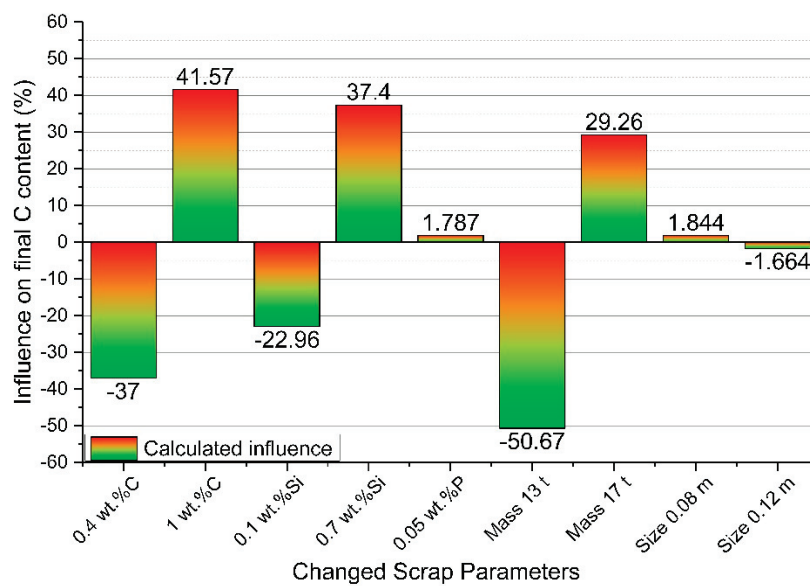
Figure 9. Calculated influence on the final carbon content.

5.4. Influence on the Final Phosphorus Content

The second main task of an LD converter is dephosphorization, and the aim of each operator is to reach low phosphorus contents in the tapped crude steel. As shown in Figures 10 and 11, the trajectories of the phosphorus content in the melt are influenced during the entire blowing period through the adjusted parameters. The interaction between an increasing amount of carbon, silicon and phosphorus in the scrap leads to higher final phosphorus contents in the tapped crude steel (Figure 10). Due to the still relatively high carbon activity and the increasing bath temperatures during the process, the stable oxides of manganese and phosphorus will be reduced. In the final stages of the blowing period, low amounts of carbon and silicon lead to an early carbon activity decrease. This results in an earlier resumption of the phosphorus oxidation.
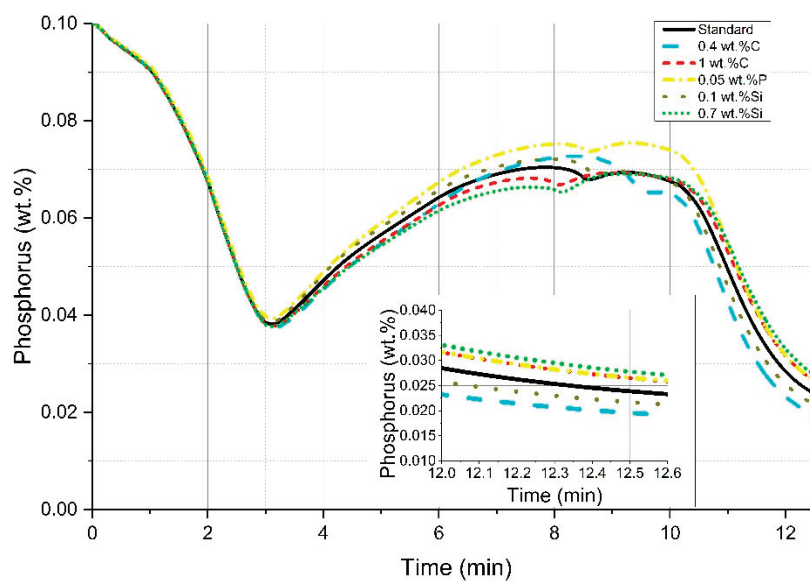
Figure 10. Influence of variable element contents in scrap on the phosphorus content of the liquid crude steel.

Figure 11. Influence of variable charging scrap amounts and scrap size on the phosphorus content of the liquid crude steel.

Because of the strong influence on the melt temperature, the slag composition and the melting behavior of low-charged scrap amounts lead to higher calculated final phosphorus contents, as pointed out in Figure 11. In the main dephosphorization period at the beginning of the process, the temperature of the melt rises faster if there is less scrap or high volume scrap charged. Therefore, the point of re-phosphorization will start earlier and this causes higher final phosphorus contents in the melt. A possibility to counteract this behavior would be a different charging concept for lime and a modified slag metallurgy.

The percentage of influence on the final phosphorus content in the liquid melt according to the adjusted parameters is shown in Figure 12. It shows that the dynamic LD converter model reacts sensitively to the final phosphorus contents on variations in the chemical scrap composition and charged scrap mass.
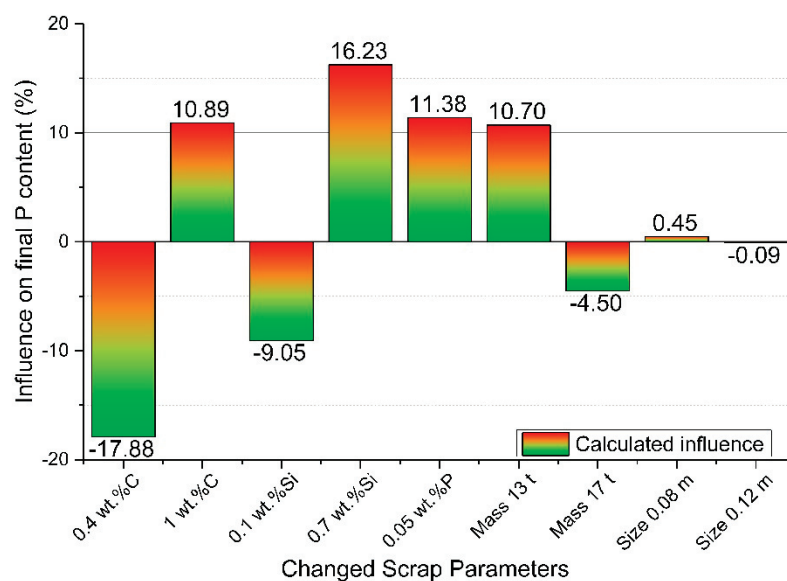
Figure 12. Calculated influence on the final phosphorus content.

6. Conclusions

The present study was done to clarify the relevance of the obtained deviations for the final temperature, composition and scrap melting behavior. Therefore, adjustments in chemical composition, size and mass of charged scrap were considered. The aim was to focus on the detailed description of the melting and dissolution behavior of scrap during the LD converter process for future work. The BOF model used was coded in MatLab® (R2014b, MathWorks Inc., Natick, MA, USA) and describes the behavior of the metal and slag phases during the blowing period of the BOF process using thermodynamic and kinetic equations.

The LD converter model used includes literature-based scrap melting equations. In the literature they are discussed, but insufficient validation reports are available. The model calculations show that around three quarters of the blowing process are dominated by diffusive scrap melting. A faster melting of the scrap could be indicated if the carbon or silicon content of the scrap were increased in comparison to the standard composition. This behavior is based on a lower melting point of scrap due to the higher contents of those elements. In this research, the phosphorus content of the scrap was also investigated. It has to be mentioned that it has no influence on the melting behavior of the scrap, but with increasing phosphorus in the scrap, the final phosphorus content in the liquid crude steel will also increase. It was shown that the amount of charged material has a very strong influence on the melting behavior as well as the final compositions of carbon and phosphorus. The scrap size changes those values solely in a small frame. It is worth pointing out that particularly low contents of carbon and silicon in the scrap also lower the final phosphorus and carbon content in the melt.

To sum up, the calculations reported in this paper clearly indicate that the dynamic BOF model reacts very sensitively to the chemical composition of the scrap as well as the charged scrap mass and size and therefore, the whole melting and dissolution behavior of scrap. Experiments will be necessary for validation of the diffusive scrap melting model. Based on that, reliable conclusions could be drawn to improve the theoretical and practical description of the dissolution and melting behavior of scrap. This description should be as precise as possible if it is necessary to be able to implement a complete dynamic LD converter model for usage in the industry.

References

1. Turkdogan, E.T. *Fundamentals of Steelmaking*; The Institute of Materials: London, UK, 1996; pp. 209–244.
2. Ghosh, A.; Chatterjee, A. *Ironmaking and Steelmaking Theory and Practice*; PHI Learning Private Limited: Delhi, India, 2015; pp. 285–292.
3. Chigwedu, C. Beitrag zur Modellierung des LD-Sauerstoffaufblasverfahrens zur Stahlerzeugung. Ph.D. Thesis, Technische Universität Clausthal, Clausthal-Zellerfeld, Germany, 1997.
4. Penz, F.M.; Bundschuh, P.; Schenk, J.; Panhofer, H.; Pastucha, K.; Paul, A. Effect of Scrap Composition on the Thermodynamics of Kinetic Modelling of BOF Converter. In Proceedings of the 2nd VDEh-ISIJ-JK Symposium, Stockholm, Sweden, 12–13 June 2017; pp. 124–135.

5. Hiebler, H.; Krieger, W. Die Metallurgie des LD-Prozesses. *BHM* **1992**, *137*, 256–262.

6. Kruskopf, A.; Holappa, L. Scrap melting model for steel converter founded on interfacial solid/liquid phenomena. *Metall. Res. Technol.* **2018**, *115*, 201–208. [CrossRef]

7. Kruskopf, A.; Louhenkilpi, S. 1-Dimensional scrap melting model for steel converter (BOF). In Proceedings of the METEC & 2nd ESTAD, Düsseldorf, Germany, 15–19 June 2015; pp. 1–4.

8. Kruskopf, A. A Model for Scrap Melting in Steel Converter. *Metall. Mater. Trans. B* **2015**, *46*, 1195–1206. [CrossRef]

9. Guo, D.; Swickard, D.; Alavanja, M.; Bradley, J. Numerical Simulation of Heavy Scrap Melting in BOF steelmaking. *Iron Steel Technol.* **2013**, *10*, 125–132.

10. Sethi, G.; Shukla, A.K.; Das, P.C.; Chandra, P.; Deo, B. Theoretical Aspects of Scrap Dissolution in Oxygen Steelmaking Converters. In Proceedings of the AISTech, Nashville, TN, USA, 15–17 September 2004; Volume II, pp. 915–926.

11. Shukla, A.K.; Deo, B. Coupled heat and mass transfer approach to simulate the scrap dissolution in steelmaking process. In Proceedings of the International Symposium for Research Scholars on Metallurgy, Materials Science & Engineering, Chennai, India, 18–20 December 2006; pp. 1–14.

12. Shukla, A.K.; Deo, B.; Robertson, D. Scrap Dissolution in Molten Iron Containing Carbon for the Case of Coupled Heat and Mass Transfer Control. *Metall. Mater. Trans. B* **2013**, *44*, 1407–1427. [CrossRef]

13. Lytvynyuk, Y.; Schenk, J.; Hiebler, M.; Sormann, A. Thermodynamic and Kinetic Model of the Converter Steelmaking Process. Part 1: The Description of the BOF Model. *Steel Res. Int.* **2014**, *85*, 537–543. [CrossRef]

14. Lytvynyuk, Y. Thermodynamic and Kinetic Modelling of Metallurgical Processes. Ph.D. Dissertation, Montanuniversität Leoben, Leoben, Austria, 2013.

15. Hirai, M.; Tsujino, R.; Mukai, T.; Harada, T.; Masanao, O. Mechanism of Post Combustion in the Converter. *Trans. ISIJ* **1987**, *27*, 805–813. [CrossRef]

16. Bundschuh, P.; Schenk, J.; Hiebler, M.; Panhofer, H.; Sormann, A. Influence of CaO Dissolution on the Kinetics of Metallurgical Reactions in BOF-process. In Proceedings of the 7th European Oxygen Steelmaking Conference, Trinec, Czech Republic, 9–11 September 2014.

17. Boychenko, B.; Okhotskiy, V.; Kharlashin, P. *The Converter Steelmaking*; Dnipro-VAL: Dnipropetrovsk, Ukraine, 2006; pp. 22–69.

18. Ohguchi, S.; Robertson, D.; Deo, B.; Grieveson, P.; Jeffes, J. Simultaneous dephosphorization and desulphurization of molten pig iron. *Iron Steelmak.* **1984**, *11*, 202–213.

19. Kitamura, S.; Kitamura, T.; Shibata, K.; Mizukami, Y.; Mukawa, S.; Nakagawa, J. Effect of stirring energy, temperature and flux composition on hot metal dephosphorization kinetics. *ISIJ Int.* **1991**, *31*, 1322–1328. [CrossRef]

20. Kitamura, S.; Kitamura, T.; Aida, T.; Sakomura, E.; Koneko, R.; Nuibe, T. Development of analyses and control method for hot metal dephosphorization process by computer simulation. *ISIJ Int.* **1991**, *31*, 1329–1335. [CrossRef]

21. Kitamura, S.; Shibata, H.; Maruoka, N. Kinetic Model of Hot Metal Dephosphorization by Liquid and Solid coexisting slags. *Steel Res. Int.* **2008**, *79*, 586–590. [CrossRef]

22. Pahlevani, F.; Kitamura, S.; Shibata, H.; Maruoka, N. Kinetic Model Dephosphorization in Converter. In Proceedings of the SteelSim, Leoben, Austria, 8–10 September 2009.

23. Mukawa, S.; Mizukami, Y. Effect of stirring energy and rate of oxygen supply on the rate of hot metal dephosphorization. *ISIJ Int.* **1995**, *35*, 1374–1380. [CrossRef]

24. Ishikawa, M. Analysis of hot metal desiliconization behaviour in converter experiments by coupled reaction model. *ISIJ Int.* **2004**, *44*, 316–325. [CrossRef]

25. Higuchi, Y.; Tago, Y.; Takatani, K.; Fukagawa, S. Effect of stirring and slag condition on reoxidation on molten steel. *ISIJ* **1998**, *84*, 13–18.

26. Lytvynyuk, Y.; Schenk, J.; Hiebler, M.; Mizelli, H. Thermodynamic and kinetic modelling of the devanadization process in the steelmaking converter. In Proceedings of the 6th European Oxygen Steelmaking Conference, Stockholm, Sweden, 7–9 September 2011.

27. Penz, F.M.; Bundschuh, P.; Schenk, J.; Panhofer, H.; Pastucha, K.; Maunz, B. Scrap melting in BOF: Influence of particle surface and size during dynamic converter modelling. In Proceedings of the 3rd ABM week, São Paulo, Brazil, 2–6 October 2009.

28. Grigoryan, A.H.; Stomakhin, A.J.; Ponomarenko, A.G. *Physico-Chemical Calculations of the Electric Steel Process*; Metallurgy: Moscow, Russia, 1989.

29. Kolesnikova, K.; Gogunskii, V.; Olekh, T. Calculation of equilibrium in the system metal-slag during steelmaking in electric arc furnace. *Metall. Min. Ind.* **2016**, *6*, 8–13.

30. Sigworth, G.K.; Elliot, J.F. The thermodynamics of liquid dilute iron alloys. *Met. Sci.* **1974**, *8*, 298–310. [CrossRef]

31. Lytvynyuk, Y.; Schenk, J.; Hiebler, M.; Sormann, A. Thermodynamic and Kinetic Model of the Converter Steelmaking Process. Part 2: The Model Validation. *Steel Res. Int.* **2014**, *85*, 544–563. [CrossRef]

32. Wadell, H. Volume, shape, and roundness of quartz particles. *J. Geol.* **1935**, *43*, 250–280. [CrossRef]

33. Penz, F.M. Charakterisierung des Hochofeneinsatzstoffes Sinter, Mittels Optischer 3D-Partikelanalyse. Bachelor's Thesis, Montanuniversitaet Leoben, Leoben, Austria, 2014.

34. Medhibozhskiy, M.Y. *Basis of Thermodynamic and Kinetic of Steelmaking*; Vischa shkola: Kyiv, Ukraine, 1979; p. 229.

35. Isobe, K.; Maede, H.; Ozawa, K.; Umezawa, K.; Saito, C. Analysis of the Scrap Melting Rate in High Carbon Molten Iron. *ISIJ* **1990**, *76*, 2033–2040.

36. Zarl, M. Development and Evaluation of a BOF Pre-Processor Model. Master's Thesis, Montanuniversität Leoben, Leoben, Austria, 2017.

Publication 4:

Dissolution of Scrap in Hot Metal under Linz–Donawitz (LD) Steelmaking Conditions

Reproduced with permission of open access Creative Commons CC BY 4.0 license

Article

Dissolution of Scrap in Hot Metal under Linz–Donawitz (LD) Steelmaking Conditions

Florian Markus Penz [1,*] **, Johannes Schenk** [1,2] **, Rainer Ammer** [3] **, Gerald Klösch** [4] **and Krzysztof Pastucha** [5]

[1] K1-MET GmbH, Stahlstraße 14, A-4020 Linz, Austria; Johannes.Schenk@unileoben.ac.at
[2] Chair of Ferrous Metallurgy, Montanuniversität Leoben, Franz Josef Straße 18, A-8700 Leoben, Austria
[3] voestalpine Stahl GmbH, voestalpine Straße 3, A-4020 Linz, Austria; Rainer.Ammer@voestalpine.com
[4] voestalpine Stahl Donawitz GmbH, Kerpelystraße 199, A-8700 Leoben, Austria;
    Gerald.Kloesch@voestalpine.com
[5] Primetals Technologies Austria GmbH, Turmstraße 44, A-4020 Linz, Austria;
    Krzysztof.Pastucha@primetals.com
* Correspondence: Florian-Markus.Penz@K1-MET.com; Tel.: +43-3842-402-2244

check for updates

Abstract: One of the main charging materials of the Linz–Donawitz oxygen steelmaking process (LD) is scrap. Scrap acts as a coolant for the exothermic reactions inside the LD vessel and as an iron source in addition to hot metal. The optimization of the LD process is focused, amongst other factors, on thermodynamic and kinetic modelling. The results of simulations have to be validated in close to reality laboratory-scale experiments. A study was made on the dissolution behavior of common steel scrap in carbon-saturated hot metal which is charged into LD converters. In order to examine the effect of several parameters on diffusive scrap melting, the difference between stagnant and dynamic dissolution as well as the influence of the hot metal temperature were investigated. Using a literature-based equation the mass transfer coefficient of carbon between the solid scrap and the liquid hot metal was evaluated. The ranges of values of the ablation rate and the mass transfer coefficient for the appropriate systems are pointed out, resulting in a significant dependence of the investigated parameters.

Keywords: basic oxygen furnace steelmaking; mass transfer coefficient; scrap dissolution; thermodynamics; process modelling

1. Introduction

Since the early 1950s, oxygen steelmaking in a Linz–Donawitz oxygen steelmaking process (LD) converter has been the dominant method of crude steel production. Since the beginning, scrap has been charged as a cooling agent and an additional iron source besides hot metal. Cooling is necessary due to heat generation through the oxidation reactions of carbon, silicon, manganese, and phosphorus. The whole process cycle is influenced by the dissolution and melting behavior of scrap in hot metal. Since the early 1970s, the investigation of the melting and dissolution behavior of scrap in iron melts with different carbon contents has been investigated, whereby only a few authors have taken into account the fluid flow of the liquid phase together with the initial process composition of hot metal [1–12].

To examine the effects of several parameters on diffusive scrap melting, an experimental investigation of the melting behavior of a common steel scrap in carbon saturated hot metal was executed. This work specifically points out the differences in the melting and dissolution rate of scrap in hot metal between stagnant and turbulent fluid motion of the liquid melt.

2. Background of Diffusive Scrap Melting

According to the literature, two processes control scrap melting and they change when the temperature exceeds the melting point of the scrap, which is defined by the liquidus temperature in the phase diagram for the given chemical composition of the scrap. Below the scrap melting point, the diffusion process of carbon controls the scrap dissolution and so-called diffusive melting occurs. Above the scrap melting point, forced or convective scrap melting starts. In this case, the mass transfer can be neglected since the heat transfer becomes dominant for the dissolution process [5,6,13]. Forced scrap melting is not relevant for this research work, since the melting point of the used steel scrap was above the hot metal temperature.

The main influence on diffusive scrap melting is the diffusive mass transport of carbon between the liquid metal and the charged scrap. Equation (1) is a mathematical model, proposed by L. Zhang and F. Oeters in ref. [6], where the mass transfer coefficient k_{met} in $[m \cdot s^{-1}]$ is a second decisive factor to define the ablation rate of a scrap particle.

$$- \frac{\mathrm{d}r}{\mathrm{d}t} = k_{met} * \ln \left(\frac{\%C_{Scrap} - \%C_{HM}}{\%C_{Scrap} - \%C_{liq}} \right) \tag{1}$$

In equation (1) the radius of the particle is r in unit [m]. C_{liq} describes the carbon concentration of the scrap on the liquidus line at a given temperature. The carbon concentrations in the scrap and hot metal are C_{HM} and C_{scrap} in [wt%] [6]. In this work, the liquidus line was determined for the actual silicon and manganese content of the scrap using the Fe Fe$_3$C phase diagram generated by the FactSage^{TM} FSstel database (licensed to Montanuniversität Leoben, Department Metallurgie; Version 7.1, ©Thermfact and GTT-Technologies, Montreal, QC, Canada and Herzogenrath, Germany) [14–16].

3. Description of the Experiment

The steel scrap investigated in this study was an S235JR construction steel, submerged in carbon saturated hot metal. The hot metal (330 g) was charged into an alumina crucible and positioned in a high temperature vertical tube furnace. To reach the starting temperatures, the heating rate was specified at 300 K/min. Before the first and between each further dissolution experiment, a holding time of 30 min was set. The vertical tube furnace was flushed with nitrogen during the heating and melting process to prevent oxidation of the hot metal. The scrap geometry was cylindrical. The diameter of the cylinder was 12 mm and the length 30 mm. The submerging depth into the hot metal was 25 mm. The axial heat flow to the specimen holding was diminished through a notch. The starting temperature of the specimen was 25 °C. The axial movement of the cylinder to the melt was carried out with a vertical pneumatic controlled cylinder. In order to realize a turbulent fluid motion in the hot metal, the sample was rotated at 100 rpm for the dynamic investigations. The determination of the real level of turbulence during the entire blowing process will, inter alia, be possible through CFD-simulation or related methods. Measurements directly in an LD converter are difficult to realize but it may be reasonable to assume that turbulent conditions are present. According to the geometric and physical parameters of the experiments and the present case of a rotating cylinder in a cylindrical crucible the theory of Taylor–Couette flow is used to define when laminar flow becomes unstable and further turbulent. The mathematical executions are not explained in detail in this work but are well described by A. Esser and S. Grossmann in [17] or A. Racina in [18]. For the present system a rotating sample with 100 rpm was found to be definitely in turbulent mixing regime. For static conditions, stirring by rotation of the cylinder was not performed.

To determine the effect of the initial temperature of the hot metal, three starting temperatures were defined (1305 °C, 1370 °C, and 1450 °C). Through pre-experiments as well as a heat and mass balance, published by the authors in ref. [19] the equilibrium temperature between the scrap center

and the hot metal was reached after less than 10 s. The starting and equilibrium temperatures as well as the chemical composition of the hot metal and the steel scrap are listed in Table 1.

Table 1. Specification of the hot metal and the scrap.

Definition	Hot metal	Scrap
Carbon content [wt%]	4.58	0.1
Silicon content [wt%]	0.37	0.0733
Manganese content [wt%]	0.63	0.479
Phosphorus content [wt%]	0.07	0.01
Mass [g]	330	26.3
Initial temperature [°C]	1305/1370/1450	25
Equilibrium temperature [°C]	1230/1300/1385	1230/1300/1385

To fulfil the variables for Equation (1), the carbon concentrations on the liquidus line of the scrap (C_{liq}) for the three determined equilibrium temperatures, given in Table 1, are shown in the appropriate phase diagram of the scrap in Figure 1. In the same figure the red line defines the liquidus line of the used scrap. The carbon concentrations (C_{liq}) are marked with the star symbol and their values are written beside it.
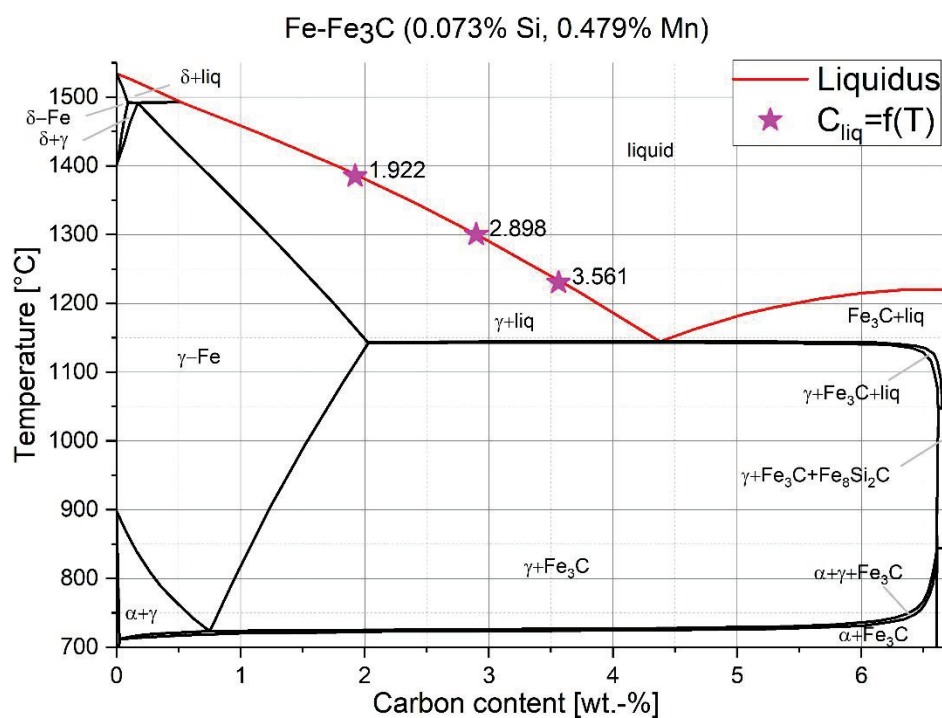

Figure 1. Carbon concentration of the scrap on the liquidus line at a given temperature.

The weight of the cylinder was measured before each experiment. After a defined dissolution time, the sample was extracted from the melt. Immediately after the extraction, the sample was quenched in water to avoid weight changes through oxidation. For the evaluation of the ablation rate (dr/dt), the radius was determined through the mass ($m_{\Delta t}$) of the sample after the measured dissolution time. For this evaluation, the density of the cylinder, defined by Equation (2), published by Miettinen in ref. [20], was used. The density $\rho_{T=T_{eq}}$ is assumed to be equal to the density at the equilibrium temperature ($T = T_{eq}$, austenitic) as well as the density of the hot metal. It was observed that only melting in the radial direction occurred, which can be explained through local density differences according to the temperature gradient in the boundary layer of the hot metal. Therefore, the length l of the cylinder was assumed to be constant for the evaluation of the radius r after a certain dissolution

time Δt. Further hot metal droplets stuck to the ground surface of the cylinder after its removal from the melt. The adherent hemispheres were included for the determination of the radius $r_{\Delta t}$. Due to the fact that the hot metal droplet is not always a perfect hemisphere, it has to be multiplied by a geometric factor g. The factor is 1 if the droplet is a hemisphere or 0 if there is no hot metal sticking on the ground surface. The geometric factor was determined through pictures, which were taken at eight circumferential positions. The equation for the determination of the radius after a certain time $r_{\Delta t}$ was done by goal seek application with Microsoft Excel and is shown in Equation (3), where $m_{\Delta t}$ is the mass of the cylinder after the defined submerging period.

$$\rho_{T=T_{eq}} = 8099.79 - 0.506T + (-118.26 + 0.00739T) * C_{C,scr} - 68.24 * C_{Si,scr} - 6.01 * C_{Mn,scr} \quad (2)$$

$$0 = \frac{2}{3} * r_{\Delta t}^3 * g + r_{\Delta t}^2 * l - \frac{m_{\Delta t}}{\rho_{T=T_{eq}} * \pi} \quad (3)$$

The derivates of the ablation rate ($\Delta r/\Delta t$) were solved by a Lagrange polynomial of the second grade for uneven time steps. The basic polynomial used is shown in Equation (4) [21].

$$f'(x) = f(x_{i-1})\frac{2x-x_i-x_{i+1}}{(x_{i-1}-x_i)*(x_{i-1}-x_{i+1})} + f(x_i)\frac{2x-x_{i-1}-x_{i+1}}{(x_i-x_{i-1})*(x_i-x_{i+1})} \\ + f(x_{i+1})\frac{2x-x_{i-1}-x_i}{(x_{i+1}-x_{i-1})*(x_{i+1}-x_i)} \quad (4)$$

In Equation (4), x is the value where the derivative has to be estimated, which in this case is the radius r as derivative from the time.

4. Discussion of the Experimental Results

The experimental data is based on a test series where three to six specimens were submerged for a specific time into hot metal. The submerging times were 10 s, 20 s, 30 s, 60 s, 120 s, 180 s, and 240 s. At the highest equilibrium temperature 140 s was the longest submerging time. From each cylinder, photographs were made in the circumferential position for further processing. In Figure 2 the cylinders after the given submerging time are shown in comparison to the initial state of the cylinder.
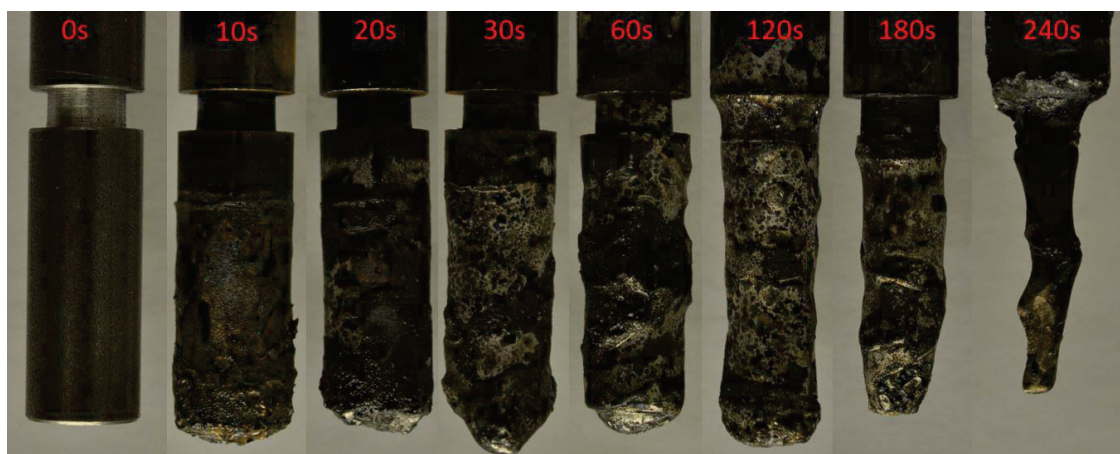

Figure 2. Recent photography's of the steel cylinders after a specific dissolution time (red marks) in comparison to the initial state (0 s).

In Figure 3 the calculated dimensionless average radius, using Equation (3), is shown for static approaches (no rotation of the sample). Figure 4 shows the determined values in turbulent conditions (dynamic sample, rotation velocity 100 rpm) inside the hot metal, which are more valuable for the conditions during the LD process, where high turbulence according to the oxygen blowing arises. The light areas in Figures 3 and 4 show the standard deviation of the measurements. Especially at the

higher temperatures and long dissolution times, problems of oxidation through air inside the furnace lead to higher fluctuations of the final determined radius.

In the initial stage of the dissolution, a small shell formation appears that lasts longer the lower the temperature of the liquid hot metal. At an equilibrium temperature of 1385 °C no shell formation is obvious after 10 s. In this case, the freezing and melting of the hot metal layer are already finished after the first measurement point. Furthermore, it is clearly shown that the shell formation will be shorter during turbulent conditions. With increasing temperature, the decrease of the radius is faster. This effect appears in both settings.
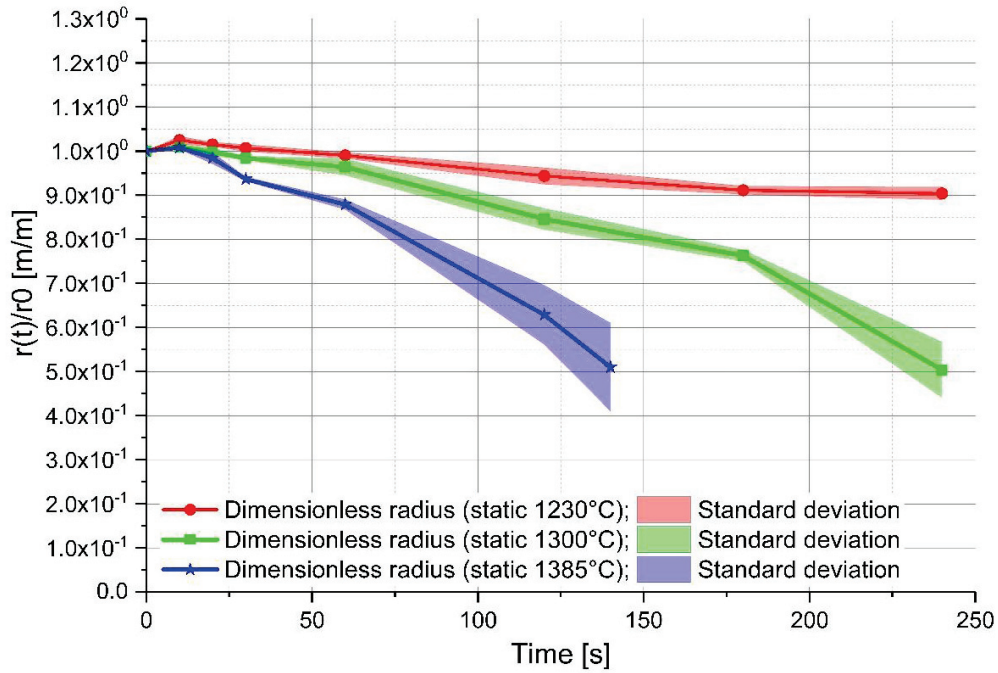
Figure 3. Dimensionless radius of the experiment with stagnant hot metal (static approach).
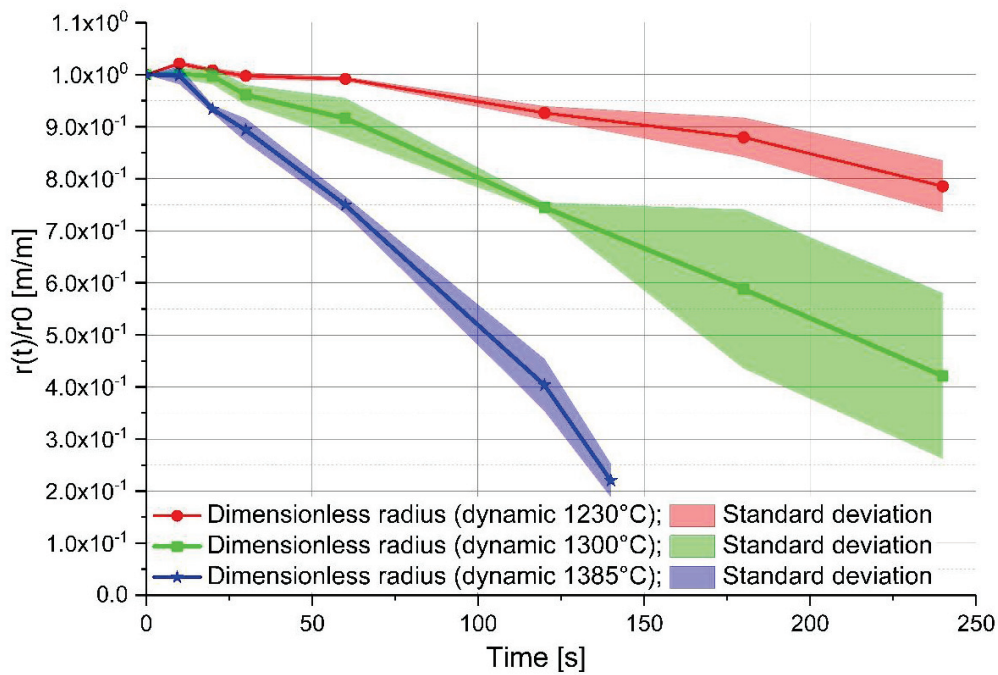

Figure 4. Dimensionless radius of the experiment with turbulent conditions in hot metal (dynamic approach).

In Figure 4 it can be seen that diffusive melting proceeds faster in comparison to static conditions. After a process time of 150 s and an equilibrium temperature of 1385 °C, the cylinder dissolved completely.

Based on the determined radius, the derivates of the ablation rates were quantified based on a second grade Lagrange polynomial. The graphical results are shown in Figure 5. It is visible that the ablation rate stays close to constant after shell formation. This could be observed at the two lower equilibrium temperatures. At the equilibrium temperature of 1385 °C, a slight decrease in the ablation rate is visible. This is a result of the oxidizing atmosphere in the vertical tube furnace. The surface of the sample that is not submerged in the hot metal starts to be oxidized after long holding times and higher temperatures. At all temperatures, the absolute value ($|\Delta r/\Delta t|$)of the ablation rate under turbulent hot metal conditions is higher than under static surroundings, which means that the scrap melts faster under turbulent conditions. This is explainable due to the higher mass transport from the sample surface to the melt according to the turbulence. In Equation (1) there is no factor for turbulence included, so a modification has to be defined.
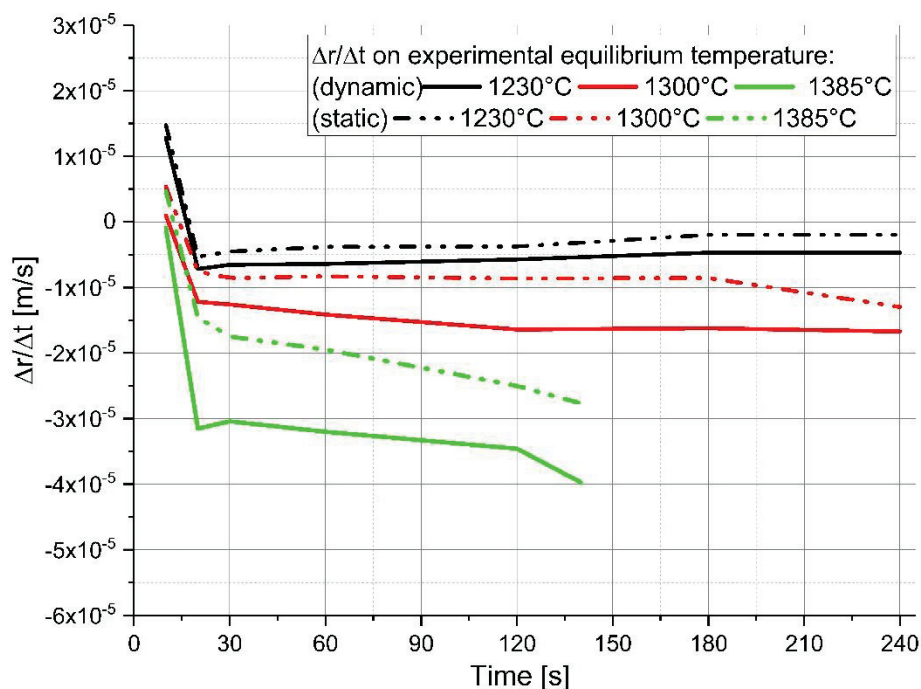

Figure 5. Comparison of the radial ablation rates in stagnant or turbulent conditions of the liquid hot metal with different equilibrium temperatures.

The mass transfer coefficients for the appropriate systems were evaluated with Equation (1) using the chemical parameters from Table 1 and Figure 1 as well as the determined derivates. The mass transfer coefficients for the stagnant and dynamic systems are presented in Figure 6 and listed in Table 2. After the shell formation ends, a quite constant mass transfer coefficient occurs at the temperatures of 1230 °C and 1300 °C. In all cases, the mass transfer is higher under turbulent conditions in the hot metal. At a temperature of 1385 °C, again a slight increase in the mass transfer with increasing dissolution time is obvious according to the oxidation of the sample holding device.

Table 2 lists the range of the calculated ablation rate and the mass transfer coefficients above 20 s of dissolution time. In the case, presented in this work, the freezing of a hot metal layer and its melting is finished. As shown in Table 2, the ablation rate is always negative after 20 s which means the scrap melts according to the diffusive melting theory. Thereby, it is clearly shown that the mass transfer is influenced strongly by the temperature and the experimental condition. Higher temperatures and a turbulent surrounding increase the mass transfer.
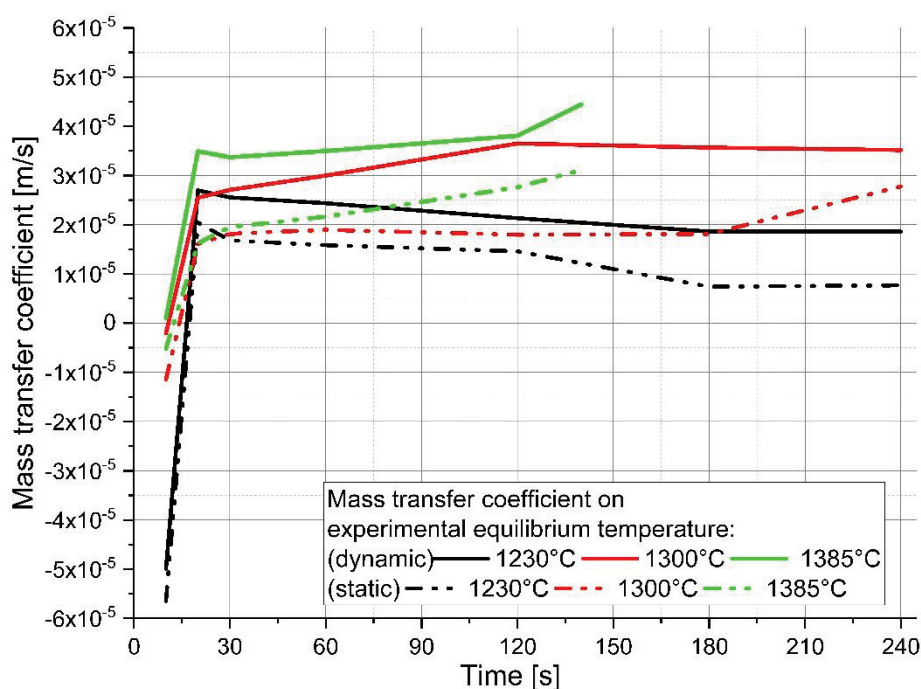
Figure 6. Comparison of the determined mass transfer coefficients under stagnant or turbulent conditions of the liquid hot metal with different equilibrium temperatures.

Table 2. Range of the calculated ablation rate and mass transfer coefficient above 20 s dissolution time.

Equilibrium temperature [°C]	1230	1230	1300	1300	1385	1385
Experimental condition	static	dynamic	static	dynamic	static	dynamic
Ablation rate [(m/s) $\times$ 10^{-6}]	-1.98 to -5.30	-4.68 to -7.19	-7.5 to -12.9	-12.1 to -16.7	-14.6 to -27.7	-30.4 to -39.7
Mass transfer coefficient [(m/s) $\times$ 10^{-6}]	7.39–20.4	18.5–27.0	16.1–26.8	25.5–36.5	18.2–31.1	33.7–44.4

5. Discussion

The intention of this work was to present the results of laboratory-scale experiments on the dissolution and melting behavior of common construction steel scrap in hot metal under stagnant or turbulent conditions of the melt and with a variation in temperature. The conditions were used because they are similar to the initial stages of the LD steelmaking process.

For the investigation of the differences between the two assumed conditions, the ablation rate of the radius of the dissolved scrap cylinder was determined. A shell formation of the hot metal on the scrap surface occurred in the initial stages at the experiment equilibrium temperatures of 1230 °C and 1300 °C. It was clearly pointed out that the shell formation lasts longer the lower the equilibrium temperature. At the highest temperature, the shell formation and its melting is finished after the first measurement point of a submerging time of 10 s. Turbulent conditions decrease the time of shell formation significantly. Based on the measured and calculated radius, the derivates for the ablation rate of the radius were determined using a second grade Lagrange polynomial. The ablation rate observed was shown to be constant after the turning point of the shell formation at temperatures of 1230 °C and 1300 °C. At 1385 °C, a decrease in the ablation rate was visible. Finally, it was observed that turbulent bath conditions have a higher absolute value of the ablation rate than in a stagnant melt.

In summary, the results of the work clearly indicate that the actual temperature and the motion of the melt have a strong impact on the melting and dissolution behavior of scrap. More research has to be done to develop a close to reality equation for the melting and dissolution behavior under the LD steelmaking process conditions. The conclusions should be used in further works to improve the

theoretical and practical description of the scrap melting for online and offline dynamic LD converter models, used in the industry. Better predictions of scrap melting may result in a decrease in lance damages due to breakage induced by non-molten big scrap pieces. Furthermore, a more precise description of the scrap melting and dissolution may decrease tap-to-tap times.

Author Contributions: Conceptualization, F.M.P.; Data curation, F.M.P.; Investigation, F.M.P.; Methodology, F.M.P.; Project administration, F.M.P., J.S. and K.P.; Resources, F.M.P.; Software, F.M.P. and J.S.; Supervision, F.M.P. and J.S.; Validation, J.S., R.A., G.K., and K.P.; Visualization, F.M.P.; Writing—original draft, F.M.P.; Writing—review and editing, F.M.P., J.S., R.A., G.K., and K.P.

Conflicts of Interest: The authors declare no conflict of interest.

References

1. Turkdogan, E.T. *Fundamentals of Steelmaking*; The Institute of Materials: London, UK, 1996; pp. 209–244.
2. Ghosh, A.; Chatterjee, A. *Ironmaking and Steelmaking Theory and Practice*; PHI Learning Private Limited: Delhi, India, 2015; pp. 285–292.
3. Asai, S.; Muchi, I. Effect of scrap melting on the process variables in LD converter caused by the change of operating conditions. *Trans. ISIJ* **1971**, *11*, 107–115.
4. Gaye, H.; Wanin, M.; Gugliermina, P.; Schittly, P. Kinetics of scrap dissolution in the converter. Theoretical model and plant experimentation. In Proceedings of the 68th Steelmaking Conference, AIME, Detroit, MI, USA, 14–17 April 1985; pp. 91–103.
5. Isobe, K.; Maede, H.; Ozawa, K.; Umezawa, K.; Saito, C. Analysis of the scrap melting rate in high carbon molten iron. *ISIJ* **1990**, *76*, 2033–2040.
6. Zhang, L.; Oeters, F. *Schmelzen und Mischen von Legierungsstoffen in Stahlschmelzen*; Verlag Stahleisen GmbH: Düsseldorf, Germany, 2012; pp. 38–40.
7. Szekely, J.; Chuang, Y.K.; Hlinka, J.W. The melting and dissolution of low-carbon steels in iron-carbon melts. *Metall. Trans.* **1972**, *3*, 2825–2833. [CrossRef]
8. Shukla, A.K.; Deo, B.; Robertson, D.G.C. Scrap Dissolution in Molten Iron Containing Carbon for the Case of Coupled Heat and Mass Transfer Control. *Metall. Mater. Trans. B* **2013**, *44*, 1407–1427. [CrossRef]
9. Den Hartog, H.W.; Kreyger, P.J.; Snoeijer, A.B. Dynamic model of the dissolution of scrap in BOF process. *CRM Rep.* **1973**, *37*, 13–22.
10. Kawakami, M.; Takatani, K.; Brabie, L.C. Heat and Mass Transfer Analysis of Scrap Melting in Steel Bath. *Tetsu-to-Hagané* **1999**, *85*, 658–665. [CrossRef]
11. Kruskopf, A.; Holappa, L. Scrap melting model for steel converter founded on interfacial solid/liquid phenomena. *Metall. Res. Technol.* **2018**, *115*, 201–208. [CrossRef]
12. Sethi, G.; Shukla, A.K.; Das, P.C.; Chandra, P.; Deo, B. Theoretical Aspects of Scrap Dissolution in Oxygen Steelmaking Converters. In Proceedings of the AISTech 2004 Proceedings Volume II, Nashville, TN, USA, 15–17 September 2014; pp. 915–926.
13. Medzhibozhskiy, M.Y. *Basis of Thermodynamic and Kinetic of Steelmaking*; Vischa shkola: Kyiv, Ukraine, 1979; p. 229.
14. Lytvynyuk, Y.; Schenk, J.; Hiebler, M.; Sormann, A. Thermodynamic and Kinetic Model of the Converter Steelmaking Process. Part 1: The Description of the BOF Model. *Steel Res. Int.* **2014**, *85*, 537–543. [CrossRef]
15. Penz, F.M.; Bundschuh, P.; Schenk, J.; Panhofer, H.; Pastucha, K.; Paul, A. Effect of Scrap Composition on the Thermodynamics of Kinetic Modelling of BOF Converter. In Proceedings of the 2nd VDEh-ISIJ-JK Symposium, Stockholm, Sweden, 12–13 June 2017; pp. 124–135.

16. Zarl, M. Development and Evaluation of a BOF Pre-Processor Model. Master's Thesis, Montanuniversität Leoben, Leoben, Austria, 2017.

17. Esser, A.; Grossmann, S. Analytic expression for Taylor-Couette stability boundary. *Phys. Fluids* **1996**, *8*, 1814–1819. [CrossRef]

18. Racina, A. *Vermischung in Taylor-Couette Strömung*; Universitätsverlag: Karlsruhe, Germany, 2009; pp. 29–40.

19. Penz, F.M.; Schenk, J.; Ammer, R.; Maunz, B.; Pastucha, K. Dissolution behavior of ULC steel in carbon saturated hot metal. In Proceedings of the 2nd International Congress on Science and Technology of Steelmaking, Venice/Mestre, Italy, 12–13 June 2018. CD-ROM.

20. Miettinen, J. Calculation of solidification-related thermophysical properties for steels. *Metall. Mater. Trans. B* **2018**, *28 B*, 281–297. [CrossRef]

21. Chapra, S.C.; Canale, R.P. *Métodos Numéricos para Engenharia*, 4th ed.; McGraw-Hill International do Brasil Ltda: São Paulo, Brazil, 2008; p. 549.

Publication 5:

Dissolution behaviour of ULC steel in carbon saturated hot metal

Industry news

Dissolution behaviour of ULC steel in carbon saturated hot metal

edited by: **F. M. Penz, J. Schenk, R. Ammer, K. Pastucha, B. Maunz**

In addition to hot metal, the Linz-Donawitz oxygen steelmaking process (LD) uses scrap as an iron source. Aside from this fact, scrap acts as a coolant for the exothermic reactions inside the LD converter and will be dissolved in the hot metal. The optimization of the LD process is also focussed on the thermodynamic and kinetic modelling where literature-based dissolution equations are used. In laboratory scale experiments the dissolution behaviour of ULC steel scrap in hot metal with two different carbon concentrations was investigated. For the evaluation of the experiments, a literature model for diffusive melting of scrap in hot metal was examined. Based on the measured ablation rate of cylindrical scrap samples submerged in hot metal, the mass transfer coefficient for the dissolution of ULC steel was determined.

> **KEYWORDS:** BASIC OXYGEN FURNACE – STEELMAKING – SCRAP DISSOLUTION – THERMODYNAMICS –PROCESS MODELLING

Florian Markus Penz
K1-MET GmbH, Linz, Austria;

Johannes Schenk
K1-MET GmbH, Linz & Chair of Ferrous Metallurgy Montanuniversitaet Leoben, Austria;

Rainer Ammer
voestalpine Stahl GmbH, Linz, Austria;

Krzysztof Pastucha
Primetals Technologies Austria GmbH, Linz, Austria;

Bernhard Maunz
voestalpine Stahl Donawitz GmbH, Donawitz, Austria;

INTRODUCTION

Oxygen steelmaking in an LD converter was developed in the early 1950s in Linz and Donawitz (LD) and it gradually became the most dominant method of crude steel production. Large quantities of scrap are used for an ordinary blowing process in an LD converter besides hot metal, which is the main charging material. Scrap is mainly used as a coolant for the process due to heat generation from the oxidation reactions of carbon, silicon, manganese and phosphorus. The dissolution and melting behaviour of scrap influences the whole process cycle in the converter. Many articles concerning the scrap melting process have been published in the past, whereby only a few describe the kinetics of a special steel scrap like ULC in hot metal with changing carbon content. (1 - 12) In this work, an experimental investigation of the melting behaviour of ULC (ultra-low carbon) steel scrap in hot metal with different carbon content was executed. The experiments are based on thermodynamic and kinetic calculations through a MatLab® coded single-zone LD model. Detailed descriptions of the model are published in (13 - 16). In previous calculations it was shown that low alloyed scrap types tend toward a stagnation of dissolution and melting during the oxygen blowing process using literature-based analytical equations (15). Based on these results, laboratory scale experiments were done for validation.

DERIVATIONS OF THE OBSERVED DATA

A collection of measurement data from LD-converters by various authors on the carbon concentration of the molten steel and the melt temperature during the blowing process is presented in (3). It was found that the change of the carbon content is a function of the melt temperature and its trend is parallel to
the liquidus line (austenite-liquid melt) in the Fe Fe$_3$C phase diagram. Most of the data points are in the liquid phase but some are in the two-phase area of austenite and liquid melt. A similar behaviour is also modelled with the LD model used and was partly published in (15). To describe the scrap melting and dissolution behaviour following literature-based considerations were applied.

The literature describes the melting of scrap in different phases where the diffusion process of carbon controls the scrap dissolution as long as the metal phase temperature is below the melting point of the scrap. If the temperature exceeds the melting point of the scrap a model for forced scrap melting is used. The scrap melting point is defined by the liquidus temperature in the phase diagram for the given chemical composition of the scrap.

The rate of diffusive melting of scrap is determined by the diffusive mass transport of carbon between the liquid metal and the charged scrap. Equation [1] is a mathematical model, proposed by Zhang L. and F. Oeters (6), where the mass transfer coefficient k_{met} in [m s^{-1}] is a decisive factor.

$$(1)$$

$$-\frac{\partial r}{\partial t} = k_{met} * \ln\left(\frac{\%C_{Scrap} - \%C_{HM}}{\%C_{Scrap} - \%C_{liq}}\right)$$

The scrap particles are assumed as spheres in the model used and the radius of the particle is r in unit [m]. C_{scrap} and C_{HM} are the carbon concentrations in the scrap and hot metal in [wt.-%]. C_{liq} describes the carbon concentration of the scrap on the liquidus line at a given temperature. (6) In this work, the liquidus line was determined for the actual silicon and manganese content of the scrap using the Fe-Fe$_3$C phase diagram generated by the FactSageTM FSstel database. (13, 15, 17)
When the temperature exceeds the scrap melting point, forced or convective scrap melting starts, where the mass transfer could be neglected since the heat transfer becomes dominant for the dissolution process. (5, 6, 18) In comparison to diffusive scrap melting, the driving force the temperature difference between scrap and hot metal during forces scrap melting. The equation for the forced scrap melting is cited in other publications. (15, 16) Forced scrap melting is not relevant for this research work, since the melting point of the ULC scrap was above the hot metal temperature in all experiments.

DESCRIPTION OF EXPERIMENTS
Dissolution tests

For the experimental procedure, an alumina crucible was charged with 320 g to 345 g of hot metal and positioned in a high temperature vertical tube furnace. The heating rate was 300 K/min to reach the starting temperatures, which are listed in Tab. 1. Before the first and between each further dissolution experiment, a holding time of 30 min was set. To prevent oxidation of the hot metal, the vertical tube furnace was flushed with nitrogen during the heating and melting process. The scrap geometry was cylindrical with a diameter of 12 mm and a length of 30 mm. The whole specimen, including the sample holding, is shown in Fig. 1. The cylinder was submerged into the hot metal with a depth of 20 mm, whereby the axial heat flow to the specimen holding was diminished through a notch. The starting temperature of the specimen was 25 °C. The axial movement of the cylinder to the melt was carried out with a vertical pneumatic controlled cylinder. No stirring by rotation of the cylinder or crucible was performed during the dissolution experiment (i.e. static conditions).
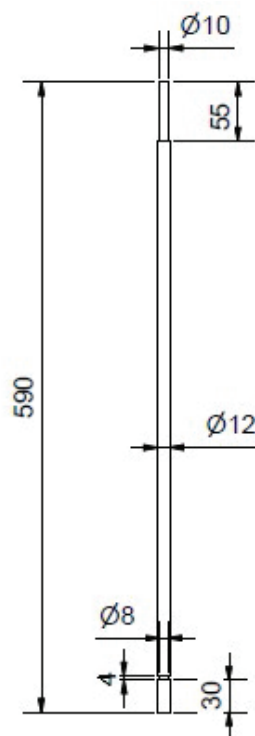
Fig. 1 - Sample geometry including the sample holding part (units in mm)

Before each dissolution experiment, the mass of the cylinder was determined. After a defined dissolution time, the cylinder was extracted from the melt and immediately quenched with water to inhibit further carbon diffusion in the sample and weight change by oxidation with air. Through the mass difference (Δm), the ablation rate of the radius Δr/Δt was evaluated. For this evaluation, the density of the cylinder, defined by equation [2], was used and assumed to be equal at the equilibrium temperature. After the experiments, it was observed that only a melting in radial direction occurred. Local density differences can explain this according to the temperature gradient in the boundary layer of the hot metal. The denser liquid will move downwards along the cylinder surface and inhibit a melting on the bottom surface of the cylinder, which is why the length of the cylinder remains nearly constant in all experiments.

The density of the scrap ρ_{scr} is defined by equation [2] published by Miettinen in (19) and is dependent on the temperature (in °C) and the scrap composition. The scrap is assumed to be ferritic and the density for a multicomponent system (composition $C_{i,scr}$ in wt.-%) is, according to the considered elements i of the scrap, explained with equation [2]. (19)

(2)

$$\rho_{scr} = 7875.96 - 0.297T - 5.62 * 10^{-5}T^2 + (-206.35 + 0.00778T + 1.472 * 10^{-6}T^2) * C_{C,scr} + 36.86 *$$
$$C_{Si,scr} - 30.78 * C_{Mn,scr}$$

The compositions of the hot metal and scrap samples used in the experiments are listed in Tab. 1 and Tab. 2, respectively. The dissolution tests were executed with ULC scrap in carbon saturated hot metal (hot metal 1) at three different temperatures (experiment numbers 1 to 3). Experiment number 4 was executed with hot metal 2 (carbon content of 1 wt.-%), which has a composition close to the liquidus line of the ULC at 1443 °C. The starting temperature of the experiment was assumed to be 1550 °C according to the calculation of the equilibrium temperature, which will be explained subsequently. According to Zhang and Oeters' model, a stagnation of the melting behaviour should occur when the driving concentration difference (%Cs$_{crap}$ - %C$_{liq}$) in equation [1] should become zero.

Tab. 1 – Hot metal specification

	Hot metal specification				
	Hot metal 1				Hot metal 2
Carbon content [wt.-%]	4.58				1
Silicon content [wt.-%]	0.37				0.1
Manganese content [wt.-%]	0.63				0.161
Phosphorus content [wt.-%]	0.07				0.015
Mass of hot metal [g]	320				345
Starting temperature [°C]	1305	1370	1450		1550
Experiment number [-]	1	2	3		4

Tab. 2 – Scrap specification

Scrap specification		
	ULC scrap	S235JR
Carbon content [wt.-%]	0.002	0.1
Silicon content [wt.-%]	<0.001	0.0733
Manganese content [wt.-%]	0.05	0.479
Phosphorus content [wt.-%]	0.003	0.01
Mass of hot metal [g]	26.3	26.3
Starting temperature [°C]	25	25
Experiment number [-]	1-4	Pre-test

Pre-Tests for Verification of Starting Conditions

Before the dissolution experiments, pre-tests were executed to verify the starting conditions for the individual dissolution tests. The starting temperature of the melt was measured with a thermocouple type B, which was directly submerged into the melt. This temperature is shown in Tab. 1 for experiments 1 to 4.

In a preceding test series of this research work, the melting and dissolution behaviour of S235JR scrap was investigated. In the course of this investigation, S235JR specimens (see Tab. 2) were used for verification of the equilibrium temperature between the liquid metal and the submerged sample, which results from the heat exchange between hot melt and cold scrap. For this purpose, a thermocouple type S was located in a bore with a diameter of 1.7 mm in the cylinder centre and at a distance of 10 mm from the cylinder tip. The cold cylinder was submerged into the liquid hot metal and the temperature was monitored until the equilibrium between the melt and the cylinder was reached. This temperature was always below the starting temperature of the hot metal, according to Tab. 1. The S235JR has a very similar enthalpy to ULC steel as a function of temperature. Fig. 2 shows these functions for ULC steel and S235JR, calculated with the FactSage™ FSstel and FactPS database. Accordingly, it was assumed that the equilibrium temperature measured for S235JR should be the same as for ULC steel.

The equilibrium temperature was evaluated with a heat balance, based on equations [3] and [4]. Whereas mScrap and mhot metal are the masses of the scrap and the hot metal in [kg], Q is the heat flux in [W m^{-2}], cp,hot metal is the specific heat capacity in [J kg^{-1} K^{-1}], $T_{start\ scrap/hot\ metal}$ and $T_{equilibrium}$ are the starting temperature of the melt or scrap and the equilibrium temperature in [K]. $H_{Scrap}(T)$ is the temperature dependent enthalpy in [J kg^{-1}]. For the determination of Tequilibrium, the heat fluxes of the scrap and hot metal must be equal. (20)

$$Q_{Scrap} = m_{scrap} * \left(H_{Scrap}\left(T_{equilibrium}\right) - H_{Scrap}\left(T_{start\ scrap}\right)\right) \tag{3}$$

$$Q_{Hot\ metal} = m_{hot\ metal} * c_{p,hot\ metal} * \left(T_{equilibrium} - T_{start\ hot\ metal}\right) \tag{4}$$
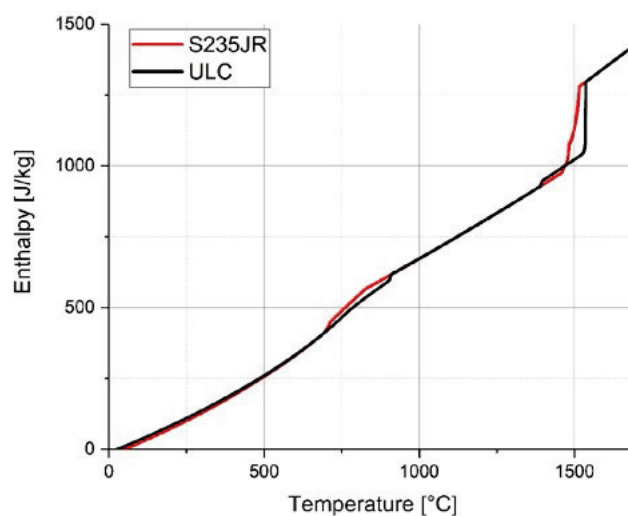

Fig. 2 - Enthalpy of ULC steel and S235JR

DISCUSSION AND RESULTS

The increase in the scrap core temperature based on the four investigated starting temperatures of the melt is shown in Fig. 3.
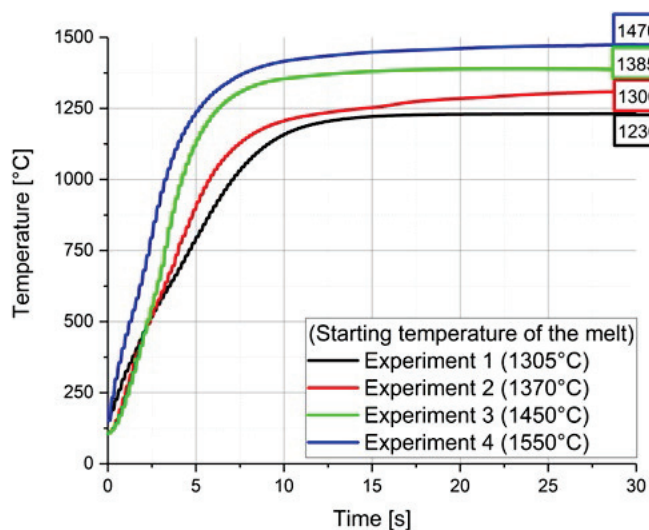

Fig. 3 - Measurement of the core temperature in the cylinder centre and equilibrium temperature

As seen in Fig. 3, the equilibrium temperature is reached within 10 seconds. The higher the starting temperature, the steeper the temperature gradient is. The measurement also shows that the equilibrium temperature is 65 °C to 80 °C below the starting temperature of the melt. In Tab. 3 the mea-

sured starting and equilibrium temperatures of the hot metal and the scrap are listed and compared with the calculated equilibrium temperatures from the heat balance obtained from equations [3] and [4] as well as the data from Fig. 3.

Tab. 3 – Starting and equilibrium temperatures of the hot metal and the scrap

	Starting temperature melt[°C]	Starting temperature scrap[°C]	Equilibrium temperature calculated[°C]	Equilibrium temperature measured [°C]	Temperature drop measured [°C]
Experiment 1	1305	25	1239	1230	75
Experiment 2	1370	25	1301	1300	70
Experiment 3	1450	25	1377	1385	65
Experiment 4	1550	25	1452	1470	80

Based on the well-fitting results of the thermocouple measurements, the determination of heat transfer coefficient k_{met} according to equation [1] becomes possible. In the following phase diagram (Fig. 4) of the present ULC scrap, the measurement points according to the hot metal composition (magenta) and the temperature development of experiment 4 with a carbon content of 1 wt.-% are shown. The blue line indicates the way of the equilibrium temperature between 10 to 30 s.,

whereby the liquidus line is exceeded during this time. Such behaviour does not occur during the experiment with hot metal with 4.58 wt. % carbon. For each equilibrium temperature, the carbon concentration on the liquidus line (cliq) in the Fe-Fe$_3$C phase diagram was determined. The terms of the carbon differences from equation [1] for each experiment are presented in Tab. 4.
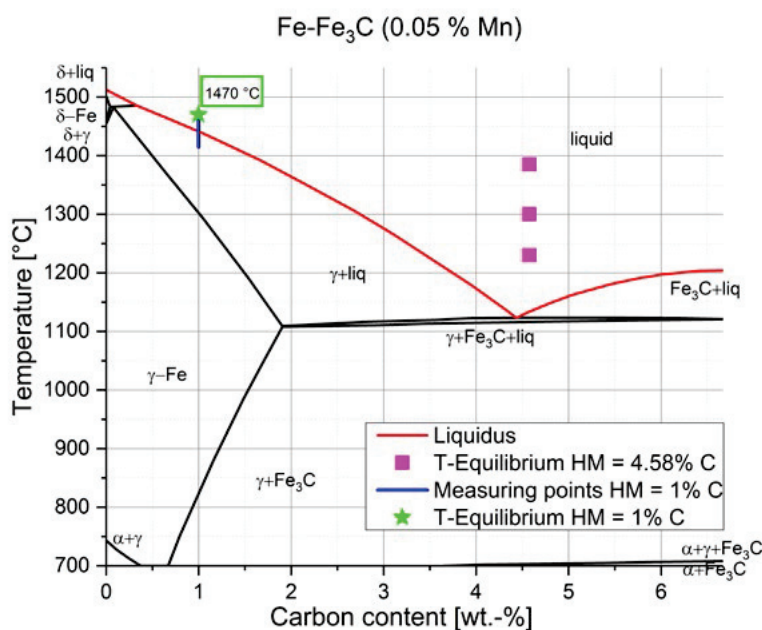

Fig. 4 - Measured equilibrium temperature based on the present ULC scrap composition phase diagram

Tab. 4 – Carbon differences based on equation [1]

	Carbon differences of equation 1		
	Equilibrium temperature [°C]	(%Cscrap - %Cliq) [wt.-%]	(%Cscrap - %CHM) [wt.-%]
Experiment 1	1230	-3.4651	-4.5763
Experiment 2	1300	-2.7467	-4.5763
Experiment 3	1385	-1.7612	-4.5763
Experiment 4	1470	-0.5930	-0.9980

The experimental determination of the ablation rate of the radius (Δr/Δt) for experiments 1 to 3, executed in hot metal with a carbon content of 4.58 wt.-%, is presented in Fig. 5.
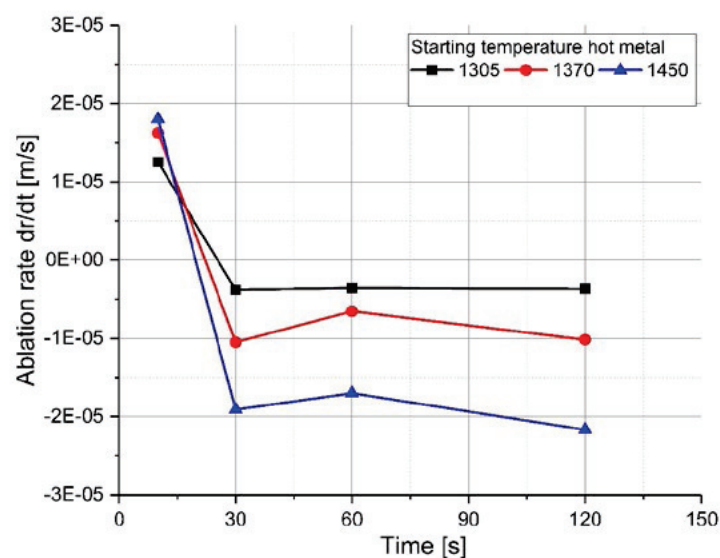

Fig. 5 - Ablation rate of ULC steel scrap in carbon saturated hot metal

At the beginning of the process, a positive ablation rate occurs. This phenomenon is attributed to a shell formation due to solidification of the liquid hot metal on the cold scrap surface. After a certain progressing time, the turning point is reached, the shell formation stops, and the melting of the shell starts. When the ablation rate turns negative, the melting of the mother scrap starts. The melting and dissolution is dependent on the equilibrium temperature, which is reached in this case, according to the measurements in Fig. 3, after 10 s. By using equation [1] the mass transfer coefficient for this system is calculated. According to the negative sign in the equation, a positive heat transfer is expected if the melting of the mother scrap is in progress. In Fig. 6 the calculated mass transfers of the three starting temperatures are plotted. As mentioned, the mass transfer is negative during the growth and melting of the shell layer at the beginning of the process and becomes positive after 25 s dissolution time at the latest. According to the progress, it could be established that the mass transfer coefficient will increase slightly with the temperature after the equilibrium temperature has been reached.
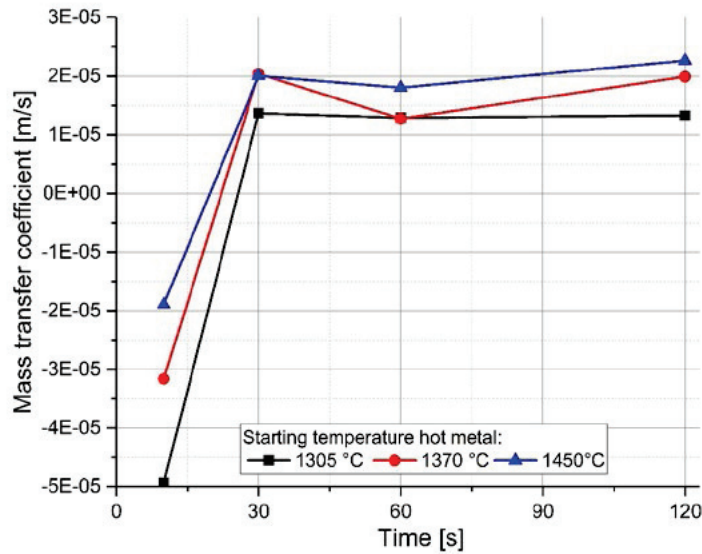
Fig. 6 - Experimental mass transfer coefficient

During the LD-process, the carbon content in the liquid melt decreases and the temperature increases in line with the exothermic reactions of oxidation. Therefore, the melting behaviour of ULC steel scrap was determined in modified hot metal with 1 % C. In Fig. 7 the mass transfer coefficient and the ablation rate of experiment 4 are presented. According to the heat balance calculation and measurement the specimen temperature increases to 1415 °C after 10 s and 1470 °C after 30 s, which is just above the liquidus line in the quasi-binary phase diagram..
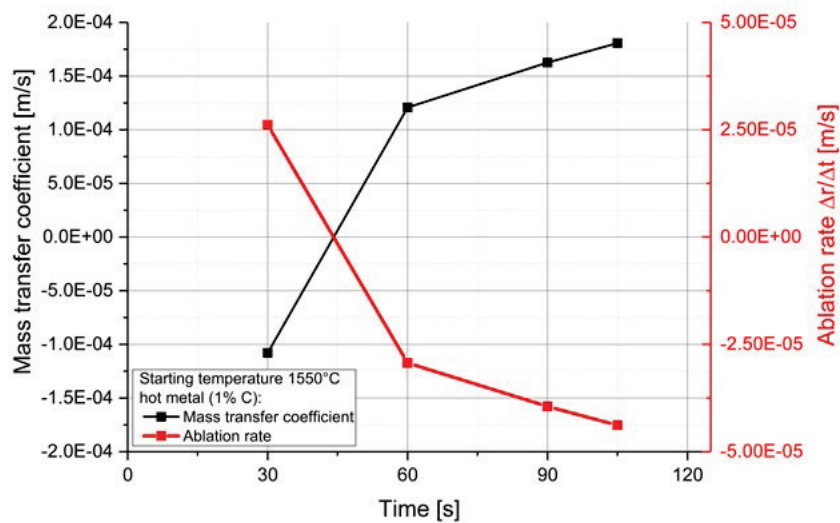

Fig. 7 - Mass transfer coefficient and ablation rate of ULC scrap in hot metal containing 1 %C

The smaller carbon content in the hot metal results in a strong shell formation at the beginning of the process with a higher negative mass transfer coefficient in comparison to experiments 1 to 3, with higher carbon contents in the hot metal. However, under real process conditions, shell formation will not occur. The scrap will be, due to heat conduction, almost at the equilibrium temperature when those amounts of carbon are reached. This will result in a higher expected negative mass transfer coefficient with an approach to 0. For that reason, a stagnation of the melting behaviour, described by equation [1], where the driving of (%Cscrap - %Cliq) would become zero or negative could be neglected. An explanatory argument is therefore that in this measurement just above the liquidus line, a dissolution of the ULC steel with high mass transfers occurs, which would not be stopped immediately when reaching the liquidus line or ends in an abrupt negative mass transfer coefficient when the temperature falls below the liquidus line.

CONCLUSION

This publication presents the results of laboratory scale experiments on the dissolution and melting behaviour of ULC steel scrap in hot metal with two different carbon concentrations. For the investigation, four different experiments with various hot metal temperatures were performed. For the evaluation of the hot metal mass transfer coefficient of the diffusive scrap melting process, a literature-based equation was used. To get the true process equilibrium temperature, a pre-test with a thermocouple in the core position of the specimen was executed, resulting in a temperature drop of more than 65 °C. Based on these measurements, the carbon concentrations on the liquidus line of the current available Fe-Fe$_3$C-Mn phase diagram were evaluated. With the measurements, the ablation rates of the radius were determinable and furthermore, the mass transfer coefficients were defined. What is mentionable is that the mass transfer coefficient is slightly dependent on the temperature. At the beginning of the process a shell formation occurs, which results in a negative mass transfer. If the carbon content in the melt decreases and the temperature increases, an increase in the mass transfer is observable. This results in a high melting rate of ULC scrap just above the liquidus line which would not turn into an abrupt negative mass transfer coefficient if the liquidus line were undercut.

In summary, the outcomes of this work clearly indicate that the actual temperature and melt composition have a strong impact on the melting and dissolution behaviour of ULC steel scrap. However, the difference in the dissolution behaviour of hot metal with 4.58 and 1 wt.-% carbon is not fully explainable. More research work must be done to investigate and describe the melting and dissolution of scrap for the conditions in the LD process.

REFERENCES

[1]   Turkdogan ET. Fundamentals of steelmaking. The institute of materials. London. 1996.

[2]   Ghosh A, Chatterjee A. Ironmaking and Steelmaking theory and practice. PHI Learning Private Limited. Delhi. 2015.

[3]   Asai S, Muchi I. Effect of scrap melting on the process variables in LD converter caused by the change of operating conditions. Transactions ISIJ. Vol. 11; 1971. p. 107 – 115.

[4]   Gaye H, Wanin M, Gugliermina P, Schittly Ph. Kinetics of scrap dissolution in the converter. Theoretical model and plant experimentation. 68th Steelmaking conference, AIME, Detroit, USA. 1985. p. 91 – 103

[5]   Isobe K, Maede H, Ozawa K, Umezawa K, Saito C. Analysis of the scrap melting rate in high carbon molten iron. ISIJ. Vol. 76; No.11, 1990. p 2033 – 2040.

[6]   Zhang L, Oeters F. Schmelzen und Mischen von Legierungsstoffen in Stahlschmelzen. Verlag Stahleisen GmbH. Düsseldorf. 2012.

[7]   Szekely J, Chuang YK, Hlinka JW. The melting and dissolution of low-carbon steels in iron-carbon melts. Metallurgical Transactions; Vol. 3; 1972. p. 2825 – 2833.

[8]   Shukla AK, Deo B, Robertson DGC. Scrap Dissolution in Molten Iron Containing Carbon for the Case of Coupled Heat and Mass Transfer Control. Metallurgical and Materials Transactions B; Vol. 44; 2013. p. 1407 – 1427.

[9]   Den Hartog HW, Kreyger PJ, Snoeijer AB. Dynamic model of the dissolution of scrap in BOF process. C.R.M. Rep. Vol. 37; No. 12, 1973. p. 13 – 22.

[10]   Kawakami M, Takatani K, Brabie LC. Heat and Mass Transfer Analysis of Scrap Melting in Steel Bath, Tetsu-to-Hagané. Vol. 85; No. 9, 1999. p. 658 – 665.

[11]   Kruskopf A, Holappa. Scrap melting model for steel converter founded on interfacial solid/liquid phenomena. Metallurgical Research and Technology. Vol. 115; 2018. p. 201 – 208.

[12]   Sethi G, Shukla AK, Das PC, Chandra P, Deo B. Theoretical Aspects of Scrap Dissolution in Oxygen Steelmaking Converters. AISTech 2004 Proceedings Volume II, Nashville, USA. 2014. p. 915 – 926.

[13]   Lytvynyuk Y, Schenk J, Hiebler M, Sormann A. Thermodynamic and Kinetic Model of the Converter Steelmaking Process. Part 1: The Description of the BOF Model. Steel Research int. Vol. 85; No. 4, 2014. p. 537 – 543.

[14]   Bundschuh P. Thermodynamische und kinetische Modellierung von LD-Konvertern. Dissertation. Montanuniversität Leoben, Austria. 2017.

[15]   Penz FM, Bundschuh P, Schenk J, Panhofer H, Pastucha K, Paul A. Effect of Scrap Composition on the Thermodynamics of Kinetic Modelling of BOF Converter. 2nd VDEh-ISIJ-JK Symposium, Stockholm, Sweden. 2017.

[16]   Penz FM, Bundschuh P, Schenk J, Panhofer H, Pastucha K, Paul A. Impact of Carbon, Silicon and Manganese contents on the dissolution and melting behaviour of scrap in a dynamic BOF model. 3rd European steel technology and application days (ESTAD), Vienna, Austria. 2017.

[17]   Zarl M. Development and evaluation of a BOF pre-processor model. Master Thesis. Montanuniversität Leoben, Austria. 2017.

[18]   Boychenko B, Okhotskiy V, Kharlashin P. The converter Steelmaking. Dnipro-VAL, Dnipropetrovsk. 2006.

[19]   Miettinen J. Calculation of solidification-related thermophysical properties for steels. Metallurgical and materials transactions B. Vol. 28 B; No. 4, 1997. p. 281 – 297.

[20]   Seshadri V., Tavares Parreiras R., Da Silva C.A., Da Silva I.A. Transport phenomena: fundamentals and applications in Metallurgical and Materials Engineering. ABM, Sao Paulo. 2011.

Publication 6:

Diffusive steel scrap melting in carbon-saturated hot metal – phenomenological investigation at the solid-liquid interface

materials

Article

Diffusive steel scrap melting in carbon-saturated hot metal—phenomenological investigation at the solid–liquid interface

Florian Markus Penz [1,*], Johannes Schenk [1,2], Rainer Ammer [3], Gerald Klösch [4], Krzysztof Pastucha [5] and Michael Reischl [6]

[1] K1-MET GmbH, Stahlstraße 14, A-4020 Linz, Austria; Johannes.Schenk@unileoben.ac.at
[2] Chair of Ferrous Metallurgy, Montanuniversität Leoben, Franz-Josef-Straße 18, A-8700 Leoben, Austria
[3] voestalpine Stahl GmbH, voestalpine Straße 3, A-4020 Linz, Austria; Rainer.Ammer@voestalpine.com
[4] voestalpine Stahl Donawitz GmbH, Kerpelystraße 199, A-8700 Leoben, Austria; Gerald.Kloesch@voestalpine.com
[5] Primetals Technologies Austria GmbH, Turmstraße 44, A-4020 Linz, Austria; Krzysztof.Pastucha@primetals.com
[6] voestalpine Forschungsservicegesellschaft Donawitz GmbH, Kerpelystraße 199, A-8700 Leoben, Austria; Michael.Reischl@voestalpine.com
* Correspondence: Florian-Markus.Penz@K1-MET.com; Tel.: +43-3842-402-2244

Abstract: The oxygen steelmaking process in a Linz-Donawitz (LD) converter is responsible for more than 70% of annual crude steel production. Optimization of the process control and numerical simulation of the LD converter are some of the current challenges in ferrous metallurgical research. Because of the process conditions and oxidation of impurities of the hot metal, a lot of chemical heat is generated. Therefore, steel scrap is charged as a coolant with the economical side aspect of its recycling. One of the more complex aspects is, among others, the dissolution and melting behaviour of the scrap in carbon-saturated hot metal. Heat and mass transfer act simultaneously, which has already been investigated by several researchers using different experimental approaches. The appearances at the interface between solid steel and liquid hot metal during diffusive scrap melting have been described theoretically but never investigated in detail. After an experimental investigation under natural and forced convective conditions, the samples were further investigated with optical microscopy and electron probe microanalysis (EPMA). A steep carbon concentration gradient in the liquid appeared, which started at an interface carbon concentration equal to the concentration on the solid side of the interface. Moreover, the boundary layer thickness moved towards zero, which symbolized that the boundary layer theory based on thermodynamic equilibrium was not valid. This fact was concluded through the prevailing dynamic conditions formed by natural and forced convection.

1. Introduction

The iron and steel industry is one of the most important global economic sectors. An increase in crude steel production up to 1670 million tons has been registered in recent years. About 72.7% of crude steel was produced by basic oxygen furnaces (BOFs), also known as Linz-Donawitz (LD) converters [1,2]. The charging materials for crude steel in a converter (besides others like slag formers) are hot metal, steel scrap, and technically pure oxygen for the oxidation of carbon, silicon, manganese, and phosphorus. Because of the exothermic reactions of oxidation, heat is generated and the

temperatures increase. By using steel scrap as a coolant, the temperature can be controlled. Charging scrap also has important economic reasons, because it is an additional valuable iron source obtained through the recycling of steel. Additionally, emissions of carbon dioxide gas can be avoided by increasing the scrap ratio [1,3–5]. In 2017, total scrap used for steel production increased steadily to more than 600 million tons. These values show that steel scrap has become an internationally traded commodity and a worldwide symbol for the environment and recycling life cycle [2].

It is definitely desirable from the viewpoint of energy and resource improvement to utilize scrap in LD converters. In previous publications, the melting and dissolution behaviours of scrap were a common research topic conducted with the aim of increasing the scrap ratio.

A number of relevant research articles focused on the theoretical mechanisms of the different stages of scrap melting [6–14]. Some of them were combined with experimental investigations on the dissolution rate of scrap in liquid hot metal considering heat or mass transfer or simultaneous heat and mass transfer [12,15–24].

In recent publications, numerical modelling of LD converters and the dissolution and melting behaviour of scrap in carbon-saturated hot metal have become more interesting [4,25–33].

In their publications, Asai, Muchi, and Miwa [25,26,34] described theoretically—by means of a mathematical model—the LD converter operation and the mutual effect of scrap melting with process variables (e.g., melt temperature and carbon contents of scrap and melt). A more thorough theoretical description of the fundamental kinetics of the scrap dissolution process was given by Zhang and Oeters in [6] and Oeters in [7]. In [35], Szekely et al. described the heat and mass transfer phenomena involved. In [14], Glinkov et al. derived a type-III boundary condition with a slightly different approach. A more detailed theoretical description of heat and mass transfer phenomena was published by Specht and Jeschar in [13].

The authors of experimental studies mostly investigated the melting time of steel scraps of different sizes, shapes, and preheating temperatures. The pioneer works on steel scrap melting were carried out by Pehlke et al. in [12] and Olsson et al. [15]. Pehlke et al. studied the melting rate of cylindrical specimens in the temperature range of 1300 to 1650 °C dependent on bath agitation [12]. Olsson et al. [15] carried out experiments with rotating iron and iron–carbon cylinders and concluded that, in a range of Reynolds numbers of 350 to 10,700, the rate of dissolution was controlled by mutual counter diffusion of carbon and iron in the boundary layer [15]. Kim and Pehlke published their findings on transient heat transfer during the initial stages of steel scrap melting in [17], where shell freezing and melting were observed. In a later publication, Kim and Pehlke showed their results concerning the dissolution rates of solid pure iron into molten iron carbon alloys under isothermal conditions in [16]. In [18], Li et al. investigated the melting rate of steel bars with various sizes, shapes, and initial temperatures in a 1650 °C hot steel bath. The article was extended to a study of multi-piece scrap melting by Li and Provatas in [19]. Penz et al. investigated the dissolution behaviour of common carbon steel scrap in carbon-saturated hot metal and pointed out the differences between stagnant and dynamic bath conditions in [20]. Several authors have also reported their investigations of scrap melting and dissolution behaviour patterns in industrial experiments [36–40]. Experiments on a fixed reaction area were carried out by Shin et al. in [22].

As a subroutine for a dynamic model describing the LD process, a numerical solution for the scrap melting stage was published by Yorucu and Rolls in [27]. A phase-field model for the melting of scrap in the presence of convection was published by Li et al. in [28]. Their model replaced the explicit tracking of the boundary by an equation of a continuum phase field. This field described either a volume element containing only a liquid ($\Phi = 1$) or solid phase ($\Phi = -1$) and interpolates continuously from −1 to 1 in the transition area [28]. Theoretical aspects of scrap dissolution with simplifying assumptions were included in a Fourier series-based analytical solution by Sethi et al. in [29]. The model was critically compared with a finite difference solution, whereby the analytical model was concluded to be more accurate [29]. A number of modelling approaches were published and compared by Shukla et al in [30]. A 2D numerical simulation tool to investigate the melting process of heavy scrap pieces during LD heat was published by Guo et al. in [31]. In their conclusion, they mentioned that the cutting size of a slab had little influence on the melting time when the ratio

between width and thickness was greater than 2, where the location of the scrap, relative to the oxygen jet, had a more significant influence [31]. Recent publications and research activities on creating a scrap melting model were conducted by Kruskopf et al. in [4,32,33]. Kruskopf discretized his model into a moving numerical grid and solved enthalpy and carbon concentration equations for solid material [32].

One of the main recurring assumptions in all experiments, theoretical analyses, and numerical approaches reported was the definition of the boundary carbon concentration, which was assumed to be the liquidus carbon concentration in a binary Fe–Fe$_3$C phase diagram. For that reason, the authors investigated in detail the melting and dissolution behaviours of carbon steel scrap. Research findings are shown in the present paper.

2. Phenomenological understanding of scrap melting and dissolution processes

Isothermal investigations into the mass transfer from solid to liquid were carried out by Lommel and Chalmers in [41]. They investigated the transport behaviour from solid lead into liquid lead–tin alloy, whereby the diffusion of tin atoms into the solid lead was not a necessary condition for mass transfer in the absence of stirring the liquid. In the studied lead/lead–tin alloy system, the initial concentration of the liquid was lower than that of the solid. Nevertheless, mass transport in the liquid adjacent to the interface occurred by volume diffusion through a boundary layer (C$_{HM}$) of thickness δ.

In the research work of Pehlke et al., rotating or static cylindrical rods of various sizes were submerged from room temperature into hot metal baths under different conditions and temperatures [12]. Formation of a hot metal shell was reported in the initial stages, which retarded the dissolution and lasted approximately 30 s. Gol'dfarb and Sherstov pointed out that a steel scrap ball of 20 cm in diameter had shell formation and melting that lasted approximately 2 min [10]. Nomura and Mori concluded in [11] that shell formation was negligible unless the scrap was thick. During the initial stages of immersion, heat was also transferred from the melt to the scrap until an equilibrium temperature between scrap and hot metal was reached [12]. Penz et al. showed in [42] that ultra-low carbon steel scrap cylinders 12 mm in diameter, submerged into hot metal, containing approximately 4.5 wt.-%, would reach isothermal conditions after less than 15 s immersion time. Similar results were published by Penz et al. in [21], where they defined the heat transfer coefficient between the steel scrap and the hot metal in the initial stages of immersion. Olsson et al. only reported on mass transfer measurements after reaching equilibrium temperature between scrap and hot metal [15]. Penz et al. defined in [20] the ablation rate of a cylindrical specimen and mass transfer coefficient by using a diffusive scrap melting formula published by Zhang and Oeters in [6]. Moreover, Li et al. in [18,19] and Xi et al. in [23] reported experiments on scrap melting in liquid iron–carbon melts at temperatures above the liquidus temperature of iron. To summarize all these findings, it is clearly shown that scrap melting is a complex mechanism combining simultaneous heat and mass transfers. The following is a proposal on how to divide the scrap melting process into three stages:

- Stage 1: Solidification of a liquid hot metal layer on the surface of cold scrap, which will re-melt fast after enough superheat is available. Heat and mass transfer work simultaneously.
- Stage 2: Dissolution of the scrap, depending on the carbon composition of the hot metal and the scrap, also defined as diffusive melting. At this stage, superheat will be consumed for promoting necessary mass transfer. Because heat transfer is much faster than mass transfer, and the carbon content in the solid steel is much lower than in the liquid melt, only mass transfer has to be considered.
- Stage 3: A forced or convective scrap melting stage will be reached if the temperature of the hot metal exceeds the melting temperature of the scrap. In this case, only heat transfer should be considered.

To sum up the phenomenological understanding, it is necessary to highlight that mass transfer—especially from carbon—is important to investigate. Further, previous publications have shown that bath agitation and temperature influence the dissolution and melting behaviour of scrap. In Figure 1, the phenomena of heat and mass transport at the solid–liquid interface are depicted. The subscript

init stands for the initial concentration or temperature of the scrap, which is uniform at time t = 0 over the whole transverse section. The initial temperature and carbon concentration of the hot metal are T_{HM} and C_{HM}, respectively. Temperature and concentration gradients will occur in both the liquid and solid. At the interface, a slightly lower temperature T_s than the hot metal will be reached. The equilibrium concentration achieved in the liquid for the temperature T_s is C_l^* and C_s^* in the solid. The boundary layers in the liquid for heat and mass transfer are δ_T and δ_C, respectively. According to Goldberg and Belton in [43] and Bester and Lange in [44], the diffusion coefficients of carbon in liquid iron and iron–carbon alloys are significantly higher than in solids, which could diminish the concentration boundary layer in the liquid dramatically.
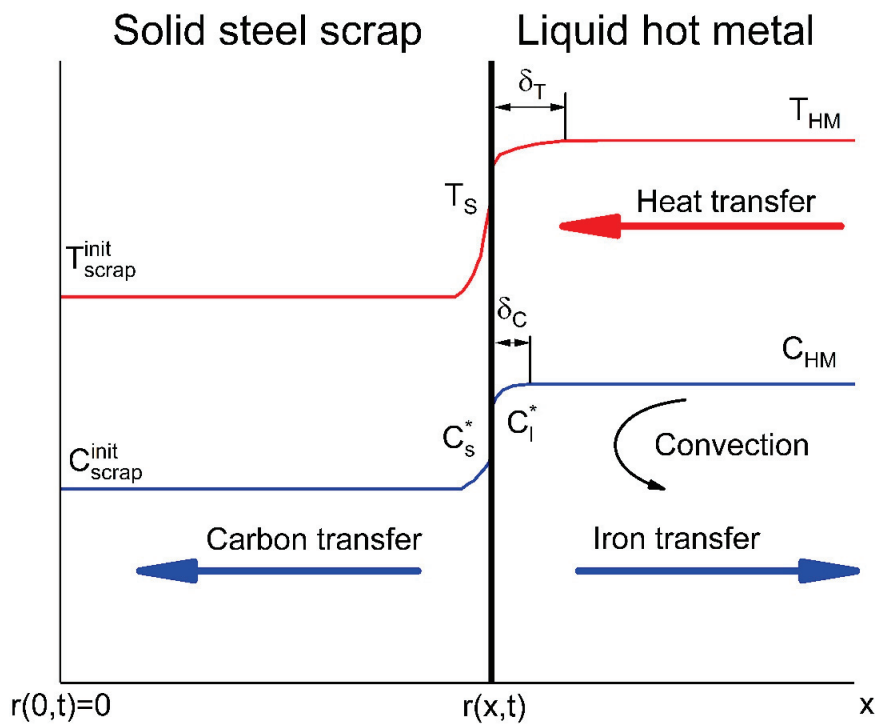

Figure 1. Schematic diagram of mass and heat transfer between cold scrap and liquid hot metal.

3. Theoretical description

In the present article, the authors focus on diffusive scrap melting under isothermal conditions. Shurygin and Shantarin proposed in [8] that the rate of dissolution of an iron disk in hot metal was limited by the diffusion of elements in the boundary layer. The expression for the boundary layer thickness δ_C they used is given by Levič in [45]. The proposed rate of dissolution, N, including Levič's expression, is given in Equation 1 [8,15,45].

$$N = \frac{D_s}{\delta_C} A\left(C_{scrap} - C_{HM}\right) = 1.95 * r^2 D_s{}^{2/3} \nu^{-1/6} \omega^{1/2}\left(C_{scrap} - C_{HM}\right). \tag{1}$$

In Equation 1, D_s is the diffusion coefficient in the solid, A is the surface area and r defines the radius of the sample. The parameters ν and ω describe the kinematic viscosity and the angular velocity. Nevertheless, Olsson et al. concluded in [15] that the expression proposed by Shurygin and Shantarin would lead to high diffusivity values. Olsson et al. noted that the liquid and solid at the interface were in an equilibrium relation. They assumed that for that reason, the liquid at the interface had liquidus composition corresponding to the bath temperature (C_{liq}), which is given in Equation

2. These findings were based on the considerations published by Lommel and Chalmers in [41]. Equation 2 is only valid if equal densities in the solid and liquid are considered [15,41].

$$-\frac{dr}{dt} = k_{met} * ln\left(1 + \left(\frac{\%C_{liq} - \%C_{HM}}{\%C_{Scrap} - \%C_{liq}}\right)\right). \tag{2}$$

In Equation 2, $k_{met} = D/\delta$ is the mass transfer coefficient (m/s), which is the ratio between the diffusion coefficient D and the boundary layer thickness δ.

Assuming that solid steel scrap has a more uneven composition than liquid hot metal, as usual in an LD converter, the melting is extended with dissolution phenomena, including multiphase systems with temperature as well as chemical composition-dependent liquidus and solidus lines. Based on Figure 2, which shows the Fe–Fe₃C phase diagram of common S235JR construction steel scrap, the solidus and liquidus lines could be estimated. The square blue points in Figure 2 show the specific isothermal carbon concentrations of the scrap (C_{scrap}) and an assumed liquid hot metal composition (C_{HM}) as well as the solidus (C_s^*) and liquidus (C_l^*) concentrations at 1300 °C. In [9], Krupennikov and Filimonov expressed the direct solution of steel in iron carbon melts in two successive stages: the transition of iron atoms through the phase boundary (kinetic stage) and the subsequent diffusion through the boundary layer into the melt (diffusion stage). The result of their theoretical consideration was that the carbon concentration at the surface of the solid had to be equal to C_s^* at the solidus temperature. This led to a chemical potential difference $\Delta\mu(C_s^*, C_l^*)$ between the iron atoms on the surface of the solid and in the melt at the phase boundary. Because of the breakdown of the solid's crystalline structure, which results in a reduction of activation energy characterizing the kinetic stage, a liquid phase will form in the decomposition of a supersaturated solid. However, they mentioned that no significant kinetic factors retarding the melting process had been observed yet [9]. As the authors presented in [46] with their dynamic LD converter model, and Asai and Muchi [25] showed based on the investigations of Oya in [47], the carbon concentration of the hot metal could also be just below the liquidus line in a binary phase diagram, which led to a negative logarithmic term in Equation 2. In fact, a negative logarithmic term results in an increase in scrap during the blowing period of an LD converter.
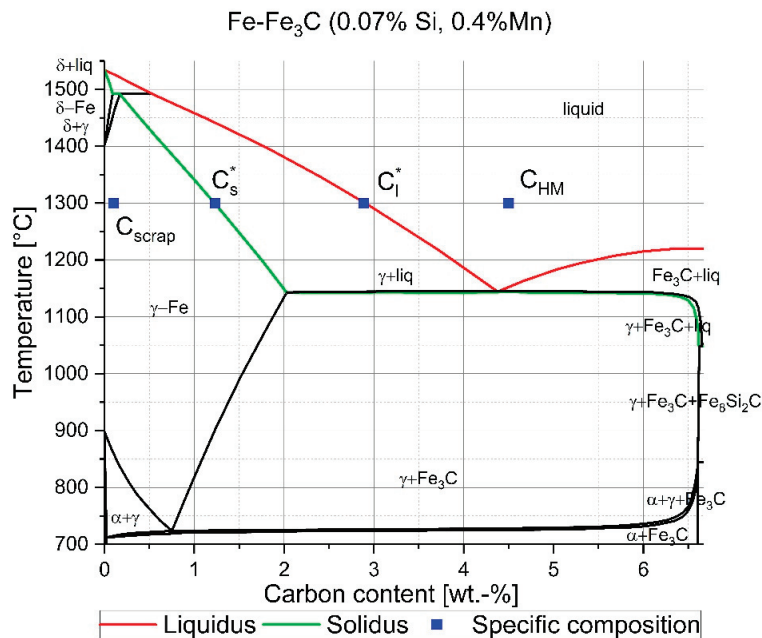

Figure 2. Fe–Fe₃C phase diagram of common S235JR construction steel scrap including schematic points of carbon concentrations.

The mass balance on the surface according to Figure 1 and the theoretical description of Specht and Jeschar in [13] is given in Equation 3, where k'_{met} is the mass transfer coefficient in m/s, D_s is the diffusivity into the solid in m²/s, and ρ_{HM} and ρ_{scrap} are the densities of the hot metal and scrap in kg/m³, respectively.

$$k'_{met} * \rho_{HM} * (C_{HM} - C_l^*) = -\rho_{scrap} * D_s * \frac{dc}{dx}_{|x=r(x,t)} - \rho_{HM} * (C_l^* - C_s^*)\frac{dr(x,t)}{dt}. \tag{3}$$

Glinkov et al. presented a slightly different aspect in [14]. In their theoretical exploration, they determined that the interface composition was equal in the solid and the liquid (C_{int}). It was not clearly defined if the interface carbon concentration in Glinkov's research work was either C_s^* or C_l^*.

From Figure 1 it is known that carbon is transported steadily to the interface through convection and will diffuse into the solid scrap. The fundamental equation for diffusion is Fick's second law, which is given in Equation 4 with the three-dimensional differential operator ∇ [48–52].

$$\frac{\partial C}{\partial t} = \nabla \cdot (D\nabla C). \tag{4}$$

The general equation can be transferred to the more common form in Equation 5, where the axial flow in the *x*-direction is given with the boundary conditions $\partial/\partial z = \partial/\partial y = 0$ and $0 < r(x,t) < \infty$ according to the sketch in Figure 1:

$$\frac{\partial C}{\partial t} = \nabla \cdot (D\nabla C), \tag{5}$$

where C is the concentration and the diffusion coefficient is D_s. Assuming that the state of constant ambience concentration (C_{HM}) is given, the melting rate can be stated as constant.

$$v = -\frac{dx}{dt} = -\frac{dr(x,t)}{dt} = const. \tag{6}$$

The boundary conditions for the mass transfer are defined in [13] and according to the sketch in Figure 1 as follows:

$$C(x = 0) = C_{scrap} \text{ and } C(x = \infty) = C_{HM}. \tag{7}$$

Kim and Pehlke reported in [16] a carbonised layer of 58 μm at 1242 °C in stagnant melt conditions. Experiments with a fixed reaction area were carried out by Shin et al. in [22] and Nomura and Mori in [11]. Shin et al. approximated the carbonised layer thickness to be 114, 108, and 57 μm at 1230, 1325, and 1415 °C, respectively, by using temperature- and carbon-dependent extrapolated diffusion coefficients [22]. Nomura and Mori reported an estimated diffusion boundary layer thickness of 50 to 100 μm at decreasing temperatures in the range of 1420 to 1200 °C, respectively [11]. According to those measurements, the boundary condition $C(x = 0) = C_{scrap}$ could be assumed for samples with a thickness >1 mm. With the boundary conditions and the constant melting rate, the solution to Equation 5 is expressed in Equation 8.

$$\frac{C - C_{scrap}}{C_s^* - C_{scrap}} = \exp\left(-\frac{v}{D_s} * X\right). \tag{8}$$

The surface gradient will be as given in Equation 9 if the interface concentration in the solid is assumed to be the solidus concentration at the presumed temperature.

$$\frac{dc}{dx}_{|x=r(x,t)} = -\left(C_s^* - C_{scrap}\right)\frac{v}{D_s}. \tag{9}$$

As long as the widely spread consideration in literature is used, that the densities of the scrap ρ_{scrap} and hot metal ρ_{HM} are equal, the mass balance of Equation 3 can be rewritten and simplified to Equation 10.

$$-\frac{dr}{dt} = k'_{met} * \left(\frac{c_{HM} - c_l^*}{c_l^* - c_{scrap}}\right).$$
(10)

According to Zhang and Oeters in [6], the mass transfer coefficient k'_{met} used in Equation 10 is connected to k_{met} by the function expressed in Equation 11 using the dimensionless value ξ [6]. It is the ratio of the velocity of the boundary movement to the mass transfer.

$$f(\xi) = \xi / \left(1 - e^{-\xi}\right).$$
(11)

With high values of ξ, the mass transfer will increase, which means that the mass transfer is only dependent on the velocity of the boundary movement. A detailed description of this explanation is given by Zhang and Oeters in [6]. Using Zhang and Oeters' expression in Equation 11 with the mass balance of Equation 10, the expression of the mass balance will result in the initial Equation 2.

From a theoretical point of view, the dissolution rates are controlled by the interdiffusion of iron and carbon in the liquid boundary layer. Therefore, the kinetics of scrap dissolution essentially belong to the class of moving boundary problems with phase changes, which is also known as a Stefan problem. A more comprehensive theoretical description of Stefan problems can be found in various research articles (e.g. [53–55]). It should be kept in mind that the values of mass transfer will also depend on scrap geometry, the condition of the liquid bath, and various physical parameters that include the diffusion coefficients.

In a literature research process, two papers investigated directly the surfaces of scrap samples. In [24], Sun et al. presented their experimental observations of spherical scrap melting in hot metal. Spherical scrap with a mass of 0.23 to 0.25 kg fixed on a molybdenum rod was immersed into a 70 kg hot metal bath with temperatures between 1300 and 1600 °C. Electron probe microanalyses (EPMAs) were carried out on the surface of specimens. They detected a slightly higher amount of carbon counts close to the surface, concluding that it might be insignificant. Xi et al. carried out thermal simulation experiments with GCr15-bearing steel samples at temperatures of 1500 °C and 1600 °C, and they published their results in [23]. With optical microscopy analyses, a sharp interface between the frozen hot metal shell (primary carbide) and the mother scrap was detected. In the inner layers of the steel bar, the microstructure changed to martensite due to water quenching. Xi et al. concluded that it was reasonable to assume that the melting process was less affected by mass transfer of carbon, and that the melting process was mainly controlled by heat transfer at the investigated temperatures [23].

4. Experimental investigation

4.1. Experimental setup and melting

In a previous study, the authors submerged S235JR construction steel in carbon-saturated hot metal with a carbon concentration of approximately 4.58 wt.-% [20]. The primary objective of Penz et al. was to determine the mass transfer coefficient under stagnant or turbulent bath conditions and various temperatures. To simulate turbulent bath conditions, the samples were rotated with a rotation speed of 100 rpm. With the geometric and physical parameters of the experimental setup, the theory of Taylor–Couette flow was used to define when laminar flow became unstable and more turbulent [20,56,57]. The initial chemical compositions and experimental data are listed in Table 1. Thereby, a mass of 330 g of hot metal was heated in an aluminum oxide crucible in a Carbolite Gero high temperature vertical tube furnace. The heating rate was specified at 300 K/min. For oxidation prevention, the furnace was flushed with nitrogen gas. Cylindrical specimens 12 mm in diameter were submerged into the hot metal. The initial temperatures of the hot metal were measured to be 1305, 1370, and 1450 °C. The initial temperature of the specimen was 25 °C before submerging. The submerged length was 20 mm. Through further experiments, published by the authors in [42], it was verified that an equilibrium temperature between the hot metal and the core of the scrap was reached

after 10 s. The equilibrium temperatures were 1230, 1300, and 1385 °C, respectively, and are listed with the initial temperatures of the scrap and the hot metal in Table 1 [20].

Table 1. Experimental data [20].

Definition	Hot metal	Scrap
Carbon content (wt.-%)	4.58	0.1
Silicon content (wt.-%)	0.37	0.0733
Manganese content (wt.-%)	0.63	0.479
Phosphorus content (wt.-%)	0.07	0.01
Mass (g)	330	26.3
Initial temperature (°C)	1305/1370/1450	25
Equilibrium temperature (°C)	1230/1300/1385	1230/1300/1385

4.2. Sample preparation

After a specified submerging time, the samples were withdrawn and quenched with water to avoid oxidation and stop carbon diffusion immediately. To prevent any influence of the microstructure and the chemical distribution of the elements inside the samples, they were cut longitudinally with wire electrical discharge machining (wire EDM). For the cutting, deionized water was used as a dielectric. Afterwards, the sectional surface of the sample was ground with SiC sand paper and polished to 1 μm. The final polishing to 0.1 μm for electron microprobe analysis (EPMA) was carried out with an alumina suspension. EPMA was done with a JEOL JXA-8230 using a tungsten filament for generating the electron beam and five wavelength-dispersive X-ray spectroscopy (WDS) detectors. The elements investigated were carbon, silicon, manganese and phosphorus. Additionally, chromium and oxygen were partially investigated. For the latter, quantification was not possible because there was a lack of standards available. The analyzed area had a size of 240 × 2000 μm, and one detection point occupied an area of 3 × 3 μm. Measurements were carried out with an acceleration voltage of 15 kV and a probe current of 580 nA. After the EPMA, the samples were etched with nitric acid and analyzed by means of optical microscopy.

5. Results and discussion

5.1. Effect of bath temperature on dissolution

As mentioned above, the authors investigated in [20] the dissolution and melting behaviours of the scrap. For each specified immersion time, three samples were submerged into fresh, hot metal. The average rate of the radius after immersion (r(t)) with the initial radius (r0) was further determined through the weight. The detailed description of the experiments and the evaluation of the ablation rate and mass transfer coefficients can be taken from [20]. In Figure 3, the average rate of the radius after the specified immersion time with the initial radius is shown for a stagnant system. In the initial 10 s, shell freezing occurred, which reached its maximum point after approximately 5 s. The maximum radius of the frozen shell was temperature-dependent and was in the range of 15% at an initial temperature of 1450 °C to 25% at 1305 °C of the initial scrap radius. After melting of the shell, a constant dissolution of the mother scrap occurred, which was faster with increasing temperature. The light areas in Figure 3 show the standard deviation of the determined radii. The results of the average dissolution rate of the radius after immersion (r(t)) with the initial radius (r0) are published in [20].
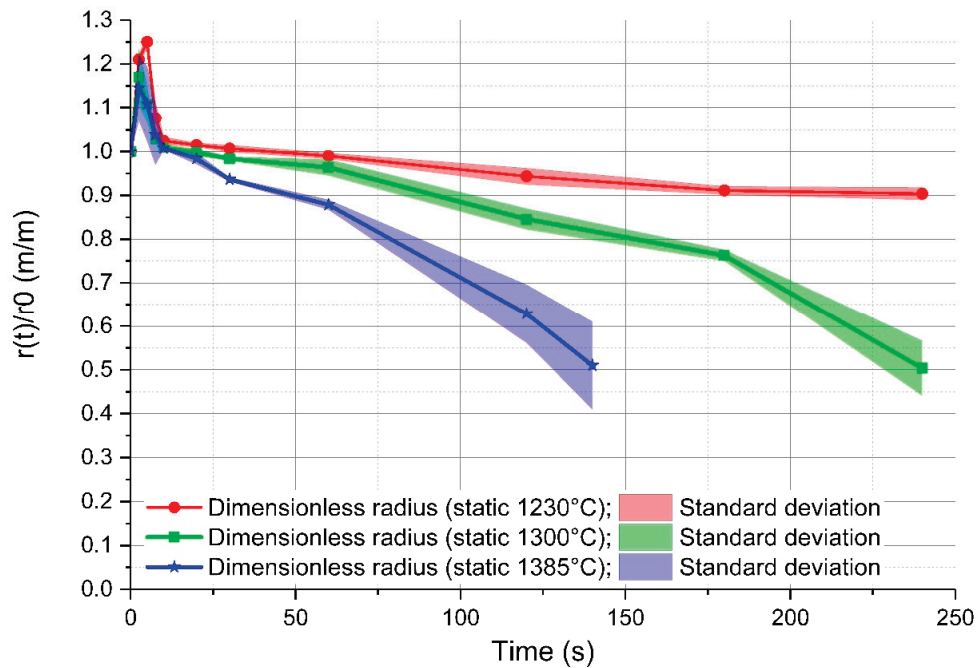
Figure 3. Effect of bath temperature on the melting rate of cylindrical scrap samples in hot metal.

5.2. Optical Microscopy Observations

To summarize the observations of optical microscopy, a few samples were taken for this publication. Two of the samples (162 and 107) presented in detail were submerged—without rotation of the sample—into the hot metal to receive stagnant conditions influenced only by natural convection. The Nital-etched longitudinal area of samples 162 and 107, which were submerged for 20 s at an initial temperature of 1305 °C and 180 s at 1370 °C, respectively, were visible in the mosaic picture in Figure 4 and Figure 5. Through the energy balance, the equilibrium temperature between scrap core and hot metal dropped to 1230 or 1300 °C, respectively. Sample number 59 was submerged into the hot metal for 60 s at an initial temperature of 1450 °C and a rotational speed of 100 rpm. Owing to this speed, turbulent conditions occurred in the hot metal. The Nital-etched longitudinal area of sample number 59 is shown in Figure 6.
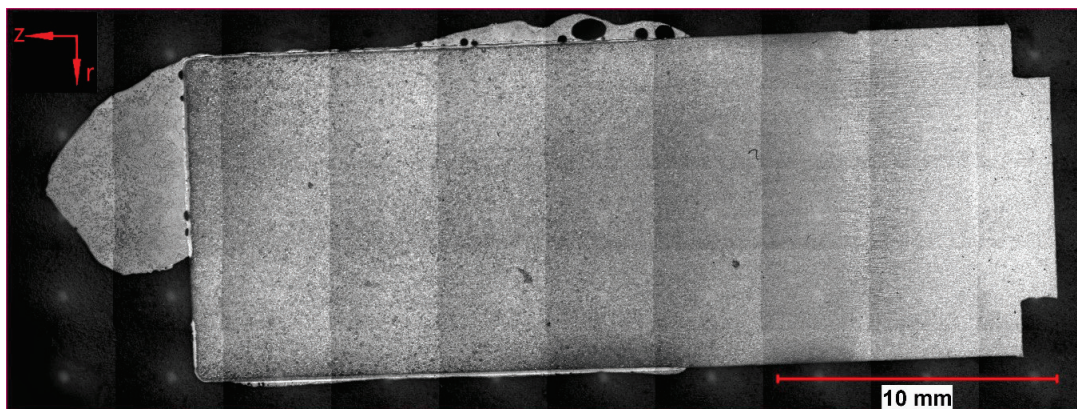
Figure 4. Nital-etched longitudinal area of stagnant sample number 162, submerged for 20 s into hot metal with an equilibrium temperature between scrap core and hot metal of 1230 °C.
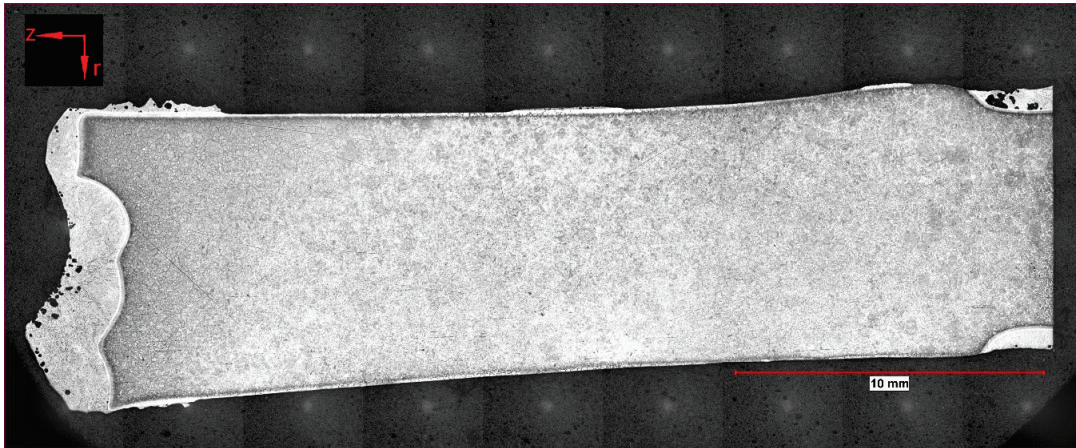
Figure 5. Nital-etched longitudinal area of stagnant sample number 107, submerged for 180 s into hot metal with an equilibrium temperature between scrap core and hot metal of 1300 °C.
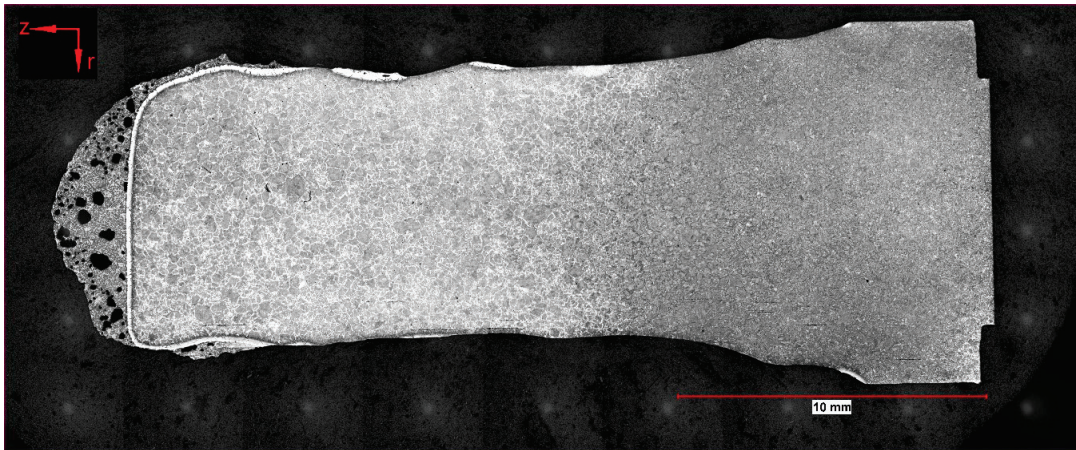

Figure 6. Nital-etched longitudinal area of rotating sample number 59, submerged for 60 s into hot metal with an equilibrium temperature between scrap core and hot metal of 1385 °C.

In Figures 4, 5, and 6, the submerging direction was in an axial direction (z). It can be seen that through the removal from the melt, a droplet of hot metal stuck to the ground surface of the scrap on the left side of the figures. On the surface of the sample in Figure 4, residuals of the frozen shell were still visible. The scrap itself melted stronger in the radial direction (r), which could be explained by local density differences according to the temperature gradient in the boundary layer of the hot metal. With increasing immersion time, dissolution also started on the ground surface. A small bright layer was visible in the mother scrap, which was an indication of a chemical event during dissolution.

After the EPMA measurements, the same section was investigated by means of optical microscopy. Between the two steps of investigation, only Nital etching was carried out. No abrasive steps, like polishing or grinding, were necessary. For this reason, the tracks of the EPMA were barely visible, and a comparison could be made with the outputs of the EPMA.

In Figure 7, the section of sample 162 is shown where the EPMA was carried out at 100× magnification. The rest of the frozen shell of primary carbide is on the left side of the picture. As a result of the measurements carried out by the authors in [42], it was known that the temperature in the scrap reached the austenite temperature and would form martensite in the subsequent water-cooling process. Between those areas, a significant layer more than 100 μm in thickness could be seen, which was identified in Figure 4 as the bright area.
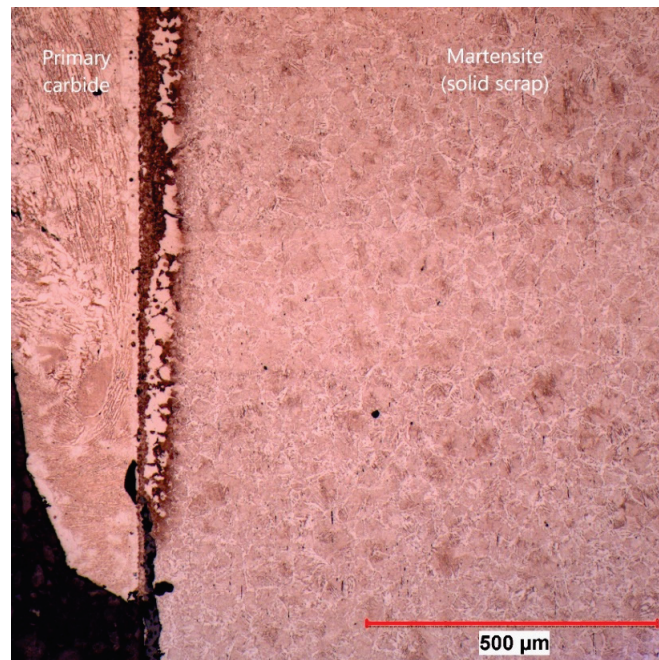
Figure 7. Section where the electron probe microanalysis (EPMA) measurement was carried out for sample 162 (20 s immersion time at 1230 °C equilibrium temperature).

The same microstructure was also found in sample 107 at an equilibrium temperature between scrap core and hot metal of 1300 °C, shown in Figure 8 at 100× magnification. In this picture, it can be clearly seen that there was a sharp interface between the primary carbide and the mother scrap. The bright area was definitely a part of the scrap. In the primary carbide, small residual grains of the scrap were also visible, which resulted from an uneven dissolution through the grain boundary diffusion of carbon.
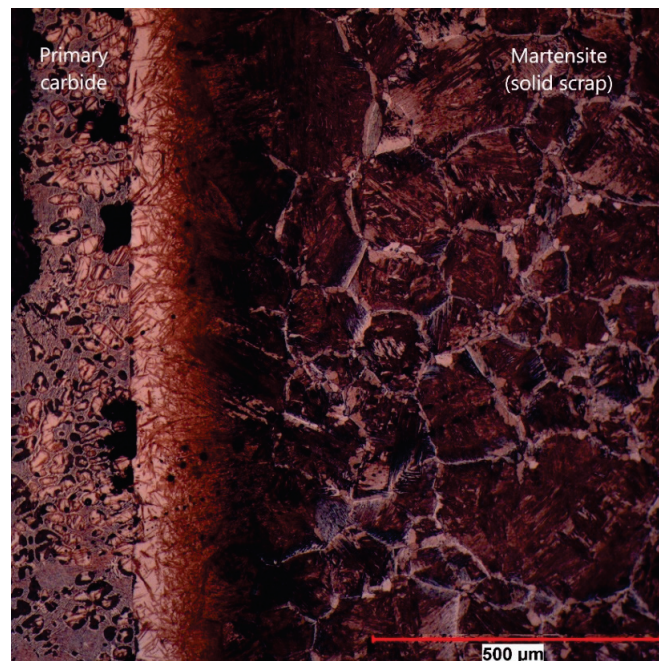
Figure 8. Section where the EPMA measurement was carried out for sample 107 (180 s immersion time at 1300 °C equilibrium temperature).

In Figure 9 the section of EPMA of sample 59 is shown at 200× magnification. The sharp interface between solid scrap and residual primary carbide as well as the diffusion of carbon between the austenite grains was clearly visible.
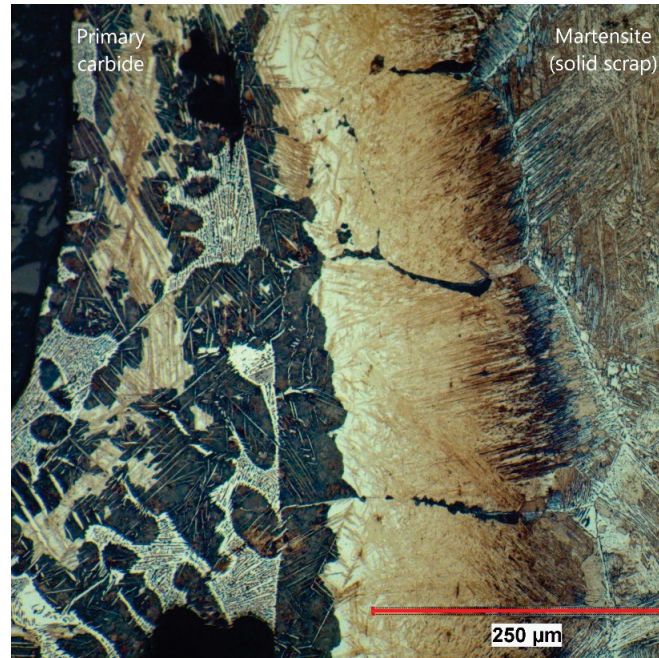

Figure 9. Section where the EPMA measurement was carried out for sample 59 (60 s immersion time at 1385 °C equilibrium temperature).

In all figures, it was noticeable that the primary carbide was in direct contact with the interface during the dissolution process. Scattered former grains of the scrap, liberated from the scrap, were still close to the dissolution interface, which was an indication of a low transportation speed of solid particles in the hot metal.

5.3. Electron Probe Microanalysis (EPMA) Observations

The EPMA measurements were carried out in the certified and accredited laboratory of voestalpine Forschungsservicegesellschaft Donawitz GmbH/Section Material Analytics. In the following figures, the measured fields on the surface of the scrap sample are shown. Through rapid removal of the sample from the hot metal and subsequent water cooling, residual melt stuck to the surface and solidified immediately. It was possible to measure with EPMA the element distribution crossing the interface between the mother scrap and the residual primary carbide. In all figures, the lower graphs show the average value of the 80 measurement points of an area 3 µm × 3 µm each in *y*-distance in the colored shape image. The legends in all figures are on the same scale to compare them to each other.

The colored shape image in Figure 10 shows the carbon distribution of sample 162. The red area on the left side shows the frozen residual melt with a carbon composition of more than 4 wt.-%, including liberated grains from the scrap with a composition below the solidus composition. To compare with the microstructure picture in Figure 7, the red area stopped at the brown sharp interface. From the average carbon composition in the graph, it can be seen that carbon from the hot metal diffused approximately 100 µm into the scrap. A steep gradient from the solidus point at the interface to higher carbon contents in the former melt region was visible. Due to distortions of the liberated grains, it is not clearly readable from the average graph that the carbon composition on the liquid side of the interface steps from the interface carbon composition directly to the hot metal carbon composition. It could be seen that the average silicon formed a layer on the scrap side surface

with silicon contents four times higher than in the scrap and one and a half times higher than in the hot metal. Inside the scrap, it was visible that the small silicon peaks were congruent with the oxygen counts, which was a sign of silicon oxide inclusions.
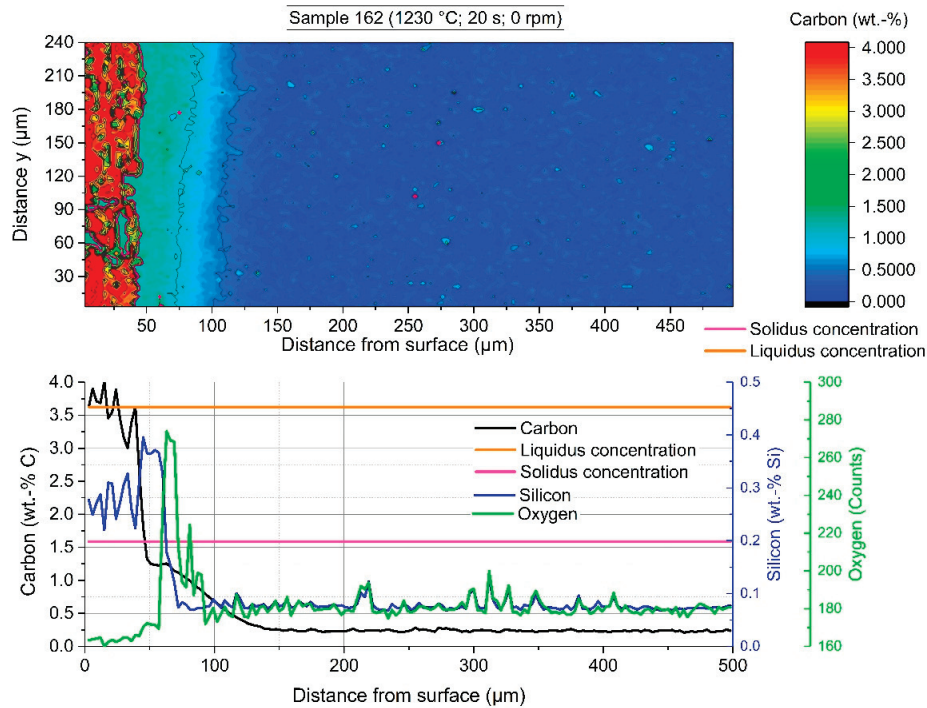

Figure 10. EPMA-measured carbon distribution of sample 162 with an immersion time of 20 s at 1230 °C equilibrium temperature.

In Figure 11, a comparison of the average carbon diffusion profiles of samples with different immersion times at an equilibrium temperature of 1230 °C and natural convection conditions in the bath is shown. The detected lines were cut at the detected interface between the solid and liquid melt. It can be seen that the diffusion profile was nearly equal, and the diffusion depth was approximately 200 μm, except at the two shortest immersion times of 10 and 20 s where the profile was not well developed. At an immersion time of 240 s, carbon diffusion was much deeper, which was a result from the measuring position being too close to the ground surface of the sample. The same behaviour and approximately the same diffusion depth of the carbon were detected for samples with a rotation speed of 100 rpm so that turbulent conditions existed in the melt. The comparison of the average carbon compositions from starting at the liquid–solid interface for turbulent bath conditions is shown in Figure 12. The received interface carbon content in the solid ($C_{interface}$) was equal to the solidus carbon content at this temperature.
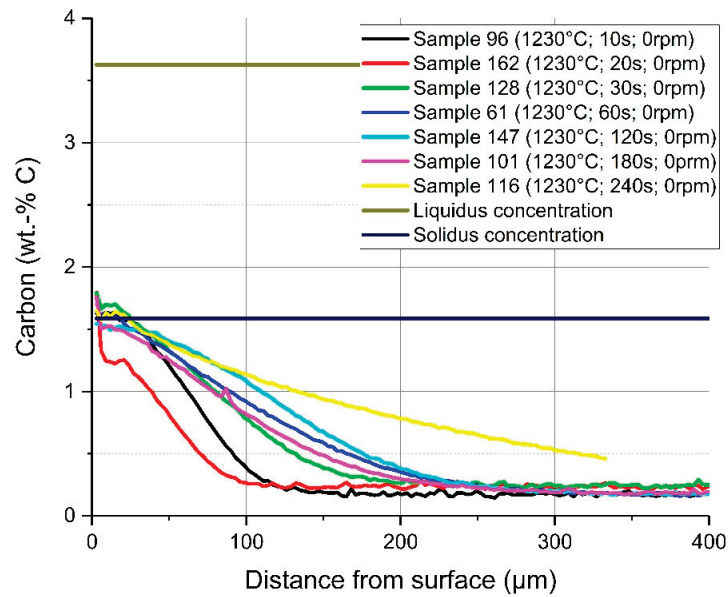
Figure 11. Average carbon composition and diffusion depth from the detected solid–liquid interface under natural convection in the melt at 1230 °C equilibrium temperature.
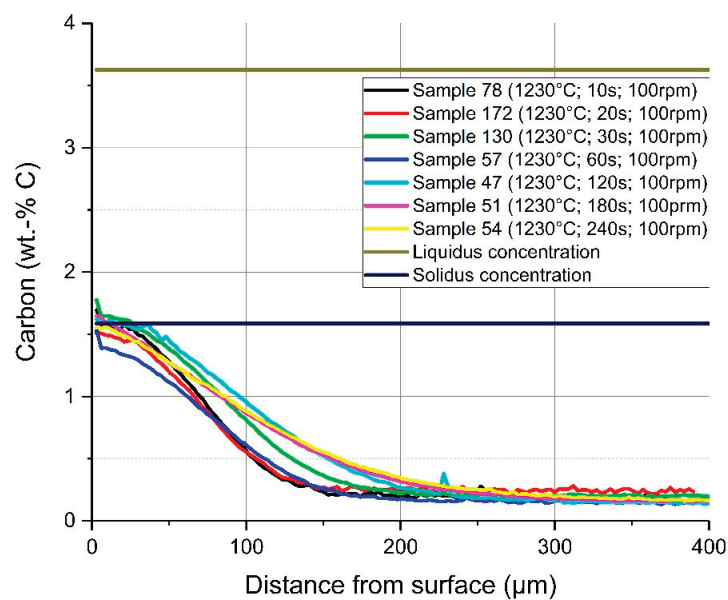

Figure 12. Average carbon composition and diffusion depth from the detected solid–liquid interface under forced convection in the melt through rotation of the sample at 1230 °C equilibrium temperature.

The colored shape image in Figure 13 shows the carbon distribution of sample 107, which was immersed for 180 s. The adjusted equilibrium temperature between scrap core and hot metal was 1300 °C. Like in Figure 10, again a sharp interface can be detected between the scrap and hot metal. In the solid area, the carbon concentration at the interface was—with approximately 1.5 wt.-% carbon—slightly higher than the solidus composition. It seemed that mass transport and dissolution were partly inhibited from the silicon layer formed in the scrap close to the surface. To compare with the microstructure picture in Figure 8, the red area stopped at the bright white, sharp interface. A few liberated grains were also visible on the left side and former liquid area. These liberated grains again led to distortions in the average carbon composition. In detail, the contour levels of the interface carbon composition in the solid, the carbon concentration of the liquidus line, and the carbon concentration of the hot metal were identical. This fact showed that there was a steep concentration gradient in the liquid and a boundary layer in the liquid several times smaller than the carbon boundary layer in the solid phase. These results showed that the boundary layer in the liquid moved towards zero in comparison to the carbon concentration boundary layer in the solid. Ultimately, there was no equilibrium between the carbon concentration of the liquidus line and the carbon concentration at the interface on the solid side. The authors concluded from those facts that the dissolution process was not describable in the liquid using Fick's boundary layer theory. It was apparent that the strong dynamic conditions, caused by natural or forced convection, influenced the dissolution process. Additionally, possible local phenomena influencing the dissolution process may be Rayleigh–Bénard convection, which is based on local density differences, or Marangoni convections, based on local surface tensions. A conspicuous characteristic was also the enrichment of silicon in the solid scrap close to the interface.
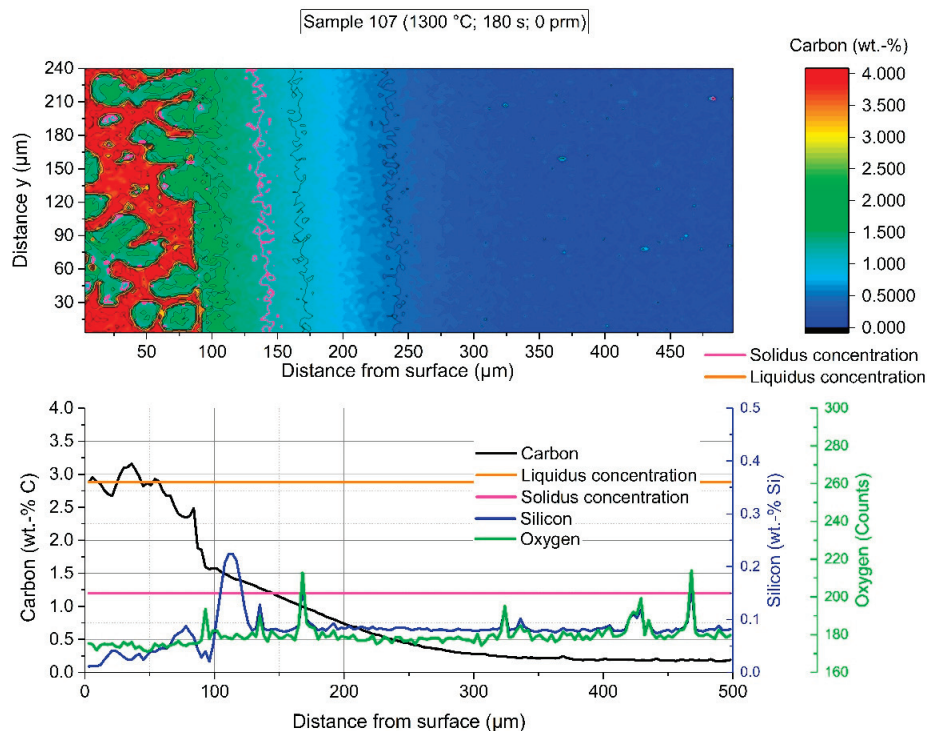

Figure 13. EPMA-measured carbon distribution of sample 107 with an immersion time of 180 s at 1300 °C equilibrium temperature.

Figures 14 and 15 depict the average carbon diffusion profiles for stagnant conditions, where only natural convection arises, and turbulent conditions of the hot metal, respectively. The measured values from various samples with specific immersion times at an equilibrium temperature between scrap core and hot metal of 1300 °C started again from the detected solid–liquid interface. As already

mentioned before, at 1230 °C, an approximately equal carbon diffusion profile in the solid arose for all immersion times. The thickness of the carburized layer was between 150 and 200 μm, which was more than double compared to previous publications. It is mentionable that diffusion depth is a little bit deeper for conditions with natural convection. This resulted from a lower bath agitation and, therefore, also a lower dissolution rate. The carbon concentration at the interface ($C_{interface}$) was approximately 1.5 wt.-%.
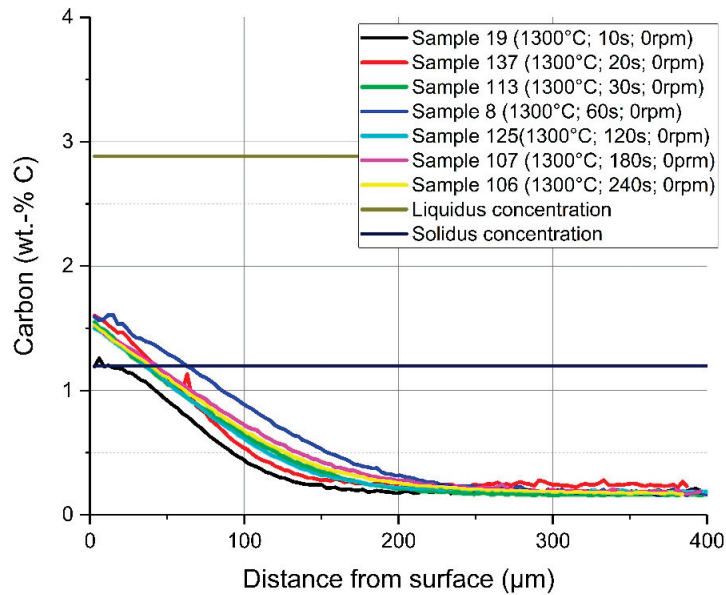

Figure 14. Average carbon composition and diffusion depth from the detected solid–liquid interface under natural convection in the melt at 1300 °C equilibrium temperature.
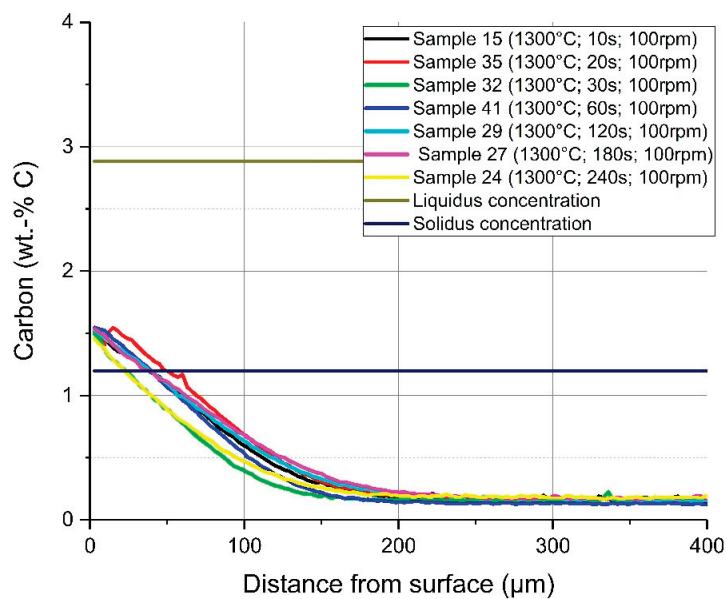
Figure 15. Average carbon composition and diffusion depth from the detected solid–liquid interface under forced convection in the melt through rotation of the sample at 1300 °C equilibrium temperature.

The colored shape image in Figure 16 shows the carbon distribution of sample 59, which was immersed for 60 s in hot metal with turbulent bath conditions realized through a rotational speed of the sample of 100 rpm. The adjusted equilibrium temperature between scrap core and hot metal reached 1385 °C. Again, there was a steep gradient between the carbon concentration at the interface ($C_{interface}$) up to the hot metal carbon concentration of more than 4 wt.-% carbon. The average carbon concentration in the graph below was influenced by liberated grains. In comparison to the microstructure in Figure 9, it was observable that the solidus concentration was deep inside the scrap, and the dissolution was again inhibited. A further point to mention is that there was no possibility to clearly define in which state (e.g., graphite or as a component) the dissolved carbon existed in the boundary layer region. As at lower temperatures the contour levels of the interface carbon composition in the solid, the carbon concentration of the liquidus line, and the carbon concentration of the hot metal were identical.
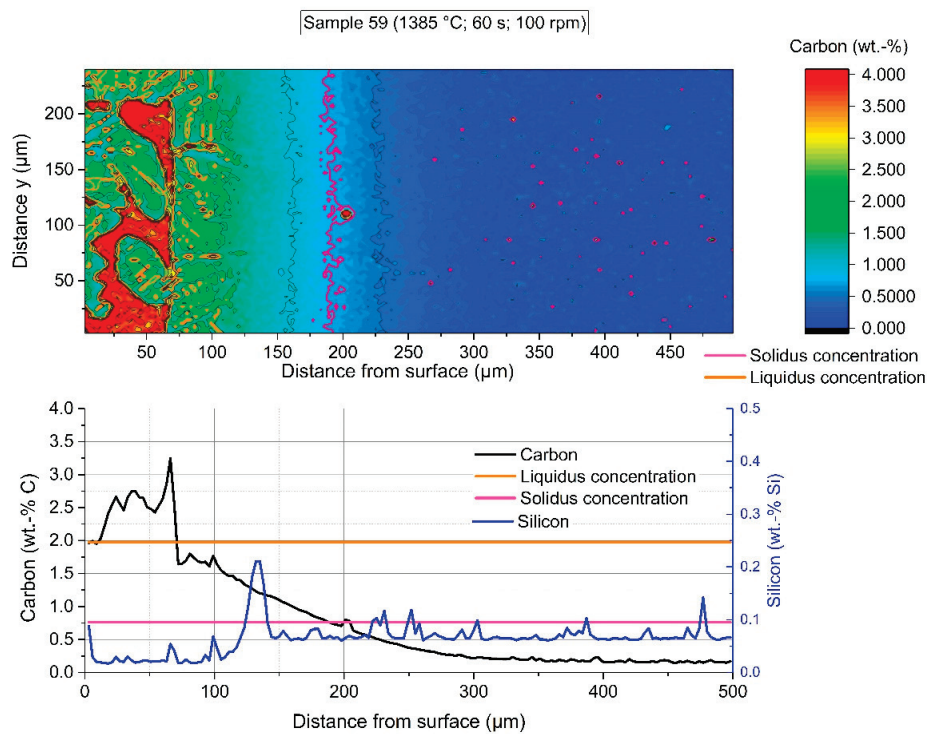

Figure 16. EPMA-measured carbon distribution of sample 59 with an immersion time of 60 s at 1385 °C equilibrium temperature and turbulent bath conditions.

The average carbon diffusion profiles for stagnant or turbulent conditions at an equilibrium temperature of 1385 °C showed similar results to those at lower temperatures. The carbon concentration at the interface ($C_{interface}$) was approximately 1.6 wt.-%.

To emphasize silicon enrichment, Figure 17 shows the EPMA-measured silicon distribution of sample 59, parallelly measured with the carbon distribution from Figure 16. It was clearly visible that a silicon-enriched layer was formed in the solid scrap at 125 μm < x < 140 μm from the measurement starting point. The first former liquid regions, detected by carbon distribution, arose at x < 125 μm. Such an enrichment was observed in all samples during the entire investigation period. In the literature, there has not been any similar behaviour reported thus far. A theory regarding this phenomenon is that the dispersed silicon oxides in the mother scrap will stay at the lowest energy

level, which is at the interface. They will be reduced by the transferred carbon, which may be a retarding factor of the dissolution process. Additionally, a possible occurrence of diffusive events at the reported temperature levels, for example mass transfer of silicon, cannot be ruled out in this case. A closer investigation into this phenomenon has to be carried out in future research and experimental investigations.
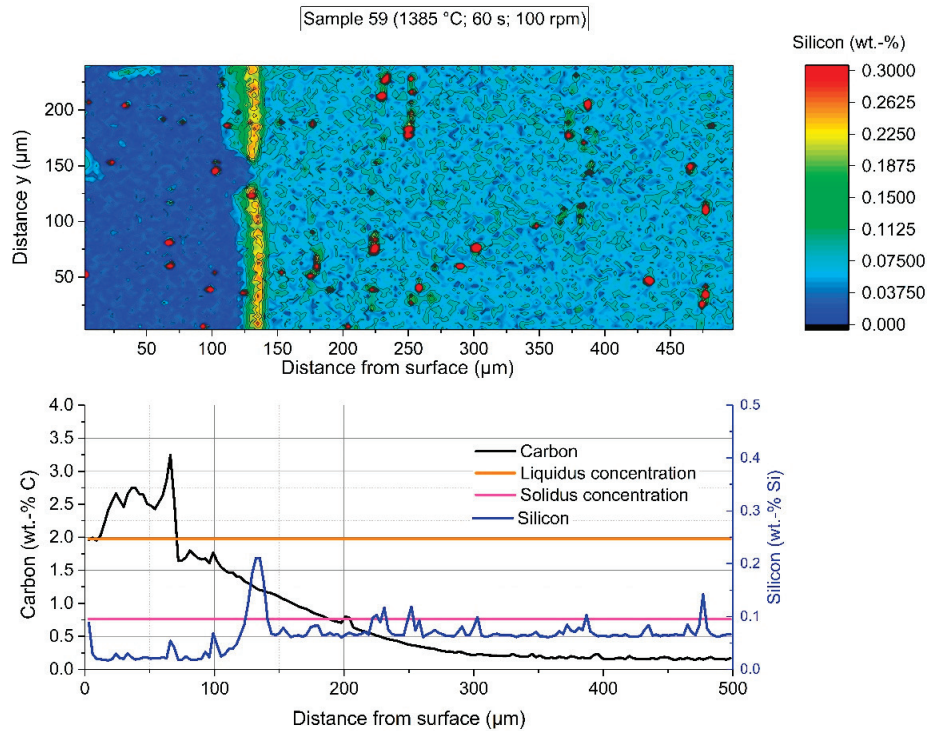

Figure 17. EPMA-measured silicon distribution of sample 59 with an immersion time of 60 s at 1385 °C equilibrium temperature and turbulent bath conditions.

5.4. Discussion of mass balance according to EPMA investigations

From the results of the EPMA measurements, it was evident that the carbon concentration on the solid side of the solid–liquid interface increased through diffusion of carbon to an interface carbon concentration ($C_{interface}$). For an equilibrium temperature between scrap core and hot metal of 1230 °C, the interface carbon concentration was defined by $C_{interface} = C_s^*$. With increasing temperature, the interface carbon concentration increased to values of 1.5 wt.-% carbon at 1300 °C and 1.6 wt.-% carbon at 1385 °C. In line with the phase diagram in Figure 2 of the scrap composition determined, these concentrations were in the two-phase area. In the liquid region, a steep gradient from the interface carbon concentration to the carbon composition of the hot metal was clearly recognized. Theoretical analyses reported in former publications always expected an equilibrium system, which was explained by means of the boundary layer theory and Fick's second law. In the case of scrap dissolution, the present paper shows with the EPMA measurements that the boundary layer in the liquid went to zero in comparison with the diffusion boundary layer inside the solid scrap. Based on the measurements, the authors will amend the mass balance of Equation 3 to the following expression given in Equation 12:

$$k'_{met} * \rho_{HM} * \left(C_{HM} - C_{interface} \right) = -\rho_{scrap} * D_s * \frac{dC}{dx}\Big|_{x=r(x,t)}. \tag{12}$$

The term on the left side of Equation 12 expresses the carbon transport in the liquid melt with the carbon concentration difference. According to the evaluated results from the EPMA, the

difference is between the hot metal composition C_{HM} and an interface carbon concentration applicable for $C_l^* > C_{interface} \geq C_s^*$. To close the mass balance, only the expression of carbon diffusion into the solid scrap will be in the counter direction. This fact is disputed through non-equilibrium and heavy dynamic conditions occurring under both natural and forced convection in the liquid. By the use of Equation 9 and the ratio of the velocity of the boundary movement of Zhang and Oeters in Equation 11, the mass balance can be transformed into the following expression, which will describe the diffusive dissolution behaviour of steel scrap in liquid hot metal. It is valid for the following temperature-dependent expression $C_l^* > C_{interface} \geq C_s^*$:

$$-\frac{dr}{dt} = k_{met} * ln\left(\left(\frac{(\%C_{HM}-\%C_{interface})*\rho_{HM}}{(\%C_{interface}-\%C_{scrap})*\rho_{scrap}}\right) + 1\right). \tag{13}$$

Additionally, it has to be mentioned that the dissolution behaviour will also be influenced through other elements, which is reasonable due to the observed enrichment of silicon. Furthermore, an influence through local phenomena (e.g., Rayleigh-Bénard convection) might be given and should definitely be investigated in detail.

6. Conclusions

Scrap melting and dissolution is indeed a complex and complicated process including simultaneous heat and mass transfer. The present study describes the analytic determination of common steel scrap dissolution tests in liquid carbon-saturated hot metal. In previous publications, a thermodynamic equilibrium between the liquid metal and the solid scrap was assumed, allowing the steel scrap dissolution to be explained using Fick's second law and by means of a binary Fe–Fe₃C phase diagram of the used scrap.

As a result of systematic approaches, the scrap samples immersed into the hot metal were removed and subsequently water-cooled. Without additional heat input, the sample preparation was carried out to perform a series of electron probe microanalysis (EPMAs) on the scrap surface and the residual melt, which could not flow away rapidly enough before quenching. By comparison with optical microscope measurements, the area analyzed using EPMA could have been used to provide further information.

It was observed that in the liquid area, a steep concentration gradient of carbon existed, which started at an interface carbon concentration equal to the interface carbon concentration in the still solid material. Through maximum increase in the concentration gradient in the liquid, ending at the hot metal carbon concentration, it was concluded that the boundary layer in the liquid moved towards zero, and no distinctive boundary layer was formed. Notably, strong dynamic conditions, caused by natural or forced convection, influence the dissolution process. The appearance of local convection phenomena influencing the dissolution process (e.g., Rayleigh-Bénard convection) cannot be excluded. Through the detected interface carbon concentration, a new approach for mass balance to describe the dissolution process was outlined. Moreover, it was visualized that the diffusion of carbon into the solid was constant at every investigated immersion time step, which was an indication of a constant dissolution rate under isothermal conditions. The carburized boundary layer thickness in the solid material reached between 150 to 200 μm, which was approximately two times more than that reported in previous publications. The new approach reported can be easily included into dynamic LD-converter process models, which are based on thermodynamic considerations. As long as the equilibrium temperature of the liquid hot metal and the scrap is below the two-phase melting stage at the initial carbon concentration of the scrap, the equation given in Equation 13 might be used. Further, it is necessary that the process model implies an approximation of the mass transfer coefficient as well as an estimation of the interface carbon concentration according to the rule $C_l^* > C_{interface} \geq C_s^*$.

Conspicuous characteristic silicon enrichments were detected in the solid scrap close to the solid–liquid interface. Due to the high temperatures and large amounts of silicon oxides in the scrap, it was concluded that the oxides will be trapped at the interface and reduced through the carbon. It

is absolutely necessary to investigate in further research the behaviour of other elements besides carbon on their diffusivity into the solid steel and mutual interference with the carbon mass transfer.

In summary, the outcomes of the present study clearly indicate that more individual and adequate experiments will be necessary in future research work to describe steel scrap melting and dissolution behaviours in hot metal.

Author Contributions: Conceptualization, F.M.P.; Data curation, F.M.P.; Investigation, F.M.P. and M.R.; Methodology, F.M.P.; Project administration, F.M.P., J.S. and K.P.; Resources, F.M.P.; Software, F.M.P. and J.S.; Supervision, F.M.P. and J.S.; Validation, J.S., M.R., R.A., G.K., and K.P.; Visualization, F.M.P.; Writing—original draft, F.M.P.; Writing—review & editing, F.M.P., J.S., M.R., R.A., G.K., and K.P.

Conflicts of Interest: The authors declare no conflict of interest.

References

1. Ghosh, A.; Chatterjee, A. *Ironmaking and Steelmaking Theory and Practice*; PHI Learning Private Limited: Delhi, India, 2015; pp. 285–292.
2. Bureau of International Recycling Ferrous Division, World Steel Recycling in Figures 2013–2017: Steel Scrap—A Raw Material for Steelmaking. Available online: https://www.bdsv.org/fileadmin/user_upload/180222-Ferrous-report-2017-V07.pdf (accessed on 3 January 2019).
3. Deng, S.; Xu, A.; Yang, G.; Wang, H. Analyses and Calculation of Steel Scrap Melting in a Multifunctional Hot Metal Ladle. *Steel Res. Int.* **2019**, *90*, 1800435.
4. Kruskopf, A.; Holappa, L. Scrap melting model for steel converter founded on interfacial solid/liquid phenomena. *Metall. Res. Technol.* **2018**, *115*, 201–208.
5. Ohnuki, K.; Hiraoka, T.; Inoue, T.; Umezawa, K.; Matsumoto, N. Development of steel scrap melting process. *Nippon Steel Tech. Rep.* **1994**, *61*, 52–57.
6. Zhang, L.; Oeters, F. *Schmelzen und Mischen von Legierungsstoffen in Stahlschmelzen*; Verlag Stahleisen GmbH: Düsseldorf, Germany, 2012; pp. 38–40.
7. Oeters, F. *Metallurgie der Stahlherstellung*; Springer: Berlin/Heidelberg, Germany,1989; pp. 414–452.
8. Shurygin, P.M.; Shantarin, V.D. Растворение металлов в железоуглеродистых расплавах (engl.: Metal dissolution in liquid Iron Carbon alloy). Известия Высших Учебных Заведений, Черная Металлургия **1963**, *6*, 5–11.
9. Krupennikov, S.A.; Filimonov, Y.P. Melting of steel scrap in hot metal. *Steel Transl.* **2007**, *37*, 217–219.
10. Gol'dfarb, M.; Sherstov, B.I. Heat and mass transfer when melting scrap in an oxygen converter. *J. Eng. Phys. Thermophys.* **1970**, *18*, 342–347.
11. Nomura, H.; Mori, K. The Rate of Dissolution Iron into Liquid Fe-C Alloy. *Tetsu-to-Hagané* **1969**, *55*, 1134–1141.
12. Pehlke, R.D.; Goodell, P.D.; Dunlap, R.W. Kinetics of Steel Dissolution in Molten Pig Iron. *Trans. Metall. Soc. AIME* **1965**, *233*, 1420–1427.
13. Specht, E.; Jeschar, R. Kinetics of steel melting in carbon-steel alloys. *Steel Res.* **1993**, *64*, 28–34.
14. Glinkov, M.A.; Filimonov, Y.P.; Yurevich, V.V. Dissolution of a steel cylinder in liquid pig iron. *Steel USSR* **1971**, *1*, 202–203.
15. Olsson, R.G.; Koump, V.; Perzak, T.F. Rate of dissolution of Carbon-Steel in Molten Iron Carbon Alloys. *Trans. Metall. Soc. AIME* **1965**, *233*, 1654–1657.
16. Kim, Y.-U.; Pehlke, R.D. Mass transfer during dissolution of a solid into liquid in the iron-carbon system. *Metall. Trans.* **1974**, *5*, 2527–2532.

17. Kim, Y.U.; Pehlke, R.D. Transient heat transfer during initial stages of steel scrap melting. *Metall. Trans. B* **1975**, *6*, 585–591.

18. Li, J.; Brooks, G.; Provatas, N. Kinetics of scrap melting in liquid steel. *Metall. Mater. Trans. B* **2005**, *36B*, 293–302.

19. Li, J.; Provatas, N. Kinetics of Scrap Melting in Liquid Steel: Multipiece Scrap Melting. *Metall. Mater. Trans. B* **2008**, *39*, 268–279.

20. Penz, F.M.; Schenk, J.; Ammer, R.; Klösch, G.; Pastucha, K. Dissolution of Scrap in Hot Metal under Linz–Donawitz (LD) Steelmaking Conditions. *Metals* **2018**, *8*, 1078.

21. Penz, F.M.; Parreiras Tavares, R.; Weiß, C.; Schenk, J.; Ammer, R.; Pastucha, K.; Klösch, G. Analytical and numerical determination of the heat transfer coefficient between scrap and hot metal based on small-scale experiments. *Int. J. Heat Mass Transf.* **2019**, unpublished.

22. Shin, M.; Oh, J.S.; Lee, J.; Jung, S.; Lee, J. Dissolution rate of solid iron into liquid Fe-C alloy. *Metals Mater. Int.* **2014**, *20*, 1139–1143.

23. Xi, X.; Yang, S.; Li, J.; Chen, X.; Ye, M. Thermal simulation experiments on scrap melting in liquid steel. *Ironmak. Steelmak.* **2018**, *52*, 1–7.

24. Sun, H.; Liu, Y.; Lin, C.; Lu, M. Experimental Observation of Spherical Scrap Melting in Hot Metal. In Proceedings of the 6th ICS, Beijing, China, 12–14. May 2015; pp. 136–139.

25. Asai, S.; Muchi, I. Effect of scrap melting on the process variables in LD converter caused by the change of operating conditions. *Trans. ISIJ* **1971**, *11*, 107–115.

26. Asai, S.; Muchi, I. Theoretical Analysis by the Use of Mathematical Model in LD Converter Operation. *Trans. ISIJ* **1970**,10, 250–263.

27. Yorucu, H.; Rolls, R. A mathematical model of scrap melting for the LD process. *Iron Steel Int.***1976**, *49*, 35–40.

28. Li, J.; Brooks, G.A.; Provatas, N. Phase-Field Modeling of Steel Scrap Melting in a Liquid Steel Bath. In Proceedings of the AISTech 2004 Proceedings, Nashville, TN, USA, 8–11 May 2004; Volume I, pp. 833–843.

29. Sethi, G.; Shukla, A.K.; Das, P.C.; Chandra, P.; Deo, B. Theoretical Aspects of Scrap Dissolution in Oxygen Steelmaking Converters. In Proceedings of the AISTech 2004 Proceedings Volume II, Nashville, TN, USA, 15–17 September 2014; pp. 915–926.

30. Shukla, A.K.; Deo, B.; Robertson, D. Scrap Dissolution in Molten Iron Containing Carbon for the Case of Coupled Heat and Mass Transfer Control. *Metall. Mater. Trans. B* **2013**, *44*, 1407–1427.

31. Guo, D.; Swickard, D.; Alavanja, M.; Bradley, J. Numerical Simulation of Heavy Scrap Melting in BOF steelmaking. *Iron Steel Technol.* **2013**, *10*, 125–132.

32. Kruskopf, A. A Model for Scrap Melting in Steel Converter. *Metall. Mater. Trans. B* **2015**, *46*, 1195–1206.

33. Kruskopf, A.; Louhenkilpi, S. 1-Dimensional scrap melting model for steel converter (BOF). In Proceedings of the METEC & 2nd ESTAD, Düsseldorf, Germany, 15–19 June 2015; pp. 1–4.

34. Muchi, I.; Asai, S.; Miwa, M. Mathematical Model of LD Converter and Its Application to theoretical Analysis of Refining Process. *Proc. ICSTIC, Suppl. Trans. ISIJ* **1971**, *11*, 347–351.

35. Szekely, J.; Chuang, Y.K.; Hlinka, J.W. The melting and dissolution of low-carbon steels in iron-carbon melts. *Metall. Trans.* **1972**, *3*, 2825–2833.

36. Wright, J.K. Steel dissolution in quiescent and gas stirred Fe/C melts. *Metall. Mater. Trans. B* **1989**, *20B*, 363–374.

37. Burdakov, D.D.; Varshavskii, A.P. Melting scrap in the oxygen converter process. *Stal Engl.* **1967**, *8*, 647–648.

38. Gaye, H.; Destannes, P.; Roth, J.L.; Guyon, M. Kinetics of scrap melting in the converter and electric arc furnace. In Proceedings of the 6th International Iron and Steel Congress, Nagoya, Japan, 21–26 October 1990; Volume 4, pp. 11–17.

39. Gaye, H.; Wanin, M.; Gugliermina, P.; Schittly, P. Kinetics of scrap dissolution in the converter. Theoretical Model and Plant Experimentation. *Steelmak. Proc.* **1985**, *68*, 91–104.

40. Kawakami, M.; Takatani, K.; Brabie, L.C. Heat and Mass Transfer Analysis of Scrap Melting in Steel Bath. *Tetsu-to-Hagané* **1999**, *85*, 658–665.

41. Lommel, J.M.; Chalmers, B. The Isothermal Transfer from Solid to Liquid in Metal Systems. *Trans. Metall. Soc. AIME* **1959**, *215*, 499–508.

42. Penz, F.M.; Schenk, J.; Ammer, R.; Pastucha, K.; Maunz, B. Dissolution behaviour of ULC steel in carbon saturated hot metal. *La Metallurgia Italiana* **2018**, *11*, 36–45.

43. Goldberg, D.; Belton, G.R. The diffusion of carbon in iron-carbon alloys at 1560 °C. *Metall. Trans.* **1974**, *5*, 1643–1648.

44. Bester, H.; Lange, K.W. Abschätzung mittlerer Werte für die Diffusion von Kohlenstoff, Sauerstoff, Wasserstoff, Stickstoff und Schwefel in festem und flüssigen Eisen. *Arch. Eisenhüttenwesen* **1972**, *43*, 207–213.

45. Levič, V.G. *Physicochemical Hydrodynamics*, 2nd ed.; Prentice-Hall: New York, NY, USA, 1962; p. 69.

46. Penz, F.M.; Bundschuh, P.; Schenk, J.; Panhofer, H.; Pastucha, K.; Paul, A. Effect of Scrap Composition on the Thermodynamics of Kinetic Modelling of BOF Converter. In Proceedings of the 2nd VDEh-ISIJ-JK Symposium, Stockholm, Sweden, 12–13 June 2017; pp. 124–135.

47. Oya, T.; Furugaki, I.; Matsunaga, H.; Tominaga, T.; Miyagawa, K.; Nomura, E. On the Melting Rate of Scrap and Cold Pig Iron in the LD Process. *Tetsu-to-Hagane* **1965**, *51*, 1925–1927.

48. Mehrer, H. (Ed.) *Diffusion in Solids: Fundamentals, Methods, Materials, Diffusion-Controlled Processes*; Springer: Berlin/Heidelberg, Germany, 2007; pp. 37–51.

49. Szekely, J.; Themelis, N.J. *Rate Phenomena in Process Metallurgy*, 1st ed.; John Wiley & Sons, Inc.: New York, NY, USA, 1971; pp. 351–476.

50. Furtado, H.S.; Bhattacharya, T.; Hwang, H.; Kirmse, O.J. *Transport Phenomena: Fundamentals and Applications in Metallurgical and Materials Engineering*; ABM: Sao Paulo, Brazil, 2011.

51. Necati Özisik, M. *Heat Conduction*, 2nd ed.; John Wiley & Sons, Inc.: New York, NY, USA, 1993.

52. Guthrie, R.; Gourtsoyannis, L. Melting rates of furnace or ladle additions in steelmaking. *Can. Metall. Q.* **1971**, *10*, 37–46.

53. Kumar, A.; Singh, A.K. A Stefan problem with temperature and time dependent thermal conductivity. *J. King Saud Univ. Sci.* **2018**, 1–5, doi:10.1016/j.jksus.2018.03.005.

54. Turkyilmazoglu, M. Stefan problems for moving phase change materials and multiple solutions. *Int. J. Therm. Sci.* **2018**, *126*, 67–73.

55. Voller, V.R.; Falcini, F. Two exact solutions of a Stefan problem with varying diffusivity. *Int. J. Heat Mass Transf.* **2013**, *58*, 80–85.

56. Racina, A. *Vermischung in Taylor-Couette Strömung*; Universitätsverlag: Karlsruhe, Germany, 2009; pp. 29–40.

57. Esser, A.; Grossmann, S. Analytic expression for Taylor-Couette stability boundary. *Phys. Fluids* **1996**, *8*, 1814–1819.

2 Attachment B: Additional figures

In the attached DVD additional figures and illustrations are saved. The directories of the folders are related to the chapters in the main part of this thesis and are named as followed:

- To chapter 4.4.1 EMPA investigation of the construction steel samples
    - 20190607 EMPA 1230 stagnant
    - 20190607 EMPA 1230 turbulent
    - 20190607 EMPA 1300 stagnant
    - 20190607 EMPA 1300 turbulent
    - 20190607 EMPA 1385 stagnant
    - 20190607 EMPA 1385 turbulent
    - 20190607 EMPA Pure Iron
    - Optical microscopy and shell freezing
- To chapter 4.4.2 EMPA investigation of a scrap skull withstanding an entire converter heat
- To chapter 4.5 Comparison of the modified diffusive melting equation with the existing model
- To chapter 5.3 Analytical diffusion model
- To chapter 6.2 New scrap melting model